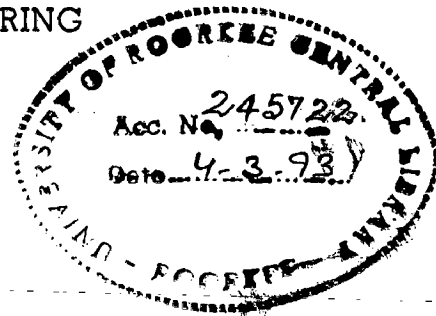


ANALYTICAL INVESTIGATION OF INTERACTION  
BETWEEN AIR MOTION AND FUEL SPRAY  
IN DIRECT INJECTION DIESEL ENGINE

1  
DG-91  
SIN

A THESIS

submitted in fulfilment of the  
requirements for the award of the degree  
of  
DOCTOR OF PHILOSOPHY  
in  
MECHANICAL ENGINEERING



By

S. K. SINGAL




DEPARTMENT OF MECHANICAL AND INDUSTRIAL ENGINEERING  
UNIVERSITY OF ROORKEE  
ROORKEE-247 667 (INDIA)

JULY, 1991

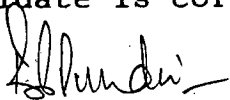
### CANDIDATE'S DECLARATION

I hereby certify that the work which is being presented in this thesis entitled "ANALYTICAL INVESTIGATION OF INTERACTION BETWEEN AIR MOTION AND FUEL SPRAY IN DIRECT INJECTION DIESEL ENGINE" in fulfillment of the requirements for the award of the Degree of DOCTOR OF PHILOSOPHY, being submitted in the Department of Mechanical and Industrial Engineering of the University of Roorkee, is an authentic record of my own work carried out during the period from October 1986 to July 1991 under the supervision of Dr P S Mehta and Dr B P Pundir.

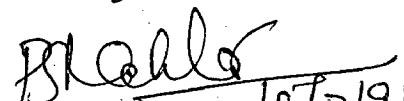
The matter embodied in this thesis has not been submitted by me for the award of any other degree.

  
(S.K. Singal)

This is to certify that the above statement made by the Candidate is correct to the best of our knowledge.




(Dr B P Pundir)  
Project Co-ordinator  
Engines Laboratory  
Indian Institute of  
Petroleum, Dehradun  
DEHRADUN - 248 005  
(INDIA)

  
(Dr P S Mehta) 15/7/91

Reader  
Department of Mechanical  
and Industrial Engineering  
University of Roorkee  
ROORKEE - 247 667  
(INDIA)

The PhD Viva-Voce examination of Sh. S K Singal, research scholar has been held on 28 Feb. 92. at 3:30 pm.

   
Signature of Guide

  
Signature of  
External  
Examiner

## ABSTRACT

In a small size direct injection diesel engine, fuel injection spray impinges on the combustion chamber wall, thus significantly affecting fuel-air mixing and burning characteristics of the spray. With decrease in engine displacement, air swirl inside the combustion chamber is considered essential to improve fuel-air mixing. Consequently, the understanding of the influence of the wall on the spray development in the combustion chamber is quite important. It is reported in the literature that the decrease in displacement volume of the engine results in a significant increase in brake specific fuel consumption (BSFC). The deterioration in the fuel economy is attributed to the wall wetting due to the spray in addition to higher heat transfer and friction losses. A proper matching of fuel injection, air motion and piston bowl geometry is, therefore, very important.

In literature, only a few attempts are seen concerning the modelling of the wall jet development in engine situation. The available models present a simplified analysis in this respect without consideration of the swirl and the wall shear effects.

The present study is an attempt to investigate the influence of spray-swirl-wall interaction in direct injection diesel engine. An analytical model has been developed to predict the fuel-air mixing and burning characteristics of small DI diesel engines. The predicted results have been validated with the available experimental data. Besides comparison with the published data of earlier investigators, the data are also measured on engines.

Four mass and momentum conservation equations are written along the tangential and normal directions to the spray for both

free and wall regions based on continuum integral approach. The flow along the smooth and impermeable wall is considered to be two dimensional. The velocity distribution in the spray along the wall is taken by the composite profile developed combining one-seventh law of velocity distribution in turbulent boundary layer at the wall and the velocity profile of Abramovich in the free jet region.

The influence of the bowl geometry in terms of moment of inertia and the wall friction on the instantaneous swirl level during compression is considered. The spray structure is multi-zonal and the simulation of atomization, droplet-size distribution, evaporation, turbulent mixing and combustion processes is included. The fuel spray is divided into a number of elemental zones in the axial and radial directions in order to simulate the heterogeneous nature of the diesel spray. It is postulated that following the ignition delay period, combustion occurs at the specified rate in the elements where the actual air-fuel vapour equivalence ratio falls within the limits of inflammability. Hence, the mass rate of burned fuel and the rate of heat release is computed. Conservation equations for the mass and energy are formulated for the spray and surrounding fluids. Solution of energy equation and equation of state gives the cylinder pressure, the temperature and the volume of the spray and temperature of the surrounding fluids. Heat transfer from gases to the walls of the cylinder is computed following Woschni's correlation.

Moment of inertia of the air, depending upon the shape of bowl-in-piston and the bowl offset, influences the angular swirl near top centre position of the piston at the time of injection. It is found that there is an appreciable variation in the air swirl at the top centre position due to the variation in bowl geometry.

From the results it is established that the rate of air entrainment is enhanced during the wall jet flow due to the combined effect of increased axial entrainment parameter, increased surface area available for entrainment and the wall shear stress. Although, early impingement in small engines results in wall wetting, it does help in enhanced mixing due to the higher rates of air entrainment.

Results of prediction concerning the effect of injection parameters on the spray motion concede that the initial rate of injection and mass averaged injection pressure play significant role in the air-fuel mixing. The rate of entrainment is higher in the central injection case in comparison to the other injector locations in the cylinder. Changes in nozzle orifice size affect fuel-air mixing. The effect is, however, predominantly injection pressure controlled.

The model predictions show good correlation with the experimental data and respond well to the variations in input parameters. The Influence of the chamber wall on the burning rates and engine performance is studied using the model. The comparison of experimental engine pressure data history and the performance parameters at various test conditions are made with the model predictions. The predictions in terms of the burning rates and undermixedness suggest that, if the spray is fully vaporized prior to the impingement, the rate of burning is found to be faster in the presence of the wall.

The level of predictions from the model is satisfactory and the model is quite suitable to optimize the injection characteristics, bowl geometry and air motion in small DI diesel engines.

## ACKNOWLEDGEMENTS

The author wishes to express his profound sense of gratitude to Dr P S Mehta of University of Roorkee and Dr B P Pundir for their kind help, keen interest and guidance throughout the course of this work.

The author wishes to thank Sh Sudhir Singhal, Head, Petroleum Products Application Division and Dr T S R Prasad Rao, Director, Indian Institute of Petroleum, Dehradun for providing the necessary facilities for carrying out this work in the Engine Laboratory.

Thanks are also to all colleagues of the laboratory for their help particularly to Sh P B Semwal.

The author expresses appreciation to his wife Anita and daughter Vinti for their support and patience.

## CONTENTS

DECLARATION

ABSTRACT

ACKNOWLEDGEMENTS

CONTENTS

NOMENCLATURE

CHAPTER - 1	GENERAL DISCUSSION AND LITERATURE REVIEW	1
1.1	INTRODUCTION	1
1.2	AIR MOTION	2
1.2.1	Induction Swirl	4
1.2.2	Compression-Induced Swirl	5
1.3	FUEL SPRAY	7
1.3.1	Fuel Injection	7
1.3.2	Spray Development	9
1.4	AIR MOTION AND FUEL SPRAY INTERACTION	15
1.5	FUEL SPRAY AND WALL INTERACTION	18
1.6	ENGINE MODELS	24
	FIGURES	33
CHAPTER - 2	PROBLEM ENUNCIATION AND FORMULATION	52
	FIGURE	54
CHAPTER - 3	MODEL FORMULATION	55
3.1	DESCRIPTION OF SWIRL MOTION	55
3.2	FUEL INJECTION	57
3.3	SPRAY MOTION	57

	3.4	TURBULENT MIXING	63
	3.5	ATOMIZATION, DISPERSION AND SPRAY STRUCTURE	65
	3.6	FUEL DISTRIBUTION	67
	3.7	IGNITION DELAY	68
	3.8	EVAPORATION	69
	3.9	COMBUSTION	69
	3.10	HEAT TRANSFER	70
	3.11	THERMODYNAMIC ANALYSIS	73
		FIGURES	78
CHAPTER - 4		COMPUTER PROGRAM STRUCTURE	80
	4.1	INTRODUCTION	80
	4.2	PROGRAM INPUT	80
	4.3	FLOW CHARTS AND PROGRAM MODULES	80
	4.4	MODEL OUTPUT	86
		FIGURES	87
CHAPTER - 5		EXPERIMENTAL PROGRAM	93
	5.1	GENERAL EXPERIMENTAL PLAN	93
	5.2	MEASURING INSTRUMENTATION	93
	5.3	MEASUREMENT OF FUEL INJECTION RATE	95
	5.4	TEST CONDITIONS	96
		FIGURES	98
CHAPTER - 6		RESULTS AND DISCUSSION	101
	6.1	EFFECT OF INJECTION PARAMETERS ON SPRAY CHARACTERISTICS	101
	6.1.1	Effect of Nozzle Size/ Flow Area	104
	6.1.2	Injector Location	105



6.1.3	Injection Quantity/ Duration Effect	106
6.1.4	Injection Rate Curve	107
6.1.5	Effect of Spray Angle	108
6.2	EFFECT OF BOWL GEOMETRY AND OFFSET ON AIR MOTION	109
6.3	VALIDATION AND PARAMETRIC STUDY OF SPRAY-SWIRL-WALL INTERACTION MODEL	112
6.3.1	Spray Penetration and Velocity	112
6.3.2	Spray Growth	113
6.3.3	Air Entrainment	114
6.4	VALIDATION OF COMBUSTION MODEL	115
6.5	STUDY OF COMBUSTION CHARACTERISTICS	115
6.6	IMPLICATION OF RESULTS FOR SMALL DI ENGINES	117
	FIGURES	119
CHAPTER - 7	CONCLUSIONS AND FUTURE WORK	152
7.1	CONCLUSIONS	152
7.2	FUTURE WORK	153
	REFERENCES	155
	APPENDIX - A	167
	APPENDIX - B	169
	APPENDIX - C	173
	APPENDIX - D	176
	APPENDIX - E	178
	APPENDIX - F	180
	LIST OF PAPERS FROM THESIS	182

## NOMENCLATURE

Symbol	Description	Units
$a_1, a_2$	Axial and normal entrainment parameters	
A	Area	(m <sup>2</sup> )
AFRS	Stoichiometric air-fuel ratio	
b	Radius of circular free spray or thickness of the wall jet	(m)
c	Concentration	
$C_d$	Discharge co-efficient	
$C_f, C_f$	Friction co-efficients	
$C_p, C_v$	Specific heat	(J/Kg-K)
CN	Cetane number	
CR	Compression ratio	
CVF	Calorific value of fuel	(J/Kg)
d	Diameter of combustion bowl	(m)
$d_e$	Equivalent diameter	(m)
$d_o$	Nozzle orifice diameter	(m)
D	Cylinder bore diameter	(m)
$D_d$	Droplet diameter	(m)
$D^*$	Normalized droplet diameter	
$D_s$	Drag force due to shear stress	(N)
DINJ	Duration of injection	(degree)
E	Entrainment function	
$E_a$	Activation energy	(J/mol)
$f(y)$	Concentration profile function	
h	Enthalpy	(J/Kg)

$h_b$	Depth of combustion bowl	(m)
$h_w$	Heat transfer co-efficient	(W/m <sup>2</sup> -K)
ID	Ignition delay	(degree)
$I_1-I_6$	Values of Integrals	
I	Moment of inertia	(Kg-m <sup>2</sup> )
m	Mass	(Kg)
n	Number of orifices	
N	Engine speed	(rev/min)
P	Pressure	(Pascal)
$P, P_1, P_2$	Constants for spray perimeter	
Q	Heat energy	(J)
r	Radius	(m)
R	Gas constant	(J/Kg-K)
$R_e$	Reynolds number	
s	Spray penetration	(m)
$s_w$	Spray penetration along wall	(m)
SMD	Sauter mean diameter	(m)
SR	Swirl ratio	
$S(\theta)$	Distance of piston crown from cylinder cover at any crank angle	(m)
t	Time	(sec)
$t_w$	Time at the instant of impingement	(sec)
T	Temperature	(K)
$T_f$	Torque force due to friction	(N)
u	Spray velocity	(m/sec)
U	Air velocity	(m/sec)
$v_p$	Mean piston speed	(m/sec)
V	Volume	(m <sup>3</sup> )

$V_E, V_R$	Fuel delivery	(m <sup>3</sup> /cycle)
$y$	Normalized radius of free spray or thickness of wall jet ( $b/b_j$ )	
$\alpha$	Spray deflection angle	(rad)
$\beta$	Density function	
$\gamma$	Some fraction	
$\delta$	Boundary layer thickness	(m)
$\epsilon$	Turbulent energy dissipation rate	(m <sup>2</sup> /s <sup>3</sup> )
$\theta$	Crank angle	(degree)
$\mu$	Viscosity	(Kg/m-sec)
$\nu$	Kinematic viscosity	(m <sup>2</sup> /sec)
$\rho$	Density	(Kg/m <sup>3</sup> )
$\tau$	Turbulent mixing time	(sec)
$\phi$	Equivalence ratio	
$\omega$	Angular swirl	(rad/sec)
$\Delta$	Change of variable during a time step	

### Subscripts

a	Air
ab	Air burnt
ae	Entrained air
ag	Average gas value
au	Air unburnt
b	Break-up, bowl, burnt
B	Burning
c	Coolant

cyl	Cylinder
C	Commulative
d	Droplet
f	fuel, friction, fixed
fb	Fuel burnt
fi	Fuel injected
fl	Liquid fuel
fv	Fuel vapour
h	Cylinder head
in	Inlet conditions
inj	Injection
IVC	Inlet valve closure
j	Jet boundary, jet
J	Refers radial position of spray elements
l	Liner, liquid
m	Centre-line, manifold
mot	Motoring
n	Normal component
o	Orifice
p	Piston crown
P	Packet
prod	Products of combustion
s	Swirl, surface, standard conditions
sp	Spray
sur	Surrounding
t	Tangential component, total
v	Volume, vapour

vap Vapour phase  
vb Fuel vapour burnt  
vu Fuel vapour unburnt  
w Wall

**Superscripts**

• Per unit time (1/sec)

## CHAPTER - 1

### GENERAL DISCUSSION AND LITERATURE REVIEW

#### 1.1 INTRODUCTION

Diesel engine has been an unrivalled power source for heavy duty vehicles and stationary applications in terms of fuel economy for almost one hundred years now. With the continuing development, it is making inroads to the light duty and automotive applications as well. In present time, research and development efforts for fuel efficient and low pollution diesel engine lay emphasis on the fluid mechanical aspects of its in-cylinder processes. The matching of fuel injection characteristics with air motion are now widely considered and has attained significance for more rigorous investigations to achieve better emission and speed characteristics in direct injection(DI) diesel engine, which is primarily a fuel efficient system.

An enhanced fuel-air mixing can be achieved either by high pressure fuel injection and/or by generating swirling air flows in the combustion chamber. The increase in the air motion is reported to have increased losses due to heat transfer, volumetric efficiency and pumping work(1). On the other side, the high pressure fuel injection, apart from its difficulties in terms of hardware development, suffers from maintaining the high pressure of injection in full operating range of engine speed and load. Even, the gains from electronically controlled high pressure fuel injection system are optimum only when the injection system is in

tune with a particular combustion chamber(2).

In a DI diesel engine, the role of injection, air motion and combustion chamber characteristics, therefore, is important from better fuel-air mixing standpoint. The present work attempts to study the interaction of the air motion and the fuel spray in a direct injection diesel engine.

## 1.2 AIR MOTION

The air motion in a diesel engine is generally caused either by the intake port and/or combustion chamber geometries during induction and compression strokes respectively. Three different elements of the air motion present during intake to expansion strokes in engine cylinder have been classified as;

- Swirl
- Squish, and
- Turbulence.

During the intake process, swirl is produced in the cylinder by the annular jet flow through the intake port and valve. This then gets modified during compression stroke. Squish is the radially inward or transverse gas motion that occurs towards the end of the compression stroke, when a portion of piston face and cylinder head approach each other closely(3). The maximum squish velocity occurs at about 10 degree before the top dead centre(TDC) position. The magnitude of the squish velocity depends on the bumping clearance and squish area (determined by bowl-entry diameter) and is affected by air leakage through piston rings, dimensions of the crevice volume and heat losses to the cylinder wall and cylinder head.

The complex fluid flow field inside the piston bowl is



determined by the swirl-squish interaction. The competing requirements of the centrifugal forces associated with the swirl and the opposing inward squish motion are demonstrated in Fig 1.1(4). This mechanism has practical relevance for diesel engine performance. In a high swirl engine, the flow near the swirl centre does not experience the squish motion and retains its solid body characteristics. It may be concluded that the squish flow alone does not influence fuel-air mixing as it affects the velocity field inside the piston bowl through interaction with the swirl. Such a resultant velocity field is complex and its prediction is beyond the scope of the present investigation.

The definition of turbulence in the engine has been a matter of debate(5). In case the flows in engines were truly periodic, the turbulence intensity is possible to be determined from the deviations of the instantaneous velocity at a particular crank angle from an ensemble average mean velocity. An ensemble averaged analysis will associate the cyclic velocity fluctuations with the turbulence intensity. The character of the turbulence at the end of compression controls the fuel-air mixing and the burning rates. Only limited reliable data are available in literature in this regard and not much is known in engine firing case. Fig 1.2 compares results of turbulent intensity obtained for flows near top centre by a number of investigators using motored engines(6). These results cover a range of engine configurations with and without the consideration of swirl. It is found that the order of magnitude of the top centre turbulent velocity is one half of the mean piston speed. Usually, the magnitude of the swirl velocities is reported to be about 15 times the mean piston speed(3) during induction which further amplifies during compression. Compared to

the swirl magnitude, the turbulence intensity seems quite low and thus the contribution of turbulence to the bulk flow affecting the fuel-air mixing may be small.

The swirl motion is generally recognized to be of greater consequence in the engine flow characterization and is amenable to some sort of analytical description. The primary swirl produced during the intake is augmented due to the effect of the piston bowl during compression. The swirl motion is the most important element of the air motion in regard to the fuel-air mixing. The swirl motion in this study, therefore, will be referred to as the 'air motion' for the following discussions. The genesis of the swirl motion in the engine cylinder is classed in two distinct stages;

- Induction swirl
- Compression swirl

### 1.2.1 Induction Swirl

The intake air enters from the port into the cylinder through the openings of the intake valve as a conical jet. There are two main types of ports producing swirl up-stream or down-stream of the valve(7). Helical ports produce swirl before the valve and directed ports have it afterwards. In the tangential plane, there are two components of the angular momentum flux as shown in Fig 1.3, which contribute to the total in-cylinder swirl(7). The details of the swirling flow in an actual operating engine are rather complex. Three dimensional analytical modelling approaches(8-13) and the advanced experimental diagnostic techniques(14-19) are employed for its characterization. The simpler techniques such as the paddle wheel(20-21), the impulse swirl meter etc. are used to measure the swirl levels on steady

flow test rigs. The swirl characterization is generally based on the premise that the flow in the engine cylinder approximates a solid body rotation. There is adequate experimental evidence to this effect on the basis of LDA measurements(22-24). The solid body rotation of the flow near the engine cylinder axis and uniform velocities near cylinder walls is amply confirmed mostly at low engine speeds. This fact is yet to be established for the higher speed range.

The relationship between the steady flow rig tests and the actual complex engine swirl patterns is also not well established(3). In practice, the swirl ratio is normally used to refer the intensity of swirl measured at the intake valve closure. The swirl ratio is defined as the ratio of angular velocity of a solid body rotating flow, having angular momentum equal to the actual flow, to the crank shaft angular speed and is expressed as;

$$SR = \frac{\omega \cdot (60)}{2\pi N} \quad (1.1)$$

Despite inability of the above relationship (equation 1.1) to represent the actual flow field, its application in the diesel engine is convincing due to the fact that the emphasis of this approach is on the estimate of the mean velocity which signifies momentum exchange between the air and the fuel spray.

### 1.2.2 Compression-Induced Swirl

Angular momentum of the air, which enters the cylinder during induction, decays throughout the compression stroke due to the friction at the walls and the turbulent dissipation within the fluid. About 25 to 30 percent of the initial angular momentum is lost at the end of compression(3). Application of momentum theorem

to the fluid flow during compression results(25) in

$$\frac{d}{dt}[I\omega] = T_r \quad (1.2)$$

Neglecting the effect of the wall friction ( $T_r = 0$ ), the equation (1.2) yields :

$$I\omega = \text{Const.} \quad (1.3)$$

In conserving angular momentum, if the moment of inertia ( $I$ ) is decreased during compression, the angular velocity ( $\omega$ ) of air must increase. However, the total angular momentum of air does decay due to the friction at the cylinder walls. The combustion chamber cavity, therefore, tends to modify the swirl as the piston approaches the top centre position.

The influence of the piston cavity on the swirl during compression is extensively studied using various experimental techniques such as;

- (i) Laser Doppler Anemometry(26-28)
- (ii) Laser Doppler Velocitimeter(29-34) and
- (iii) Hot Wire Anemometer(35-40).

Some of these investigations(26,29) compare the influence of the piston geometry, while some others(29,41) consider the influence of the bowl offset on the air motion both experimentally(29) and analytically(41). A variety of the piston cavity shapes viz. flat, circular, square, re-entrant etc. have been investigated showing;

- (i) the TDC angular momentum per unit mass is 35 percent in the square bowls compared to the circular bowls(29).
- (ii) the re-entrant bowl results in larger swirl decay compared to the flat bowl.

The larger swirl decay in the case of square and re-entrant bowls

is attributed to both the increased wall friction losses due to the larger surface to volume ratio and an increased diffusion as a result of higher turbulence at the end of compression.

The effect of the bowl offset on the swirl has been investigated both experimentally(29) and analytically(41). A decrease of six percent in angular momentum at TDC with the bowl offset of 7 percent of the bore is reported(29). It is observed(41) that the changes in the offset have noticeable influence on the flow structure near the bowl centreline(Fig 1.4). It is, therefore, concluded that the shape of the piston cavities and the bowl offset modify the swirl levels during compression and hence need consideration.

### 1.3 FUEL SPRAY

#### 1.3.1 Fuel Injection

Despite some progress reported in the fuel injection system development such as the high pressure injection and the electronically controlled injection, vehicular diesel engines mostly use the conventional features of the fuel injection system. The limitations of the conventional fuel injection system in its present form include dependence of

- i) the injection parameters (injection period and pressure) on speed and load.
- ii) the fuel injection quantity on the system dead volumes, passage lengths, plunger springs, variable flow areas, frictional and inertia forces due to moving masses, wave actions in lines etc.

It is apparent in Fig 1.5 that these disadvantages are not overcome

by mere increase in fuel injection pressures(42).

For the high injection pressures, the use of a higher air swirl is ineffective from the fuel economy and smoke formation standpoint. In such cases, the swirl can be either eliminated or minimized to reduce the thermal loading in high specific output engines. The same effect helps improving the volumetric efficiency and the pumping losses of the naturally aspirated engines. However, in case of smaller engines (less than 150 mm bore), the essential features of the conventional fuel injection system may not allow reducing the requirement of the swirl, thus the air motion may hold the key to better fuel-air mixing in these engines. The injection characteristics need to be tailored to atomization and the mixing requirements for a given combustion chamber geometry and the air motion. Injection scheduling and duration of injection are the controlling parameters influencing such an adjustment.

The injection scheduling has a strong influence on the rate of pressure rise. Maintaining a low initial rate of injection prevents the diesel knock. The steeper beginning and the end of the injection curves are considered necessary to achieve finely atomized spray free from the secondary injections and pronounced dribble(43). Figs 1.6 and 1.7 show the influence of the injection rate shapes on the atomization and spray motion(44).

The injection duration is particularly important at full load and influences the engine performance, fuel economy and smoke. Each type of combustion chamber requires an optimum duration of injection. Both shorter and longer durations are not desirable. Although with short injection duration, good fuel economy and less smoke characteristics are achieved, the engine running becomes rough. In case of the longer duration, the engine runs smoother

but the power, fuel economy and smoke levels deteriorate.

The use of digital computers for analyzing fuel injection process is now a common practice. An iterative procedure for solving the equations of continuity and equilibrium of forces at the nozzle end was proposed by Becchi(45-46). Including friction and cavitation effects, the unsteady flow in the high pressure pipe was analyzed by Knight(47). Wylie(48) has used the method of characteristics for solving the equations of unsteady flow. Thereafter, many different models have been developed to simulate the fuel injection system of diesel engine combining the above features. Many computer codes are available to simulate the fuel injection process accurately.

### 1.3.2 Spray Development

The development of fuel spray consequent to fuel injection is controlled by important physical processes viz;

Atomization,

Penetration,

Entrainment and

Vaporization.

There are numerous investigations on each of these aspects available in literature and their indepth review remains beyond the scope of the present discussion. However, salient features relating to these processes are presented here.

#### Fuel Break-up and Spray Structure

A conical spray consisting of finely atomized droplets of various sizes is formed over a short distance termed as "atomization break-up regime". Fig 1.8 shows the four regimes of

the liquid jet break-up(49). In an experimental study, it is observed that the liquid break-up is not instantaneous on injection(50). The break-up length in the spray is reported to be of the order of 10-20 mm. Arai et al(50) have proposed a correlation of the spray break-up as;

$$t_b = 28.65 \rho_l d_n (\rho_l \Delta p_{inj})^{-0.5} \quad (1.4)$$

The cyclic variations in the spray structure are observed(51) as the penetration length is found to vary from cycle to cycle as shown in Fig 1.9. The effect is attributed to the variations in the break-up process(51). It is apparent from the literature that the spray break-up is an important but least understood characteristic in the diesel engine. The difficulties are experienced in the measurements of the spray structure in the break-up region due to high density and velocity conditions near the nozzle exit. Both experimental and analytical studies relating to this phenomenon are being continuously carried out(49,52-55).

### Droplet Size Distribution

Sauter mean diameter (SMD) is the likely representative parameter of the spray(56). Chin and Lefebvre(57) have mentioned that any representative diameter is useful in describing the drop-size distribution, however, the SMD is quite appropriate in representing the fineness of the spray from the combustion viewpoint.

Droplet-size distribution for the transient spray(58) at three axial locations and five injection frequencies is shown in Fig 1.10. It is found that the SMD at each location is nearly independent of the injection frequency except at 24.4 Hz where very



high values of the SMD are obtained. Mean droplet diameter is found to decrease down-stream due to the possible breaking-up of the bigger droplets.

Correlations for the prediction of the SMD(50,59-61) and the droplet-size distribution(62-64) have been developed by several investigators using either empirical or probability considerations.

Hiroyasu and Kadota(59) reported that volume distribution of the diesel spray droplets is well correlated with Chi square distribution and their expression is validated over three types of nozzles at several back pressures and injection conditions. In their studies, the SMD varied significantly with the injection conditions. Investigations of Arai et al(50) reveal that when the viscosity of the fuel exceeds a certain value, the SMD is found to increase rapidly. This critical value of the viscosity increases with the decrease in the orifice diameter. When the injection pressure increases, the SMD decreases slightly but the critical viscosity shifts widely. This is stated to be an upper limit of the viscosity and a lower limit of the pressure to produce the fine droplet distribution of the spray. Correlation to predict the SMD is also derived(60) and the droplet distribution measured(65-66).

### Spray Penetration

The growth of the spray consisting of the atomized fuel droplets is dependent on the fuel-air interaction through their momentum exchange. From this viewpoint, the spray penetration and the entrainment processes are quite important. While the penetration is a measure of the depth of the spray, the lateral growth of the spray is expressed in terms of the amount of air engulfed by the spray from its surroundings and the consequent

vaporization of fuel in the spray.

Several correlations are available for calculation of the spray penetration in diesel engines. These are reviewed by Hay and Jones(67). Among the various correlations evaluated by them, the correlations suggested by Wakuri(68) and Dent(69) were found satisfactory over a reasonable range of operating conditions. With such a large number of correlations available in the literature, there is always a confusion regarding their suitability. However, the Dent's correlation is widely used. In general, a spray penetration correlation takes the form(70);

$$s = Ct^k \quad (1.5)$$

where 'k' is an exponent having positive value less than unity and 'C' is a proportionality constant determined from the fuel and air properties, the injection pressure and the nozzle diameter. The complexity of the relation for constant 'C', however, does not change the basic mathematical form of equation 1.5, which is rather simplistic. The value of 'k' is taken in the range of 0.4 to 0.7 in different investigations(70). Harrington(70), however, maintained that the spray-tip penetration correlations in the present form, reported in the literature, do not have the correct mathematical form. These correlations, in which penetration is proportional to a fixed power of time, predict an infinite spray velocity at zero penetration and do not exhibit the experimentally observed velocity maximum at a point down-stream from the injector as shown in Fig 1.11. Correlations for the spray-tip kinematics are most accurately developed in the velocity-distance phase plane and a simple form is expressed as;

$$ds = \frac{du_m}{dt} \quad (1.6)$$

where  $u_m$  is the centre-line tip velocity.

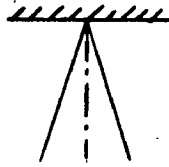
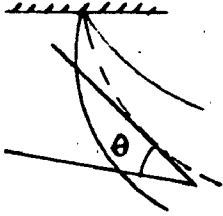
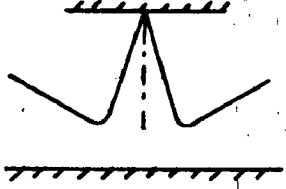
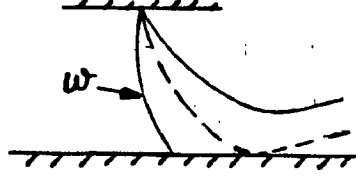
Even when a penetration correlation is obtained using integration of the velocity-time correlation instead of direct penetration-time equation, it is recommended(70) that a three regime correlation for the spray-tip penetration is necessary. The three stages- the early, the middle and the late time regimes- are dominated by the injection system characteristics, the spray-drag and the in-cylinder air flow field respectively as shown at segments A, B and C in Fig 1.11.

#### Air Entrainment

During the entrainment process, air is drawn-in the spray through its conical surface. The entrainment process controls the air-fuel mixing and thus the energy release rates in engines. A summary of the situations arising in an engine for the entrainment analysis is given in Table 1.1. This includes free and wall jets and, with or without air motion. The fuel-air interaction in the engine is commonly referred as the "confined turbulent jet". Thring and Newby(87), in their similarity analysis, suggested the concept of an equivalent diameter (defined as the nozzle diameter through which the fluid is emerging with the same initial momentum and the same velocity, but with the density of the surrounding fluid rather than the nozzle fluid) and expressed as;

$$d_e = d_n \sqrt{\frac{\rho_f}{\rho_s}} \quad (1.7)$$

**Table-1.1 Different Types of Entrainment Analysis in Turbulent Jets**

Type	Surrounding medium	Description	Representation	References
Free jet	Quiescent (surrounding medium without motion)	Injection of a fluid into an infinite stagnant reservoir		(71-72)
Free jet in cross flow	Swirl (surrounding medium with motion)	Jet flow directed normal to a fluid in motion (If jet enters the surrounding fluid at an angle, it is known as Transverse flow)	 $\theta$ - Transverse angle	(73-80)
Wall jet	Quiescent (surrounding medium without motion)	Jet flow along the wall after impingement spreading as a disc.		(81-83)
Wall jet in cross flow	Swirl (surrounding medium with motion)	Jet flow along the wall after impingement spreading in direction of swirl flow.		(84-86)

This relation became very useful in the engine models in order to consider the fuel spray as a confined jet with variable density.

For the jets in cross-flow, the entrainment rate is considered as a combined effect of the tangential and normal components of the excess velocity between the jet and the surrounding fluid. The change in the air entrainment rate with the distance along the trajectory of a non-burning spray in the presence of the air swirl is expressed following the work of Sinnamon et al(79) as;

$$\frac{dm}{ds} = 2\pi r_j (\rho_m \rho_s)^{0.5} [a_1 |u_m - U_t| + a_2 |U_s|] \quad (1.8)$$

Where  $\rho_m$  is mean jet density and  $a_1$  and  $a_2$  are two entrainment constants determined experimentally. The values of these constants are recommended as 0.035 and 0.05, respectively.

#### 1.4 AIR MOTION AND FUEL SPRAY INTERACTION

A considerable insight into the fuel-air mixing in diesel engines is gained by understanding the dynamics of the fuel spray(88). In 1971, Adler and Lyn(89) attempted a detailed solution of appropriate spray momentum equations by treating the spray as continuum and the air motion as solid body rotation. There are several other simplified assumptions made in their work in order to solve the integral equations. These assumptions are;

- i) Transient phenomenon is treated as steady state one,
- ii) Rectangular spray cross-section with constant height to width ratio, and
- iii) The velocity and temperature are represented as the average quantities viz. an equivalent velocity and an equivalent temperature.

Following this work, many subsequent investigators(75,78) made use of the continuum approach.

Elkoth and Rafat(90) computed the spray structure and the movement from the trajectory of different fuel droplets moving in the air. The effect of various operating conditions on the spray shape, trajectory, and the penetration is studied both experimentally and analytically. The correlations are suggested for fuel spray diameter and spray volume in terms of different medium pressures, initial spray velocities and injection angles.

Using mass and momentum conservation equations, Sinnamon et al(79) validated a spray model for predicting the penetration and trajectory of the spray in an engine situation through a two-dimensional spray model for a turbulent gas jet. This study has proved to be quite useful especially in terms of the evaluation of entrainment law for the spray in the presence of the air motion. A comparison between their predicted and experimental data is shown in Fig 1.12. Dent et al(91) have used Sinnamon's approach in conjunction with the spray deflection equation of Chiu et al(92) to predict the effect of the swirl on the fuel-air mixing. This approach, however, retained the limitations of the applicability of the analysis to the central injection case inherent in the correlation of Chiu et al. Prior to these attempts, the engine models have been characterizing the effect of the swirl on fuel-air mixing in quite an implicit manner through either empirical constants(93-94) or altering the local concentration values based on arbitrary mixing criteria(95).

A major criticism of the integral continuity approach is generally, made owing to the required pre-assumption of the shape

of the spray cross-sectional area and the other property distribution laws for convenience of the solution of the governing equations. This poses limitations on the use of continuum approach to predict features like vortex structure of the flow, true shape of the spray and the accurate velocity and temperature distributions(96).

As an improvement, Adler and Baron(77) took a kidney like spray cross-section shape considering the distribution of vortices along the boundaries of the spray in the lagrangian coordinates following Chen(97) and Strauber(98). The cross-sectional area was assumed to grow at a rate, which was the sum of the growth rate for a jet in the stagnant fluid and the growth rate of the vortex pairs following Tulin and Schwartz(99). Fig 1.13 shows a typical computation of the development of the kidney shaped cross-section compared with the measurements of Kamotani and Greber(80). Except the spray geometry details, the approach of Adler and Baron(77) was implemented in the work of Mehta and Gupta(100) through two momentum equations written along the tangential and normal spray directions characterizing the spray-swirl interaction effects. This eliminated the need of three momentum equations necessary in orthogonal system of coordinates. All through, vectorial approach has been used in their calculations generalized for a compact analysis procedure. They made comparison of the predicted results with the experimental data from several sources. Fig 1.14 shows the effect of the injection pressure on the spray movement. The results indicate that the spray is shifted to the centre of the cylinder with the increase in injection pressure due to the increased initial velocity causing reduced deflection.

Wilson et al(101,102) adopted the approach of Adler and

Baron(77) and extended it to the general case of a jet incorporating temperature and concentration distributions making it suitable for incorporation in a combustion model. In addition to equations for momentum change, area growth and cross-section shape following Adler and Baron, two extra equations for conservation of mass and energy were written by them in order to predict temperature and concentration. Fig 1.15 shows the predicted axial temperature decay in agreement with the experimental data(102).

Despite the limitations inherent in the integral models and its assumptions, they are widely accepted as means for predicting the trajectory of the turbulent jets in cross-flow to meet developmental requirements of the engine designs mainly due to the computational economy and ease of use in comparison to multi-dimensional models. However, the combination of multi-dimensional calculations and the experimental measurements are considered to provide valuable insight into the flow evolution in diesel engines of variety of designs and operating features. There are some very useful review papers on the in-cylinder air motion(4,7,103) which provide very comprehensive informations on the topic. The multi-dimensional models are also being developed and studied considering spray development(52,104-106). These studies are presently not under discussion here.

## 1.5 FUEL SPRAY AND WALL INTERACTION

In the development of small direct injection diesel engines, the interaction of the spray with the cylinder wall of the combustion chamber is of significance. On impingement, the spray mixing is governed by the pattern of spray growth along the wall.



This growth pattern has different consideration than the spray growth in the free region discussed earlier. Therefore, an understanding of the growth of the wall jet and the related processes viz. air entrainment and the wall shear stress etc. is essential.

A few attempts only have been made to model the wall jet development the diesel engines particularly in the case of engines having the swirl motion. Table 1.2 includes the list of the empirical correlations of the spray penetration applicable in the wall region of a quiescent chamber DI diesel engine(107-110). The correlations of Katsura et al(107) and Lakshminarayan and Dent(108) are obtained based on the measurements made in combustion bombs under quiescent conditions. The correlations used in the diesel combustion model by Dent and Mehta(109) and Payri et al(110) are derived following the work of Rajaratnam(111) and Lakshminarayan and Dent(108) respectively. These correlations are empirical in nature and are derived based on the experimental data without consideration of the air motion. These correlations, therefore, can not be accurately applied to the engine situations in the presence of air motion without proper correction co-efficients for the effect of the air motion.

The irrotational flow induced by an impinging spray may be related to the rate of the mass entrainment like the free spray. The uncertainties experienced in calculations of the rate of the mass entrainment for the free spray continue to persist in the case of an impinging spray(83). There are still fewer experimental results available concerning the entrainment aspect. The situation is further complicated in the wall jet case. Most of the entrainment data, based on the integration of the measured velocity

Table 1.2 Correlations of Spray Penetration in Wall Region

Investigator(s)	Correlation
N. Katsura et al(107)	$s_w = 3.87(\Delta p)^{0.89} \rho_s^{-0.24} (t-t_w)^{0.48}$
Lakshminarayan and Dent(108)	$s_w = 0.75 \sqrt{\left(\frac{2\Delta p}{\rho_f}\right)^{0.5} d_s(t-t_w)}$
Dent and Mehta(109)	$s_w = \sqrt{2.06 u_s d_s(t-t_w)}$
Payri et al(110)	$s_w = 0.89 \sqrt{\left(\frac{\Delta p}{\rho_f}\right)^{0.5} d_s(t-t_w)}$

profiles, show more or less a linear relationship of the mass flow rate in the wall jet with the radius, similar to the development region of a free jet. Harris et al(112) reported a correlation from studies conducted at Cranfield(82,113) as;

$$\frac{\dot{m}}{\dot{m}_a} = 0.68 \left( \frac{r}{d_s} \right) \left( \frac{T_j}{T_a} \right)^{0.5} \quad (1.9)$$

Where 'r' is the radius of the wall jet and  $T_j$  and  $T_a$  are the temperatures of the jet and the air respectively.

A detailed analysis procedure of the entrainment in the turbulent boundary layer and the wall jet based on the "Unified theory" of Spalding(114) is suggested by Escudier and Nicoll(85). The assumptions made for the free flow developed into the boundary layers or the wall jets are:

- the fluid properties are uniform,
- the wall is hydrodynamically smooth and impermeable,
- the flow is two-dimensional.

A two-parameter velocity profile having two components - one accounting for the effects of the mass and the momentum transfer to the wall, and the other for the interactions with the main stream - was recommended as;

$$Z = Z_w \left[ 1 + \left( \frac{\ln \xi}{1} \right) \right] + \frac{1}{2} (1 - Z_w) (1 - \cos \pi \xi) \quad (1.10)$$

Where  $Z$  is the velocity ratio,  $\xi$  is the non-dimensionalized distance and  $Z_w$  is a profile parameter and can be interpreted physically as the ratio of the law-of-the-wall velocity at the outer edge of the boundary layer to the main stream velocity. The quantity  $(1 - Z_w)$  is a measure of the relative magnitude of the work components of the

velocity profile. Typical wall and wake components and the total velocity profiles are shown in Fig 1.16. In correlating the experimental data, Escudier and Nicoll(85) recommended the following entrainment functions in terms of the profile parameter  $Z_E$  as;

$$0 \leq Z_r \leq 1 \quad \dot{m} = 0.075(1 - Z_r)\rho_s U_s \quad (1.11)$$

$$Z_r > 1 \quad \dot{m} = (0.03Z_r - 0.02)\rho_s U_s \quad (1.12)$$

A comparison of predictions from equation (1.10) with the experimental velocity profiles for the flat plate boundary layers is shown in Fig 1.17.

In the diesel modelling work, there are attempts to include the wall jet features which is an important aspect in the development of small DI diesel engines. Khan et al(94,115) adopted the velocity and the jet thickness equations following Glauert(81) but neglected the time and loss of the kinetic energy in the direction of the flow during transition from the free to wall jet.

In a quiescent chamber diesel engine model, Dent and Mehta(109) adopted the wall jet description following Rajaratnam(111), where the effects of the viscous friction is neglected and the similarity profiles for the velocity and the concentration related to the free jet are assumed to hold in the wall region as well. The wall jet penetration is also determined in a manner similar to that for the free jet(69) and the entrainment of air into the wall jet is calculated using Hertel's correlation(116);

$$\dot{m}_{w} = \left( 0.868 \frac{s_w}{d_s} - 1 \right) \dot{m}_f \quad (1.13)$$

Subsequently, the wall jet model is modified by Dent and co-workers(86,91) following the work of Escudier and Nicoll(85) and Campbell(84) for incorporating predictive capability of the influence of swirl motion in the engine simulation model. Investigations using Campbell's approach have been reported to overestimate the air entrainment rates(91). The wall jet model following Escudier and Nicoll(85) is successfully adopted by these authors in the engine including the effect of the wall in an implicit manner by solving the von Karman integral momentum equation.

Recently, Naber and Reitz(117) considered the impingement of the oblique spray on the walls of the combustion chamber of an engine following Taylor(118). Three different droplet-wall interaction sub-models considered by them are shown in Fig 1.18. The predicted results from this study are given in Fig 1.19 and Fig 1.20. However, the basic model used in this study has the multi-dimensional consideration.

In a recent experimental investigation(107) using a laser light extinction method, the shape of the impinging spray and the temporal and spatial distribution of the droplets density are measured. It is reported that

- (i) the droplets density is greater near the wall and the peripheral region of the impinging spray and its distribution has two peaks (Fig 1.21) - one near the spray axis and the other at the peripheral region on the radial distribution,
- (ii) the SMD is found to be about 30 micron and remains approximately constant with the time,

(iii) there is not much difference between the results of the SMD in the impinging spray and that in the free spray region.

These observations tend to suggest that the correlations used for the SMD of a diesel spray in the free region can as well be applicable near the wall region.

## 1.6 ENGINE MODELS

The engine models so far developed are either phenomenological or multi-dimensional. Each of these approaches have their own merits depending upon the purpose for which the models are to be used. The former describe the processes based on the experimental correlations, while the later are developed around basic conservation laws of thermo-fluid mechanics. The adjustment of both of these types of models to make accurate predictions is inevitable in case of their application to a particular engine. While the phenomenological models use constants despite the properly evolved relationships with the controlling parameters, the multi-dimensional models remain handicapped due to the use of empirical details of chemical kinetics, turbulence etc. In the present work, only the phenomenological diesel models developed so far are reviewed, particularly, the models which include the wall jet aspects in their formulation.

Table 1.3 lists the purpose and the approach used in the several phenomenological models from the early sixties till date. Earlier models, until the early seventies, concerned the engine performance predictions formulated on the single zone basis with

**Table 1.3 Phenomenological Models of Direct Injection Diesel Engines (In chronological order)**

Author(s)	Year	Purpose	Concept used
1. W.T. Lyn(119)	1963	Heat release	Burning rate law
2. G.L. Borman(120)	1964	Performance	Thermodynamic cycle
3. N.D. Whitehouse and R.Ray(121)	1969-70	Heat release	Single zone burning law
4. J. Shipinski, P.S. Myers and O.A. Uyehara(122)	1969-70	Heat release	Single droplet spray burning
5. D. Adler and W.T. Lyn(123)	1969-70	Evaporation and mixing	Quasi-steady integral approach
6. H.C. Grigg and M.H. Syed(124)	1969-70	Heat release	Fuel-spray air entrainment
7. E.K. Bastress, K.M. Chung and D.M. Dix(125)	1971	Performance and Nitric oxide	Thermodynamic analysis with empirical rate processes
8. I.M. Khan, G. Greeves and D.M. Probert(94)	1971	Nitric oxide and soot	Spray mixing
9. S.M. Shahed, W.S. Chiu and V.S. Yumlu(126)	1973	Nitric oxide	Burning rate law
10. N.D. Whitehouse, W.S. Chiu and B.K. Sareen(127)	1974	Heat release	Two zone spray mixing
11. S.M. Shahed W.S. Chiu and W.T. Lyn(128)	1975	Combustion and Nitric oxide	Spray mixing
12. D. Hodgetts H.S. and H.D. Shroff(129)	1975	Nitric oxide	Multi zone spray mixing
13. H. Hiroyasu and T. Kadota(93)	1976	Combustion, Nitric oxide and soot	Intermittent spray mixing
14. C.J. Kau, T.J. Tyson and M.P. Heap(130)	1976	Heat release, Nitric oxide and soot	Spray mixing
15. M. Meguerdichian and N. Waston(95)	1978	Heat release	Multi zone spray mixing

Table 1.3 continue...

16. J.C. Dent and P.S. Mehta(109)	1981	Combustion and soot .	Spray mixing
17. J.C. Dent, P.S. Mehta and J. Swan(91)	1982	Combustion and soot	Spray mixing in swirling air
18. H. Hiroyasu, T. Kadota and M. Arai(131)	1983	Combustion and Emissions	Spray mixing
19. S. Kono, A.Nagao and M. Motooka(132)	1985	Combustion and Emissions	Spray mixing
20. S.C. Kriakides, J.C. Dent and P.S. Mehta(86)	1986	Smoke and emissions	Spray mixing
21. A.K. Gupta, P.S. Mehta and C.P. Gupta(133)	1986	Combustion and soot	Multi zone spray mixing from spray-swirl interaction
22. W.H. Lipkea and A.D Deejoode(134)	1987	Performance and (NO) <sub>x</sub>	Spray mixing
23. P. Payri, J. Benajes and P.V. Tinaut(110)	1988	Performance and heat release	Spray mixing

---



empirical burning rate laws. A detailed integral approach to consider a spray structure was first incorporated by Adler and Lyn(123) in their work. Thereafter, the concepts like spray mixing(94), two-zone(127) and multi-zone(129) spray structures were used in the diesel models as the predictions of the oxides of nitrogen(125), soot(94) etc. became necessary. The efforts to improve the models are still continuing by incorporating new features and complexities to make more and more accurate predictions.

The details of the various physical and chemical processes involved in the description of the earlier models are highlighted in Table 1.4. For characterizing the injection process, the experimental injection pressure data(91,133), constant injection rates(130,132,139) and the detailed fuel injection simulation models(93,131,143) are utilized. The air motion considerations are made in these models by either using empirical coefficients in the parametric analysis(94,110,130,131,135-137,139,143) or detailed calculations of the air motion considering solid body rotation(91,93,100,132,134). The consideration of the impingement and the wall effects of the spray is either not made(100,132) or, wherever considered, the description similar to the free spray(93,110,131,134) is extended. In a few cases, the experimental correlations are used for predicting penetration(91,109,110) and the air entrainment (86,94,130,135-137,143) in the wall region.

For evaporation rate calculations, the gas jet assumption eliminated the need of detailed evaporation models in several cases(94,132,134,135-137,143). Wherever, the evaporation calculations are necessary, the models for the SMD and the droplet-

Table 1.4 Summary of the Process Description in Diesel Engine  
Combustion Model

Model -->	CAV (94,135-137)	Ultrasystem (130,139)	Hiroshima (93,131)	Imperial (143)	Loughborough (86,91,109)	
Process	1	2	3	4	5	6
Injection		Assumes uniform injection	Uses an injection simulation programme	Fuel injection system model with governing	Experimental injection pressure diagram approximated through straight line segments	
Penetration	Schweitzer's equation(138)	-	Their own experimental correlation in two regimes	Dent's(69) equation with an impulsive jet factor correction	In quiescent case, correlation of Hiroyasu(131) for early period and Dent's(69) in latter part. In case of Swirl, Chiu et al(92)	
Evaporation	Not considered	Droplet evaporation through upper limit size distribution function	Single spray droplet evaporation through SMD and droplet size distribution	Not considered	Isolated droplet evaporation through SMD and droplet size distribution equation	
Entrainment	From conical spray and its movement	Using steady state jet theory along with empirical constant	From spray configuration	No explicit expression, implied through concentration value obtained from profile shape, and conservation equations	Ricou and Spalding(71) correlation	

Table 1.4 continue...

Impingement and wall jet growth	Characterized as un-confined wall jet using Glauert's equation(81)	Characterized un-confined jet impinging on a plane wall following Abramovich[140]	Spray configuration and amount and temperature of air entrained are modified	Extends free jet analysis using Glauert's equation(81)	Relations of Giralt et al(144), Rajaratnam (111), Era and Saima(145)
Swirl	Suggests an empirical entrainment ratio to increase air entrainment in presence of swirl	Air entrainment and evaporation rates modified through constants	Arbitrary factor introduced to modify air entrainment rate (131) or detailed analysis of spray carried out(93)	Entrainment in the jet is modified by changing local concentration values	Based on Sinnamon's (79) assumptions, spray trajectory, air entrainment, wall impingement and turbulent mixing calculations modified
Heat Transfer	Based on experimental data	Anand's equation(141)	Woschni's equation(142)	Woschni's equation(142)	Woschni's relation(142)
Ignition	Experimental ignition delay values	Shipinski's correlation(122) for ignition delay	Own ignition delay correlation in terms of pressure, temperature and equivalence ratio	Ignition is recognized by the onset of a rapid rise in burning rate	Hardenberg & Hase(188) relation
Energy Release	Triangular burning rate law	Cloud combustion phenomenon with three models of energy release, premixed, homogeneous and heterogeneous diffusion combustion	Local Stoichiometric combustion	Mixing controlled Arrhenius type equation accounts for premixed and diffusion combustion	Local Stoichiometric combustion

Model -->	UOR (100,133)	SPANISH (110)	JOHN DEERE (134)	MAZDA (132)
Process				
1	7	8	9	10
Injection	Experimental injection pressure diagram is used to evaluate mass flow rate by assuming constant discharge coefficient	-	-	Experimental equation(154) by Hiroyasu has been applied to the initial condition of the jet velocity. Constant injection rate is assumed
Atomization	Break-up is computed following Arai et al (50), SMD from Elkoth and Abdalla(61) and Droplet size distribution from Simon's BDM(146)	Break-up length is computed following Levich (153) and related to break up period through constants	Not considered	Not considered
Penetration	The centre-line velocity vector/continuum approach is used(100)	Based on Hiroyasu's model(154)	Jet penetration is calculated using Dent's approach(69)	By solving mass and momentum equations
Entrainment	Sinnamon's correlation(79)	A modified version of Lakshminarayan and Dent(108) relation is extended for liquid spray by considering three different regions	The correlation of Patrick(74, 157-158) for a round jet in cross flow is used	Is assumed to be proportional to the contact area between spray and air, the turbulence intensity and the jet relative velocity
Impingement and wall jet growth	Not considered	Wall penetration is considered following Rajaratnam(111) spray width is assumed following Lakshminarayanan (108). Entrainment as in a free jet	Wall jet penetration is similar to free jet	Not considered

Table 1.4 continue...

Swirl	Swirl is calculated following Dent and Derham(25)	In order to account for air motion, the air entrainment is corrected by means of coefficient	Following Dent and Derham(25)	Mean flow model of Borgnakke et al(159) is adopted
Evaporation	A Spherico-symmetrical droplet evaporation model using empirical correlations for convection is used(147)	The evaporation is calculated by $d^2$ -law model (155) and is corrected by Ranz and Marshal correlation(156) for relative motion	The fuel jet is assumed to be all vapour	Not considered
Turbulent Mixing	The rate of change of kinetic energy is calculated from the algebraic sum of changes of K.E. due to air motion, viscous losses, injection and energy release. Turbulent dissipation rate is computed following (148-150)	Not considered	Not considered	As proposed by Dent et al(109)
Heat Transfer	Woschni's equation(142)	Woschni's equation(142)	Anand's equation(141)	Woschni's relation(142)
Ignition	Hardenberg and Hase(151) relation	Expression proposed by Hiroyasu et al(154)	Ignition delay is not input but is the result of combined effect of kinetic and mixing rates	Some experimental determined time 0.5 msec is assumed.
Energy Release	Local Stoichiometric combustion within limits of flammability following Glassman(152)	Local Stoichiometric combustion	Local Stoichiometric combustion with no artificially imposed flammability limits	Local Stoichiometric

size distribution laws are adopted (86,91,93,109,131). Mostly, a spherico-symmetrical droplet evaporation model(147) has been popular in engine simulation studies.

In these models, predictions are compared with the experimental data. The response of the models to the variations such as injection scheduling(93,109,131), injection pressure(91,109,131,133,136), injection duration (131,133) and injection timing (86,93,131,133,136) on the engine performance and the emissions are reported. The effect of the air swirl(91,93,131,133,136), engine speed (86,93,131,136), engine load(93,133,136) and exhaust gas recirculation(86) are also studied. The typical trends are shown in Figs 1.22-1.27. Besides these, the influence of the air swirl on the spray deflection(91,100,131) and the wall jet growth(86,91,131) are also considered in earlier investigations.

Although there are numerous diesel simulation models available but so far only few of these have included the wall jet features. There is a definite scope for improvement of the description of the wall jet using more comprehensive analysis in the presence of air swirl. The present work has been formulated on this motivation.

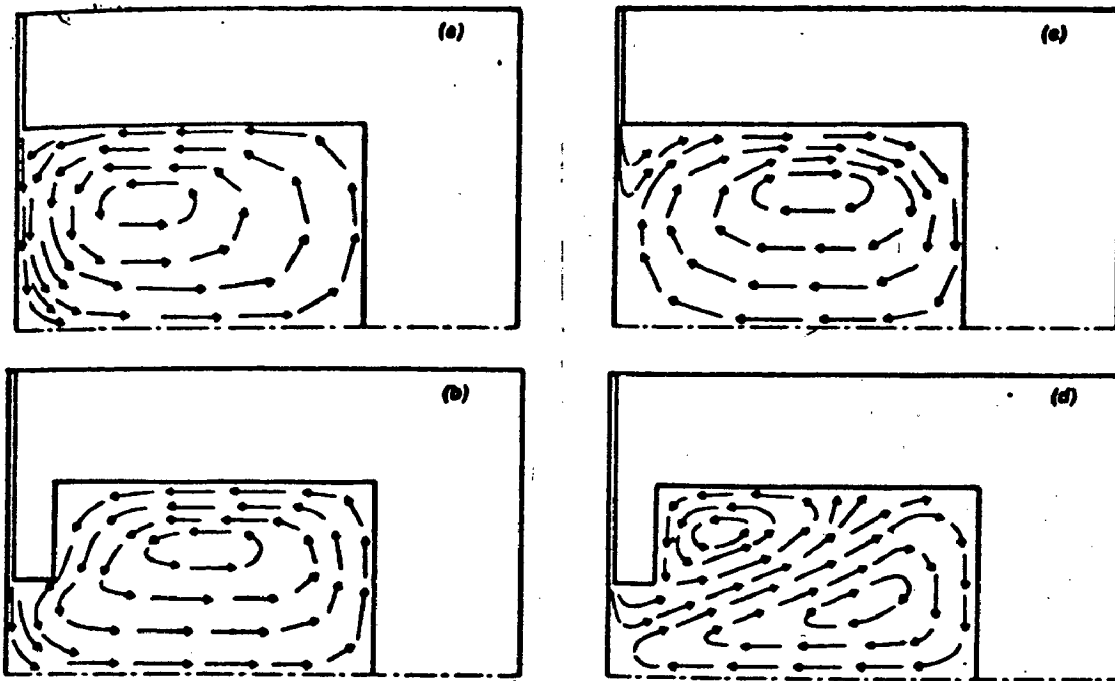


Fig 1.1 Schematic diagrams of air flow in piston bowls at TDC. a and b without swirl, c and d with swirl(4).

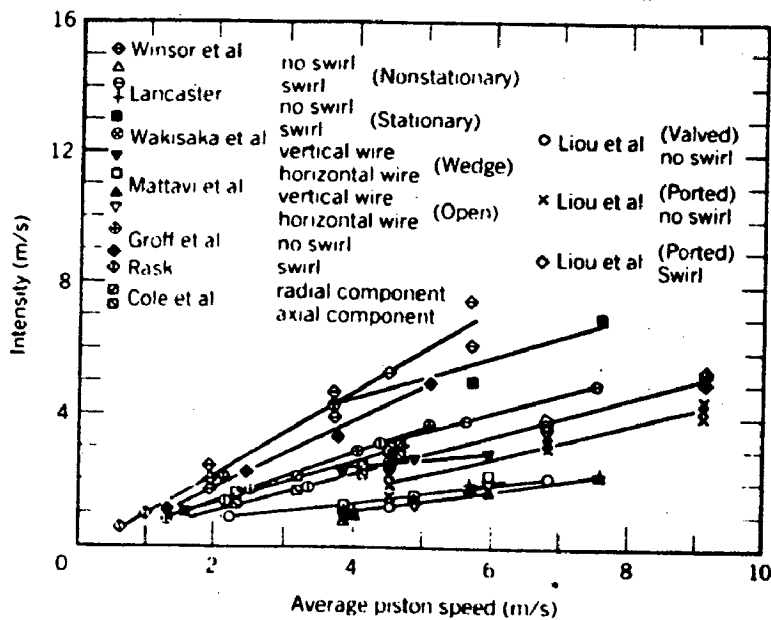


Fig 1.2 A comparison of fluctuation or turbulence intensity versus average piston speed(6).

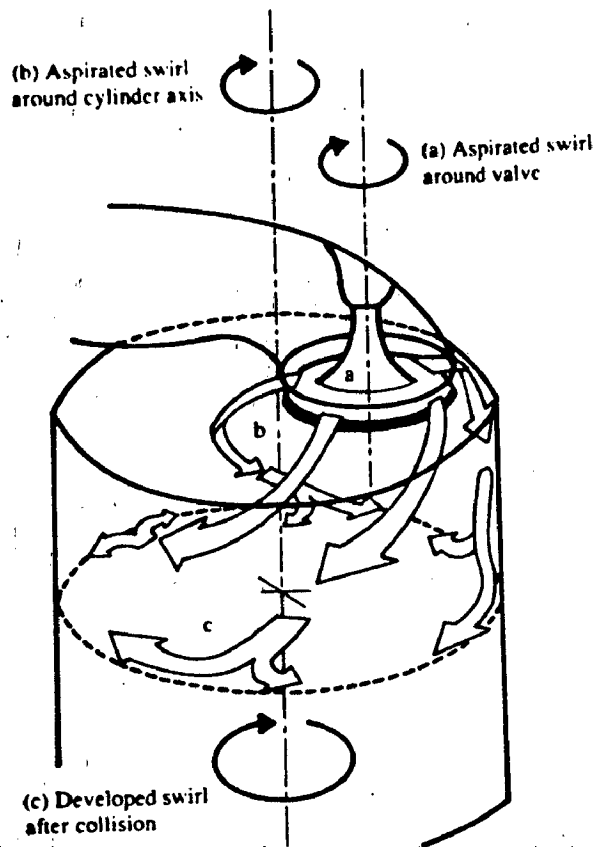


Fig 1.3 Components of the swirl motion generated by a helical port during induction(7).

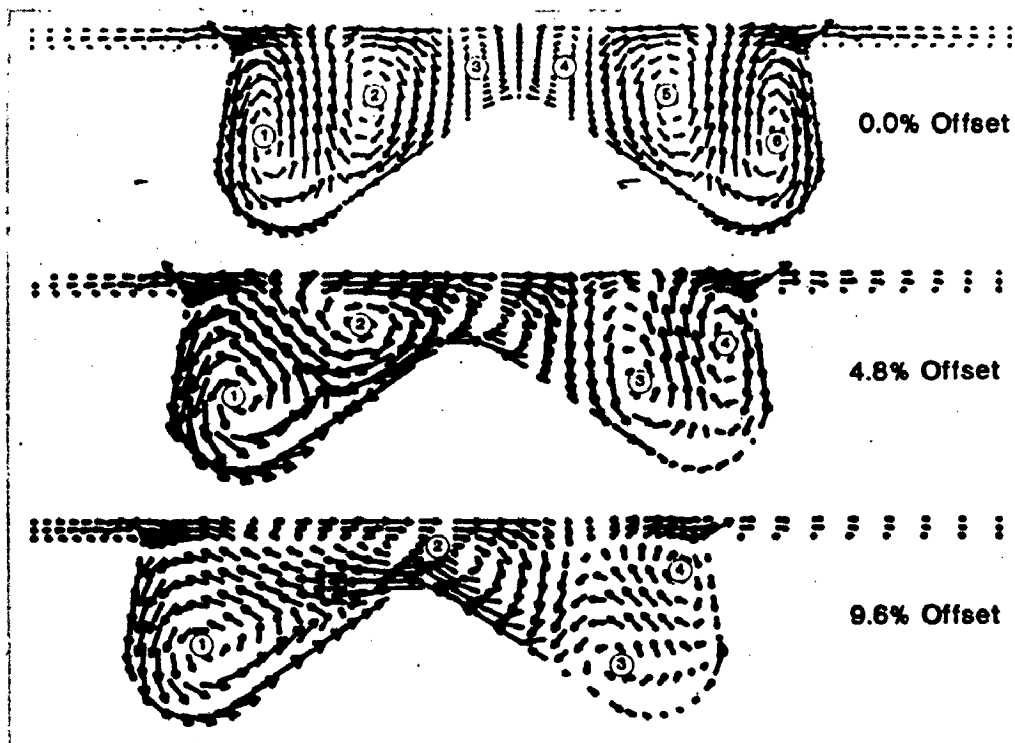


Fig 1.4 Effect of bowl offset on TDC bowl vortex structure, swirl ratio = 4.27(41).



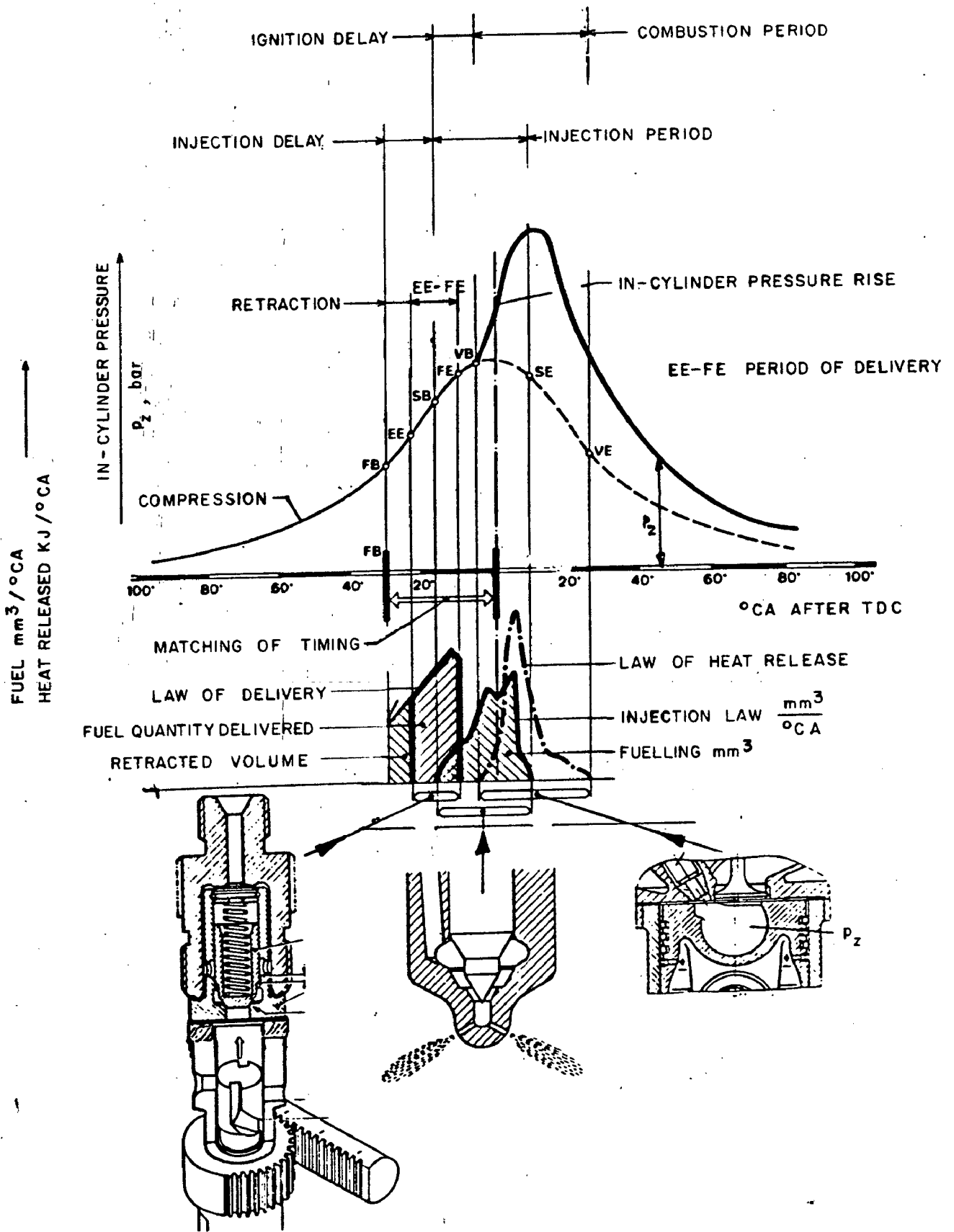


Fig 1.5 Fuel injection and In-cylinder parameters diagram(42).

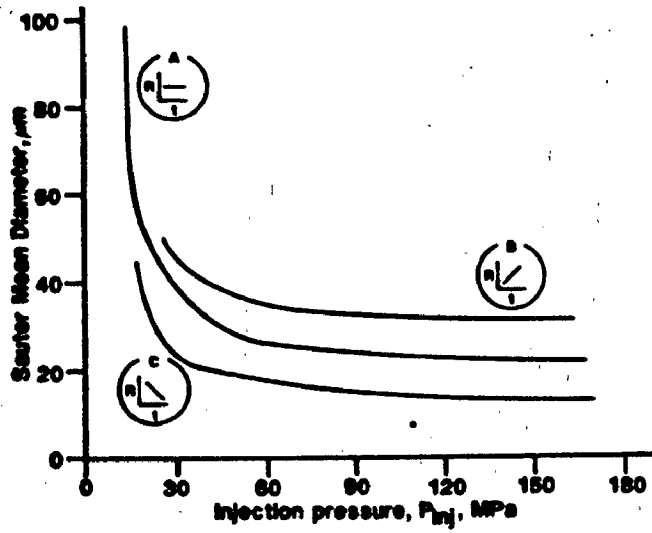


Fig 1.6 Effects of injection rate shape and pressure on droplet size(44).

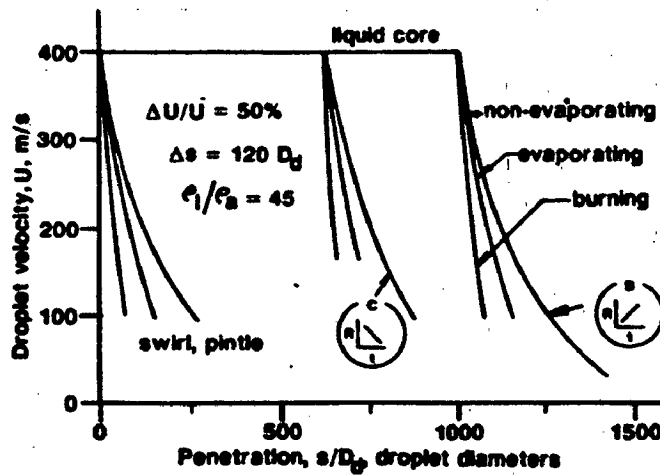


Fig 1.7 Droplet transport history(44).

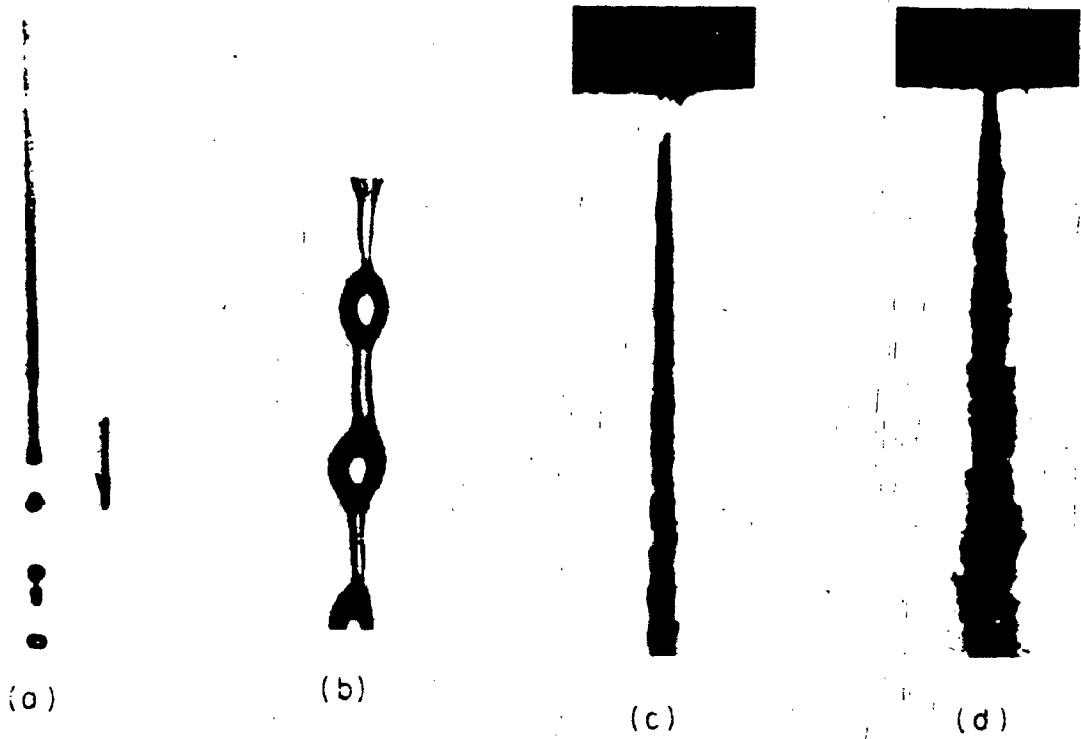


Fig 1.8 Four regimes of liquid jet break-up(49).

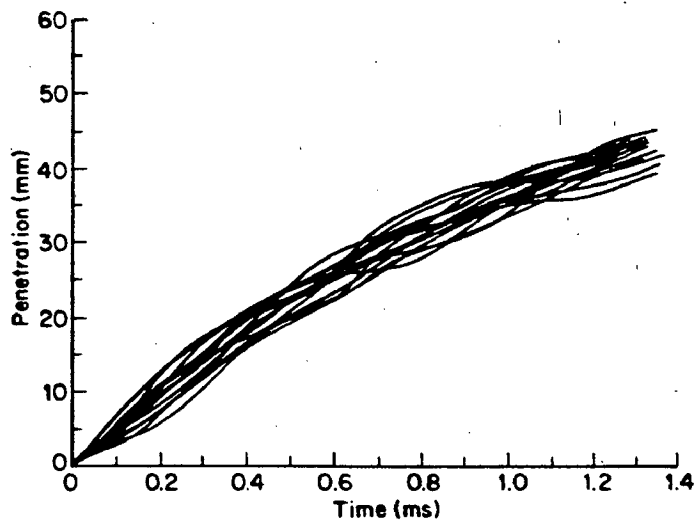


Fig 1.9 Penetration curves for spray pulses, with crossflow 12.5 m/s, pressure 4.3 MPa, temperature 293 K(51).

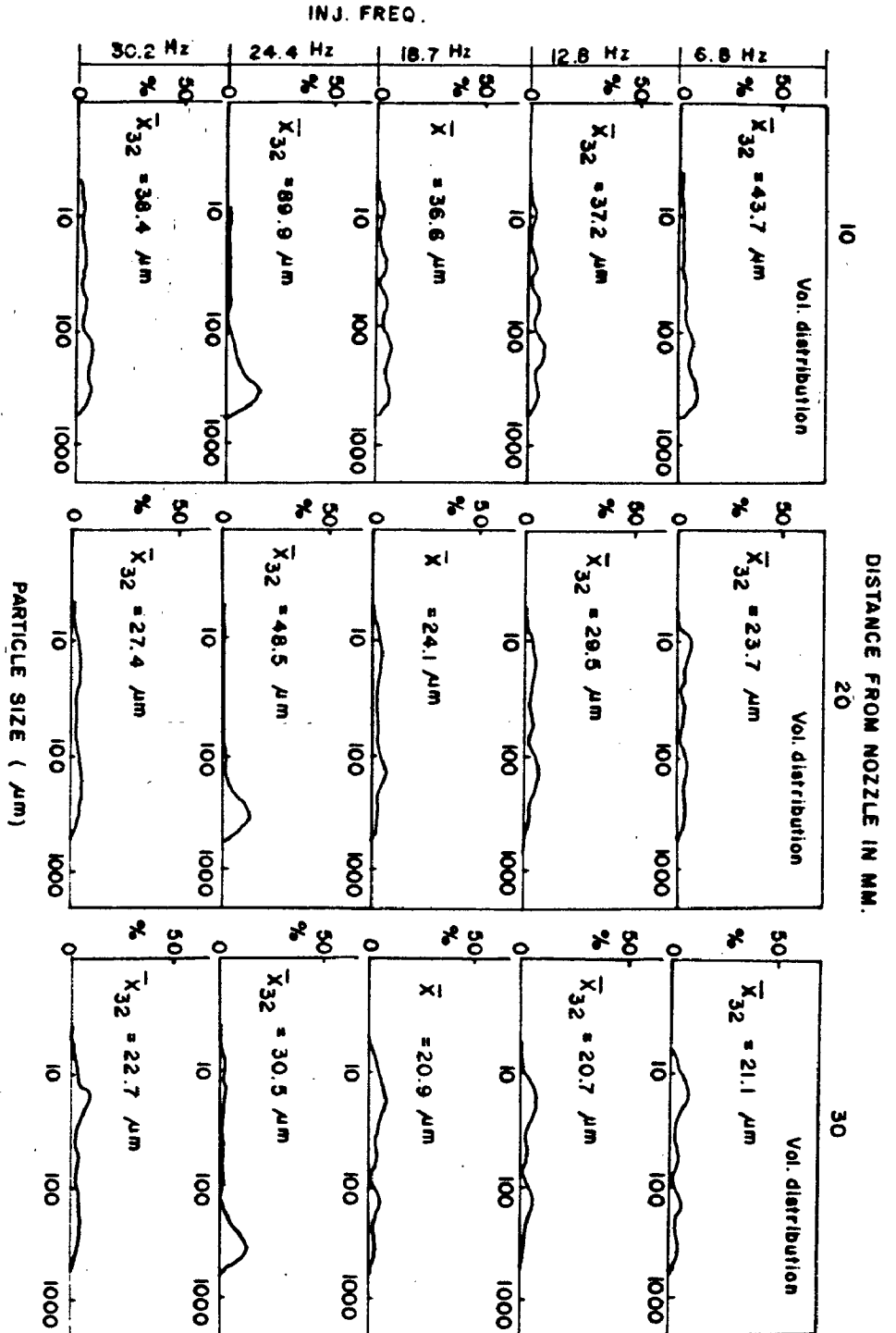


Fig 1.10 Droplet size distribution at 10, 20, 30 mm from the nozzle(58).

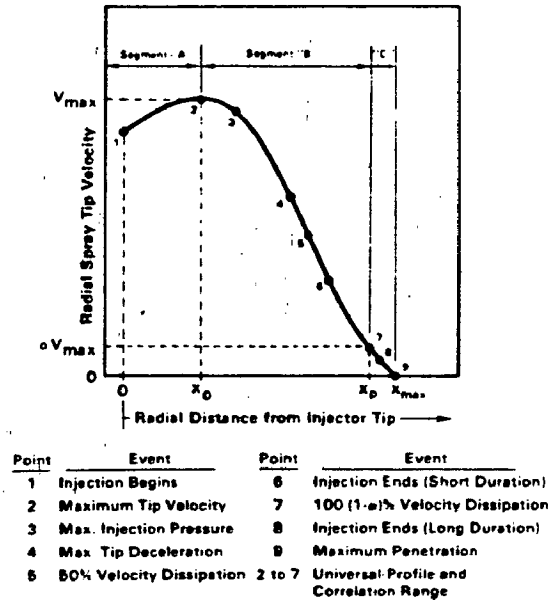


Fig 1.11 Three segments of the spray-tip velocity curve and the corresponding injection events(70).

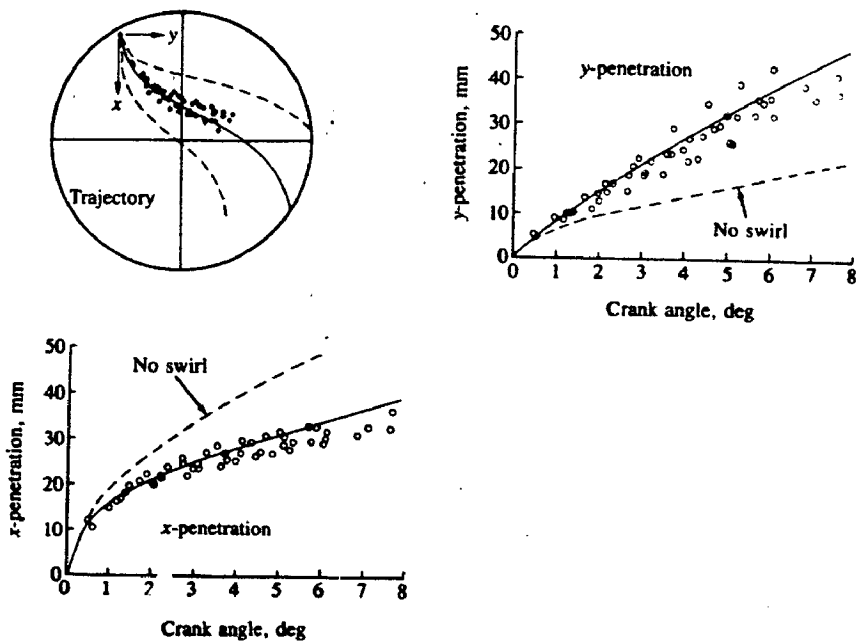


Fig 1.12 Spray trajectory and width calculated using one dimensional quasi-steady spray model compared with experimental data taken in special visualization direct injection stratified charge engine(79).

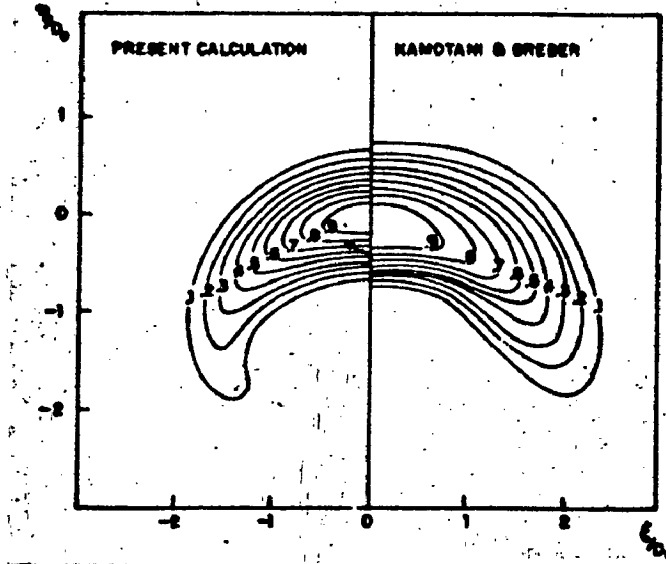


Fig 1.13 Comparison of cross sections and velocity contours measured by Kamotani and Greber(80) with calculated results(77), where the velocity maximum is located on the centre-line.

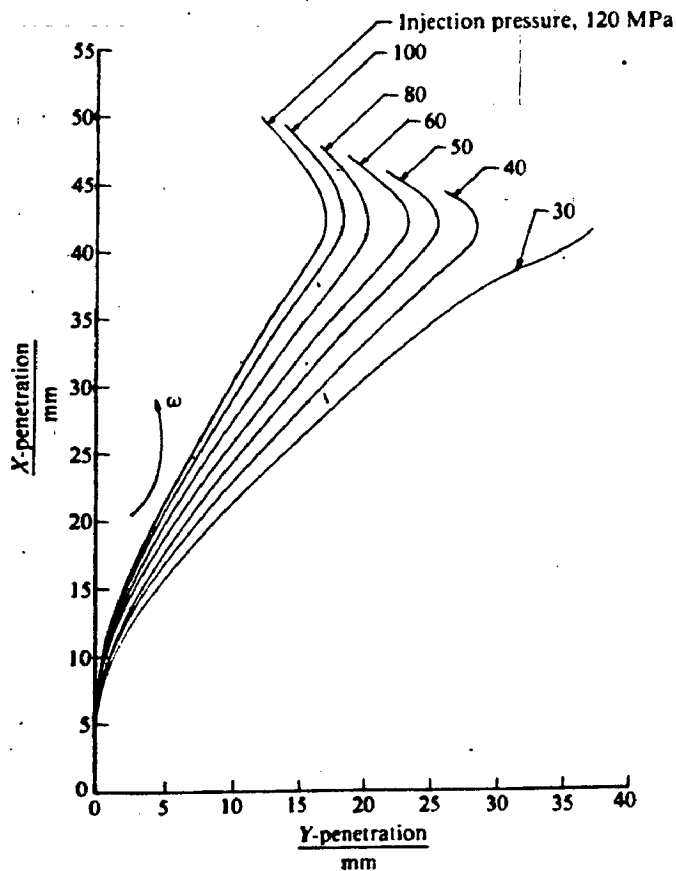


Fig 1.14 Effect of injection pressure on spray trajectory(100).

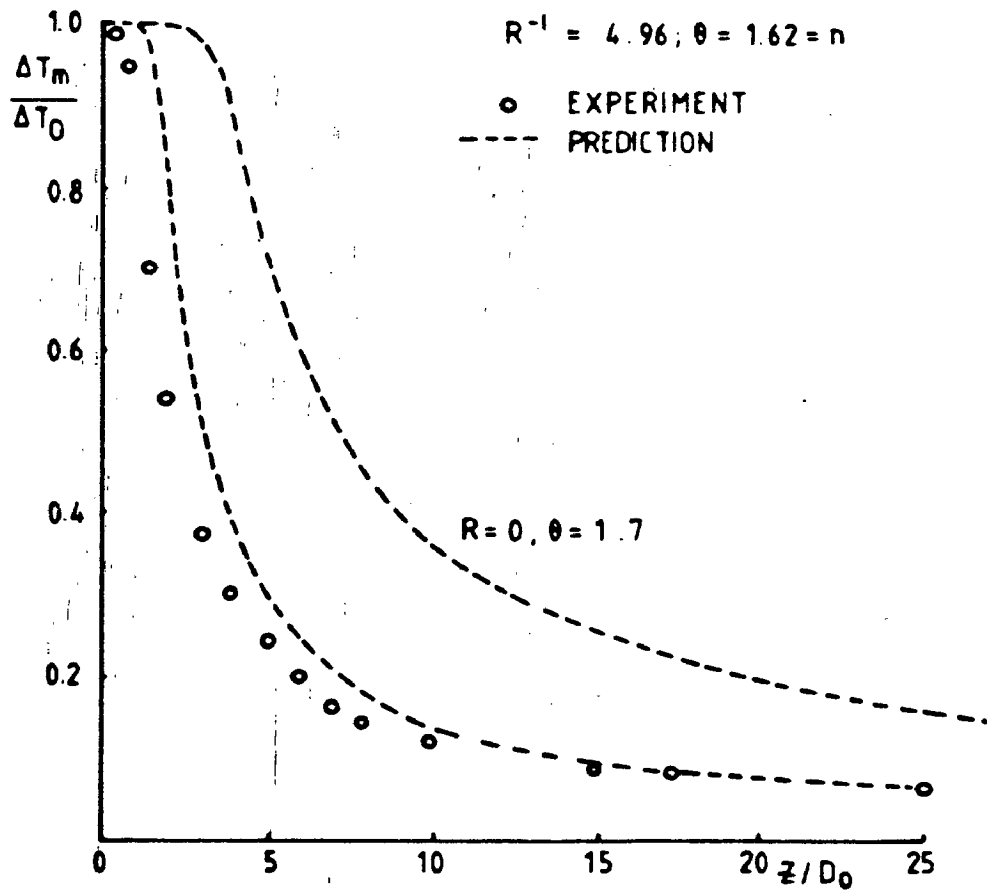


Fig 1.15 Effect of a uniform crossflow on axial temperature decay(102).

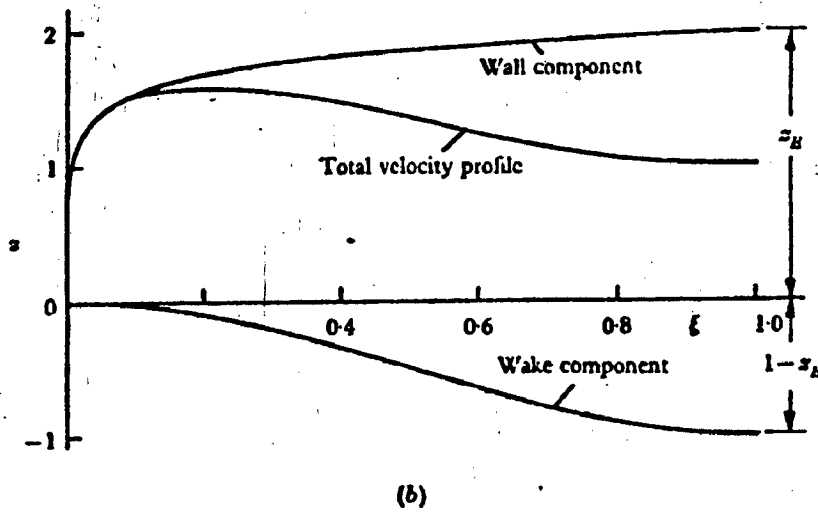
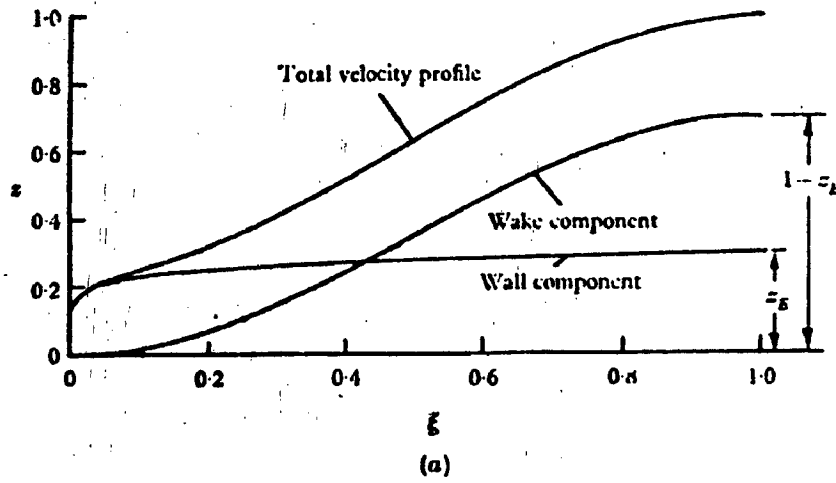


Fig 1.16 Typical velocity profiles (a) Boundary layer profile, (b) Wall jet profile(85).



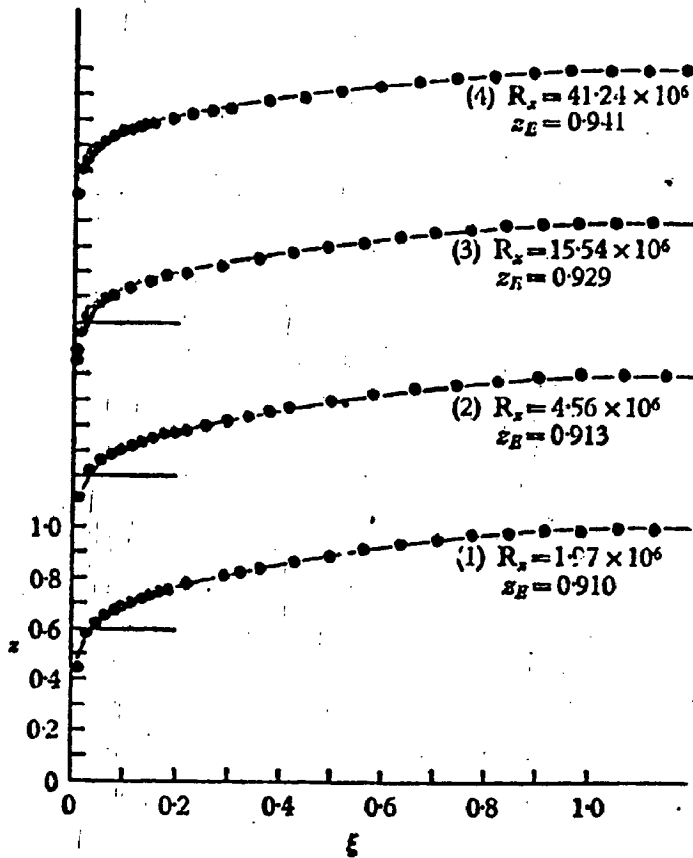


Fig 1.17 Comparison of calculated and experimental velocity profiles for flat plate boundary layers(85).

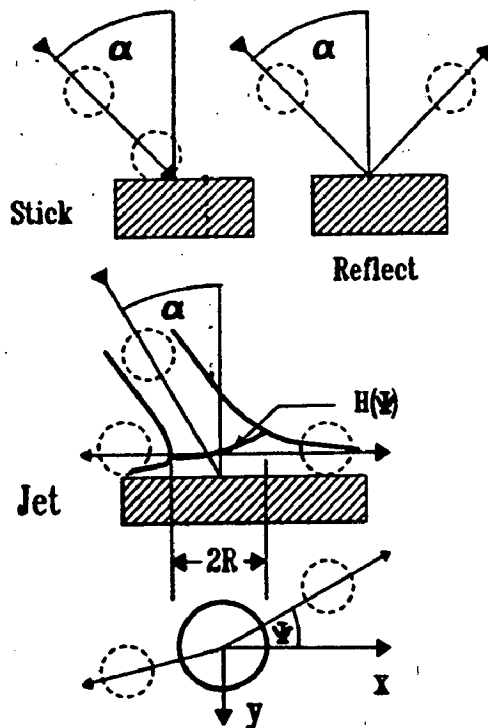


Fig 1.18 Schematic diagrams of the Stick model (drops adhere to wall), Reflect model (drops rebound) and liquid jet analogy model(117).

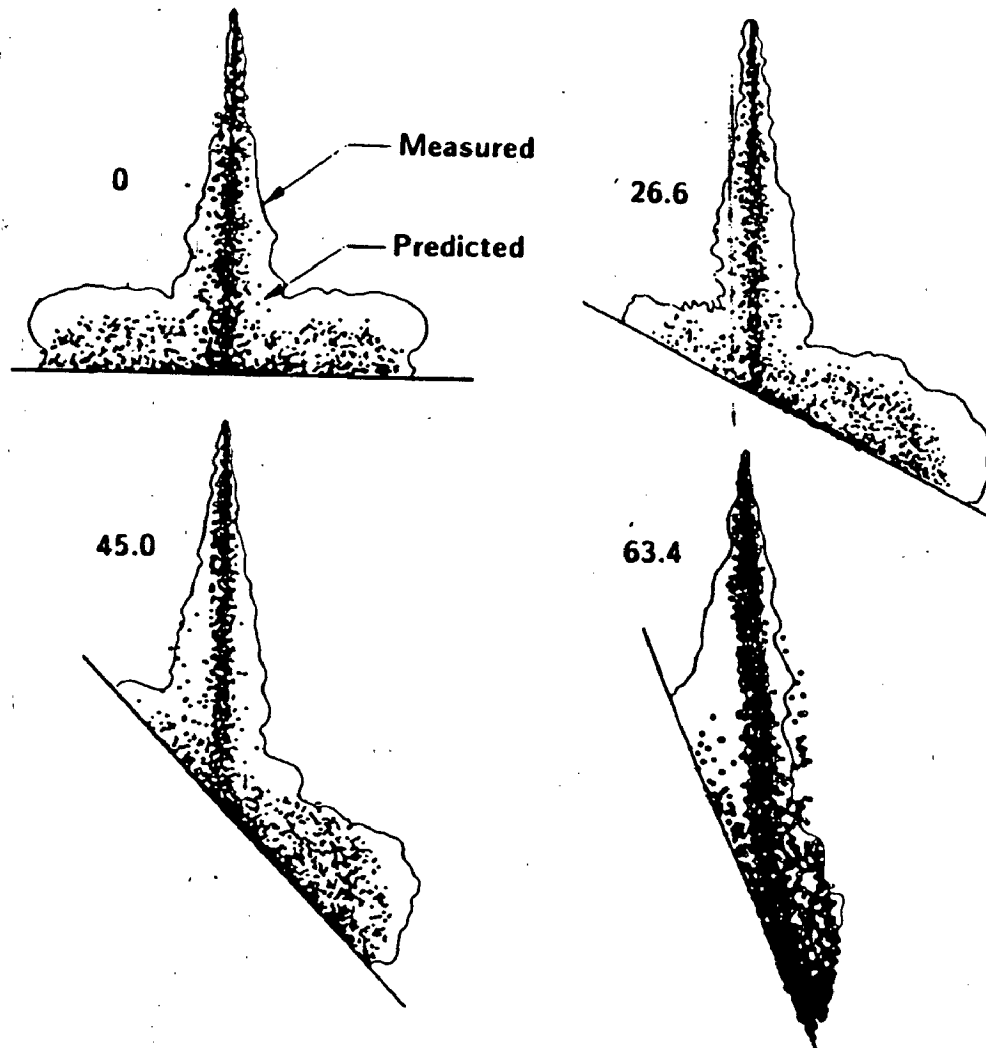


Fig 1.19 Comparison of predicted spray parcel locations (in the line of sight) with spray outlines, 5.3 msec after the start of wall impingement at inclination angles of 0, 26.6, 45 and 63.4(117).

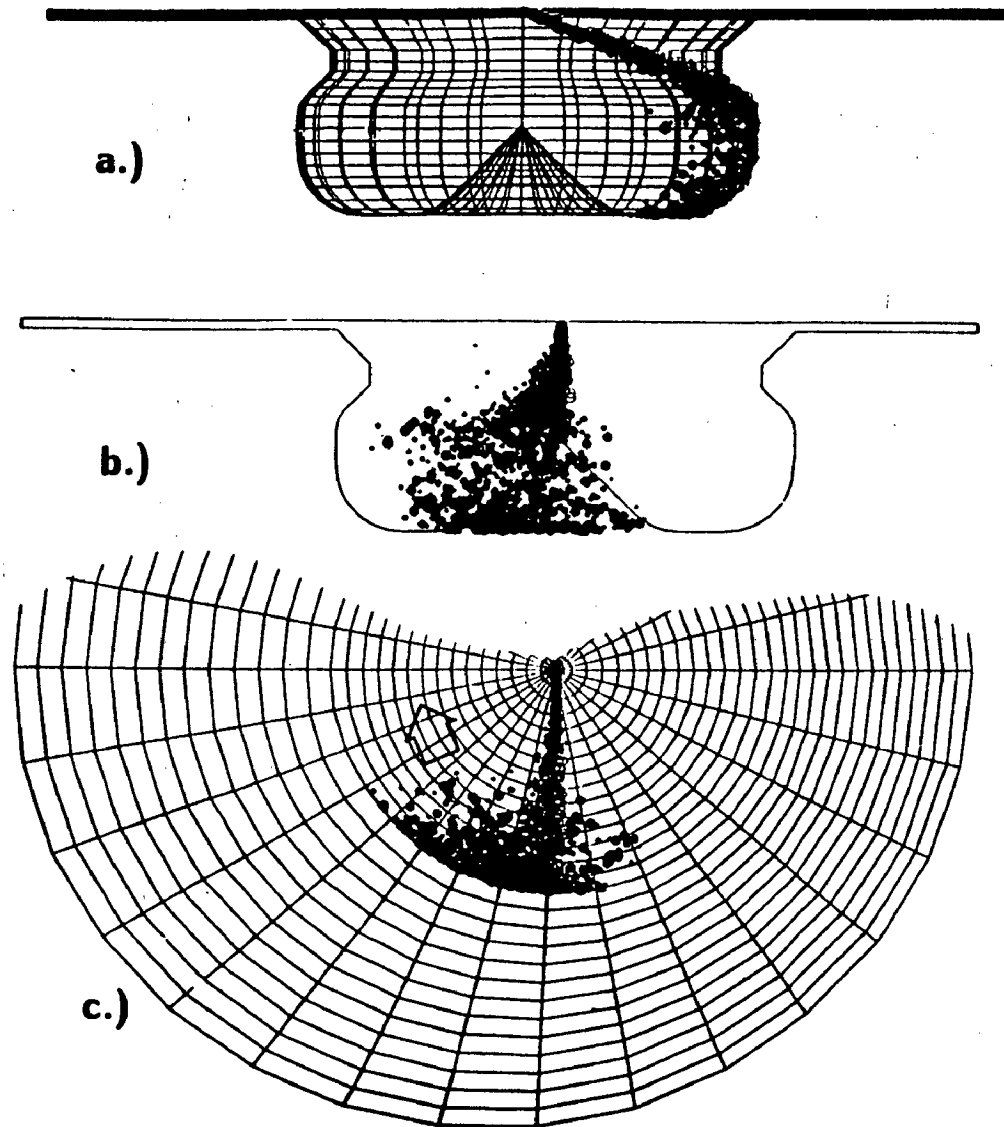


Fig 1.20 Computed engine spray wall impingement details at TDC for swirl ratio 2.9. a) end view b) spray is directed towards the reader c) plan view(117).

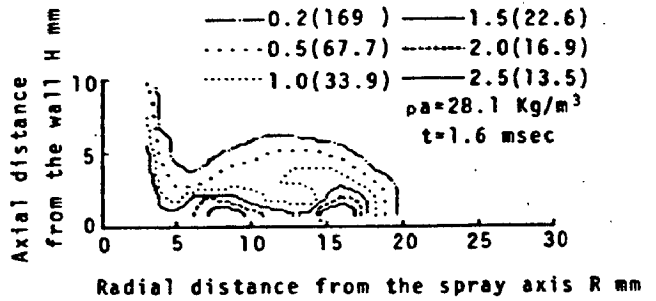
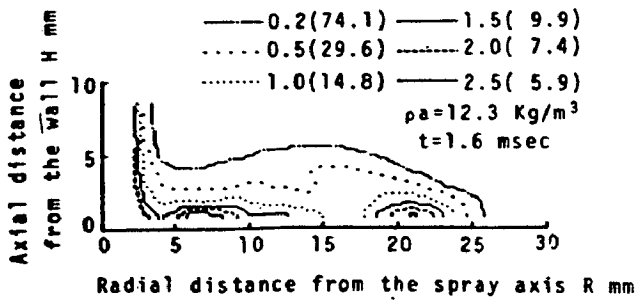
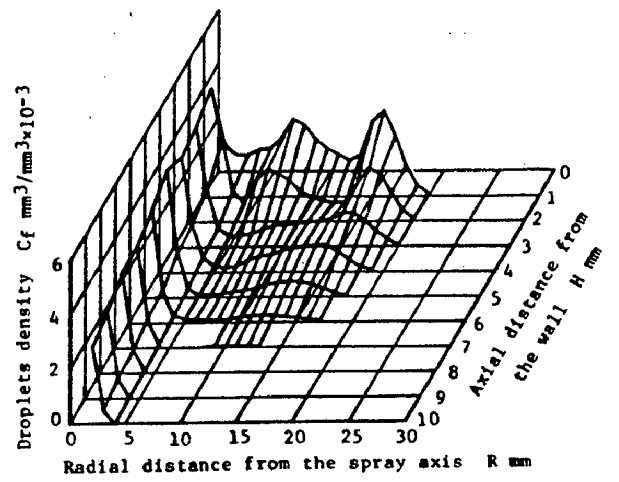
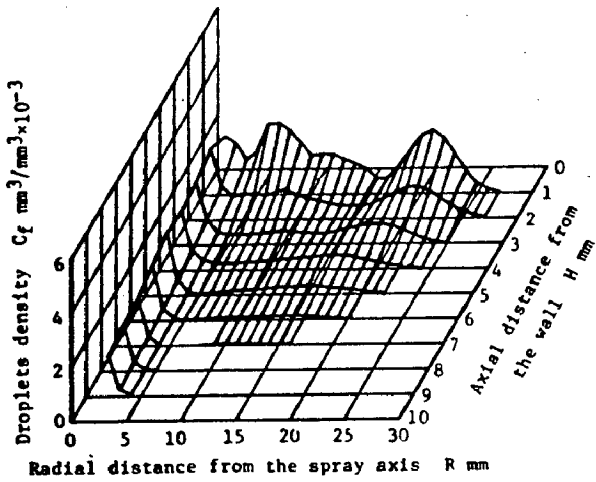
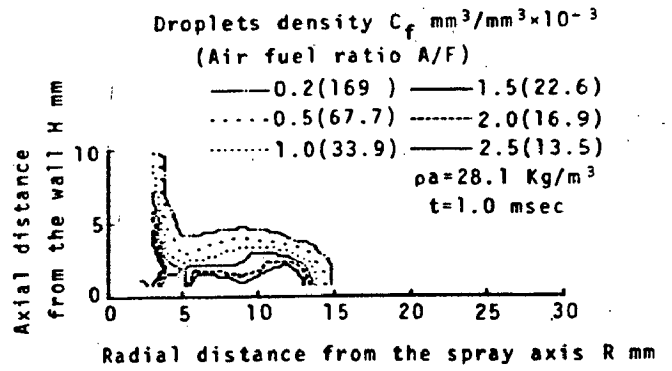
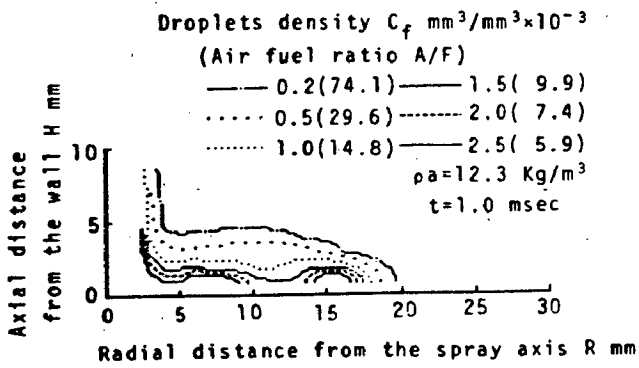
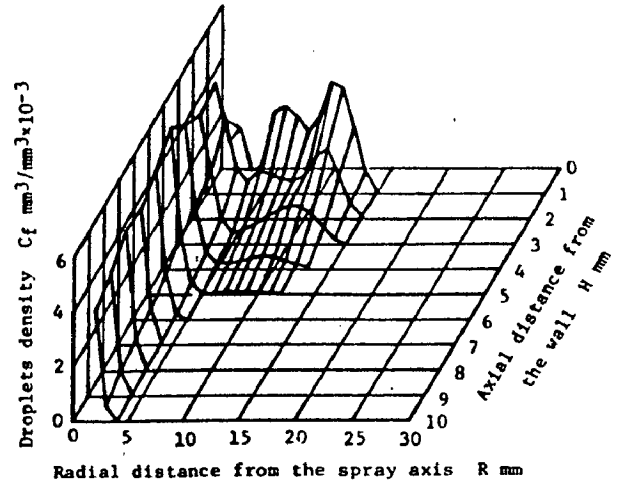
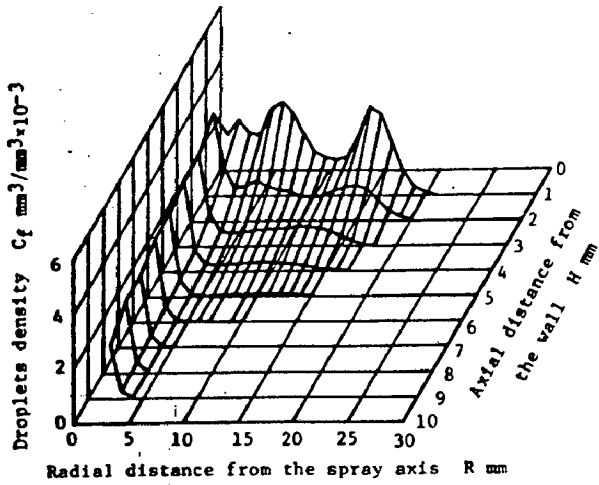


Fig 1.21 Spatial distribution of droplets density and profiles of equal droplets density curves showing the effect of ambient density(107).

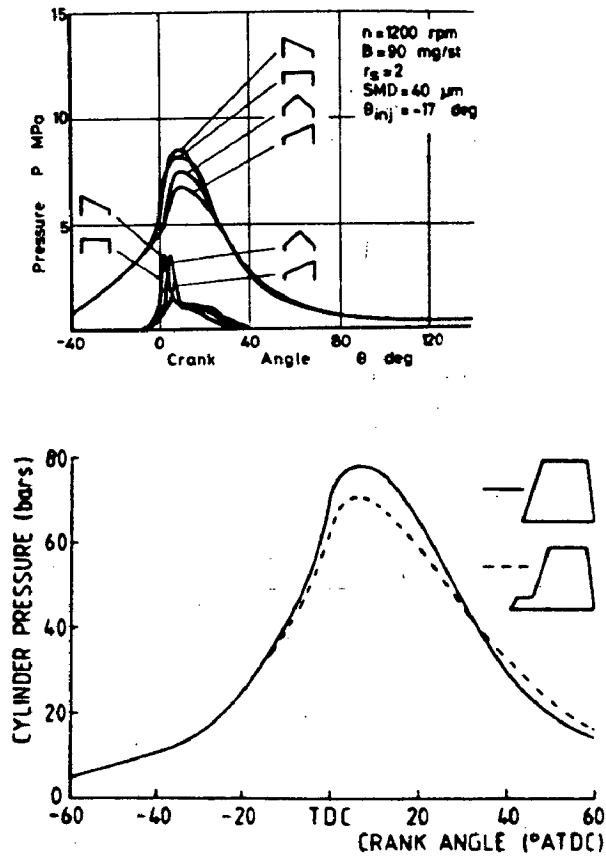


Fig 1.22 Effect of injection rate shape on cylinder pressure (109,131).

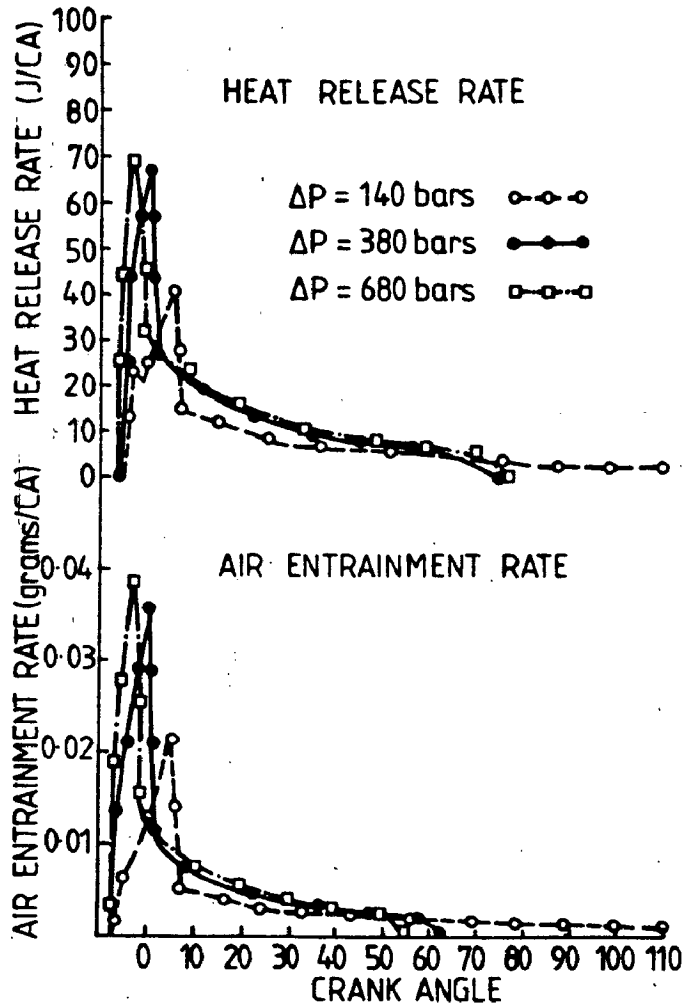
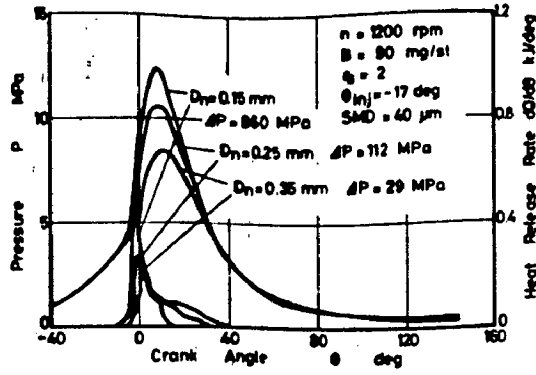


Fig 1.23 Effect of injection pressure(91,131).

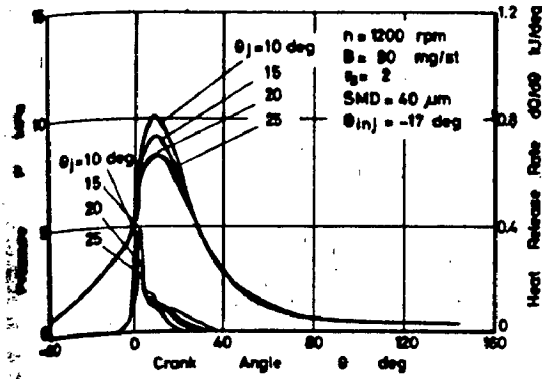


Fig 1.24 Effect of injection duration on cylinder pressure (131).

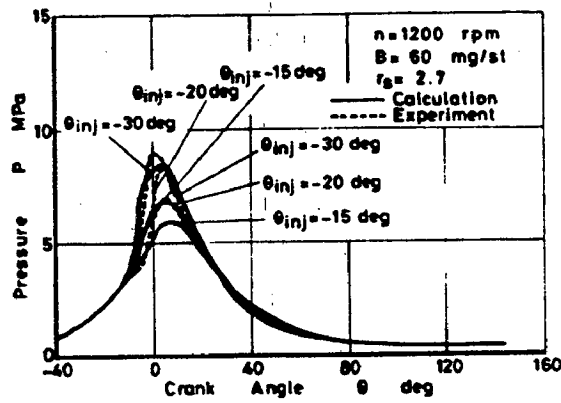


Fig 1.25 Effect of injection timing on cylinder pressure(131).

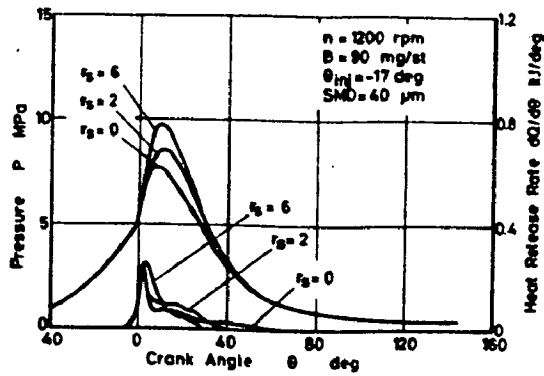
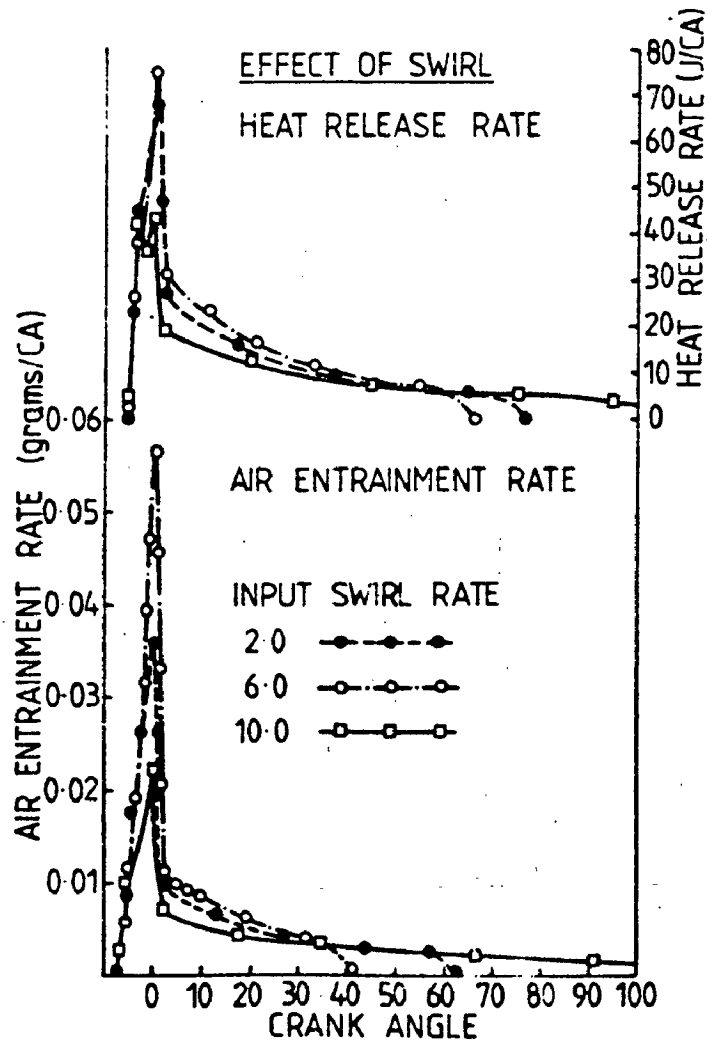
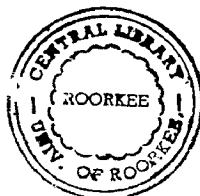


Fig 1.26 Effect of swirl ratio on air entrainment rate and cylinder pressure(91,131).



245722.



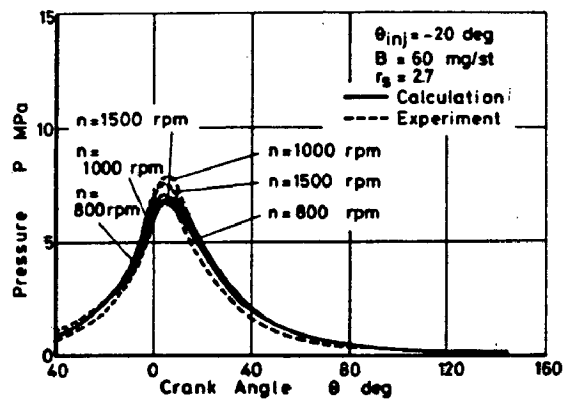


Fig 1.27 Effect of engine speed on cylinder pressure(131).

## CHAPTER - 2

### PROBLEM ENUNCIATION AND FORMULATION

In development of small DI diesel engines, availability of a limited combustion chamber space is a major constraint. High brake specific fuel consumption (BSFC) of smaller engines results, as reported in literature, primarily due to the wall wetting and higher heat transfer and friction losses. The wall wetting causes in-adequate vaporization, mixing and burning, resulting in thermal efficiency losses and higher exhaust emissions. In a detailed comparison of performance data of over a hundred different engines, Uyehara et al (44, 160) observed a linear relationship between BSFC and PCDIL (per cylinder displacement in litres)-the BSFC increases as the PCDIL is decreased (Fig 2.1). Further, it is found that for PCDIL below 2, the trends of BSFC depart from larger engines substantially. The wall wetting is expected to commence, when the combustion chamber radius is less than about three hundred times the nozzle orifice diameter. The air swirl in small DI diesels acts as means of reducing the wall wetting by the injected fuel. It is noted that, the well developed engines show lesser increase in the BSFC, when the PCDIL is reduced from 0.8 to 0.4 (160). This underlines the desirability of bringing in the considerations of the chamber geometry, air motion and fuel injection process calculations simultaneously in the engine design evolution. The intricacies of these three critical elements, needing consideration here, suggest the usefulness of mathematical simulation model.

There is a definite gap found in existing engine simulation models in terms of characterization and prediction of the wall jet effects. Therefore, the characterization of the wall jet processes has to be modelled to improve the predictive capabilities of the phenomenological as well as multi-dimensional engine models.

The present work is an attempt to analyze spray/wall interaction in the presence of swirling air motion in a diesel combustion chamber. The modelling of spray impingement and other wall jet characteristics is central to the present work in view of the objective of improving the engine performance of small DI engines for automotive applications.

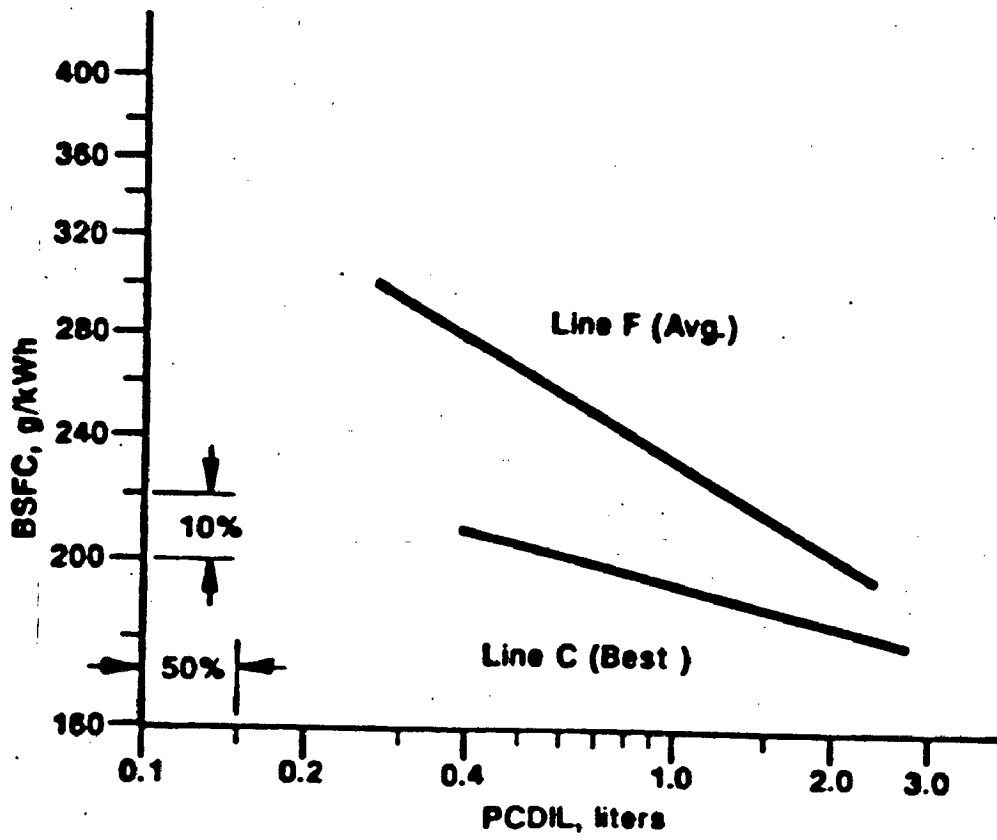


Fig 2.1 BSFC vs. PCDIL (44,160)

## CHAPTER - 3

### MODEL FORMULATION

#### 3.1 DESCRIPTION OF SWIRL MOTION

The relations for the analysis of compression-induced swirl are generally described considering the cylindrical shape of piston geometry(25,161). Moment of inertia of the air depends upon the shape of bowl-in-piston and bowl offset and thus influence the angular swirl velocity near top centre position of the piston. Therefore, the influence of piston bowl geometry on the air swirl is important.

The actual angular momentum of the air at the end of compression will be lower than the angular momentum at the closing of inlet valve due to the wall friction. This friction is estimated using friction formulae developed for flow over a flat plate, with a suitable definition of characteristic length and velocity scales as suggested by Heywood(3) and estimations made by Dent and Derham(25), where side wall effects of the bowl are not considered.

The rate of change of angular momentum at any crank angle is equal to the sum of all the torque forces acting on the fluid and is expressed as;

$$\frac{d}{d\theta}[I\omega] = T, \quad (3.1)$$

Moment of inertia of the trapped mass inside the cylinder(I) for different shapes and offset of the bowl is estimated by splitting

the boundary of the bowl into a number of segments and obtaining best fit equations using various mathematical functions. The torque force due to the wall friction ( $T_f$ ) is estimated as given in Appendix-A.

Equation(3.1) is evaluated numerically by iteration to determine instantaneous swirl ( $\omega$ ). The computation is initiated from the instant of inlet valve closure(IVC). The swirl at IVC is estimated as :

$$\omega_{IVC} = \frac{2\pi(SR)N}{60} \quad (3.2)$$

The swirl velocity vector can be obtained as the cross product of the swirl velocity( $\omega_i$ ) and the position vector of the spray( $r_i$ ) with respect to the combustion chamber axis;

$$U_i = \omega_i \cdot r_i \quad (3.3)$$

The suffix  $i$  represents X, Y and Z components of vectorial quantities in question. Owing to the assumption of solid body rotation for air motion about the Z-axis, the angular swirl velocity vector becomes;

$$\omega_i = \omega \cdot \hat{k} \quad (3.4)$$

Where  $\hat{k}$  is a unit vector along Z-axis. The swirl velocity vector( $U_i$ ) can be resolved in two components, one parallel to the spray axis (called tangential component,  $U_t$ ) and the other in a direction perpendicular to the plane of the axis(called normal component,  $U_n$ ). These are obtained by using

$$U_i = (U_i \cdot \hat{t}) \hat{t} \quad (3.5)$$

and

$$U_s = U_s - U_t \quad (3.6)$$

where  $\hat{t}$  is the unit vector along the tangential direction.

### 3.2 FUEL INJECTION

Fuel injection rate is a function of fuel injection system characteristics, and its computation requires complete simulation of the injection unit. The fuel injection rate is synthesized by solving continuity and forces equilibrium equations at different sections of the fuel injection system like pump chamber, relief valve, high pressure pipe and injector etc. The geometrical flow area of different sections and discharge co-efficients are calculated by correlations, which are well proven, showing fairly good agreement between calculated and measured data of effective flow areas of barrel intake and spill ports, delivery valve and injector nozzle and are available elsewhere(42). The scheme of calculation of fuel injection simulation is included in Appendix-B along with the method of solution. The model for the fuel injection simulation is well validated and can predict injection characteristics to a high degree of accuracy.

### 3.3 SPRAY MOTION

The model is formulated based on the aspects related to the nature of spray and air motion and the growth of spray in the impingement region. The basis of the model formulation is as follows;

1. A transient liquid fuel spray is characterized as a quasi-steady isothermal incompressible turbulent jet.
2. The presence of spray potential core region is taken into consideration in the analysis. The conditions at the end of potential core region act as initial values and it is assumed that no entrainment of air during potential core length takes place.
3. The free jet is axi-symmetric and has a circular cross-section. The wall jet is taken to be semi-elliptical in shape with major and minor axes as perpendicular and parallel to the chamber wall respectively. The major axis is taken to be twice the minor axis and their values are determined by considerations of circular jet flow area at the time of transition from free to the wall region. This simplification is merely taken for the convenience of the analysis.
4. The impingement of the free spray penetrating through the swirling air, on walls of the piston is taken on the basis of geometrical considerations as described in Appendix-C. The criterion of Skifstad(83) is used to determine the point of deflection of the free jet near the wall. Fig 3.1 represents the schematic of the wall jet.
5. The three-dimensional formulation is made following the approach of Adler and Baron(77) for the free jet, in which, two momentum equations are written: one along the spray centre-line and another normal to the centre-line. The wall jet flow is considered two-dimensional and the wall as smooth and impermeable.
6. A composite velocity distribution is arrived at by combining one-seventh law of velocity distribution in turbulent boundary



layer at the wall

$$\frac{u}{u_m} = (y)^{1/7} \quad (3.7)$$

and velocity profile of Abramovich(140) in the free jet region

$$\frac{u}{u_m} = \left(1 - y^2\right)^2 \quad (3.8)$$

on the basis that the boundary layer to total wall jet thickness  $\left(\frac{\delta}{b_j}\right)$  is 0.1(140). The concentration distribution is

$$\frac{c}{c_m} = \left(\frac{u}{u_m}\right)^{0.5} \quad (3.9)$$

The assumption makes use of powerful integral method, which transforms partial differential equations into ordinary differential equations.

7. The two components Sinnamon's equation(79) for the rate of air entrainment of the free spray in swirling environment

$$\frac{d\dot{m}}{ds} = 2\pi b_j (\rho_m \rho_a)^{1/2} [a_1(u_m - U_t) + a_2(U_s)] \quad (3.10)$$

is also adopted in the wall region by suitably modifying the value of the co-efficient of axial component of entrainment( $a_1$ ) based on the experimental data concerning entrainment of air in the wall jet taken from the reference(83), details of which are included in Appendix-D.

Four conservation equations of mass and momentum are formulated for spray motion both as free and wall jet.

(a) Conservation of fuel mass

The fuel mass flow rate at any cross-section of the jet

remains constant and is expressed as:

$$\frac{d}{ds} \left[ \int_A c \rho u dA \right] = 0 \quad (3.11)$$

(b) Conservation of total mass

The conservation of total mass (fuel plus entrained air mass) is given by

$$\frac{d\dot{m}}{ds} = \frac{d}{ds} \left[ \int_A \rho u dA \right] = P \pi b_j (\rho_m \rho_a)^{1/2} [a_1 (u_m - U_t) + a_2 (U_a)] \quad (3.12)$$

Where  $P$  is constant, the value of which depends upon whether the spray is free or wall jet.  $b_j$  is the radius of circular free jet before impingement or the thickness of the wall jet after impingement.  $P = 2$  for free spray and  $P = 0.79$  for spray motion along the wall.

(c) Momentum equation along axial direction

For steady flow, momentum equation neglecting the effect of gravity, represents the balance between the momentum entrained, wall friction force and momentum change along the spray as :

$$\frac{d}{ds} \left[ \int_A \rho u^2 dA \right] = U_t \left( \frac{d\dot{m}}{ds} \right) + D_f \quad (3.13)$$

$D_f$  represents the drag force due to shearing stresses, which emanate from viscosity usually expressed in terms of skin friction co-efficient  $C_f$  and is given by;

$$D_f = C_f b_j \frac{\rho_a}{2} (u_m - U_t)^2 \bar{t} \quad (3.14)$$

The value of  $C_x$  is taken from (162).  $D_x$  is not valid for the free region.

(d) Momentum equation in direction normal to spray

The normal momentum equation represents a balance between the drag force (form drag), centrifugal body forces and the momentum flux due to entrainment. On neglecting the buoyancy term and the drag force due to normal stresses, the expression is written as :

$$-\left[ \int_A \rho u^2 dA \right] \frac{d\alpha}{ds} = U_a \left( \frac{dm}{ds} \right) \quad (3.15)$$

Where  $d\alpha$  is the angle by which the jet is deflected as it advances by a distance  $ds$ .

The local density at any point in the jet can be expressed as a function of the density of surrounding air and the density and concentration of fuel as:

$$\rho = \rho_a \left[ 1 - \left( \frac{m_l}{m_t} \right) \left( 1 - \frac{\rho_a}{\rho_l} \right) + \frac{m_v}{m_t} \left( 1 - \frac{\rho_a}{\rho_l} \right) \right] \quad (3.16)$$

In the absence of evaporation ( $m_v = 0$ ), equation (3.16) reduces to the form of reference (79), that is

$$\rho = \frac{\rho_a}{1 - c\beta} \quad (3.17)$$

where  $\beta = \left[ 1 - \frac{\rho_a}{\rho_l} \right]$

The composite concentration profile shape as developed for wall jet is given as :

$$f(y) = 1.24(1 - y^{1.93})y^{0.62} \quad (3.18)$$

and for free jet following Abramovich(140), the profile shape is;

$$f(y) = (1 - y^{3/2}) \quad (3.19)$$

$$\frac{u}{u_m} = [f(y)]^2 \quad (3.20)$$

$$\frac{c}{c_m} = f(y) \quad (3.21)$$

Fig 3.2 is the plot showing comparison of predictions from individual similarity profiles and the composite profile thus developed.

Substitution of equations(3.17,3.20 and 3.21) into equations(3.11-3.15) and subsequent simplification results in a set of the following four first order linear differential equations in terms of four dependent variables. The details of the derivation of these equations is included in Appendix-E.

$$b_1 u_m I_1 \frac{dc_m}{ds} = b_1 I_2 \frac{du_m}{ds} + 2u_m I_2 \frac{db_1}{ds} = 0 \quad (3.22)$$

$$b_1 u_m I_3 \frac{dc_m}{ds} + b_1 I_4 \frac{du_m}{ds} + 2u_m I_4 \frac{db_1}{ds} = P_1 E \quad (3.23)$$

$$b_1 u_m^2 I_5 \frac{dc_m}{ds} + 2b_1 u_m I_6 \frac{du_m}{ds} + 2u_m^2 I_6 \frac{db_1}{ds} = P_1 U_1 E + \left[ \frac{C_t (u_m - U_1)^2 \hat{t}}{\pi} \right] \quad (3.24)$$

$$-\frac{da}{ds} = \frac{P_1 U_1 E}{b_1 u_m^2 I_6} \quad (3.25)$$

Where  $P_1$  is constant.  $P_1 = 1$  for the free spray and  $P_1 = 1.58$  for wall jet. The equations(3.22-3.25) contain the derivatives of four dependent variables viz; concentration, velocity, free jet radius or wall jet thickness and the direction. Of these four

derivatives, the value of the directional derivative is available directly from equation (3.25). The other three derivatives can be evaluated by solving equations(3.22-3.24) algebraically. Thus, the model reduces to an initial value problem. The integration at each step is carried out using modified Euler's technique.

### 3.4 TURBULENT MIXING

At the end of the injection period, the jet momentum due to fuel injection process becomes zero. Hence, the entrainment of air can not be computed in a manner, it is done during the injection period using spray-swirl-wall interaction formulation of section 3.3. However, the mixing and spray growth still continues and is thought to be controlled by the turbulence kinetics of the system.

Following Dent(150), turbulent energy dissipation rate(  $\epsilon$  ) is

$$\epsilon = \gamma \cdot (\text{Rate of energy input to the flow/mass}) \quad (3.26)$$

Where  $\gamma$  is some fraction, and after Corsin(148), is taken as 1/2.

For a solid body forced vortex air swirl, the rate of energy input is ;

$$\frac{1}{2} I \omega^2 \omega \quad (3.27)$$

For a cylinder rotating about its axis

$$I = \frac{m D^2}{8}$$

$$\epsilon = \frac{\omega^3 D^2}{32} \quad (3.28)$$

and

$$\tau_{swirl} = \left( \frac{\gamma}{\epsilon} \right)^{1/2} \quad (3.29)$$

Putting equation(3.28) into equation(3.29),

$$\tau_{swirl} = \left( \frac{32\nu}{\omega^3 D^2} \right)^{1/2} \quad (3.30)$$

Considering also the turbulent mixing rate by the energy input to the fuel sprays during the injection process(109),

$$\epsilon_{inj} = C \left( \frac{N}{DINJ} \right)^3 \left( \frac{V_f}{d_n^2} \right)^2 \quad (3.31)$$

on various substitutions, the value of constant C comes out to be  $4.924 \times 10^{-5}$ .

The mixing rate equation, therefore, becomes,

$$R_{inj} = \frac{1}{\tau_{inj}} = \left( \frac{\epsilon_{inj}}{\nu} \right)^{1/2} \quad (3.32)$$

Considering these rates to act in parallel(91),

$$R = \frac{R_{inj} R_{swirl}}{R_{inj} + R_{swirl}} \quad (3.33)$$

Where  $R_{swirl} = \frac{1}{\tau_{swirl}}$  from equation (3.30)

Hence total mixing time becomes,

$$\tau = \frac{1}{R} \quad (3.34)$$

The mass transfer rate of the air by turbulent mixing into the burning spray from the surrounding regions is expressed as,

$$\dot{m}_a = C_2 m_s / \tau \quad (3.35)$$

Where  $m_a$  is the mass of air, and  $C_2$  is constant, which is evaluated by equating the entrainment rate computed at the instant of termination of injection process of the right hand side of

expression(3.35).

### 3.5 ATOMIZATION, DISPERSION AND SPRAY STRUCTURE

Atomization is the process of breaking-up of continuous lump of injected liquid into a large number of small droplets and consequently enhancing total surface area of the liquid. This enables rapid evaporation and combustion of the fuel. The disintegration of injected liquid is understood to be the result of the oscillations and perturbations caused by the mutually opposing surface tension and aerodynamic forces acting on the surface of the liquid. The atomized fuel spray consists of droplets of various sizes.

Sauter mean diameter(SMD) is the diameter of a droplet that has the same volume to surface area ratio as that of the actual spray. The instantaneous sauter mean diameter(SMD) is computed from the correlation of Knight(47);

$$\text{SMD} = 8(\Delta p)^{-0.468} (\dot{V}_i)^{0.209} (\nu)^{0.216} \quad (3.36)$$

Where  $\Delta p$  is pressure difference in Pascals,  $\dot{V}_i$  is the injection rate in  $\text{m}^3/\text{sec}$  and  $\nu$  is the kinematic viscosity of the fuel.

The fuel spray is divided into many elemental zones. The axial divisions are formed in terms of each packet of injection in discrete time step. When time step is taken equal to 1 degree angle, the number of axial divisions become equal to the injection duration in degrees of crank angle. The spray in the free region is divided radially in 16 equal divisions starting from central portion and upto the periphery of the spray. In the wall region,

the radial divisions are assumed to begin from the surface of wall. The correlation of sauter mean diameter for the free spray is used for the spray motion after impingement as well as suggested by a recent investigation(107). The droplet-size distribution is assumed to follow Simmons's binary droplet division model (BDM). Simmons(146) suggested the BDM considering successive break-up of droplets from their maximum size to the various sizes in lower range such that every break-up stage results in two equal size droplets of diameter =  $(0.5)^{1/3}$  x the diameter of the originating droplet. The model assumes that

- i) there are total 16 classes of droplet sizes in the normalized droplet diameter(  $D^* = D_d/SMD$ ) range of  $0.112 < D^* < 3.6$ ,
- ii) the droplets in each class are spheres of the equivalent volume, and
- iii) the probability of division associated with each droplet size is such that a portion of the droplets remains undivided and constitutes the droplet-size/number distribution.

Simmons's BDM not only describes the physical phenomenon of droplet division, but has a added practical advantage of upper and lower size limits similar to upper limit distribution functions(59,163). The applicability of Simmons's model is well established for diesel spray and hence chosen in the present work.

### 3.6 FUEL DISTRIBUTION

The fuel distribution pattern in the spray is established assuming that the droplets of biggest size are distributed in the centre of spray in the free region and at the wall in the wall



region and subsequent zones towards the outer periphery of the spray contain smaller size droplets according to 16 classes of droplet sizes of the Simmons's model(146). Therefore, the following correlations establish the fuel distribution in each packet ;

Total no of drops

$$N_T = \frac{5.183 \dot{V}_R}{(\text{SMD})^3 6N} \quad (3.37)$$

Commulative number of drops of class J

$$N_{CJ} = 1.3882 e^{-(4D_{pj}^*/1.2)} N_T \quad (3.38)$$

Commulative number of drops of class J+1

$$N_{CJ+1} = 1.3882 e^{-(4D_{p,j+1}^*/1.2)} N_T \quad (3.39)$$

where  $D_{p,j+1}^* = (0.5)^{1/3} D_{pj}^*$

Number of droplets in each packet

$$N_{dJ} = N_{CJ+1} - N_{CJ} \quad (3.40)$$

Mass of fuel in each packet

$$= \frac{\pi}{6} (\text{SMD} \cdot D_{pj}^*)^3 N_{dJ} \rho_f \quad (3.41)$$

The assumption of largest droplets on the jet axis and the smallest at its edge is reasonable in the light of the experimental studies of Lee(164) and Hiroyasu et al(131). From the fuel

distribution thus calculated and the concentration distribution from the spray-swirl-wall interaction model, the equivalence ratio in all the zones in the spray is specified.

### 3.7 IGNITION DELAY

The ignition delay time is the period between the start of fuel injection and the commencement of combustion. In literature(165,166), the beginning of combustion has been defined by several methods, such as sudden increase in pressure, temperature, light emission or the concentration of free radicals. However, for engineering applications, ignition delay period in terms of pressure rise delay(151) is commonly used.

Most investigators correlate the ignition delay period with an overall Arrhenius expression. Plee and Ahmad(166) and others(167) have reported that no empirical formula can predict ignition delay in a wide range of operating conditions.

An empirical correlation of Hardenberg and Hase(151) has been widely considered suitable, hence chosen in the present model. This is expressed as :

$$ID = (0.36 + 0.22v_p) \cdot \exp \left[ E_A \left( \frac{1}{RT_m CR^{c-1}} - \frac{1}{17190} \right) + \frac{21.2}{(P_m CR^c - 12.4)} \right] \quad (3.42)$$

Activation energy  $E_A = \frac{618840}{CN+25}$

R is universal gas constant = 8.31434 j/mol

$P_m$  is absolute manifold pressure in bar

$T_m$  is absolute manifold temperature in Kelvin

$$\text{Index } c = k - \frac{k-1}{1.1v_p + 1}$$

where  $K = 1.4$  and  $v_p$  is mean piston speed in m/sec.

### 3.8 EVAPORATION

The fuel spray evaporation containing droplets of wide range of sizes is a complex phenomenon. The vaporization of an isolated droplet obeying  $d^2$ -law is a simple description widely used. Alongwith this, the spherico-symmetry of droplet is generally assumed(93,109,110,123,128,133). Many diesel engine models consider the gas jet assumptions valid. The vaporization is, therefore, instantaneous. However, Kamimoto and Matsuoka(168) suggest that the evaporation rate profile in diesel engines is similar to the fuel injection rate curve but delayed by 0.4 milliseconds. This is mainly due to the droplet break-up process. This consideration has been adopted in the present work.

### 3.9 COMBUSTION

It is postulated that following the ignition delay period, combustion occurs at the stoichiometric condition in the elements where the actual air-fuel vapour equivalence ratio falls within the limit of inflammability. The limits of inflammability selected are  $0.3 < \phi < 3$ , as recommended by Glassman(152).

The amount of fuel vapour burned( $m_{v_b}$ ) in an element of spray is expressed as

$$\Delta m_{v_b} = \Delta m_{v_s} \quad \text{for } \phi \leq 1 \quad (3.43)$$

and

$$\Delta m_{v_1} = \frac{\Delta m_{a_1}}{\text{AFRS}} \quad \text{for } \phi > 1 \quad (3.44)$$

Where  $\Delta m_{v_1}$  and  $\Delta m_{a_1}$  are the available amounts of fuel vapour and entrained air in the element respectively. AFRS is the stoichiometric air fuel ratio. The mass of burned air in any element will be

$$\Delta m_{a_1} = \Delta m_{v_1} \cdot \text{AFRS} \quad (3.45)$$

The sum of masses of burned fuel and consumed air gives the net mass of products in each element. In the small increment of time, energy burned rate due to combustion is

$$\frac{dQ_b}{d\theta} = \text{CVF} \sum_{i=1}^{i_6} \Delta m_{v_i} \quad (3.46)$$

Where CVF is the calorific value of the fuel.

### 3.10 HEAT TRANSFER

Heat transfer rate from hot cylinder gases to the walls is given by the expression :

$$\frac{dQ_w}{d\theta} = h_w A_w (T_{g_1} - T_w) \quad (3.47)$$

Where  $h_w$  is the instantaneous heat transfer co-efficient and,  $T_{g_1}$  and  $T_w$  are the mean temperature of cylinder gases and wall respectively. Heat transfer between spray elements is not considered. Heat transfer surface area ( $A_w$ ) includes the areas of cylinder head, side walls, and the piston crown.

The mean cylinder gas temperature represents the weighted mean temperature of the spray and the surrounding gas in the following form

$$T_{sg} = \frac{m_{sp} T_{sp} + m_{sur} T_{sur}}{m_{sp} + m_{sur}} \quad (3.48)$$

Where  $sp$  and  $sur$  refers to spray and surrounding fluids respectively.

The heat transfer co-efficient ( $h_w$ ) is computed using Woschni's correlation (142).

$$h_w = 0.012793 D^{-0.2} T_{sg}^{-0.53} p^{0.8} \left[ C_1 v_p + C_2 \frac{V \cdot T_{ivc}}{V_{ivc} \cdot p_{ivc}} (p - p_{mot}) \right] \quad (3.49)$$

Where  $p_{mot}$  is instantaneous motoring pressure,  $p_{ivc}$ ,  $T_{ivc}$  and  $V_{ivc}$  are the pressure, temperature and volume of cylinder at inlet valve closure. The constants  $C_1$  and  $C_2$  are taken as 2.28 and 0.00324 m/sec-k, respectively during compression and expansion strokes (142).

Total heat transfer is proportional to the surroundings and spray fluids in relation to their mass and temperature as

$$\frac{dQ_{wsp}}{d\theta} = \frac{m_{sp} T_{sp}}{m_{sp} T_{sp} + m_{sur} T_{sur}} \frac{dQ_w}{d\theta} \quad (3.50)$$

$$\frac{dQ_{wsur}}{d\theta} = \frac{m_{sur} T_{sur}}{m_{sp} T_{sp} + m_{sur} T_{sur}} \frac{dQ_w}{d\theta} \quad (3.51)$$

The mean temperatures of walls are calculated by correlations based on the basis of temperature measurements on a number of supercharged and naturally aspirated engines. The wall surface temperatures are calculated as a function of engine speed, inlet

pressure and temperature, excess air co-efficient and the bore of engine. Two correlations are used, one for fixed wall like cylinder head, piston crown etc. and another for liner.

The fixed wall temperature ( $T_{wf}$ ) is

$$T_{wf} = T_c + 30.35Z_1 \quad (3.52)$$

where,  $T_c$  is coolant temperature in Kelvin and

$$Z_1 = 7.5 \left( \frac{p_{in}}{p_s} \right)^{0.35} \left( \frac{1}{\alpha} \right)^{0.42} \left( \frac{T_{in}}{T_s} \right)^{0.35} \left( \frac{v_p}{10} \right)^{0.5} (10D)^{0.38} \quad (3.53)$$

Where,  $p_{in}$  and  $T_{in}$  are the pressure and temperature of the air at inlet conditions and  $p_s$  and  $T_s$  are the air pressure and temperature at standard conditions respectively.  $\alpha$  is the excess air co-efficient.

For cylinder liner

$$T_{wl} = T_c + 7.5Z_2 \quad (3.54)$$

where

$$Z_2 = 8.4 \left( \frac{p_{in}}{p_s} \right)^{0.35} \left( \frac{1}{\alpha} \right)^{0.42} \left( \frac{T_{in}}{T_s} \right)^{0.35} \left( \frac{v_p}{10} \right) (10D)^{0.38} \quad (3.55)$$

Therefore, equation(3.47) can be written as,

$$\frac{dQ_w}{d\theta} = h_w A_f (T_{wg} - T_{wf}) + h_w A_l (T_{wg} - T_{wl}) \quad (3.56)$$

Where  $A_f$  and  $A_l$  are the surface area of fixed wall and liner of cylinder respectively.

### 3.11 THERMODYNAMIC ANALYSIS

Thermodynamic analysis of the control volume of the system begins at the onset of injection. Conservation equations of mass and energy are written for the spray and surrounding fluids. The initial masses and composition in the spray elements are determined from spray-swirl-wall interaction and turbulent mixing models.

### Mass Conservation

A schematic diagram showing mass balance in the engine cylinder is shown in Fig 3.3.

(i) For the spray

Rate of change of mass in spray = Fuel mass injection rate + Air entrainment rate into spray

$$\frac{dm_{s3}}{d\theta} = \frac{dm_{f1}}{d\theta} + \frac{dm_{a1}}{d\theta} \quad (3.57)$$

This can be further subdivided as :

Rate of change of mass of liquid fuel in spray = Fuel injection rate - Fuel evaporation rate

$$\frac{dm_{f1}}{d\theta} = \frac{dm_{f1}}{d\theta} - \frac{dm_{fv}}{d\theta} \quad (3.58)$$

Rate of change of fuel vapour mass in spray = Fuel evaporation rate - Fuel burning rate

$$\frac{dm_{fv}}{d\theta} = \frac{dm_{fv}}{d\theta} - \frac{dm_{fb}}{d\theta} \quad (3.59)$$

Rate of change of air mass in spray = Air entrainment rate into spray - Air burned rate due to burning

$$\frac{dm_{a1}}{d\theta} = \frac{dm_{a1}}{d\theta} - \frac{dm_{ab}}{d\theta} \quad (3.60)$$

Rate of change of mass of combustion products in spray = Fuel burning rate + Air burning rate

$$\frac{dm_{prod}}{d\theta} = \frac{dm_{fb}}{d\theta} + \frac{dm_{ab}}{d\theta} \quad (3.61)$$

(ii) For the surroundings

Rate of change of mass in surroundings = - Air entrainment rate into spray

$$\frac{dm_{sur}}{d\theta} = - \frac{dm_{as}}{d\theta} \quad (3.62)$$

### Energy Balance

(i) Energy conservation equation for spray

$$\frac{d}{d\theta} [m_{sp} u_{sp}] = \frac{dQ_s}{d\theta} - \frac{dQ_{v,sp}}{d\theta} + \sum_j \frac{dm_j}{d\theta} h_j - p \frac{dV_{sp}}{d\theta} \quad (3.63)$$

L.H.S. of equation(3.63) can be expanded as ;

$$\frac{d}{d\theta} [m_{sp} u_{sp}] = \frac{d}{d\theta} [(m_{as} C_{va} + m_{fl} C_{fn} + (m_{fv} - m_{fb}) C_{v,sp} + m_{prod} C_{v,prod}) T_{sp}] \quad (3.64)$$

Which can be further written as;

$$\begin{aligned} \frac{d}{d\theta} [m_{sp} u_{sp}] = & [m_{as} C_{va} + m_{fl} C_{fn} + (m_{fv} - m_{fb}) C_{v,sp} + m_{prod} C_{v,prod}] \frac{dT_{sp}}{d\theta} \\ & + [C_{va} \frac{dm_{as}}{d\theta} + C_{fn} \frac{dm_{fl}}{d\theta} + C_{v,sp} (\frac{dm_{fv}}{d\theta} \\ & - \frac{dm_{fb}}{d\theta}) + C_{v,prod} \frac{dm_{prod}}{d\theta}] T_{sp} \end{aligned} \quad (3.65)$$

Equating equation(3.63) and equation(3.65);



$$\begin{aligned}
& [m_{as} C_{va} + m_{n1} C_{vn1} + (m_{fv} - m_{fb}) C_{vvsap} + m_{prod} C_{vprod}] \frac{dT_{sp}}{d\theta} \\
& + [C_{va} \frac{dm_{as}}{d\theta} + C_{vn1} \frac{dm_{n1}}{d\theta} + \left( \frac{dm_{n1}}{d\theta} - \frac{dm_{fb}}{d\theta} \right) C_{vvsap} \\
& + C_{vprod} \frac{dm_{prod}}{d\theta}] T_{sp} = \frac{dQ_B}{d\theta} - \frac{dQ_{vvsap}}{d\theta} - p \frac{dV_{sp}}{d\theta} \\
& + h_{n1} \frac{dm_{n1}}{d\theta} - h_{fv} \frac{dm_{fv}}{d\theta} + h_a \frac{dm_{as}}{d\theta}
\end{aligned} \tag{3.66}$$

(ii) Energy conservation equation for surrounding fluids

$$\frac{d}{d\theta} (m, u)_{sur} = - \frac{dQ_{wsur}}{d\theta} - p \frac{dV_{sur}}{d\theta} + h_a \frac{dm_{sur}}{d\theta} \tag{3.67}$$

or

$$\begin{aligned}
m_{sur} C_{va} \frac{dT_{sur}}{d\theta} + C_{va} T_{sur} \frac{dm_{sur}}{d\theta} \\
= - \frac{dQ_{wsur}}{d\theta} - p \frac{dV_{sur}}{d\theta} + h_a \frac{dm_{sur}}{d\theta}
\end{aligned} \tag{3.68}$$

putting  $\frac{dm_{sur}}{d\theta} = - \frac{dm_{as}}{d\theta}$

and volume constraint as ;

$$\frac{dV_{sur}}{d\theta} = \frac{dV_{cyl}}{d\theta} - \frac{dV_{sp}}{d\theta}$$

into equation(3.68);

$$\begin{aligned}
m_{sur} C_{va} \frac{dT_{sur}}{d\theta} - C_{va} T_{sur} \frac{dm_{as}}{d\theta} = - \frac{dQ_{wsur}}{d\theta} \\
- p \frac{dV_{cyl}}{d\theta} + p \frac{dV_{sp}}{d\theta} - h_a \frac{dm_{as}}{d\theta}
\end{aligned} \tag{3.69}$$

(iii) Equation of state for spray

$$pV_{sp} = m_{sp} R_{sp} T_{sp} \quad (3.70)$$

Differentiating both sides;

$$p \frac{dV_{sp}}{d\theta} + V_{sp} \frac{dp}{d\theta} = [m_{su} R_a + (m_{fv} - m_{fb}) R_{fv} + m_{prod} R_{prod}] \frac{dT_{sp}}{d\theta} + [R_a \frac{dm_{su}}{d\theta} + (\frac{dm_{fv}}{d\theta} - \frac{dm_{fb}}{d\theta}) R_{fv} + \frac{dm_{prod}}{d\theta} R_{prod}] T_{sp} \quad (3.71)$$

(iv) Equation of state for surroundings

$$pV_{sur} = m_{sur} R_{sur} T_{sur} \quad (3.72)$$

Differentiating equation(3.72);

$$p \frac{dV_{sur}}{d\theta} + V_{sur} \frac{dp}{d\theta} = m_{sur} R_{sur} \frac{dT_{sur}}{d\theta} + R_{sur} T_{sur} \frac{dm_{sur}}{d\theta} \quad (3.73)$$

Taking volume constraint

$$V_{sur} = V_{cyl} - V_{sp}$$

and putting it into equation(3.73) and simplifying;

$$\frac{1}{V_{sur}} \frac{dV_{cyl}}{d\theta} - \frac{1}{V_{sur}} \frac{dV_{sp}}{d\theta} + \frac{1}{p} \frac{dp}{d\theta} = \frac{1}{T_{sur}} \frac{dT_{sur}}{d\theta} + \frac{1}{m_{sur}} \frac{dm_{sur}}{d\theta} \quad (3.74)$$

Now before the commencement of injection, equation(3.69) and equation(3.74) can be used to calculate  $p$  and  $T_{sur}$  after assuming

$\frac{dV_{sp}}{d\theta}$  and  $\frac{dm_{su}}{d\theta}$  equal to zero.

The thermodynamic properties of air, fuel and combustion products are computed following procedures given in Appendix-F.

Equations(3.66,3.69,3.71 and 3.74) contain changes during time step in four variable parameters concerning the spray and surrounding conditions in the cylinder. The variables are spray volume( $V_{sp}$ ) and temperature( $T_{sp}$ ), the cylinder pressure( $p$ ) and the surroundings temperature( $T_{sur}$ ). These equations are solved by Gauss-Siedal method to give value of these variables at any instant.

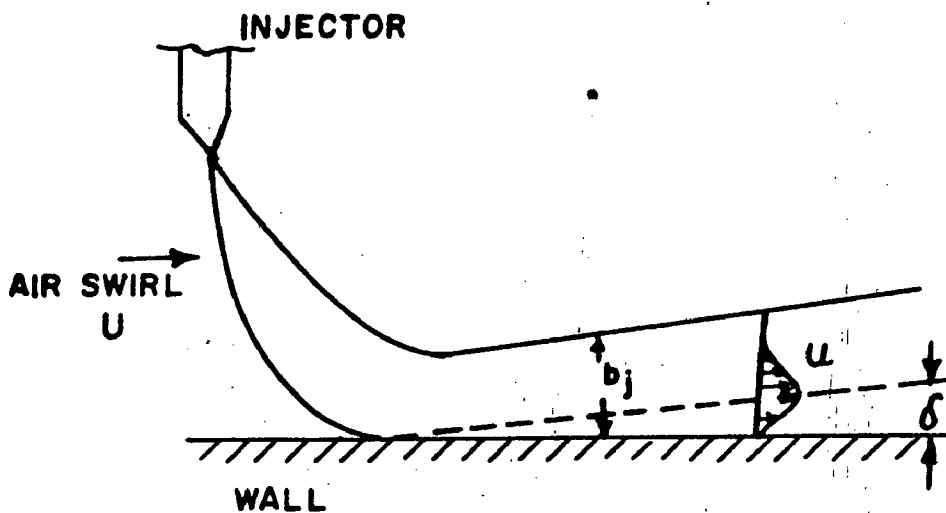


Fig 3.1 Schematic of wall jet growth

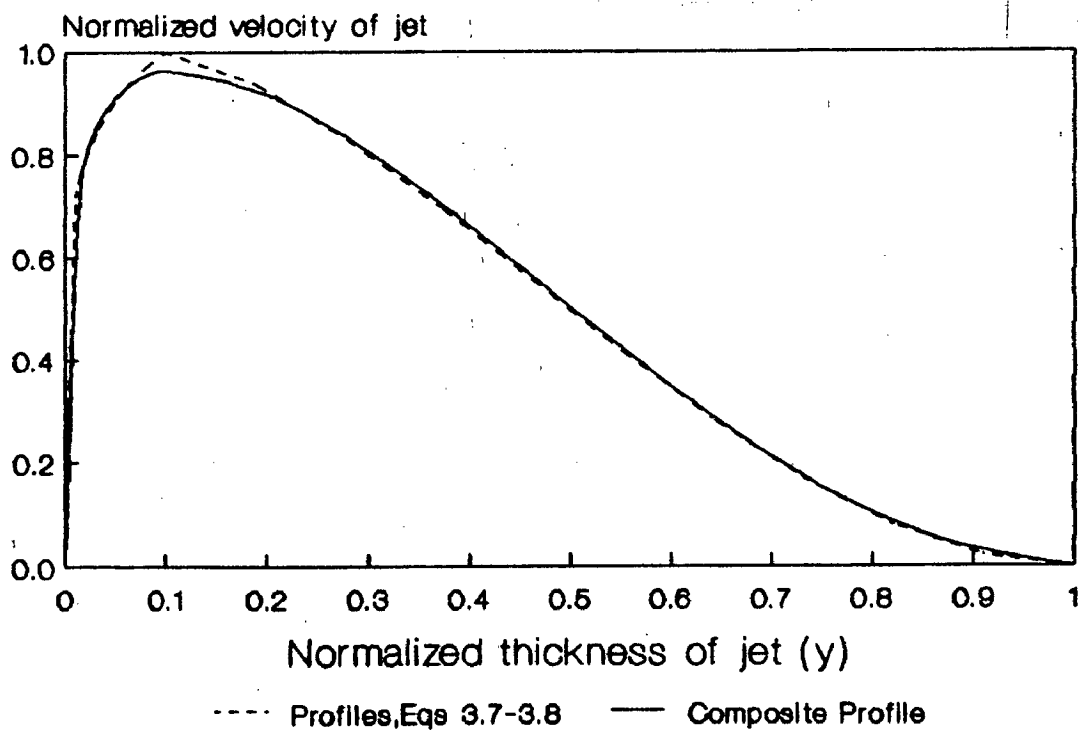


Fig 3.2 Comparison of velocity profiles

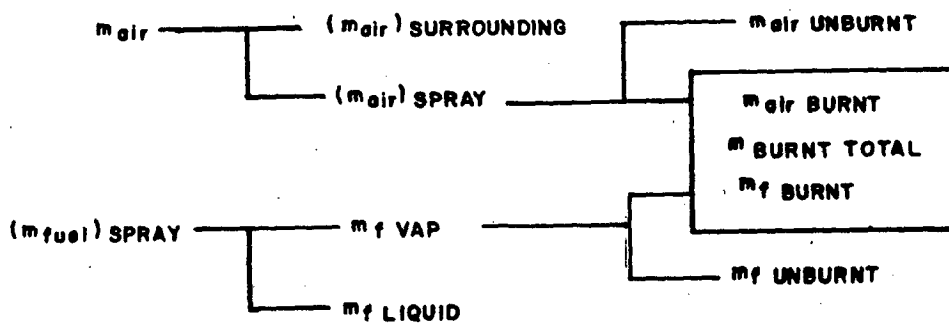


Fig 3.3 Schematic of mass balance in engine

## CHAPTER - 4

### COMPUTER PROGRAM STRUCTURE

#### 4.1 INTRODUCTION

The computer program is developed in a modular fashion based on the formulation described in Chapter-3. The program is designed to work on any operating system compatible with FORTRAN with economic use of computer storage and run time. Computations are done on the PC/386 system with 80387 math processor available at the Indian Institute of Petroleum, Dehradun.

#### 4.2 PROGRAM INPUT

Input data required in the model are listed in Table 4.1. The time step for computation is an input and has a value of 1 degree crank angle. Where necessary for accuracy, this step size is reduced to 0.1 degree crank angle.

#### 4.3 FLOW CHARTS AND PROGRAM MODULES

A flow chart of the computer program is given in Figure 4.1. The main program calls major subroutines supported by other subprograms (Table 4.2). The subprograms listed in Table 4.3 are concerning the expressions relating to similarity profiles, vectorial and integral functions and those needed for calculations of the properties of working substances.

Table 4.1 Program Input

Data concerning	variables
1. Engine dimensions	Bore, stroke, connecting rod length, compression ratio and engine speed
2. Intake conditions	Inlet temperature and pressure
3. Injection parameters	<p>(a) Number of orifices, orifice diameter, injector location angles with respect to X, Y and Z axes and injection timing</p> <p>(b) Plunger lift diagram, diameters of plunger and high pressure pipe, areas of relief valve piston, needle and needle seat, opening force and spring rate of relief valve and injector needle, mass of moving parts of relief valve and injector and length of high pressure pipe</p>
4. Piston geometry parameters	Shape of combustion chamber in X, Y and Z coordinates
5. Valve timings	Inlet valve closing and exhaust valve opening
6. Fuel properties	Number of carbon and hydrogen atoms, density, heat of combustion, surface tension, absolute viscosity, cetane number, inlet temperature and bulk modulus of elasticity

## Table 4.1 continue...

7. Coefficients/ Constants	Coefficients of heat and enthalpy properties and constants for heat transfer coefficient, universal gas constant, polytropic index, stoichiometric air-fuel ratio and drag coefficient
-------------------------------	--



Table 4.2 Usage of Subprograms

Main routines	Purpose	Supporting Subprograms	
		Subroutine	Functions
SPRAY	Defines spray structure before and after the impingement in the presence of swirl. Also calculates air entrained due to turbulent mixing.	SOLEQN CROSS DOT UNVEC SIMP WIMP	EN FW FC SQT FU SWC
ZONES	Defines zones in the spray in both radial and axial directions. Compute SMD, droplet size and fuel mass distribution and rate of burned mass.	SPRAY	
RMASS	Specifies mass of fuel injected, air entrained, spray mass, liquid fuel mass, vapour fuel mass, and mass of burned fuel, unburned air and products of combustion.	ZONES	
GASP	Computes Thermodynamic properties of gases.		
HTR	Computes heat transfer rates and temperatures of walls of cylinder, piston and head.		
COMP	Computes temperature of surrounding fluids and cylinder pressure before start of the injection.	HTR GASP	
ENERGY	Computes cylinder pressure, volume of spray and temperatures of surroundings and spray fluids after the start of injection.	RMASS HTR FL FFV GASP SOLEQN	

Table 4.2 Continue...

INJ	Computes injection rate curves	RKSSK GUPCB
WIMP	Evaluates spray impingement through coordinate geometry considerations.	

Table 4.3 List of Subprograms

Name	Purpose
SOLEQN	Solves simultaneous algebraic equations by Gauss-Siedell method
CROSS	Finds cross product of vectors
DOT	Finds magnitude and projections from vectors
UNVEC	Finds magnitude and direction cosines and angles
✓ SIMP	<u>Integrates using Simpson method</u>
EN	Evaluates entrainment functions
FW	Evaluates integrals of conservation equations both for free and wall regions
FC	Evaluates similarity profile functions of concentration both for free and wall regions
SQT	Finds square root of vectors
FL	Computes specific heat and enthalpy of liquid fuel
FFV	Computes specific heat and enthalpy of fuel vapour
✓ RKSSK	<u>Solves differential equations by Runge-Kutta method</u>
✓ GUPCB	<u>Evaluates equations for fuel injection simulation</u>

Flow chart for injection calculations (subprogram INJ) is shown in Figure 4.2. The input data related to the simulation of injection process are listed at item 2(b) in Table 4.1 and are read in subroutine INJ. In case the injection rates are available to be read directly as input, then the injection simulation routines are avoided by suppressing call of subroutine INJ. This enables the flexibility of either taking the full injection simulation or directly the injection rates as the case may be. Fig 4.3 depicts the interaction of several modules of the program developed. Flow charts for subprograms SPRAY, ENERGY and ZONES are given in Figures 4.4-4.6.

#### 4.4 MODEL OUT PUT

The program output is available in terms of the following quantities of interest:

- i) Injection rate diagram
- ii) Spray motion and trajectory
- iii) Instant and location of spray impingement on the piston
- iv) Rate of air entrainment
- v) Rate of fuel evaporation
- vi) Rate of fuel burning and heat release
- vii) Cylinder pressure, spray temperature and surrounding air temperature as a function of crank angle
- viii) Performance parameters of engine

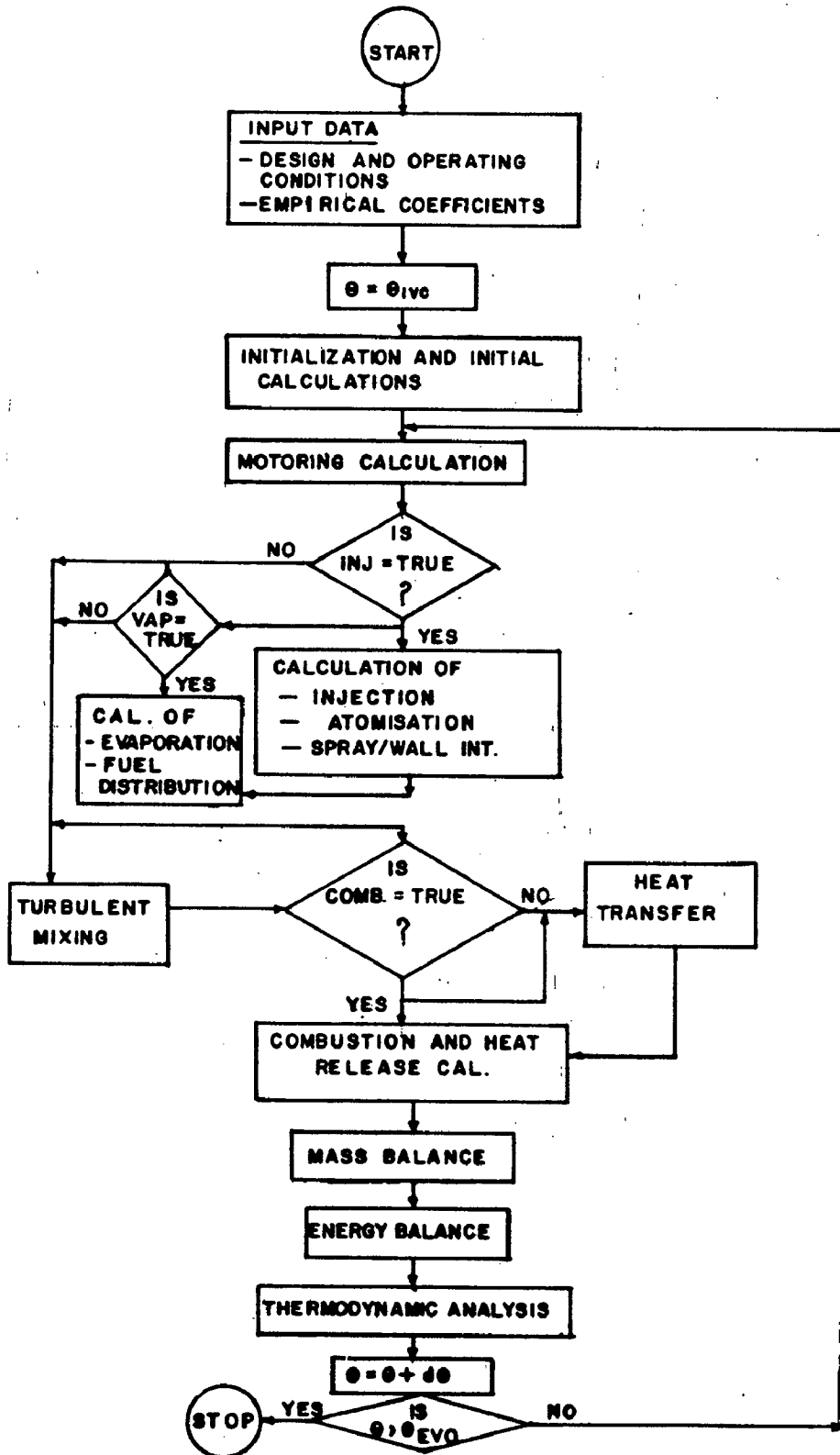


Fig 4.1 Flow chart of full computer program

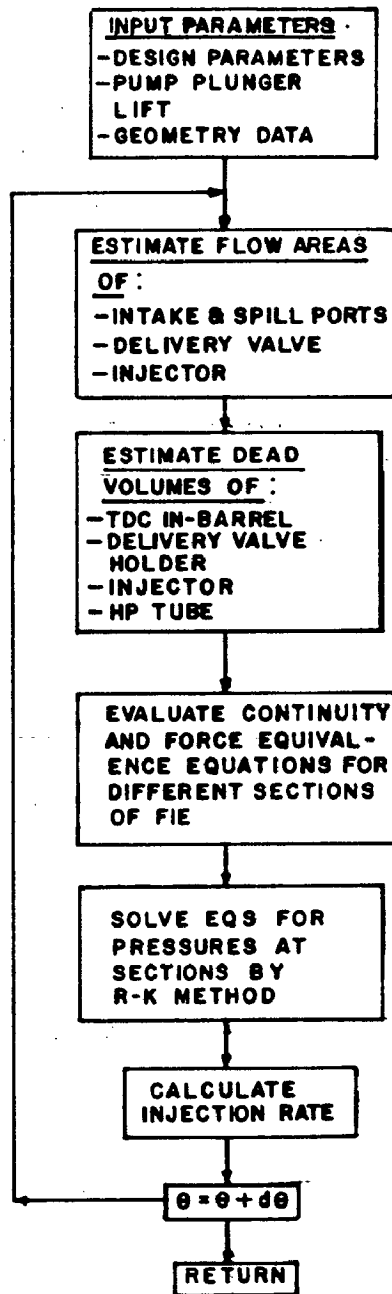


Fig 4.2 Flow chart of subprogram INJ

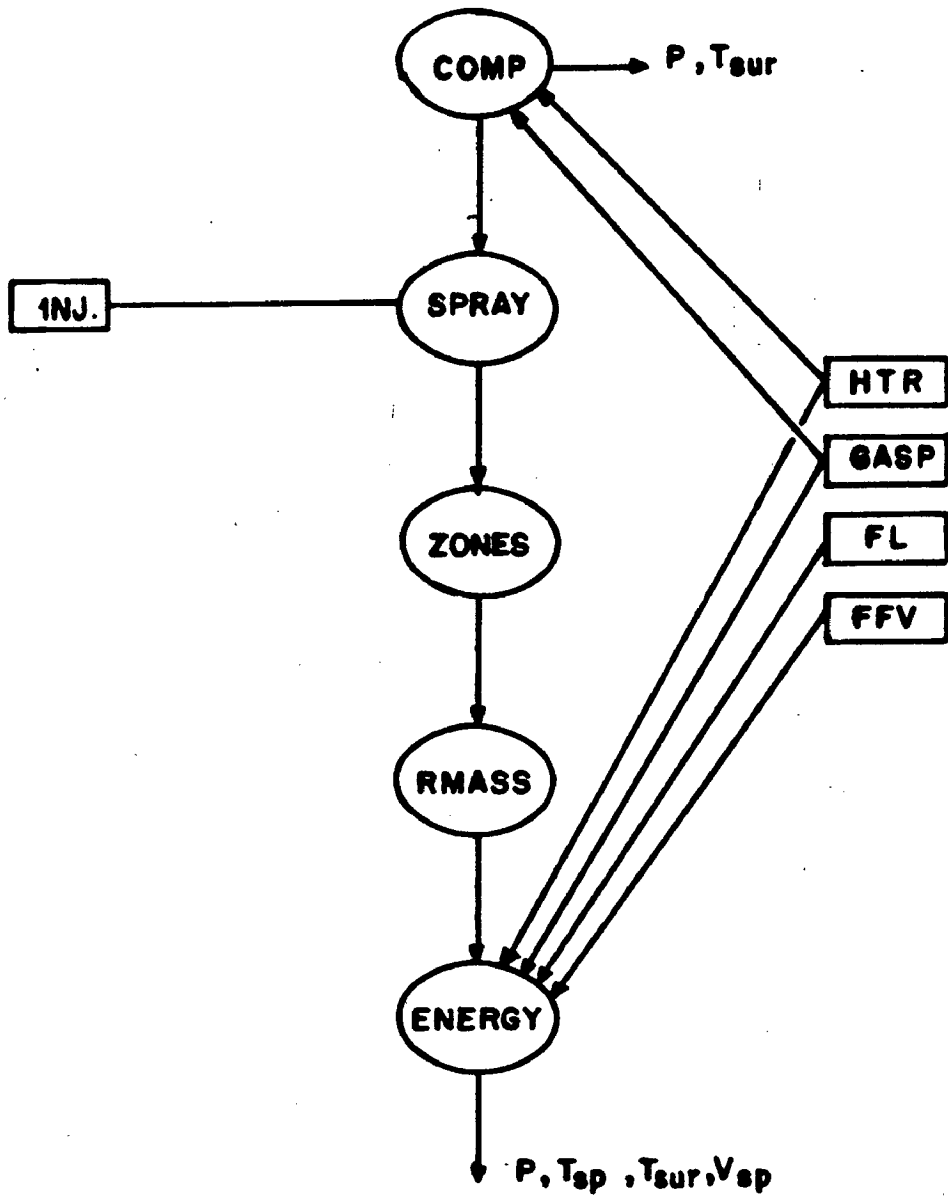


Fig 4.3 Interaction of program modules

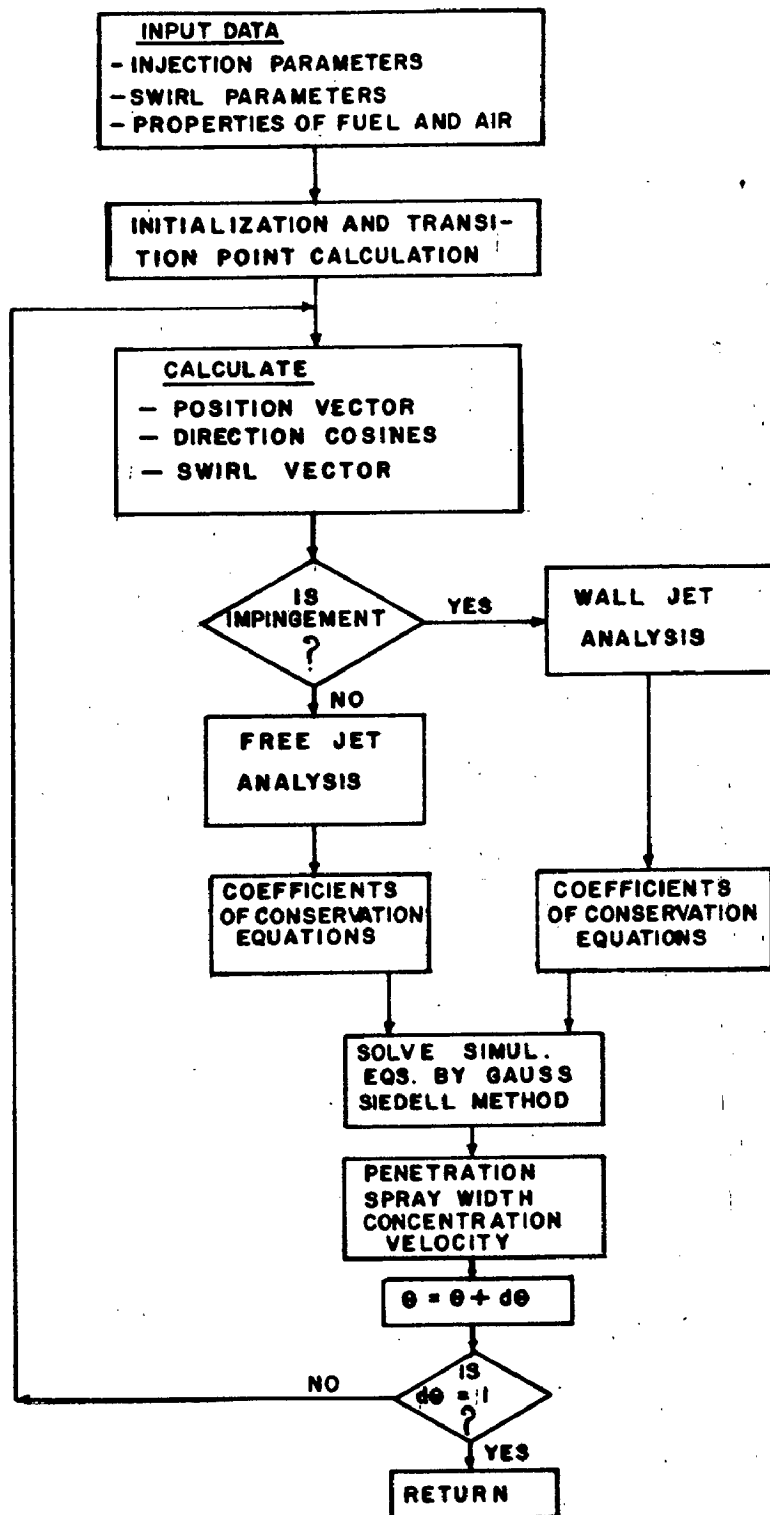


Fig 4.4 Flow chart of subprogram SPRAY



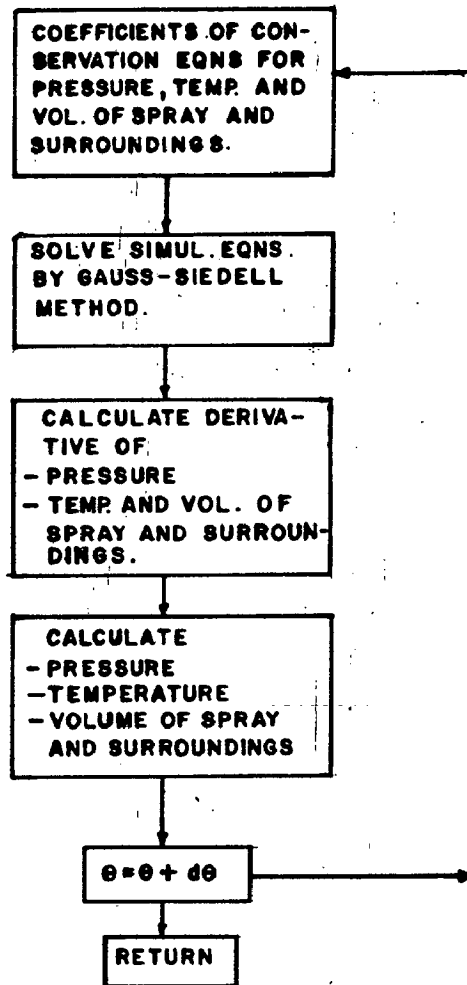


Fig 4.5 Flow chart of subprogram ENERGY

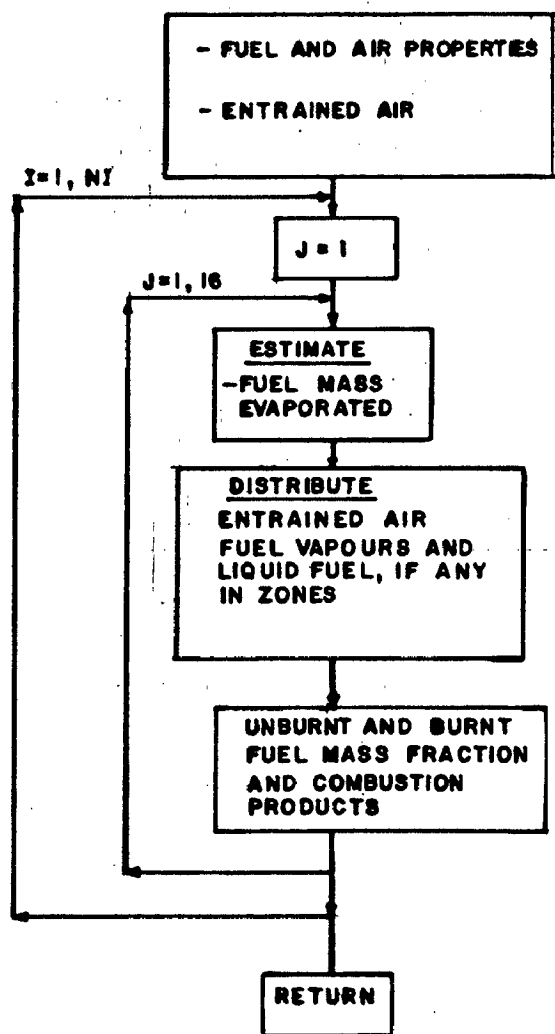


Fig 4.6 Flow chart of subprogram ZONES

## CHAPTER - 5

### EXPERIMENTAL PROGRAM

#### 5.1 GENERAL EXPERIMENTAL PLAN

Verification of the analytical results of cylinder pressure history obtained from the model is done using experimental data generated on three engines. The steady state data recorded during the study include;

- fuel consumption,
- engine speed and
- brake power.

The dynamic data recorded corresponding to crank angle positions are;

- engine cylinder pressure and
- injection characteristics.

The specifications of the three test engines are given in Table 5.1.

#### 5.2 MEASURING INSTRUMENTATION

Ricardo engine is directly coupled to an electric dynamometer which could be used either as a generator or a motor. The general view of the engine and instrumentation is shown in Figure 5.1. Eddy current dynamometer is used for other two engines (engine A and B). The cylinder pressure is measured and processed by a real time data developed by Institut Francais du Petrole. The system is

Table 5.1 Design Data of Different Engines

Parameter	Engine-A	Engine-B	Engine-C
Type of combustion chamber	Cylindrical (Open)	Semidivided (Re-entrant)	Toroidal (Ricardo research)
Bore/Stroke, mm	110/120	115/150	80.3/89
Compression ratio	17	17.7	20
No. of cylinders	2	1	1
Swept volume per cylinder, litre	1.14	1.56	0.45
Number of orifices	4	1	4
Diameter of orifice, mm	0.27	0.36	0.21

commercially available and is designated as DIGITAP an abbreviation of 'Digitization-Angle-Pressure'. A piezo-electric pressure transducer AVL CVK 8QP500CQ is mounted flush with the combustion chamber wall. The time base signal is obtained by a photo-sensitive transducer-'Angle Coder; Model MCB type G-10-76B coupled to the engine crank shaft. For analysis, an average of 128 cycles is taken.

### 5.3 MEASUREMENT OF FUEL INJECTION RATE

The instantaneous injection rates are obtained using TSNITA chamber technique. It essentially consists of injection in a small volume, from which the fuel is discharged through calibrated orifice into a calibrated burette or a fuel weight measurement system. The instantaneous pressure in the small volume of TSNITA chamber is measured by a piezo-electric pressure transducer AVL 12QP300CVK. *averaged over 128 cycles.* The technique has been developed by Research Institute for Fuel Injection Equipment, Moscow, USSR. For determination of the injection rates, the following assumptions are made while using the TSNITA chamber technique.

1. The instantaneous quantity of fuel discharged from the TSNITA chamber is equal to the fuel injected, once the chamber is filled with the fuel.
  2. The effect of fuel compressibility is neglected in the chamber as maximum pressures and rates of pressure rise in the chamber are small.
  3. The discharge co-efficient of the exit orifice of TSNITA chamber is constant for all the upstream pressures.
- The instantaneous pressure of TSNITA Chamber is measured with

the help of 'DIGITAP' pressure acquisition system. The fuel pump of the engine B is fitted on a camshaft box and a variable speed drive is used to drive the camshaft at different speeds. The angle-coder for getting signal for crank angle position is driven separately at twice the speed of camshaft by a small variable speed motor so that it corresponds with the engine speed. The arrangement is shown schematically in Fig 5.2.

#### 5.4 TEST CONDITIONS

Experiments are conducted by varying engine speed and fueling rate. Table 5.2 shows the test conditions for the three test engines. The instantaneous injection rates are only measured on engine-B at different speeds and are shown in Figs 5.3-5.6.

The results of these tests are validated with the model predictions and are included alongwith the other results and validations discussed in Chapter-6.

Table 5.2 Test Conditions of Engines

Engine	Engine Speed RPM	Fueling MM <sup>3</sup> /Cycle-Cyl	Injection Advance, deg, BTDC
Engine-A	1200	58.89	
	1600	62.5	
	1800	61.0	27
	2000	60.2	
Engine-B	1100	87	
	1300	88	27
	1500	86.4	
	1650	85	
Engine-C	1800	23.5	15
	2400	19.0	13
	2400	23.8	13
	3000	18.0	11

ENGINES LABORATORY  
INDIAN INSTITUTE OF PETROLEUM DEHRA DUN.

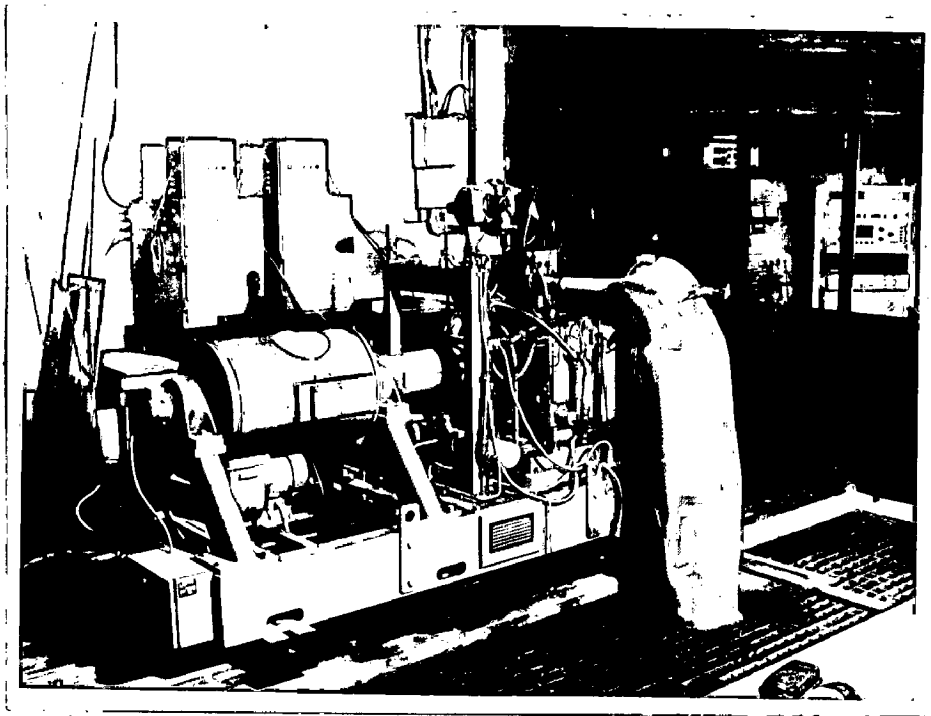


Fig 5.1 General view of Ricardo engine

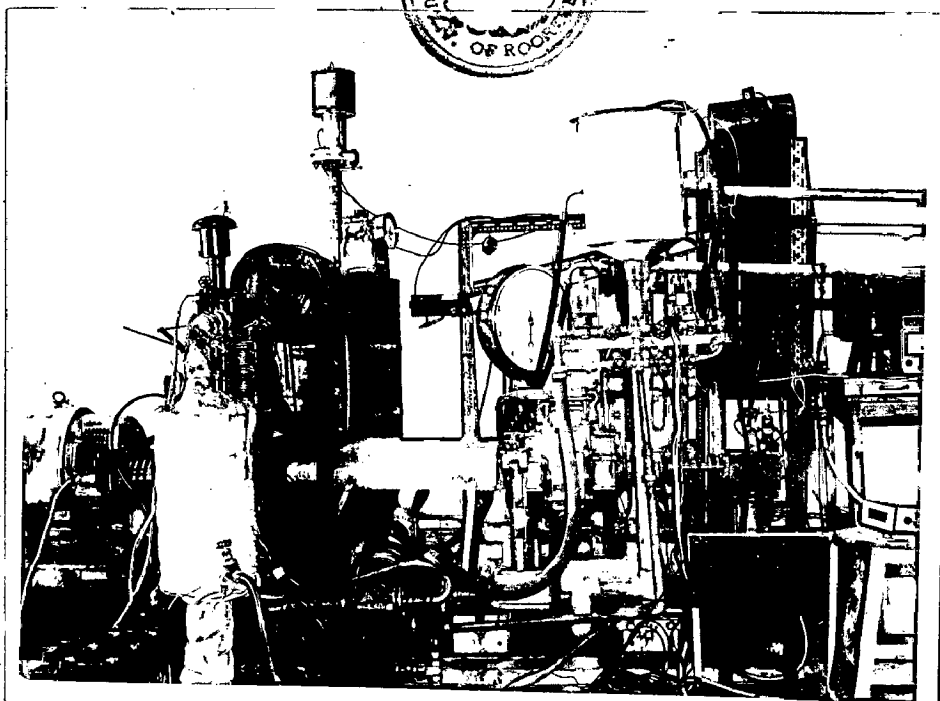


Fig 5.2 General view of arrangement for  
measurement of injection rates



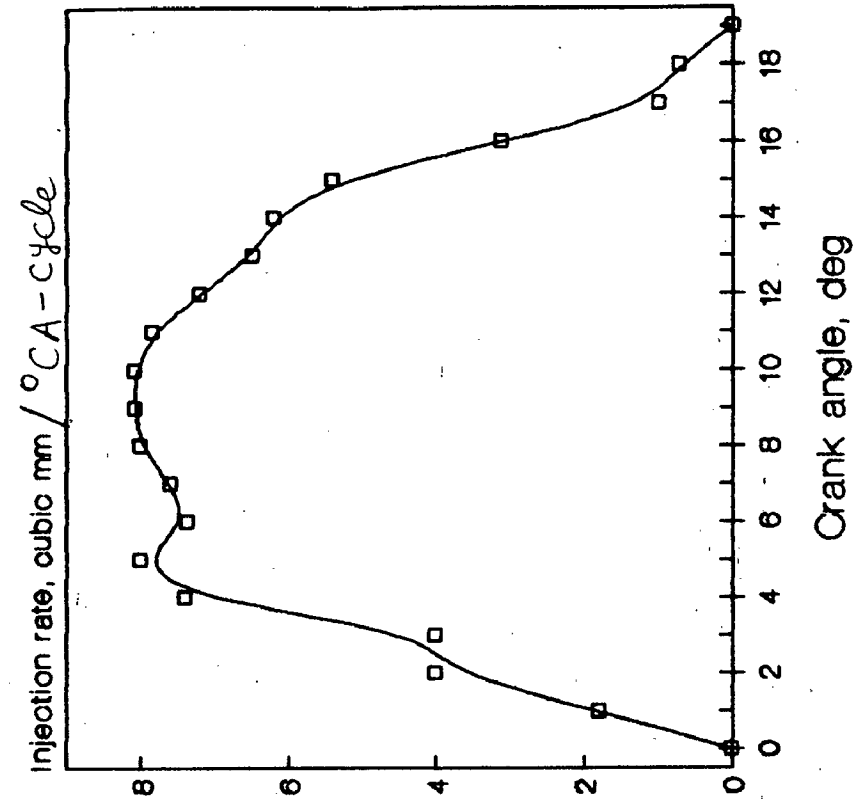


Fig 5.4 Injection rate diagram for engine-B at 1300 RPM

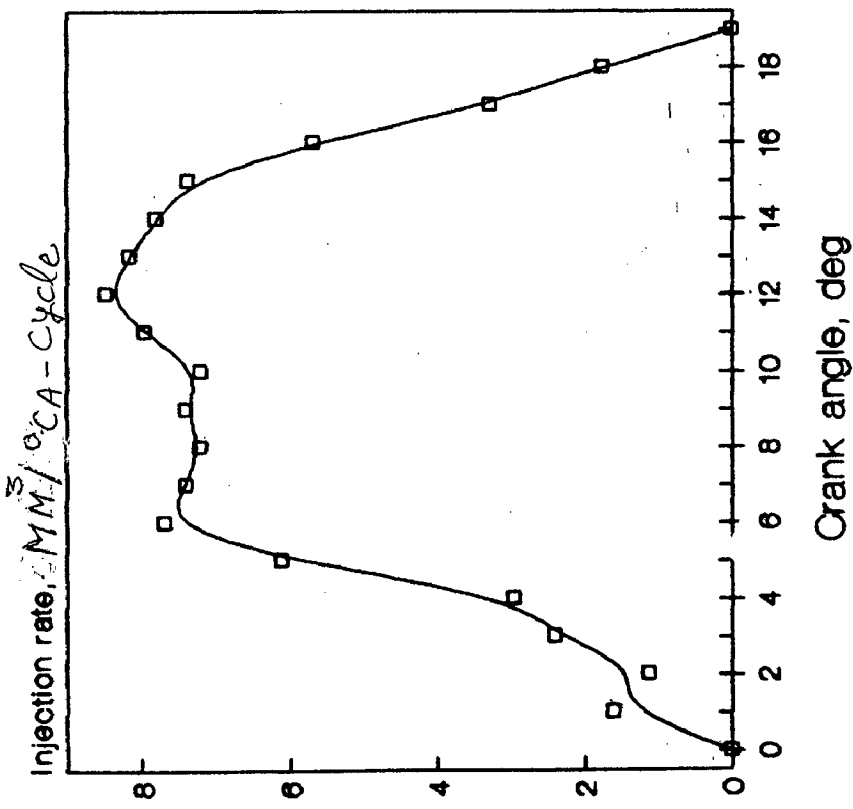


Fig 5.3 Injection rate diagram for engine-B at 1100 RPM

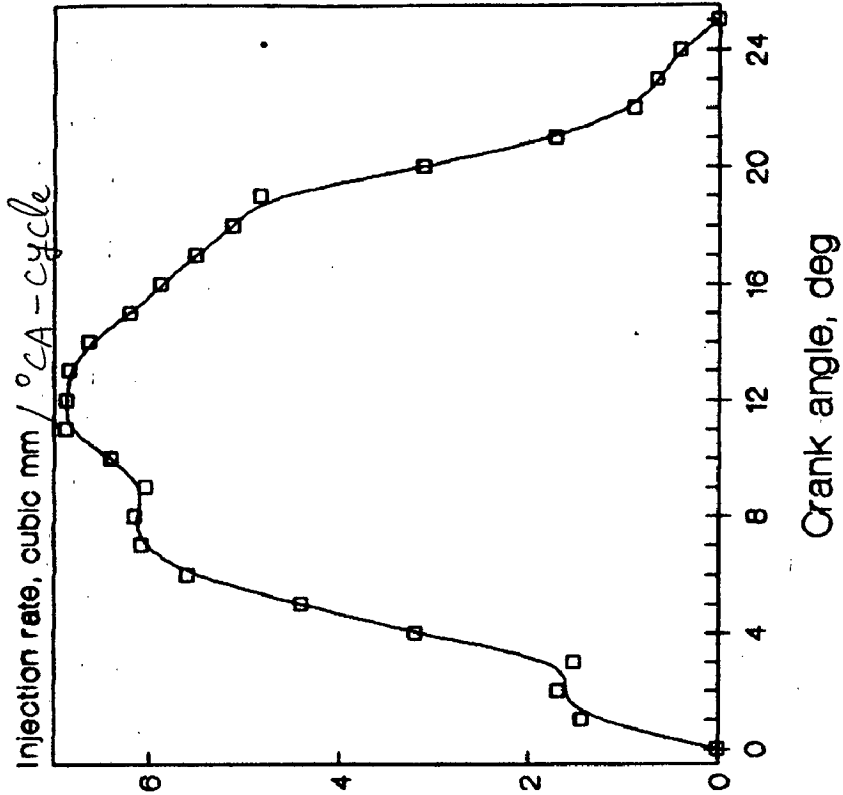


Fig 5.6 Injection rate diagram for engine-B at 1650 RPM

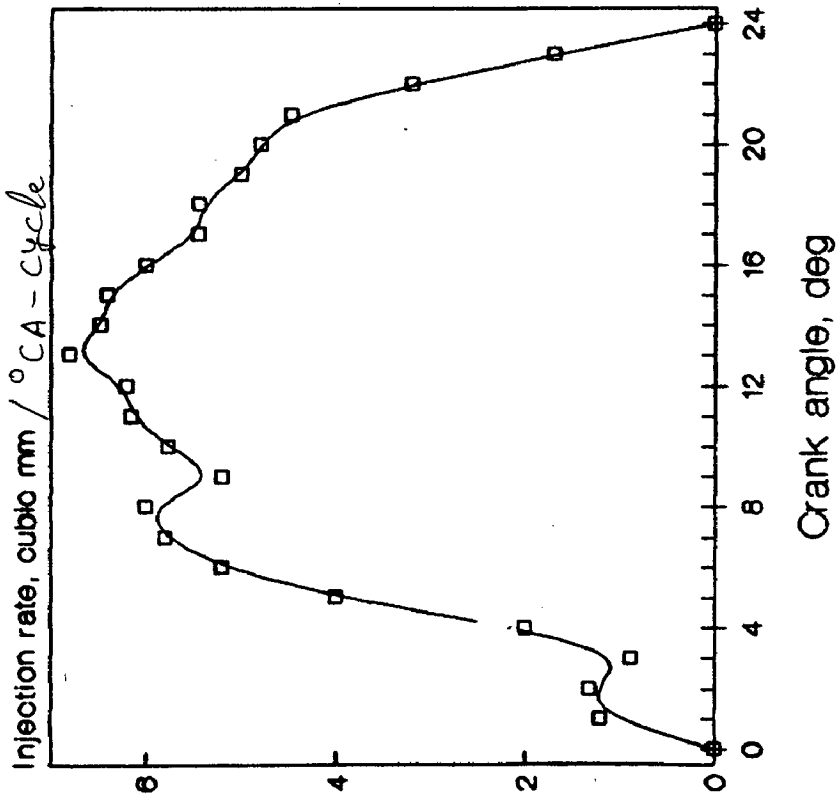


Fig 5.5 Injection rate diagram for engine-B at 1500 RPM

## CHAPTER - 6

### RESULTS AND DISCUSSION

The results of prediction for the following aspects are presented and discussed in this chapter. These include;

- (i) the effect of injection parameters on the trajectory and air entrainment rate of the free spray,
- (ii) the effect of bowl geometry and offset on the air motion during compression,
- (iii) the validation and parametric study of the spray-swirl-wall interaction model,
- (iv) the comparison of the calculated and measured pressure-time histories on three different engines to validate the combustion model, and
- (v) the deductions of the influence of bowl geometry and the air swirl on mixedness and combustion.

#### 6.1 EFFECT OF INJECTION PARAMETERS ON SPRAY CHARACTERISTICS

An effort to evaluate the effect of injection characteristics like injection scheduling, nozzle orifice size and injector location etc on spray trajectory and air entrainment etc, <sup>is made</sup> Further a parametric study is conducted with the help of model considering only the free jet formation of the spray in order to see how the injection characteristics influence the spray formation and mixing in the presence of swirl before impingement. <sup>It is essential that</sup> the free

spray must become fully formed and penetrate certain length in order to avoid wall wetting since the spray is confined to a relatively small space in small DI diesel engines.

The engine geometry and swirl conditions used in the study are given in Table 6.1. An attempt has been made to study the spray development and air-fuel mixing by varying the different injection parameters independently. The injection variables investigated are listed in Table 6.2. The base line injection rate diagram (Case 1) is a simple step function having  $5.6 \text{ mm}^3/\text{deg}$  <sup>cycle</sup> rate of fuel delivery for  $16^\circ$  duration of injection at 1800 rpm. The conditions 2 to 5 in Table 6.2 represent some of the practical combinations of the size and number of orifice holes in the injector nozzle.

In engines, when the injection quantity is varied e.g with change in engine load, both the rate and duration vary simultaneously. However, for this analysis, the injection quantity has been varied by changing the rate and keeping the injection duration constant (Case 6). The effect of shortening the injection duration is studied by increasing the rate of injection maintaining a constant fuel delivery (Case 7).

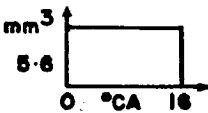
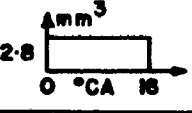
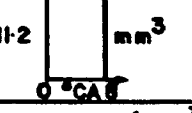
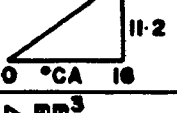

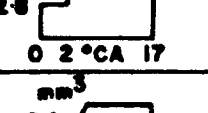
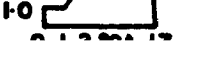
Two different extreme shapes of fuel injection rate curves- positive slope ramp (Case 8) and negative slope ramp (Case 9) are investigated. Additionally, the effect of stepped injection scheduling (Case 10 and 11), which is reported to produce lower peak pressure and a reduced and delayed peak in the energy release(109) is also studied.

By varying the injector location on the cylinder head, the effect of swirl on the spray varies. To investigate this effect, three injector positions viz. side, mid point along a radius and the centre of the cylinder are chosen. Spray angle with axis of

Table 6.1 Engine Specifications

Engine type	Single cylinder engine
Bore/stroke, mm	125/135
Compression ratio	17:1
Engine speed, rpm	1800
Injection direction	10° (from injector axis)
Swirl ratio	3
Swirl direction	Clock-wise

Table 6.2 Input parameters for injection conditions

CASE No.	NOZZLE HOLE SIZE Nos. x DIA., mm	INJECTION SCHEDULING	Calculated MASS AVERAGE MEAN INJECTION PRESSURE MPa	REMARKS
1.	4 x 0.35		24.0	BASE LINE
2.	3 x 0.4	"	25.0	NOZZLE HOLE SIZE EFFECT
3.	6 x 0.3	"	20.0	
4.	4 x 0.3	"	44.0	
5.	3 x 0.35	"	42.4	
6.	4 x 0.35		6.0	
7.	4 x 0.35		96.0	
8.	4 x 0.35		48.0	EFFECT OF INJECTION SCHEDULING
9.	4 x 0.35		48.0	
10.	4 x 0.35		22.0	
11.	4 x 0.35		21.0	

the engine cylinder is another variable considered for these parametric studies. The important parameters of the spray propagation identified are - spray tip penetration, spray to swirl momentum ratio and the air entrainment.

#### 6.1.1 Effect of Nozzle Size/Flow Area

With fixed duration and rate of injection, the nozzle flow area is varied by changing both the number of orifices and their diameter. To maintain the cyclic fuel delivery constant, different injection pressures are needed for different orifice numbers/size combinations. The momentum change experienced in the five Cases 1-5 studied here are attributed to the changes in the fuel mass flow rate and the injection velocity. The nozzle with the largest number of holes and having smallest orifice diameter (Case 3) has the lowest spray to swirl momentum ratio and shows the maximum deflection (Fig 6.1). For side injection, the air momentum at the spray tip continuously decreases as it moves towards the axis of cylinder, thus resulting in an increase of the momentum ratio giving rise to the peak seen in Fig 6.2.

Higher penetrations (Fig 6.3) are achieved when the nozzle size is large with a fewer number of orifices. However, the effect of the orifice size is more pronounced, as shown by the curve for Case 5 vis-a-vis Case 4, due to the reason that the total flow area varies as second power of the orifice diameter, as against the linear relationship with the number of holes. The effect of injection pressure (Case 5 vis-a-vis Case 3) is even more significant. Larger tip penetrations with higher injection pressure and larger hole diameter are reported in the work of Elkotb and Rafat(90) and Kuo and Bracco(171), respectively. The

experimental evidence(172) of the increased air entrainment and spray advancement with increase in the injection pressures are confirmed in the predictions of the present work.

The orifice size has a dominant effect on the air entrainment. It is illustrated by Fig 6.4, when the differences in air entrainment between Case 4 (0.3 mm dia) and Case 2 (0.4 mm dia) are compared with the differences between Case 4 (4 holes) and Case 3 (6 holes). The analysis thus, helps in selecting the orifice size fulfilling the requirement of higher air entrainment alongwith good penetration and fuel atomization requiring higher injection pressures.

#### 6.1.2 Injector Location

For injection conditions of Case 1, three different injector positions i.e side, mid-way and central are investigated. Due to variation in the location, at a given time after the start of injection, the corresponding sprays would experience different air velocities. A continually increasing velocity of the swirling air is realized by the growing spray as the origin of the spray moves towards the centre from the side. In the case of central spray, a higher entrainment (Fig 6.5) in the later stage and slightly faster drop in tip velocity (Fig 6.6) in the earlier period are observed. This is mainly attributed to the higher differences in spray and air velocities (higher excess spray velocity) in the early period.

At 7° CA after injection, the air entrainment is about 30 percent higher in the case of the central injection compared to the other cases. This may be explained on the basis that the orientation of spray relative to air velocity vectors exert a significant influence on the spray history. The point at and the

extent to which the air motion alters the spray development depends upon relative values of the momentum of swirl and momentum of injected fuel (70). Fig 6.7 and Fig 6.8 show the spray deflection and momentum ratio plot. A peak in the momentum ratio for the spray originating from the mid-position is possibly due to the spray being near to the center of cylinder at that particular instant, where very low swirling air velocity is experienced.

### 6.1.3 Injection Quantity/Duration Effect

For the base condition of Case 1, the two situations analyzed here include;

- (i) Half the injection rate ( $2.8 \text{ mm}^3/\text{deg}$  <sup>-cycle</sup>) but the same injection duration (Case 6).
- (ii) Half the injection duration and the rate of injection correspondingly increased to  $11.2 \text{ mm}^3/\text{deg}$  <sup>cycle</sup> (Case 7).

In both the cases, the cyclic fuel delivery is kept the same as in the base case.

The results for the side injection with the injector perpendicular to the cylinder axis (Figs 6.9-6.14) and the central injection with the spray angle of  $20^\circ$  with the horizontal plane (Figs 6.15-6.19) are presented. When the injection duration is reduced, the deflection of spray (Fig 6.9) by air swirl decreases considerably and results into a peak in the momentum ratio curves (Fig 6.10) due to its proximity to the centre of the cylinder. Reducing the injection duration by half amounts to only 19 percent reduction in the penetration length (Fig 6.11).

The spray penetration and the air entrainment generally follow the trend of the injection pressure effects (Fig 6.11 and 6.13). The tip velocity curves (Fig 6.12) are observed to follow the



trends of local swirl velocities (Fig 6.14) particularly in the later stages where the spray moves in the direction of swirl.

The tip penetrations in X, Y, and Z directions are compared in Figs 6.15-6.17 and the resultant spray trajectories are given in Fig 6.18 for the three-dimensional situation. The trends of the spray penetration are opposite to that of the side injection in the sense that the spray having lower rates of injection is prohibited by the swirl to penetrate towards the periphery of the cylinder. The air entrainment (Fig 6.19) process is mainly governed by the injection pressure.

#### 6.1.4 Injection Rate Curve

The effect of different shapes of the injection rate curves on the spray development are investigated for the sprays originating from the side as well as the centre of the cylinder. For the side injection, the two-dimensional spray trajectories and the corresponding momentum ratios obtained from different injection rate curves are shown in Fig 6.20 and Fig 6.21, respectively. The effect of the initial velocity of injection and the momentum ratio is quite significant on the spray deflection. The sprays with the positive slope ramp (Case 8) and the stepped injection (Case 10 and 11) having lower injection rates in the beginning are deflected considerably towards the cylinder wall. Fig 6.22 shows that, among the various cases considered, the air entrainment capability of the spray having higher mass averaged injection pressure seems superior. This may be emphasized that the injection scheduling shapes having lower injection rates in the beginning entrain less air, but the overall fuel-air mixing is controlled by the combined effect of the mass averaged injection pressure and the initial

injection rates.

For the central injection, the three-dimensional spray development is presented in Figs 6.23-6.26. Fig 6.27 shows the air entrainment rate for the central injection, where a higher air entrainment compared to the side injection (Fig 6.22) is observed for all the types of injection rate curves studied. The reason for this is, possibly, the higher excess spray velocity in the former case(100). It is observed that the initial injection rate is one important variable influencing the fuel-air mixing of the sprays.

The effect of sprays with positive slope ramp (Case 8) and negative slope ramp (Case 9) on the rate of air entrainment and the co-efficient of air utilization (ratio of air entrained to the total mass trapped in the engine cylinder) is also studied taking into account also the air entrainment during turbulent mixing. Figs 6.28-6.29 show the results. It can be observed that the higher initial rate of injection (case 9) helps in utilizing (entraining) most of the air available in the cylinder at about  $30^\circ$  CA after the start of injection, whereas smaller initial rate of injection (case 8) results in utilizing only 50 percent of the available air even after  $50^\circ$  CA. It emphasizes the significance of the initial rate of injection as far as fuel-air mixing is concerned.

#### 6.1.5 Effect of Spray Angle

The studies are carried out for central injection sprays having  $10^\circ$ ,  $20^\circ$ ,  $30^\circ$  and  $40^\circ$  inclination with the horizontal plane. The spray penetration in Z-direction and corresponding trajectories are shown in Fig 6.30 and 6.31, respectively. The sprays having higher inclination tend to go deeper in the engine bowl, while the

air entrainment (Fig 6.32) more or less remains the same for all the cases. There is a marginal variation in the air entrainment far away from the nozzle tip.

## 6.2 EFFECT OF BOWL GEOMETRY AND OFFSET ON AIR MOTION

Fig 6.33 shows a comparison between the predicted mean air motion expressed in terms of normalized angular momentum (the ratio of instantaneous angular momentum to the angular momentum at exhaust port closing) accounting for viscous friction and the data of Mckinley et al(5) computed using a multi-dimensional flow code. The generally assumed constant angular momentum is found to decay due to the effect of friction at cylinder walls. The slight variations in the predicted results of the angular momentum compared to the data of Reference 5 is attributed to the absence of criterion for turbulent dissipation effect in the present analysis. When taken into account, this should further decrease the momentum level(7). The predicted swirl ratio at TDC of 12.2 in the present analysis compares well with the average TDC swirl ratio of 12.9 for the centered cylindrical cup obtained by linear inter- and extra-polations of the velocities measured by Iijima and Bracco(29) using the Laser Doppler Anemometry technique (refer Table 6.3).

Further, the compression swirl predictions are made for commonly used piston bowl shapes, size and position. The details of bowl geometries studied are given in Table 6.4. These include the cylindrical, the re-entrant and two designs of the open chamber variety. These bowl geometries are fitted interchangeably in an engine whose specifications are given in Table 6.1. The volume of

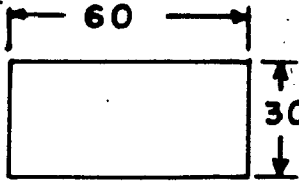
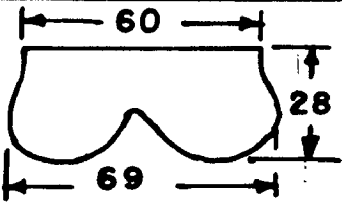
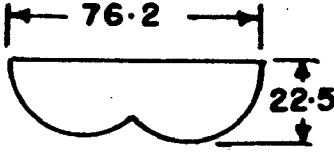
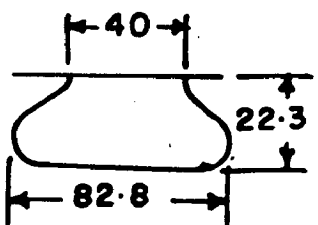
Table 6.3 Average TDC Swirl Ratio

---

Parameter	Predicted	Experimental (29)
Average TDC swirl ratio	12.2	12.9

---

Table 6.4 Different shapes of piston bowl

Shape No.	Shape of bowl mm.	Type of Combustion Chamber	Moment of inertia of bowl per unit mass, mm <sup>2</sup>
C		Cylindrical	450
1		Open	591
2		Open	641
3		Re-entrant	724

the combustion chamber and the compression ratio are therefore, maintained constant in these cases.

The results of predictions of compression swirl neglecting the wall friction for different bowl configurations are shown in Fig 6.34. It is observed that the re-entrant bowl has the minimum and the cylindrical bowl the maximum swirl level because of the maximum and minimum values of moments of inertia, respectively. The replacement of a cylindrical shape bowl with another bowl geometry having the same entry diameter and equal bowl volume (refer shape-1 in Table 6.4) shows about 12 percent decrease in swirl intensity at top centre position. It brings out that the assumption of an equivalent cylindrical bowl geometry, whenever made, is not justified and causes an overestimation in the swirl level.

On a cylindrical bowl geometry, the effect of bowl offset (distance between cylinder and bowl axes) represented as a function of engine bore are studied and the results concerning compression swirl for 0, 5 and 10 percent offset are computed (Fig 6.35). The bowl offset is accounted for in the moment of inertia calculations. An increase in the offset shows a reduction in the swirl level due to enhanced gas inertia. A decrease of about 12 percent in the swirl level at top centre position for an bowl offset of 10 percent shows that the assumption of central bowl-in-piston overestimates the swirl during compression. The wall friction is assumed to be unaffected due to the bowl offset in the analysis. It has been reported that increasing the offset virtually had no effect on friction torque on the air(41).

### 6.3 VALIDATION AND PARAMETRIC STUDY OF SPRAY-SWIRL-WALL INTERACTION MODEL

In this section, results of the predictions of the spray motion-both in free and wall regions are discussed. The predictions are validated with the experimental data taken from published literature. Results on the influence of the combustion chamber geometry on fuel-air mixing are also presented. These results are given in Figs 6.36-6.46.

#### 6.3.1 Spray Penetration and Velocity

Fig 6.36 shows the spray penetration extending in the wall region and Fig 6.37 has the spray tip velocity results. The wall jet commences after 0.8 ms from the start of injection (Fig 6.36). The predictions of the penetration and velocity data are comparing well with the experimental results of Tsunemoto and Ishitani(173) obtained on a simulated combustion chamber. There is a slight underprediction in the tip velocity results of the early period.

Fig 6.38 compares the calculated spray penetration along the wall with the experimental data observed under simulated diesel engine conditions(174) for three different rail pressures of 4.7, 6.1 and 7.8 MPa in a constant volume bomb using high speed photography technique. The predictions compare well except some overprediction after about 0.6 ms, which may be due to the fact that the experimental data were obtained from high speed movies of the back-lit spray pattern and the start of injection could not be exactly determined possibly due to the limited frame rate of the camera(174).

Fig 6.39 compares predictions of the spray tip penetration with the experimental data of Hiroyasu and Nishida(175) at

different air velocities. The spray impinges on the wall after 1 ms. Although, the general trends are in agreement, the differences in the compared results are likely due to the possible errors in reading of the experimental data from photographs(175).

The influence of the dimensions of cylindrical bowl on spray penetration at the instant of impingement normalized with maximum free jet penetration is studied and plotted against different combinations of the bowl diameter to bore ratio ( $d/D$ ) as shown in Fig 6.40. It can be observed from the results (Fig 6.40) that the penetration length of the deflected spray at the instant of impingement increases with the increase of  $d/D$  ratio from 0.4 to 0.48 but reduces with the increase of  $d/D$  ratio greater than 0.48. It is due to the fact that, in the case of  $d/D$  ratio larger than 0.48, the depth of combustion chamber becomes smaller and the spray impinges on the bottom surface of the bowl instead of the side walls. Hence, it can be said that the model predictions may help in selecting injection, air motion and bowl geometry parameters in order to make use of the benefit like increased air entrainment characteristics of the wall jet formation without suffering any penalty on account of wall wetting due to early impingement.

### 6.3.2 Spray Growth

The predicted results of the spray growth in terms of the half spray width based on the test conditions of Nishida et al(176) are compared with the experimental values in Fig 6.41. The half spray width defined as the radial distance between the spray axis and the farthest dispersed spray boundary is measured by them through microscopic observation of the real image of the spray. The

measurements are taken for the diesel spray injected into a high pressure bomb with the help of holography technique. The predictions compare well with the experimental data.

Fig 6.42 compares computed volume of the impinging spray at three ambient densities of 6.15, 9.23 and 12.3 Kg/m<sup>3</sup> with the experimental data of Katsura et al(107). The spray tip reaches the wall at 0.2 ms after the start of injection. The predictions of model compare well with the experimental data at different air densities.

### 6.3.3 Air Entrainment

Air entrainment is an important parameter controlling air-fuel mixing. Variations in the mass of air entrained as a function of penetration (non-dimensionalized with the equivalent orifice diameter  $d_e$ ) for free and wall regions are plotted in Fig 6.43, showing that the presence of swirl and the wall both enhance the mixing. The comparison of the air entrainment data of the free region taken from Reference 110 given at several injection pressures to that predicted in the model is found to be satisfactory.

The prediction of the rate of air entrainment and the mass of air entrained during the spray formation obtained on an engine specified in Table 6.1 are given in Fig 6.44 and Fig 6.45, respectively. In these results, the instant of commencement of wall influence and the enhanced air entrainment due to wall jet flow are depicted. The increased air entrainment after impingement is the combined effect of increased axial entrainment, the spray surface area available for entrainment and the wall shear stress.

Fig 6.46 compares the influence of the depth of a cylindrical



bowl keeping the same volume on the rate of air entrainment. The effect shown is due to different instant of impingement of the spray for different combinations of the bowl to piston diameter ratio ( $d/D$ ) studied here. The smaller bowl diameter (50 mm) results in a higher amount of air entrainment (Fig 6.46).

#### 6.4 VALIDATION OF COMBUSTION MODEL

The model prediction results are validated with the measured pressure-time histories obtained in the laboratory on three different engines specified in Table 5.1 of Chapter-5.

Figs 6.47-6.58 show the comparison of measured and predicted pressure-time histories for data obtained on three test engines at varying operating conditions. Figs 6.47-6.50, Figs 6.51-6.54 and Figs 6.55-6.57 are the results at different speeds for the engine-A, engine-B and engine-C respectively. Fig 6.58 shows the result of varying the fuel delivery from 19 to 23.8 mm<sup>3</sup>/stroke at 2400 rpm for engine-C.

The above comparison of experimental and predicted pressure-time histories shows that the model responds well to the changes in the engine size, injection and combustion system of each engine design. The variations between the model and the experimental values are found to be within 3 percent.

#### 6.5 STUDY OF COMBUSTION CHARACTERISTICS

Since the rate of air entrainment and the mixing rate are controlling the combustion process, it is considered necessary that

the relationship between the air entrainment rate and fuel mass burning rate be studied from the model. For this purpose the test data of a research engine (engine-C), having combustion chamber geometry as shown in Fig 6.59 are chosen.

Fig 6.60 shows the rates of fuel injected, vaporized and burned. The fuel injection rate is computed with the help of fuel injection simulation model. The fuel mass burning rate curve contains the three distinct stages of combustion (Fig 6.60):

- (i) premixed combustion phase which occurs at the end of the ignition-delay period and consumes the fuel which gets mixed with enough air during ignition delay to form a flammable mixture,
- (ii) diffusion-combustion phase during which the rates of burning and heat release are considerably lower than those during the premixed phase and
- (iii) the combustion tail region in the end.

It is clearly observed here that a major portion of the fuel is burned in the diffusion mode which is mixing controlled.

Fig 6.61 contemplates the fuel mass fraction burned comparing the influence of the combustion chamber wall on the fuel burning. It may be seen that the fuel burning is accelerated on impingement due to a higher amount of air entrainment. Fig 6.62 shows the time history of the fuel mass injected, vaporized, combusted and under-mixed as a percent of fuel injected. The combustible fuel mass fraction is defined by integrating those fuel-air mixtures which have the equivalence ratios within the rich and lean limits of combustion specified in the model formulation. The amount of under-mixing is defined by integrating the amount of fuel available in the mixtures richer than the rich limit of combustion.

The effect of swirl on the preparation of a combustible fuel mass and the fuel mass burned are shown in Fig 6.63 and Fig 6.64 respectively. The swirling air enhances mixing, due to an increased air entrainment, resulting in a higher amount of combustible mixture formation (Fig 6.63) and a faster fuel burning (Fig 6.64).

The effect of the cylindrical bowl diameter keeping the same bowl volume on combustible fuel mass and the fuel mass fraction burnt are shown in Fig 6.65 and Fig 6.66 respectively. The three bowl diameters, 30 mm, 40 mm and 50 mm having the bowl depth corresponding to the fixed bowl volume are considered. The smallest bowl diameter of 30 mm allows the faster formation of the combustible mixture (Fig 6.65) and the early burning of fuel in the cycle (Fig 6.66) due to an early impingement of the spray on the walls of the combustion chamber and the higher amount of air entrainment. In the case of 50 mm bowl diameter, the spray impinges on the bottom surface of the bowl instead of the side walls due to the reduced depth, resulting in higher air entrainment compared to 40 mm diameter bowl. These plots relate the influence of the size of the bowl on the rates of fuel burning.

These results alongwith the experimental pressure-time data establish a consistent prediction capability of the model developed.

## 6.6 IMPLICATION OF RESULTS FOR SMALL DI ENGINES

The results of model prediction show that the analysis of the spray growth along the wall of the combustion chamber is central to the accurate prediction of the fuel-air mixing and combustion for

small DI diesel engines due to the reasons as discussed in Chapter-2. Since an earlier analysis of data, concerning the effect of engine size, made by Uyehara et al(44,160) suggest that in a well developed engine, the negative effect of reduction in per cylinder displacement on fuel efficiency is reduced considerably, a proper matching of the fuel injection, air motion and piston bowl shape particularly, in small diesel engines assumes a very high importance. The consideration of the fuel impingement on the wall is an important aspect and the usefulness of mathematical simulation models with this feature is ever increasing. The work presented in this thesis is an attempt in this direction.

The results of the model prediction suggest that the deflected spray should be so oriented as to obtain the minimum wall wetting and the maximum air entrainment during spray growth along the wall. The model has a potential to compute wall wetting also, if a detailed analysis of the spray break-up and evaporation characteristics is made.

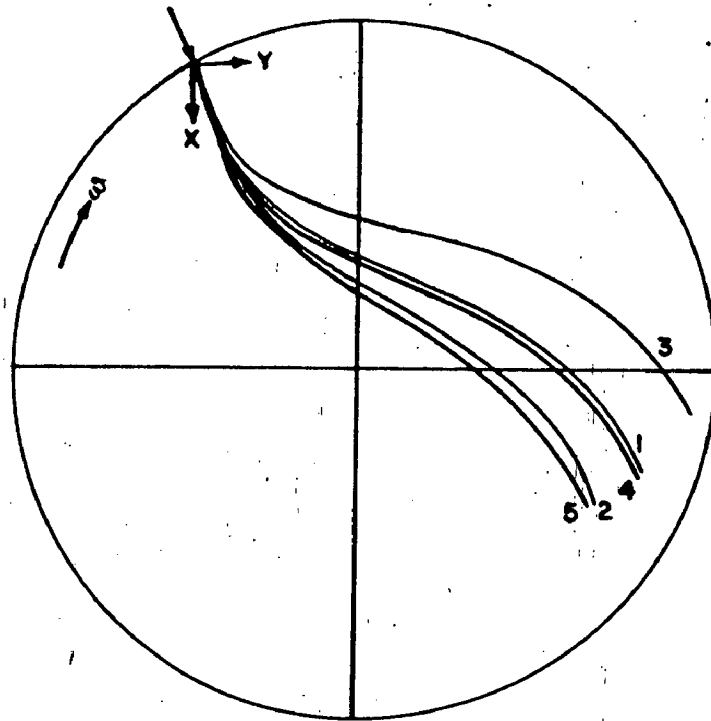


Fig 6.1 Effect of nozzle geometry on spray trajectory

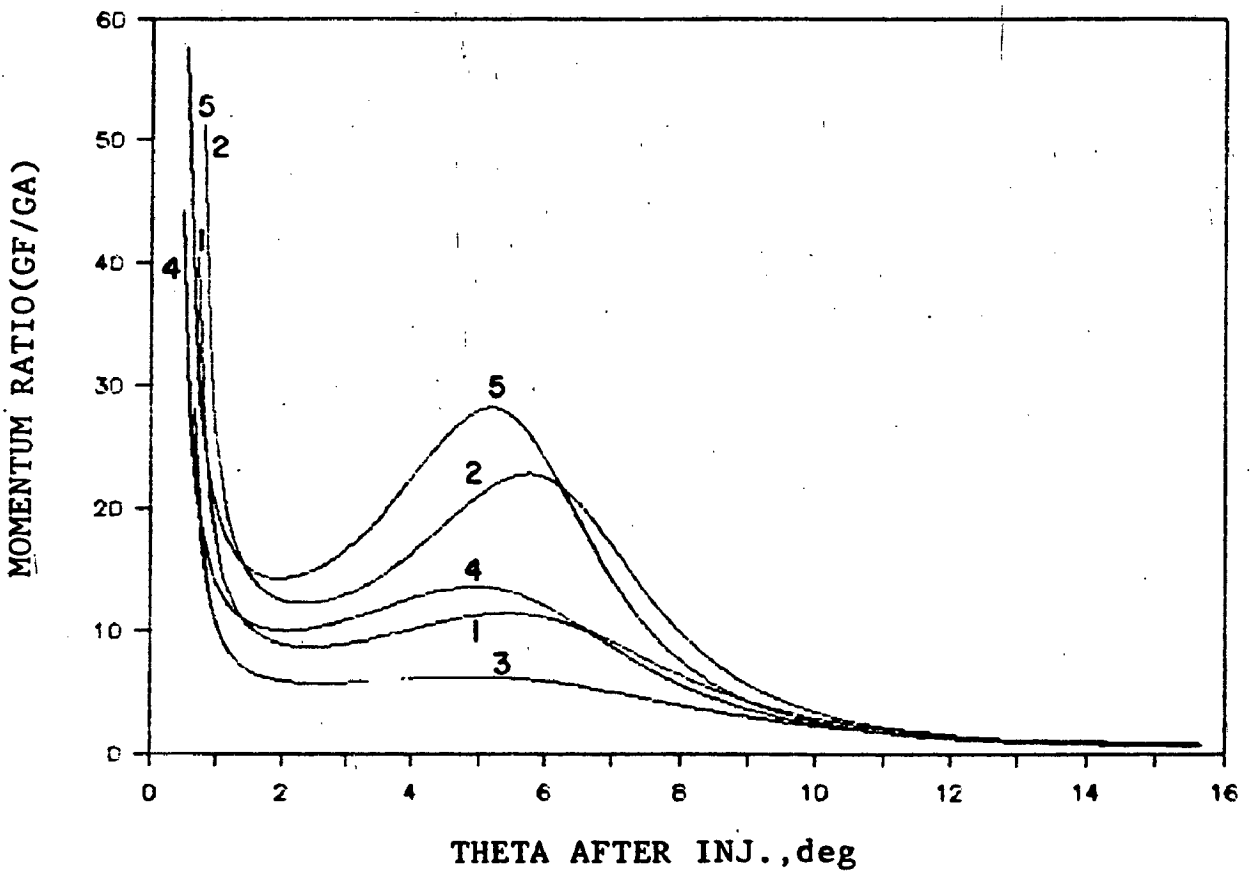


Fig 6.2 Effect of nozzle hole size on momentum ratio

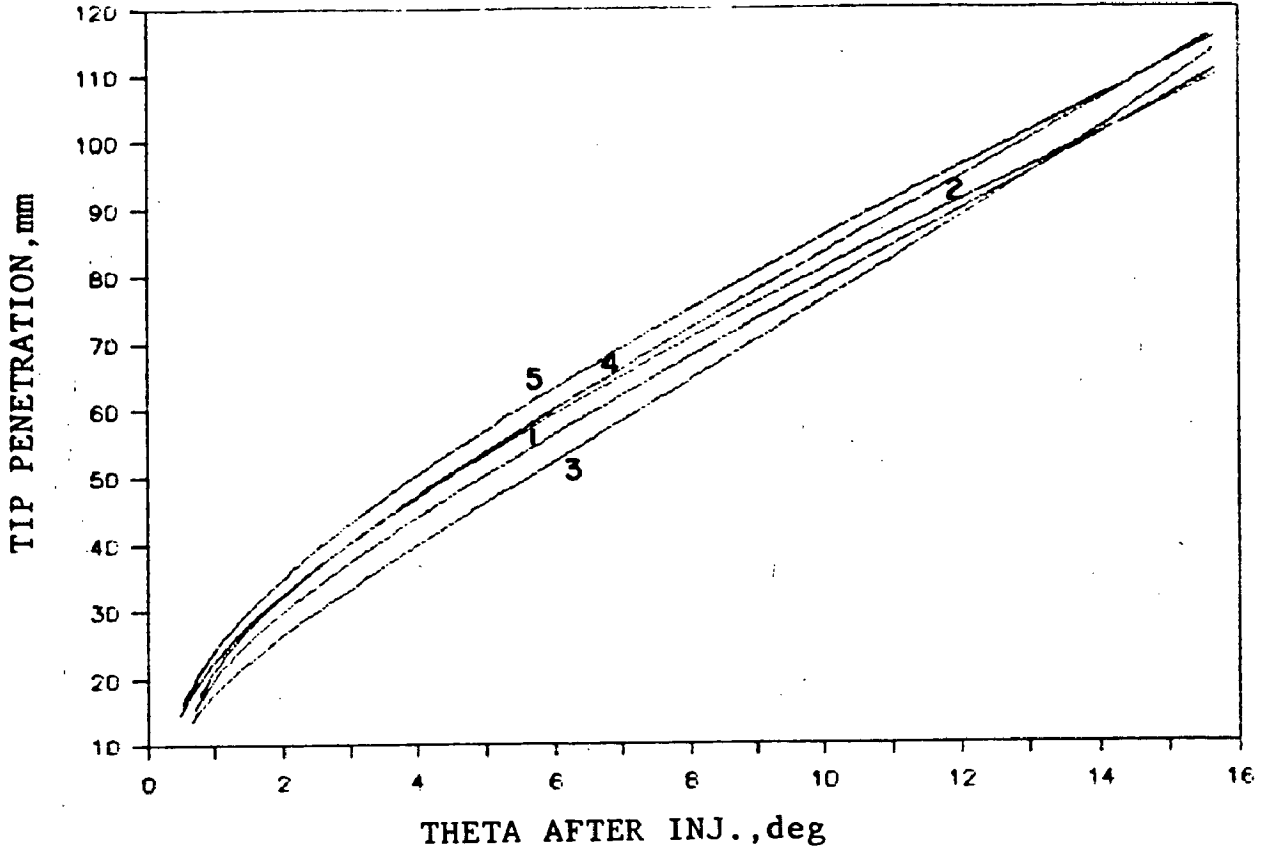


Fig 6.3 Effect of nozzle hole size on tip penetration

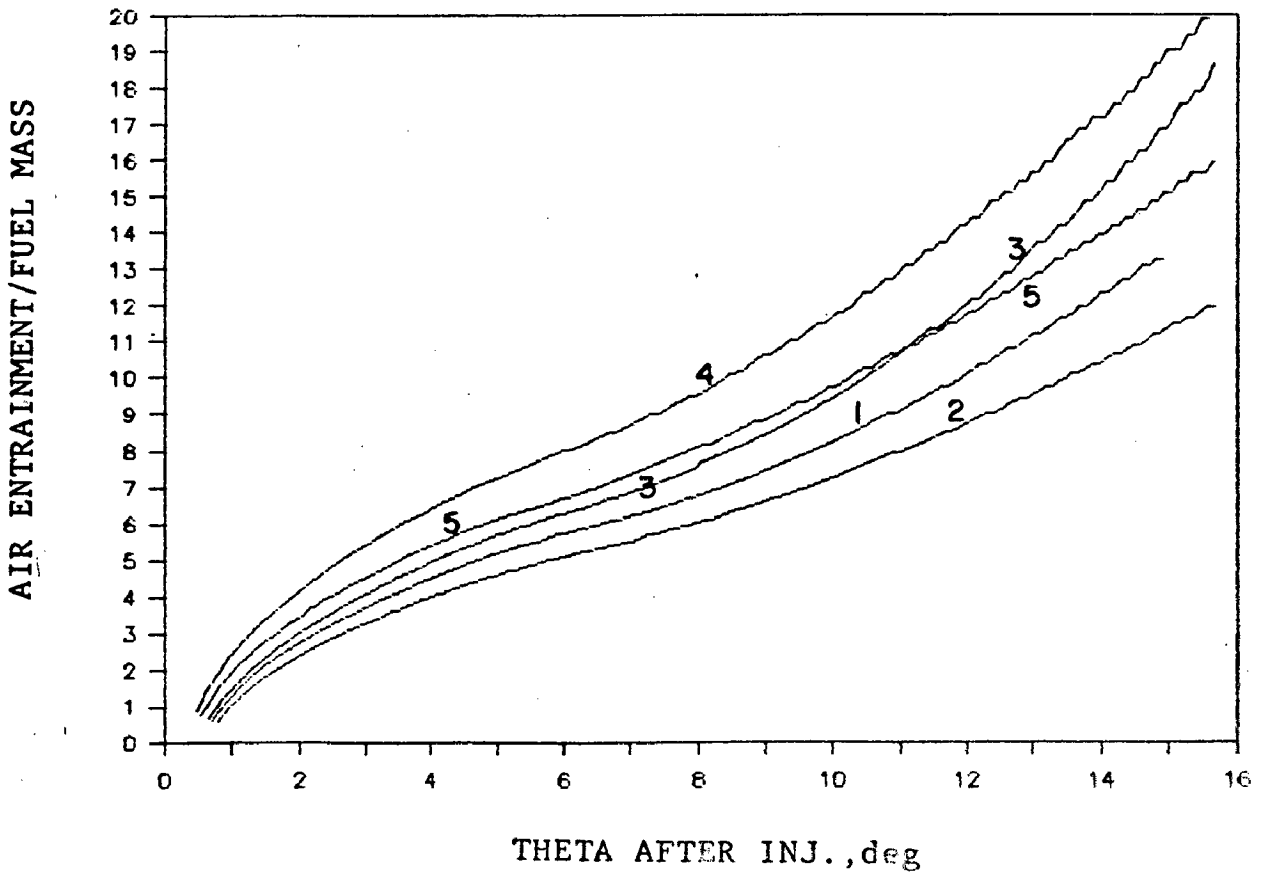


Fig 6.4 Effect of nozzle hole size on air entrainment

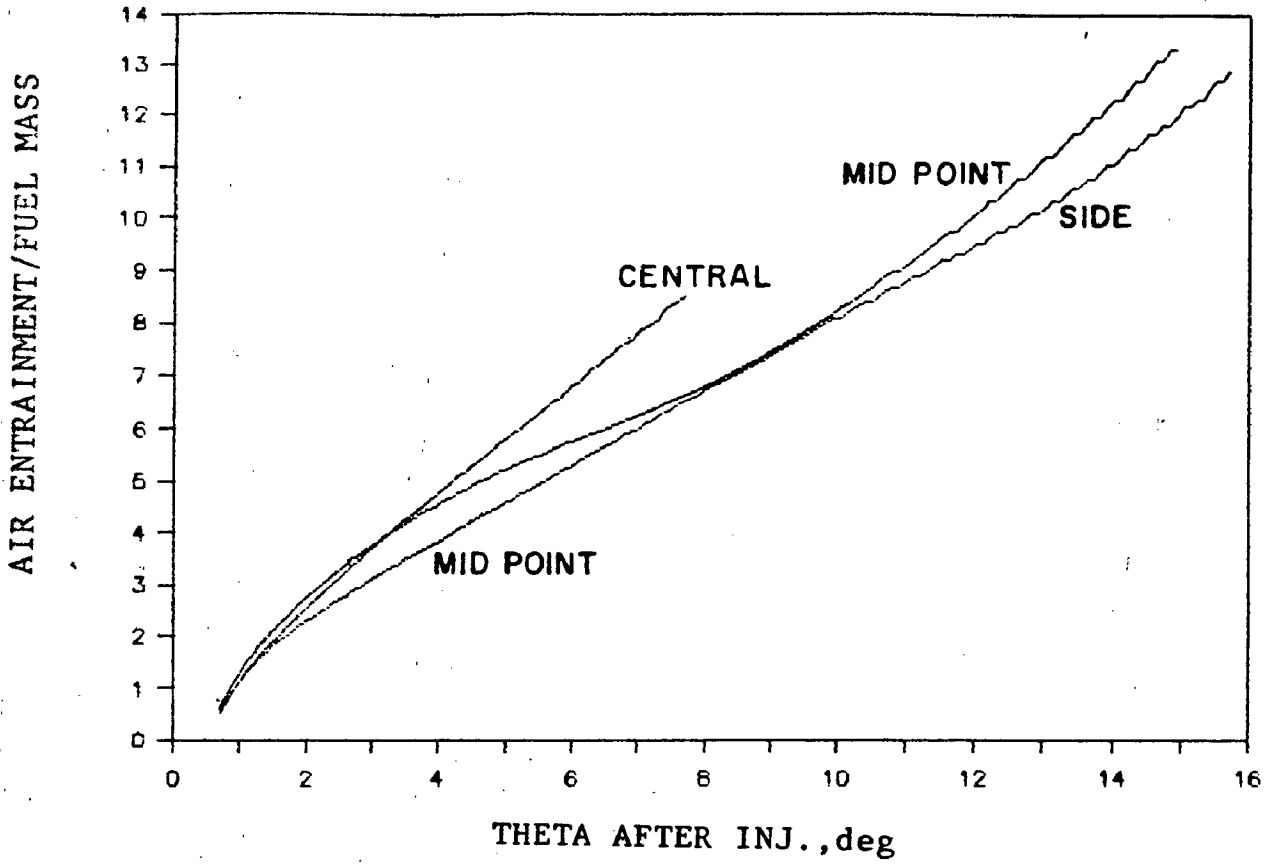


Fig 6.5 Effect of injector location on air entrainment

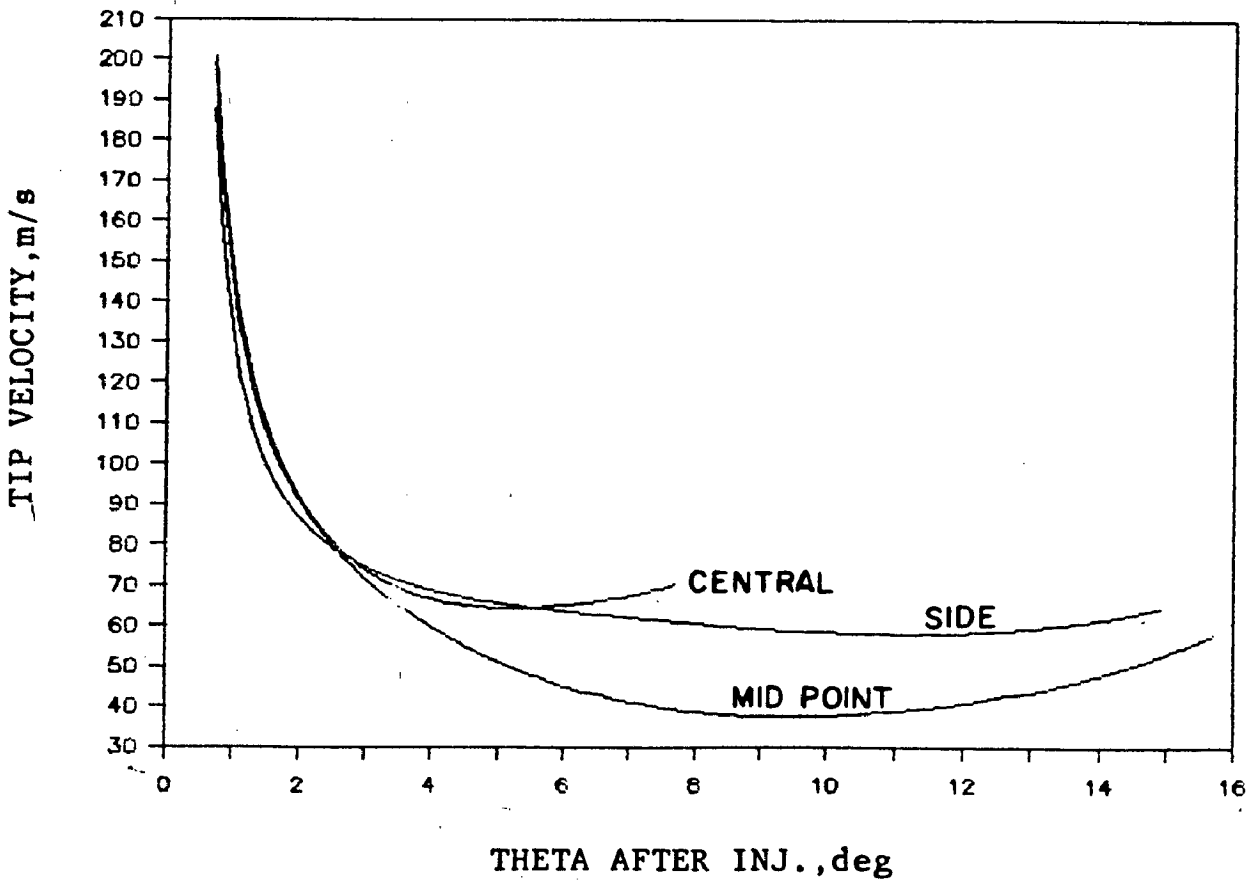


Fig 6.6 Effect of injector location on tip velocity

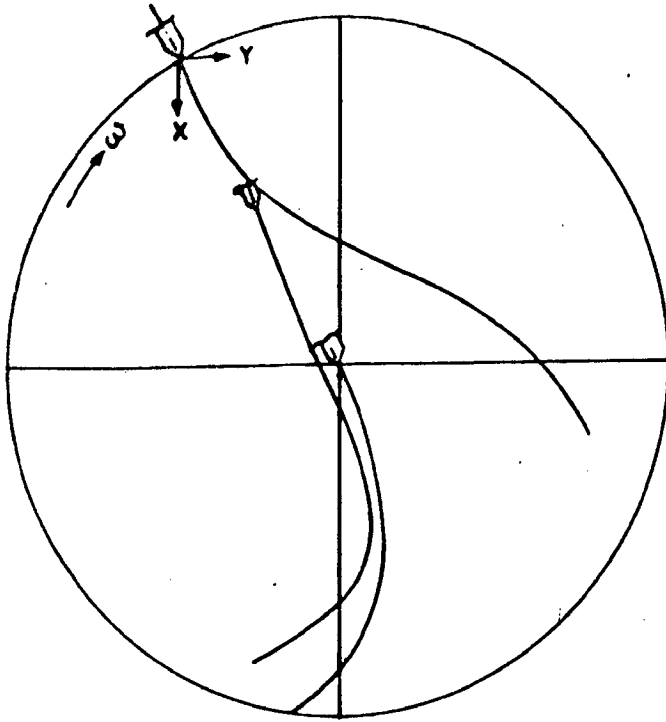


Fig 6.7 Effect of injector location on spray trajectory

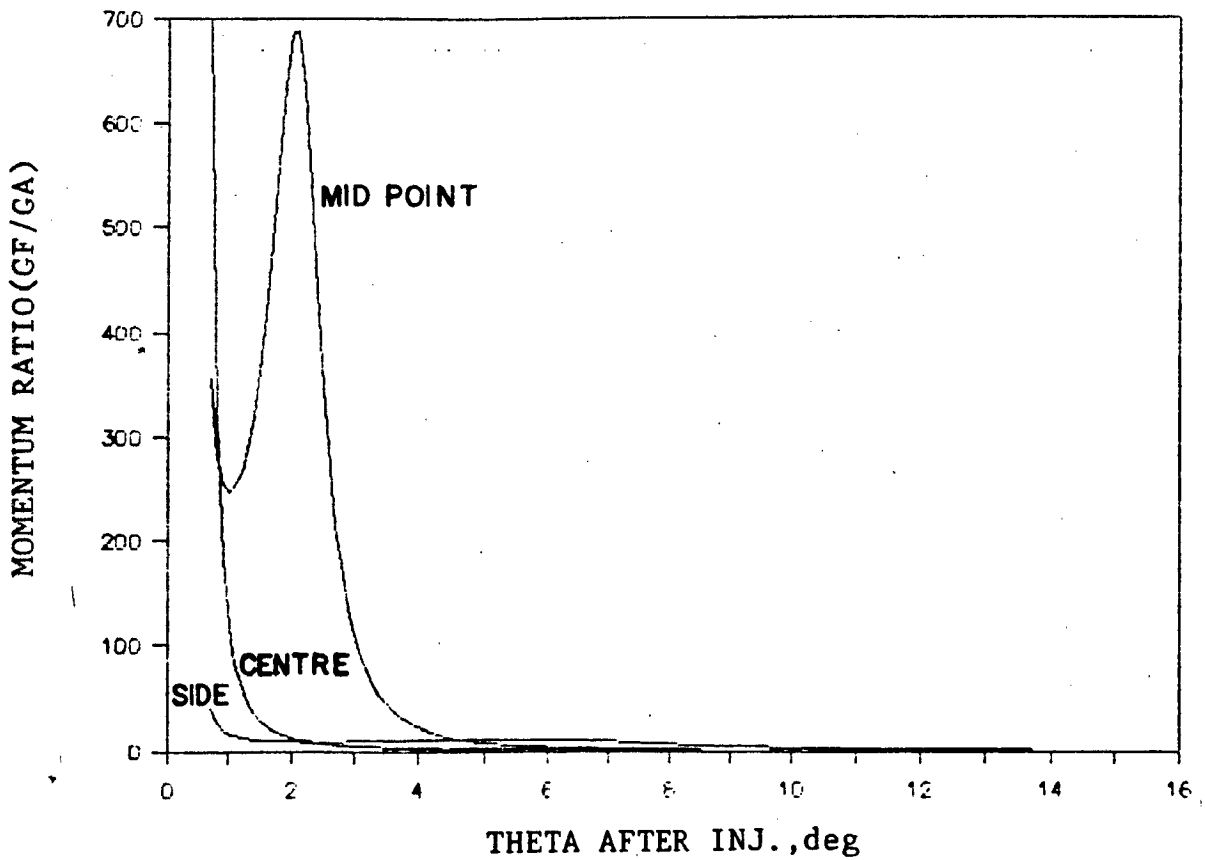


Fig 6.8 Effect of injector location on momentum ratio



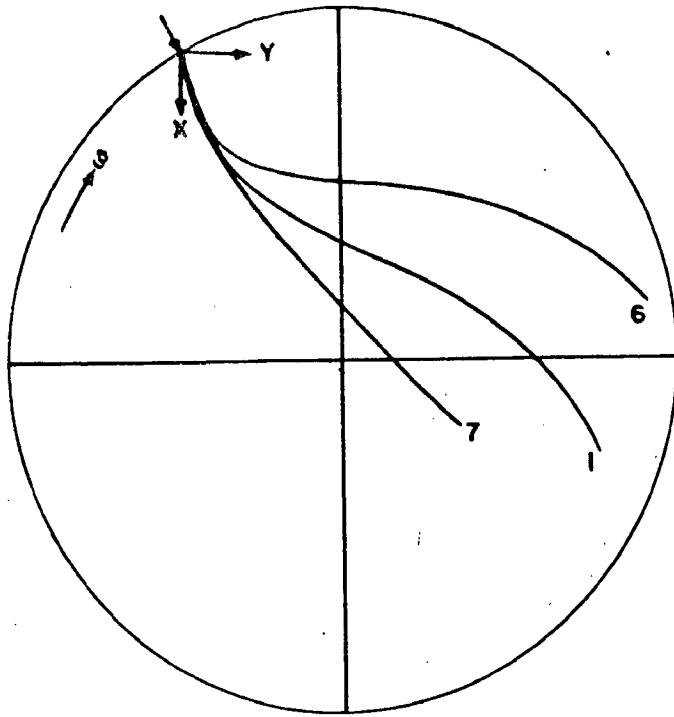


Fig 6.9 Effect of rate/duration of injection on trajectory

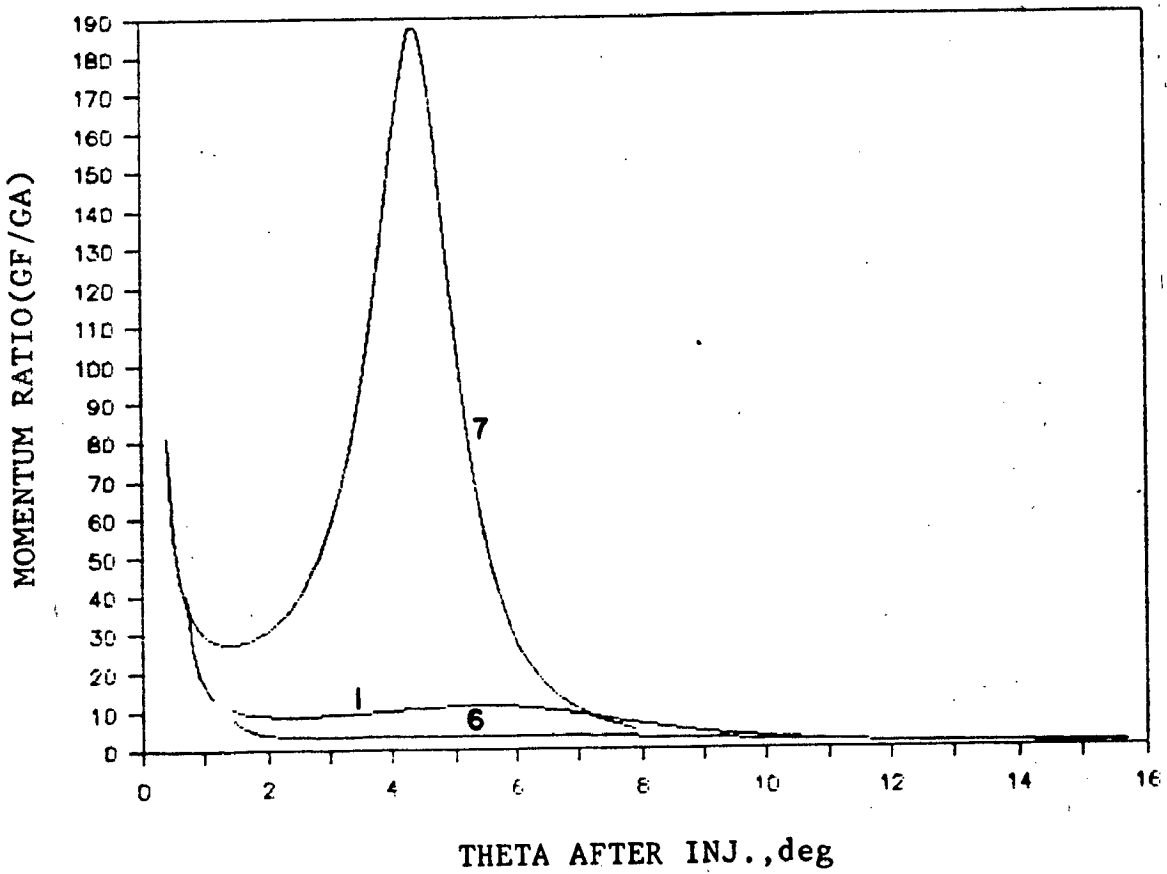


Fig 6.10 Effect of rate/duration of injection on momentum ratio for side injection spray

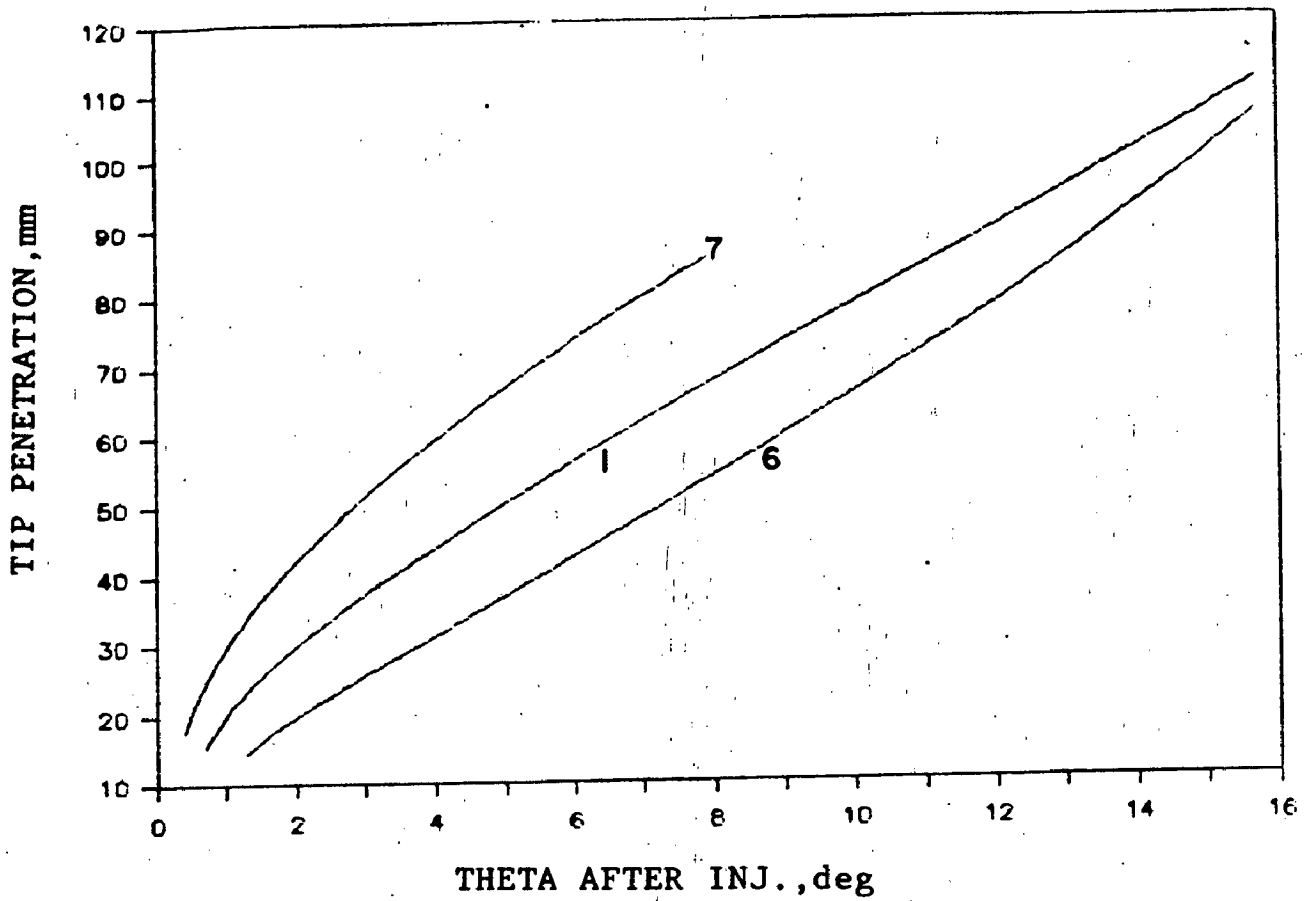


Fig 6.11 Effect of rate/duration of injection on penetration length for side injection

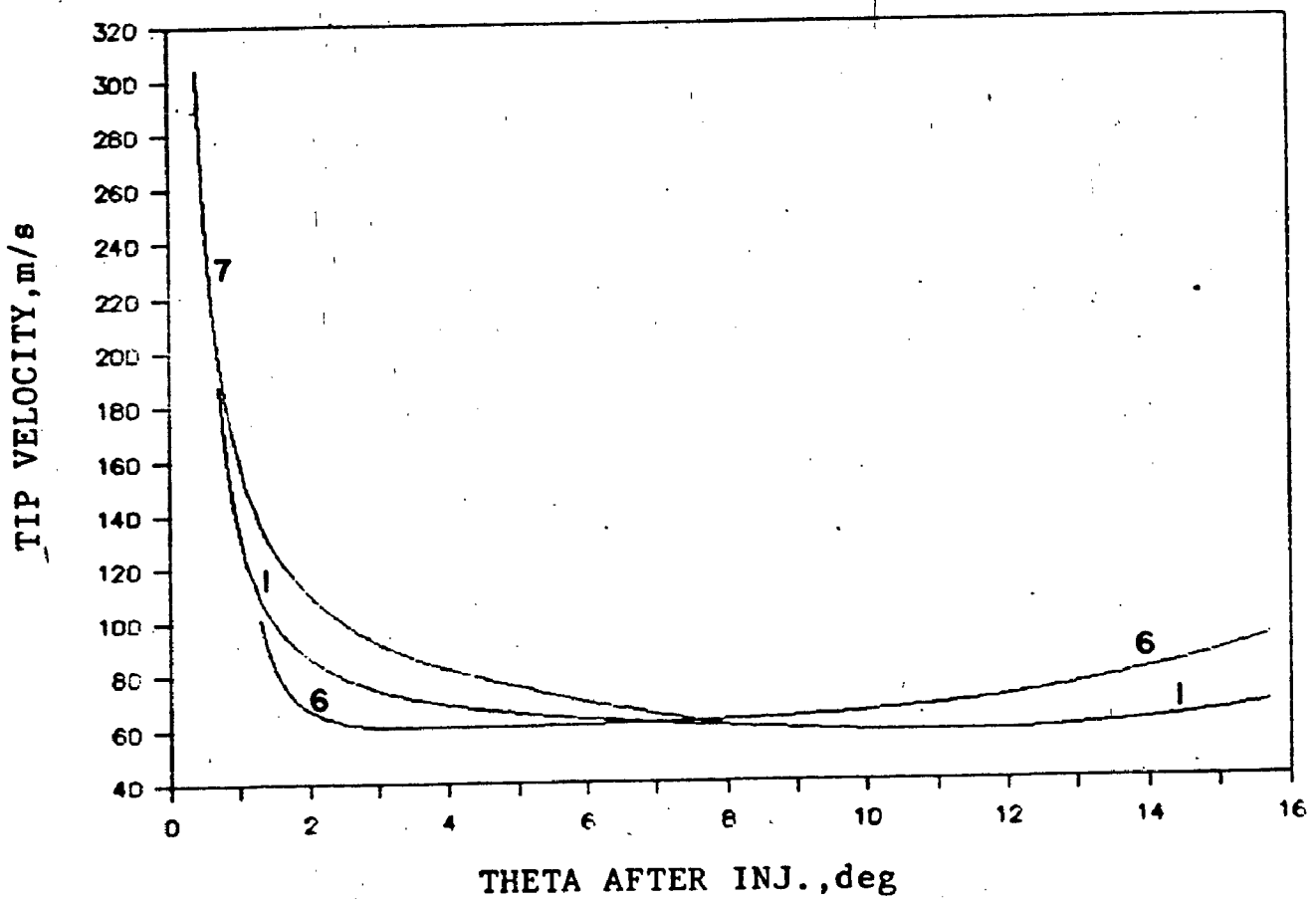


Fig 6.12 Effect of rate/duration of injection on tip velocity for side injection spray

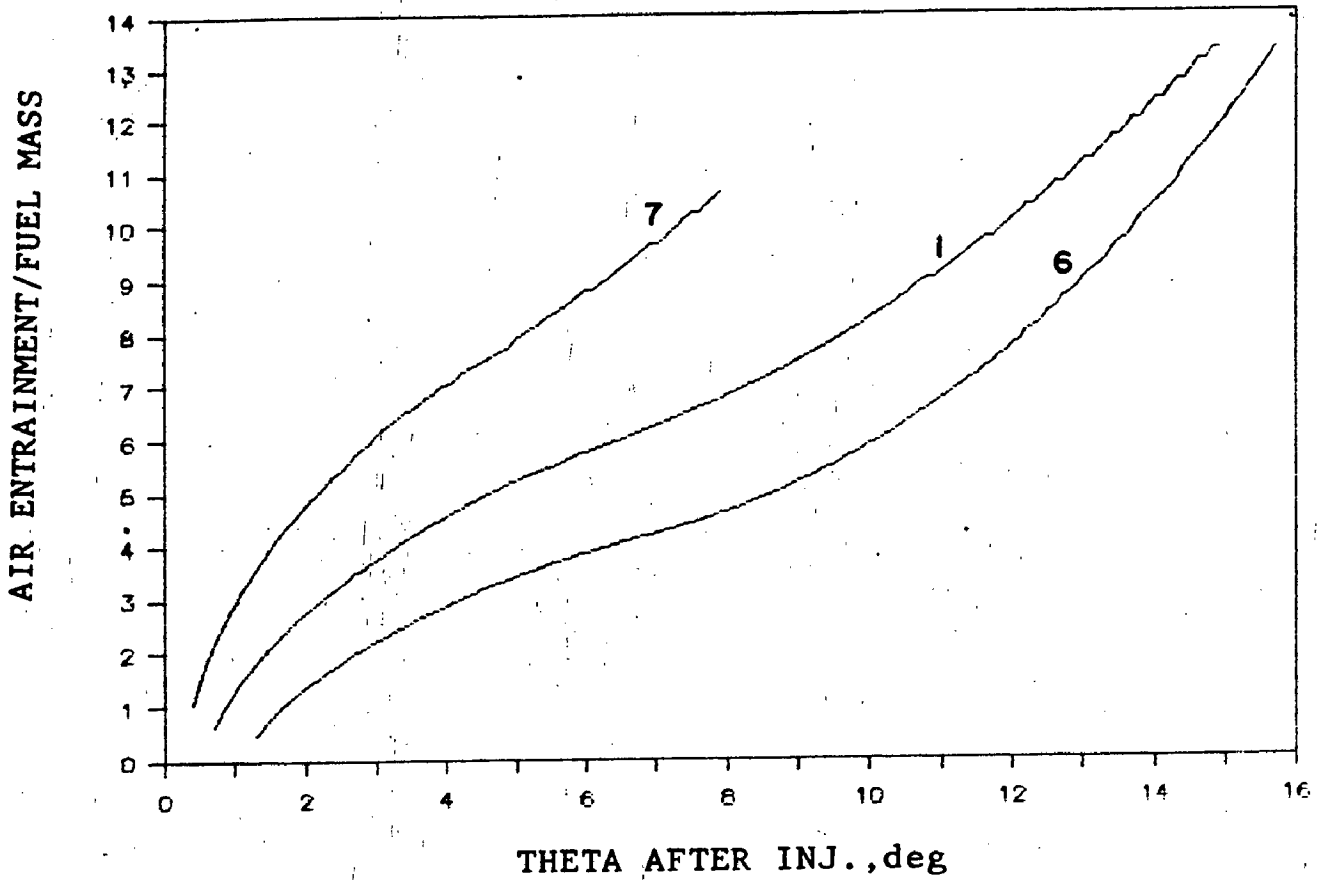


Fig 6.13 Effect of rate/duration of injection on air entrainment for side injection spray

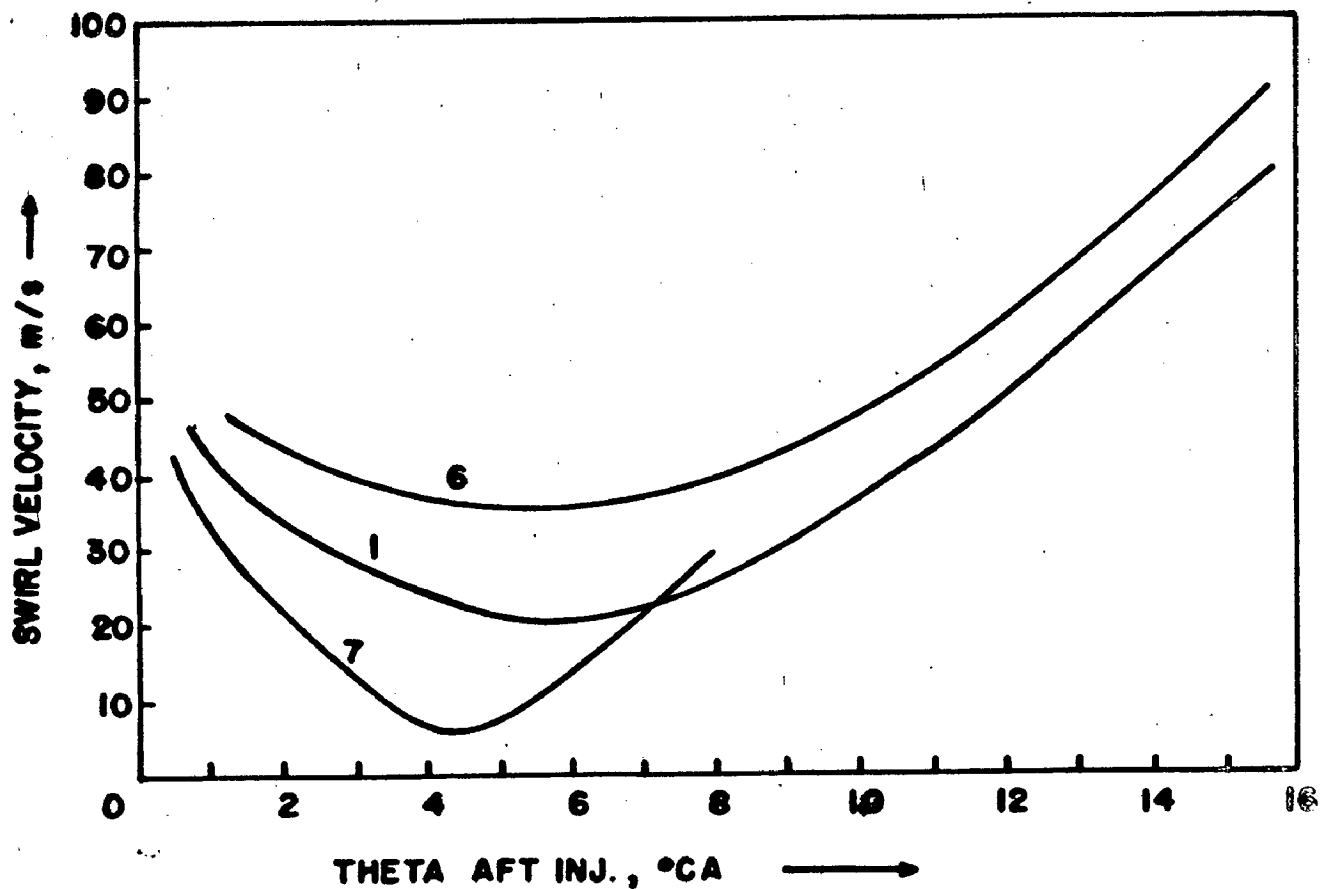


Fig 6.14 Air velocity encountered by spray for side injection

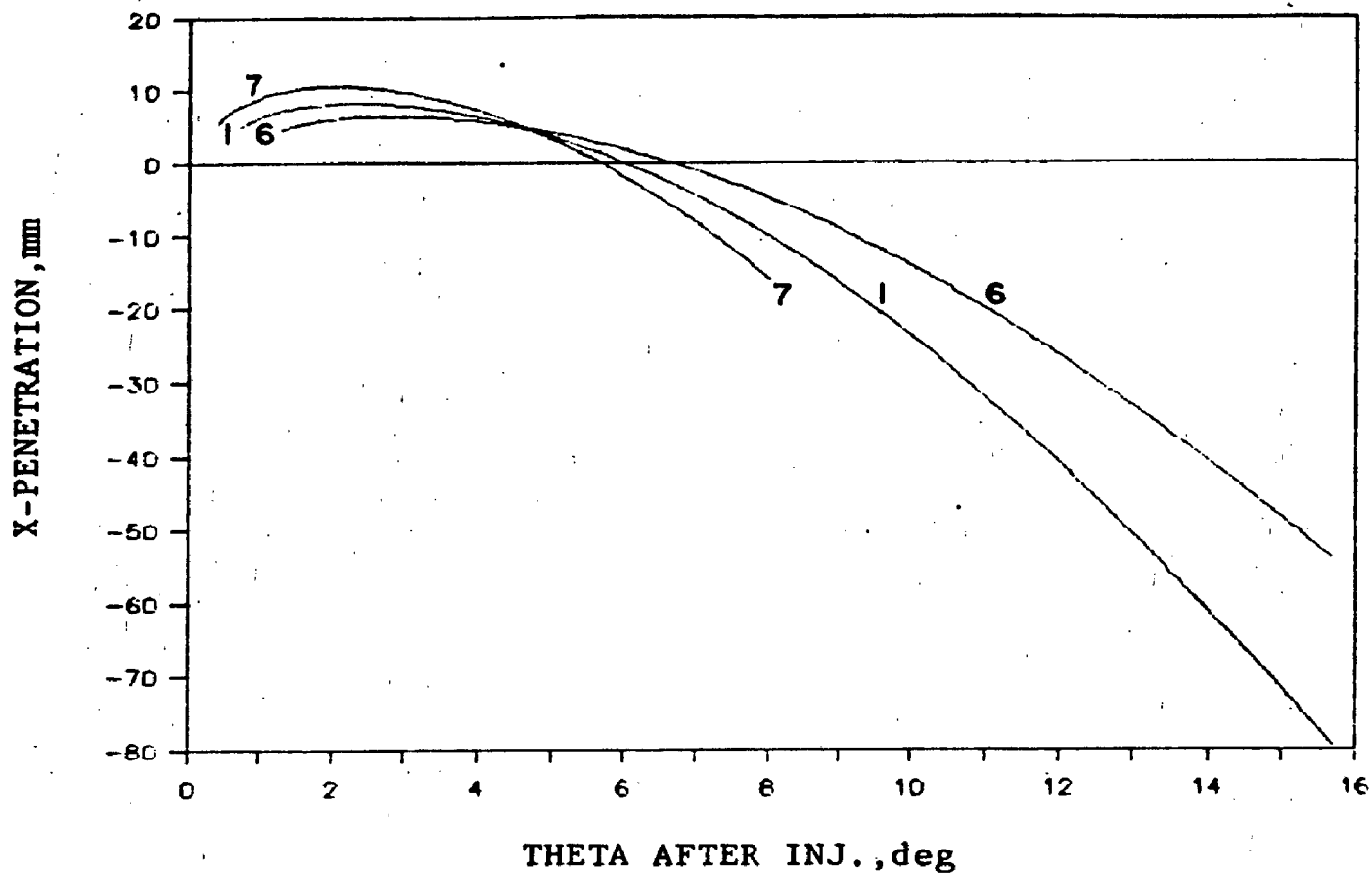


Fig 6.15 Effect of rate/duration of injection on x component of penetration for central injection

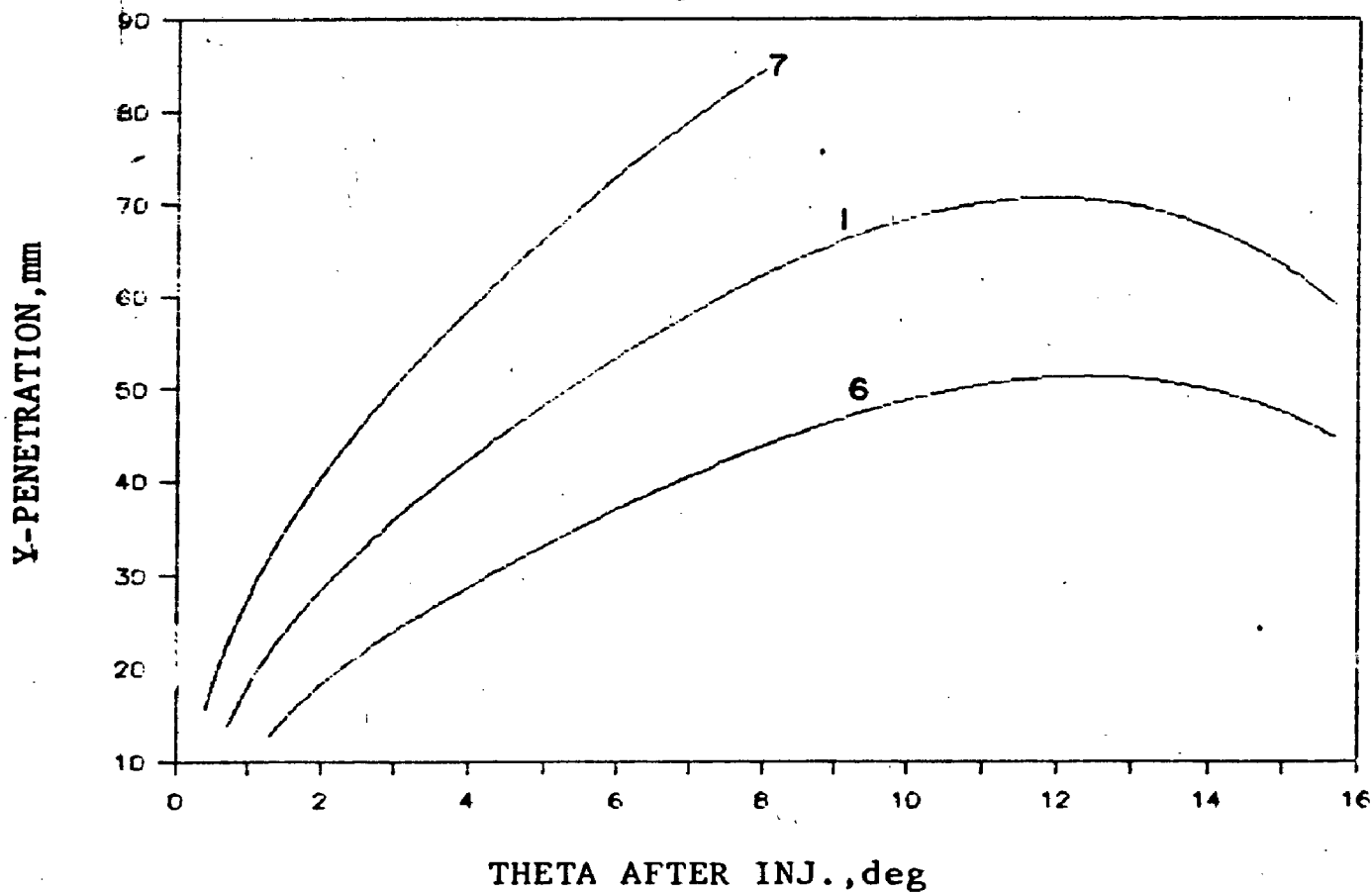


Fig 6.16 Effect of rate/duration of injection on y component of penetration for central injection

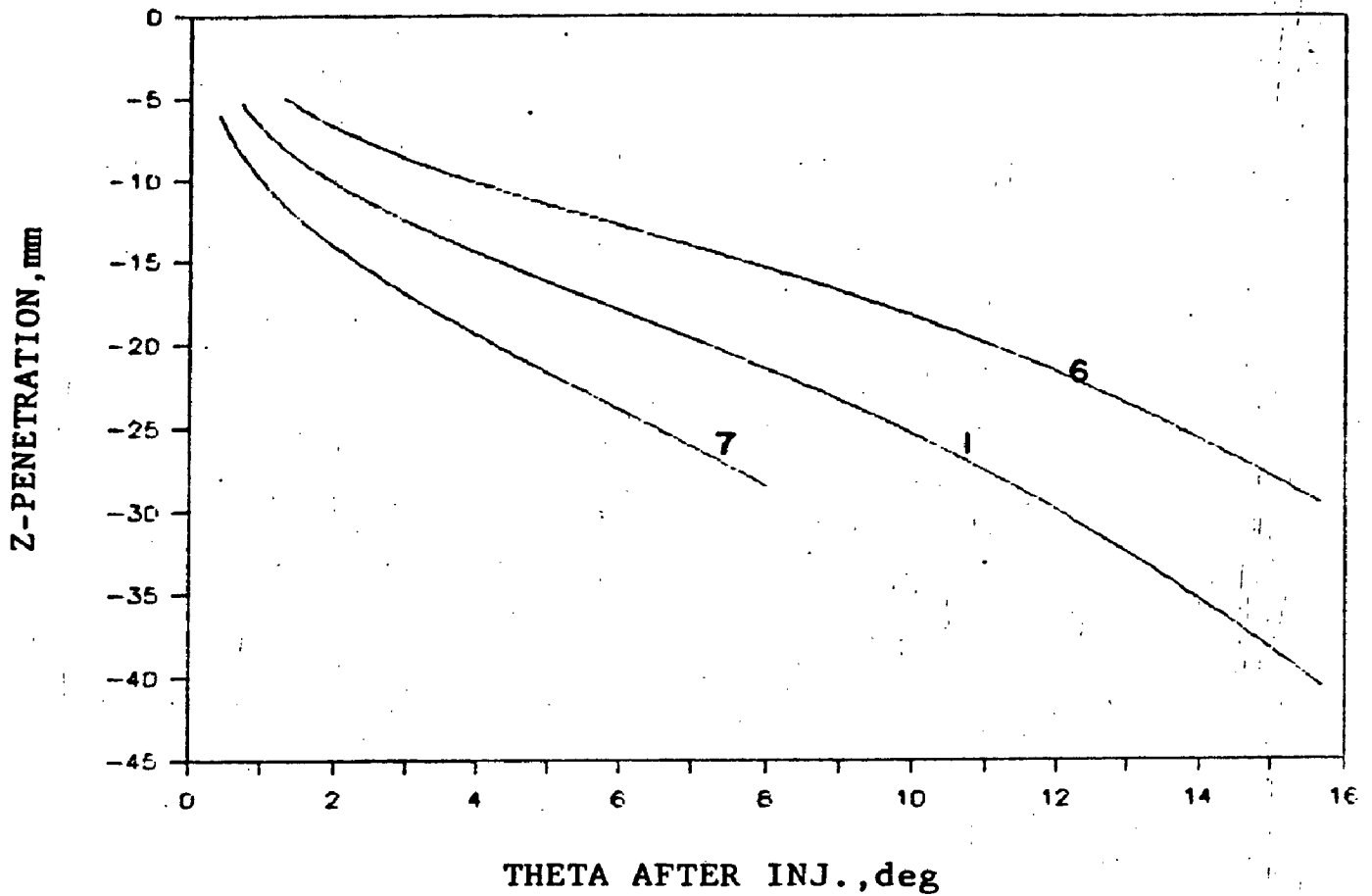


Fig 6.17 Effect of rate/duration of injection on z component of penetration for central injection

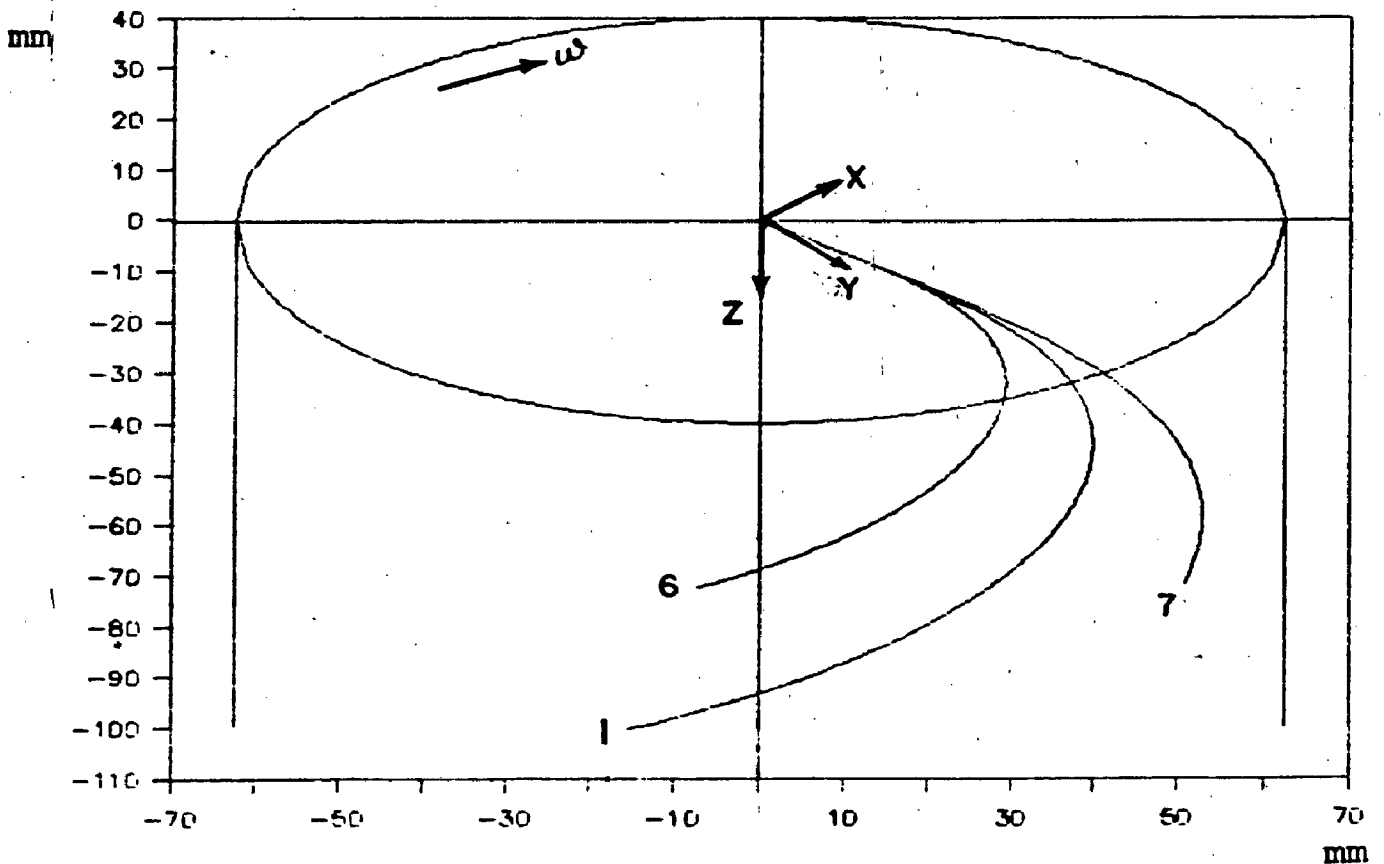


Fig 6.18 Effect of rate/duration of injection on trajectory for central injection

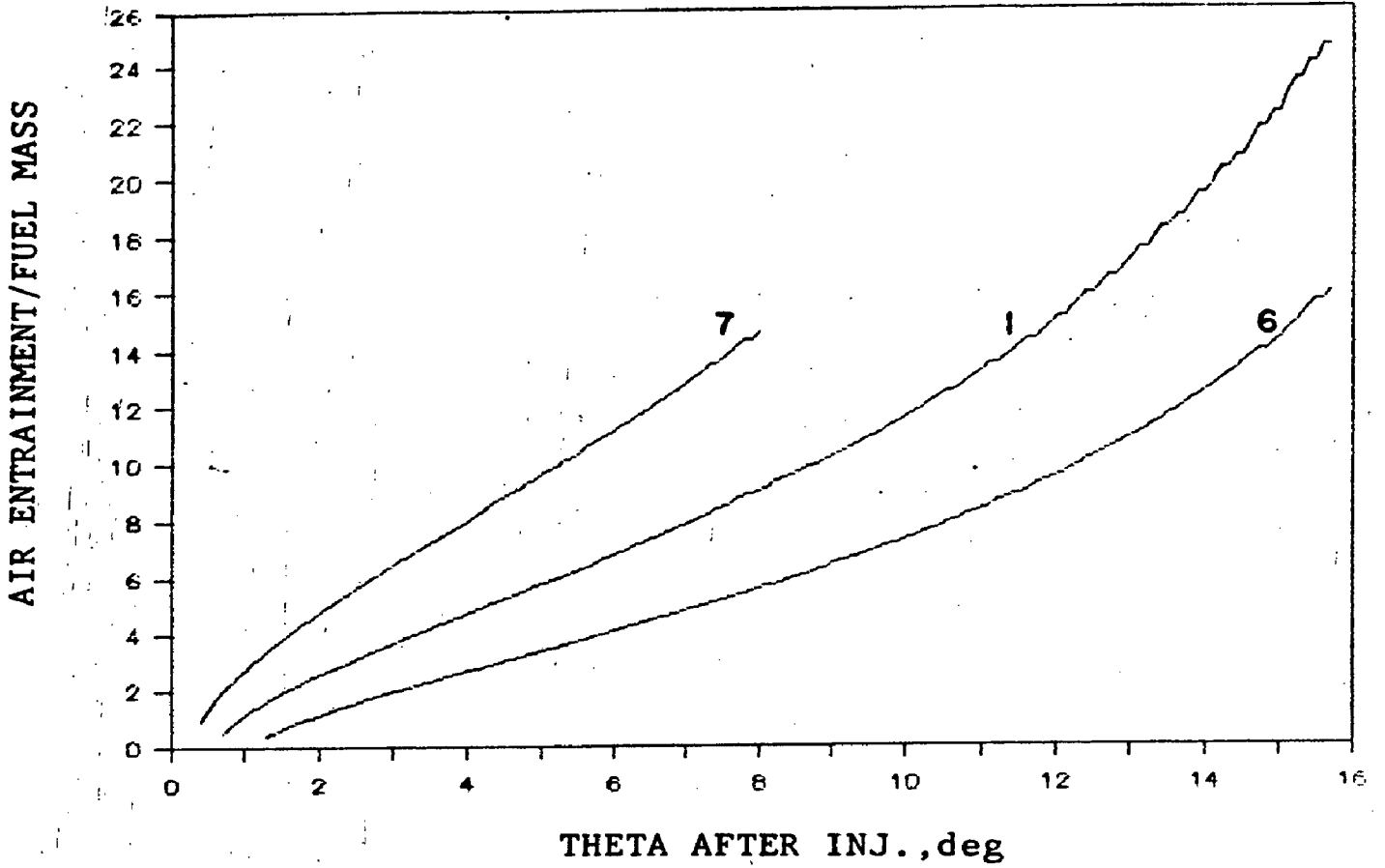


Fig 6.19 Effect of rate/duration of injection on air entrainment for central injection

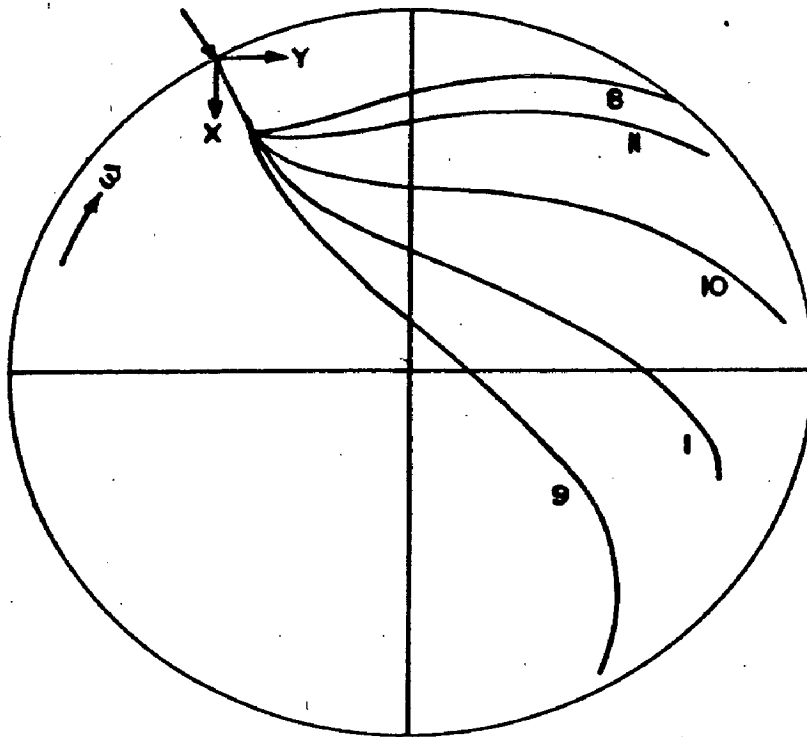


Fig 6.20 Effect of injection scheduling on spray trajectory

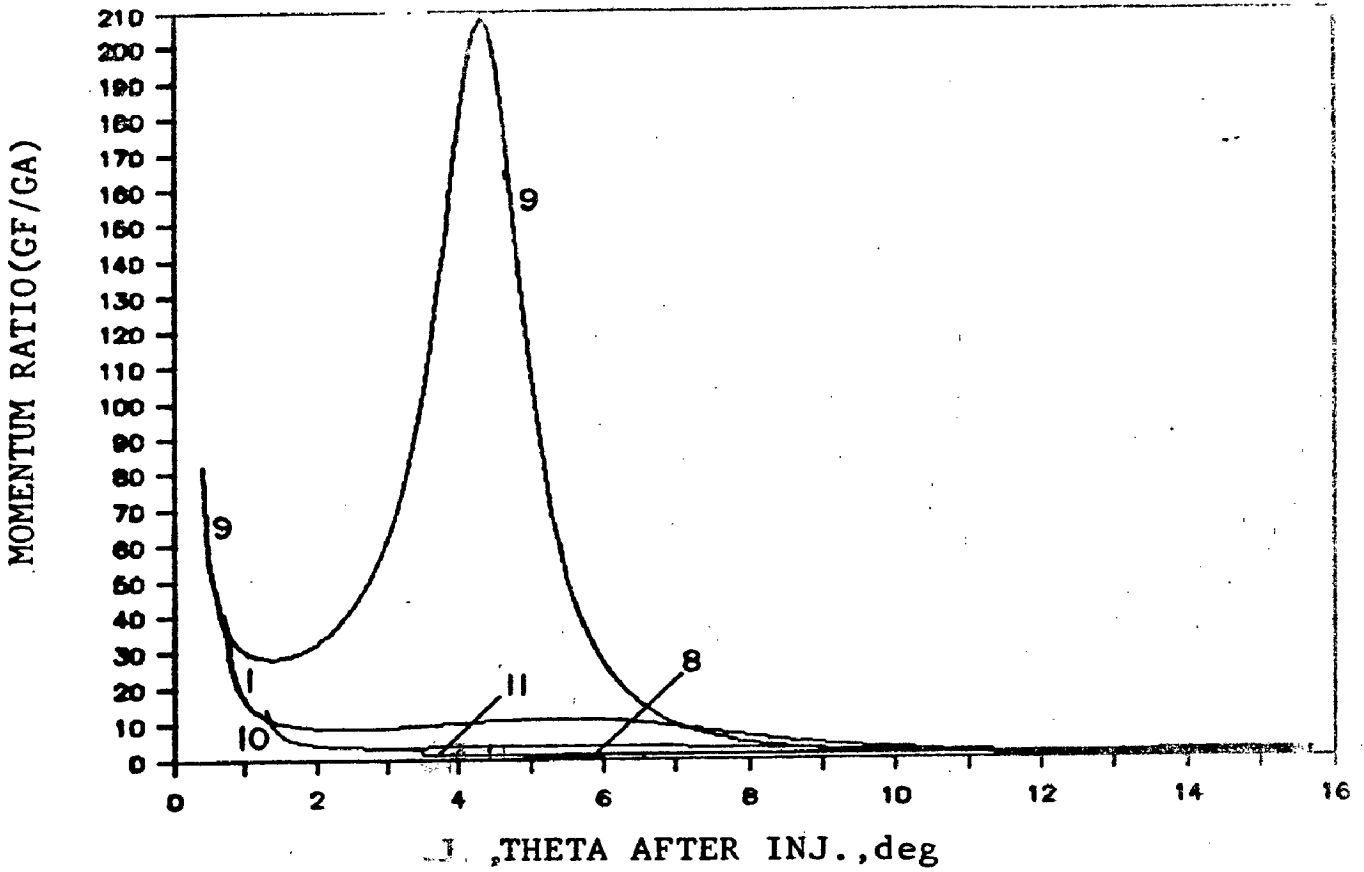


Fig 6.21 Effect of injection rate shape on momentum ratio for side injection

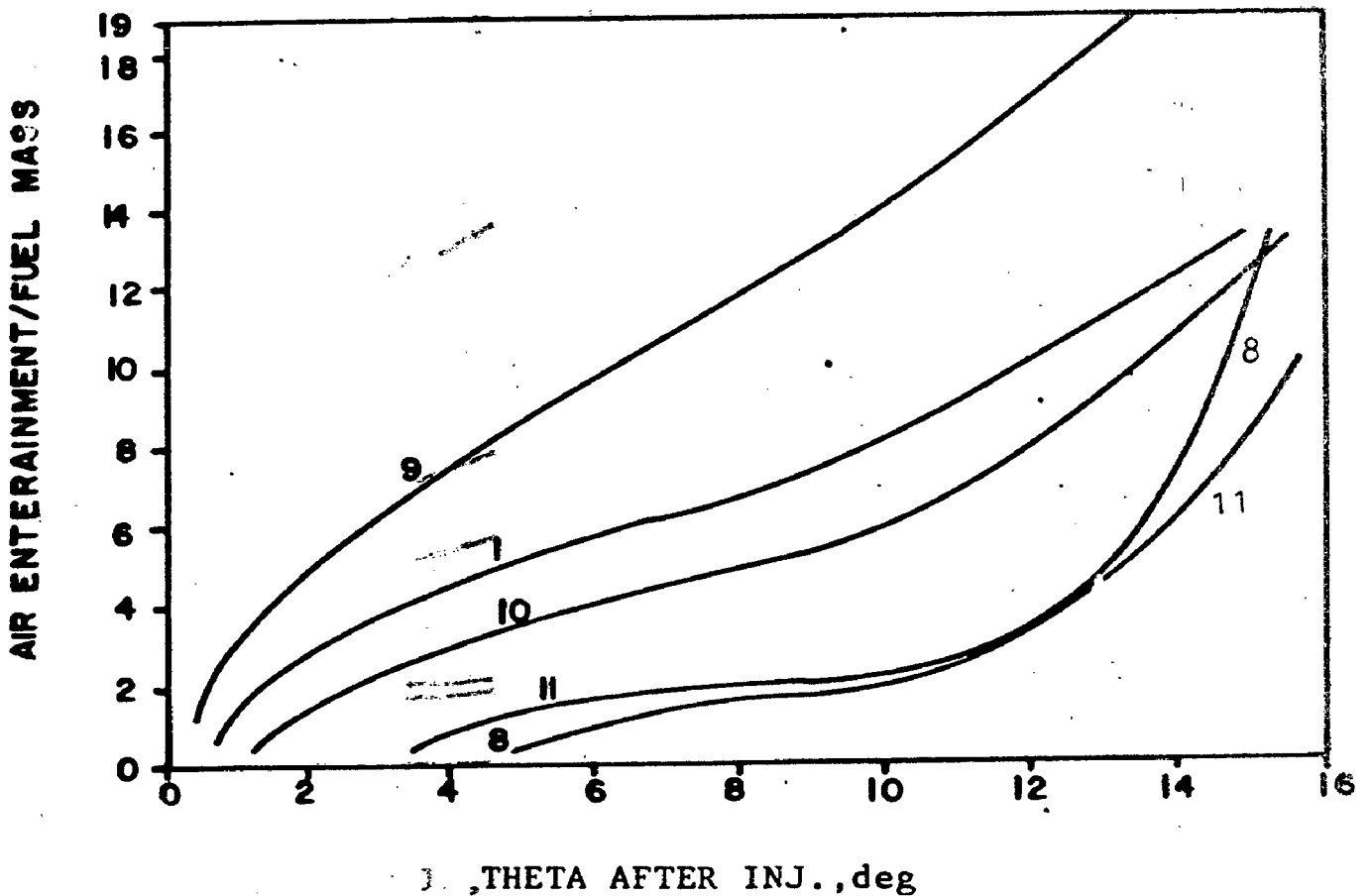


Fig 6.22 Effect of injection rate shape on air entrainment for side injection

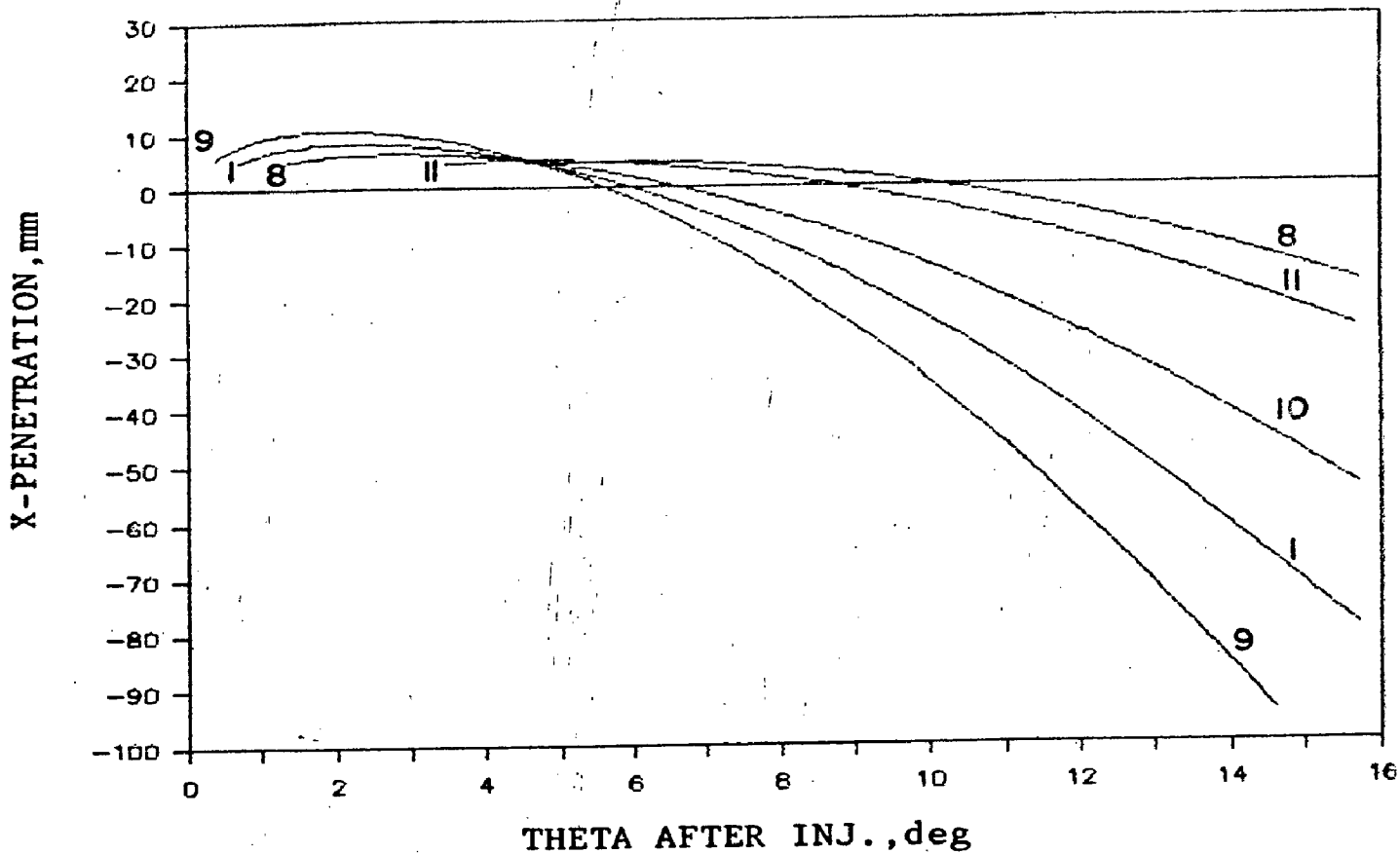


Fig 6.23 Effect of injection rate shape on x component of penetration for central injection

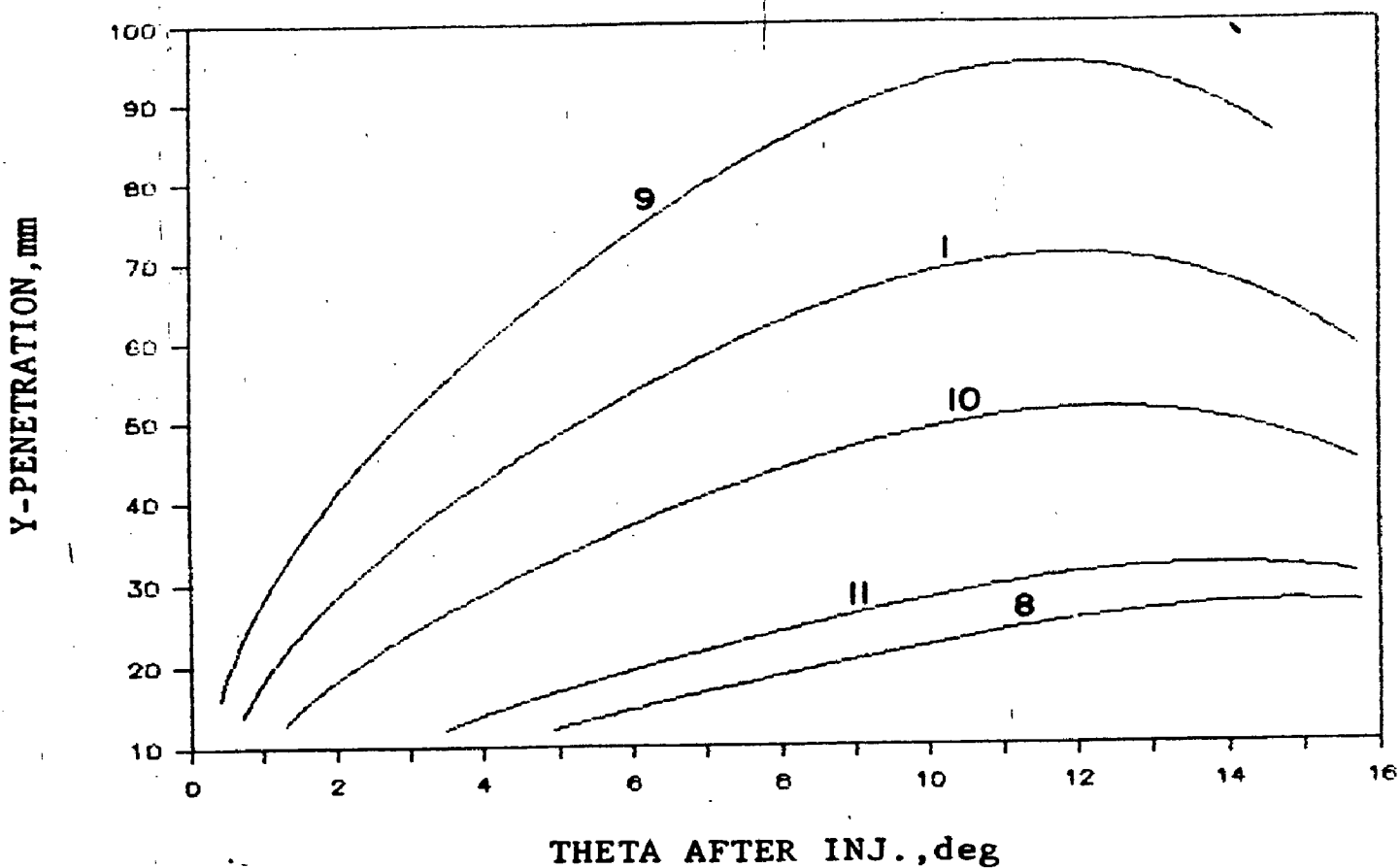


Fig 6.24 Effect of injection rate shape on y component of penetration for central injection



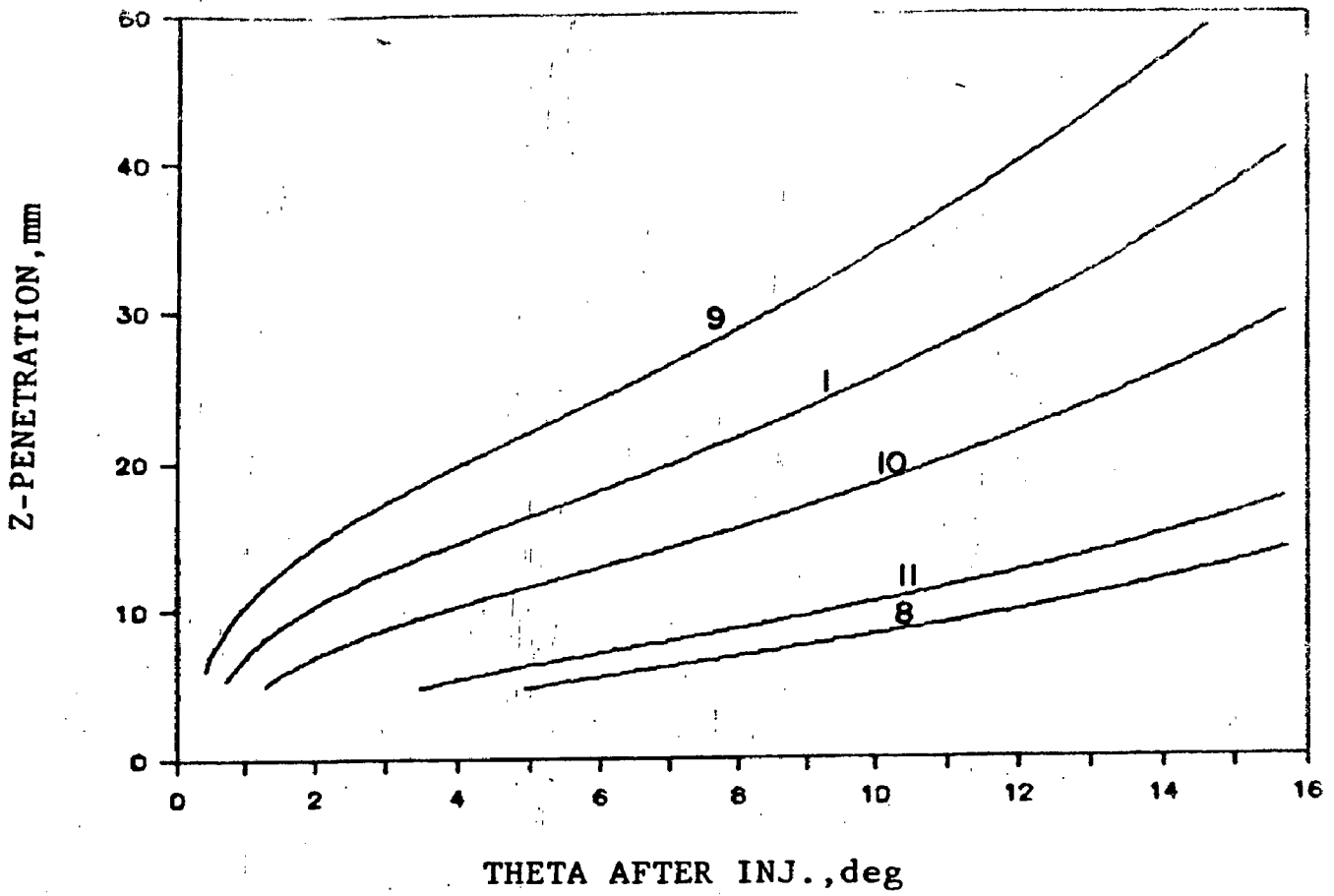


Fig 6.25 Effect of injection rate shape on z component of penetration for central injection

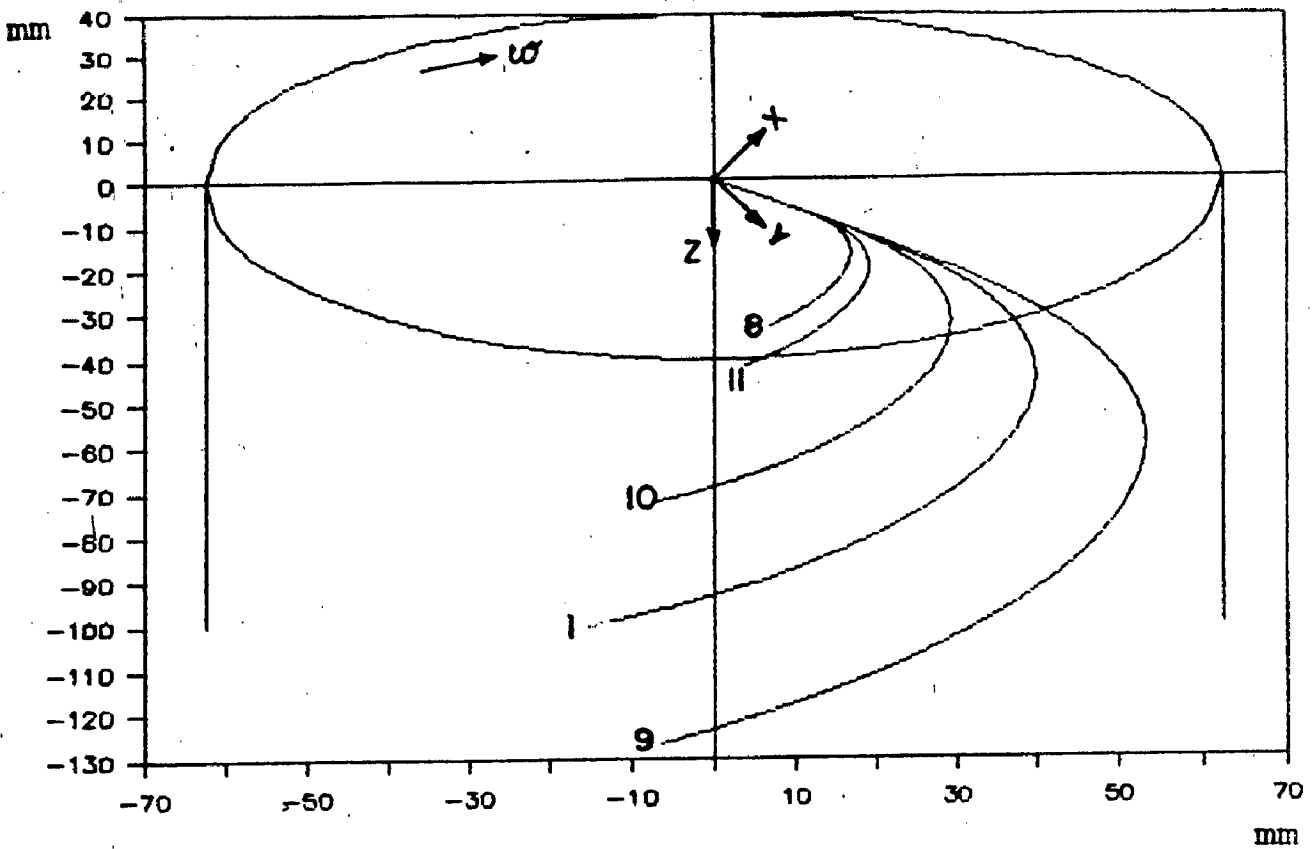


Fig 6.26 Effect of injection rate shape on trajectory for central injection

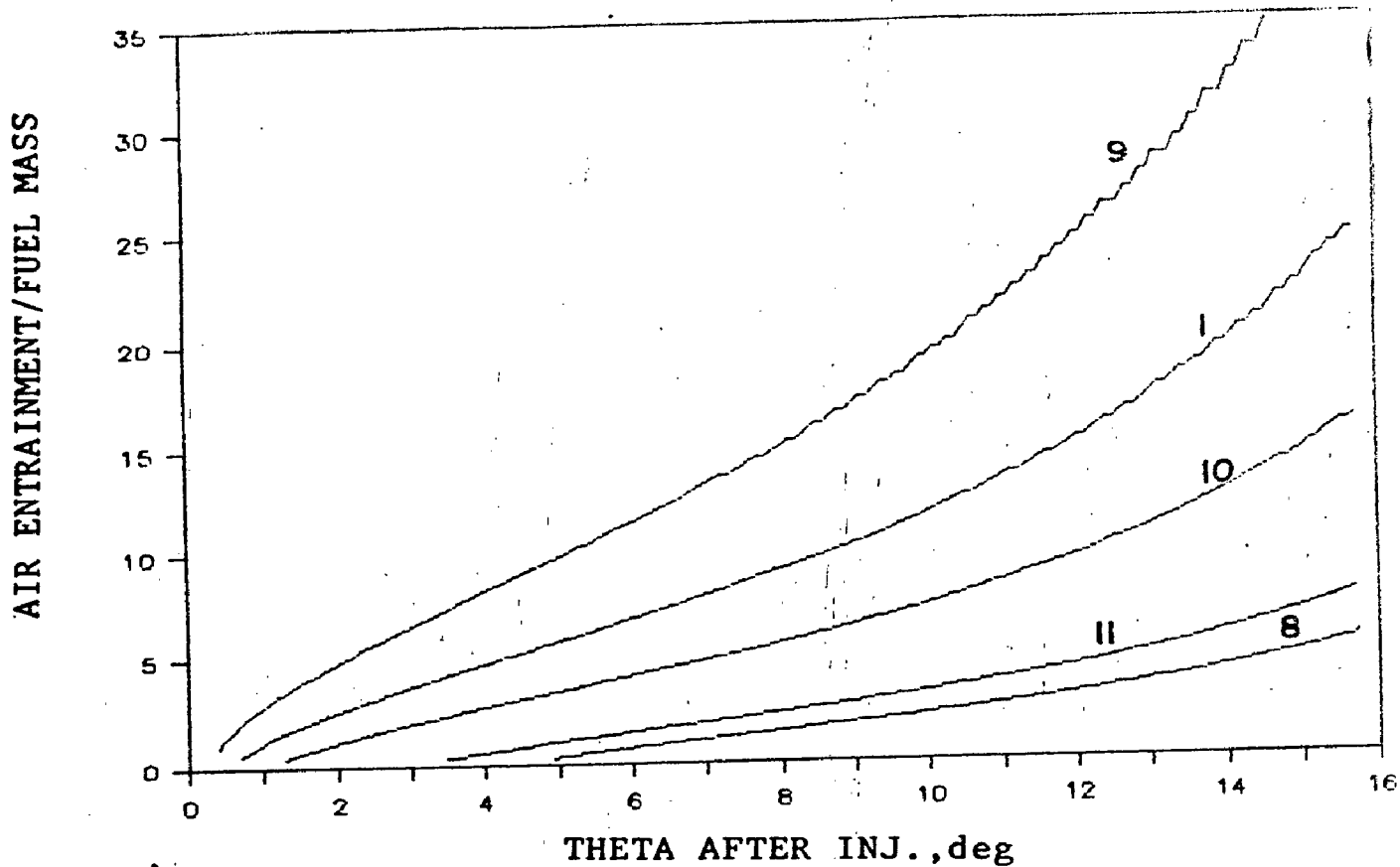


Fig 6.27 Effect of injection rate shape on air entrainment for central injection

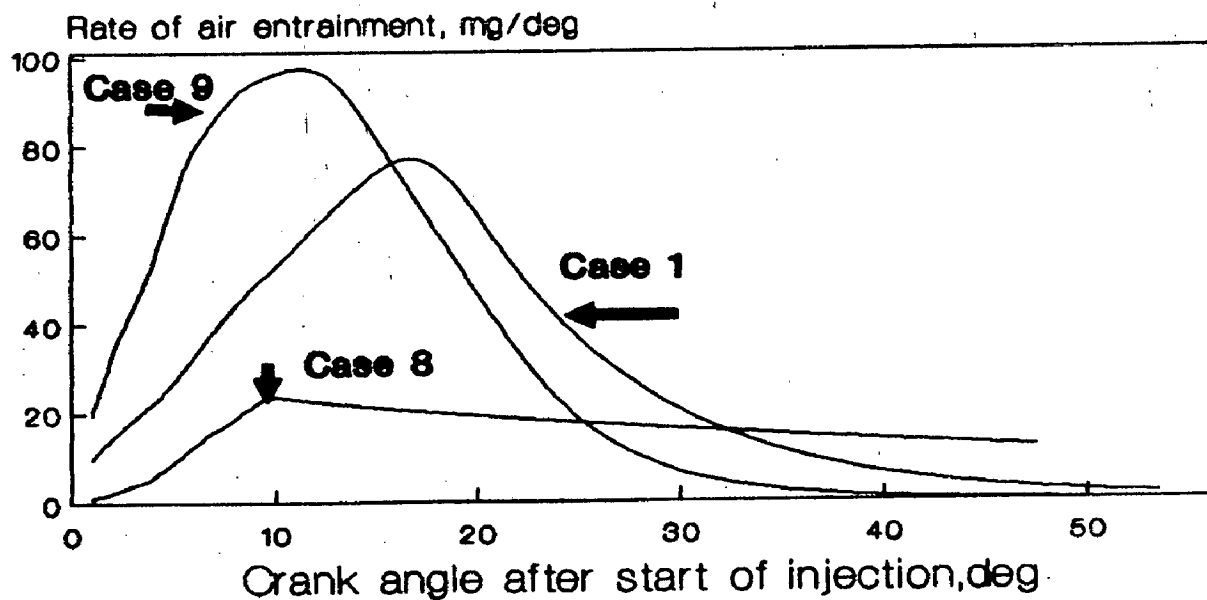


Fig 6.28 Effect of injection rate shape on rate of air entrainment

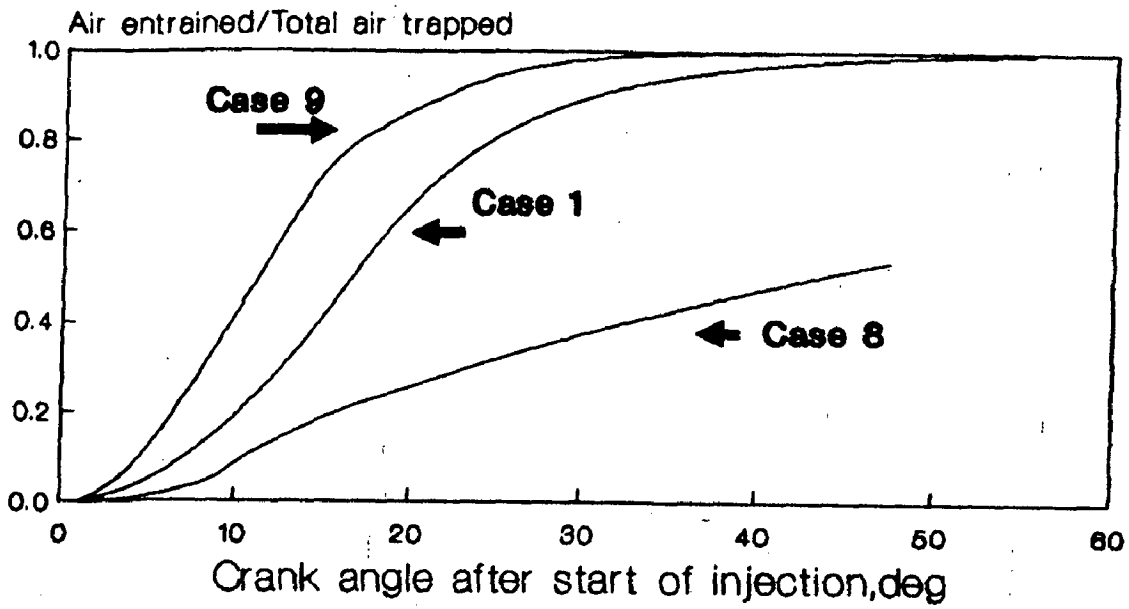


Fig 6.29 Effect of injection rate shape on air utilization

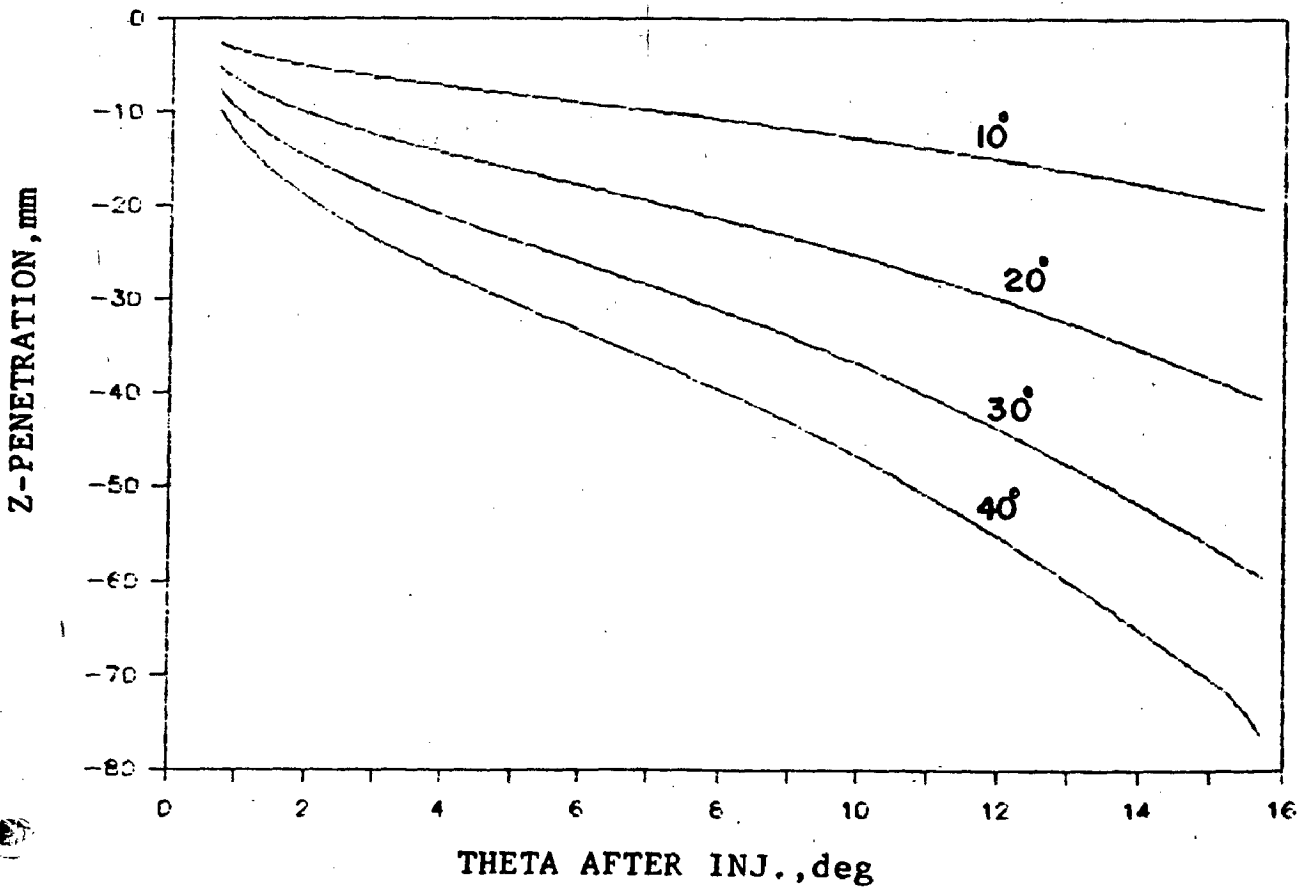


Fig 6.30 Effect of spray angle on z component of penetration

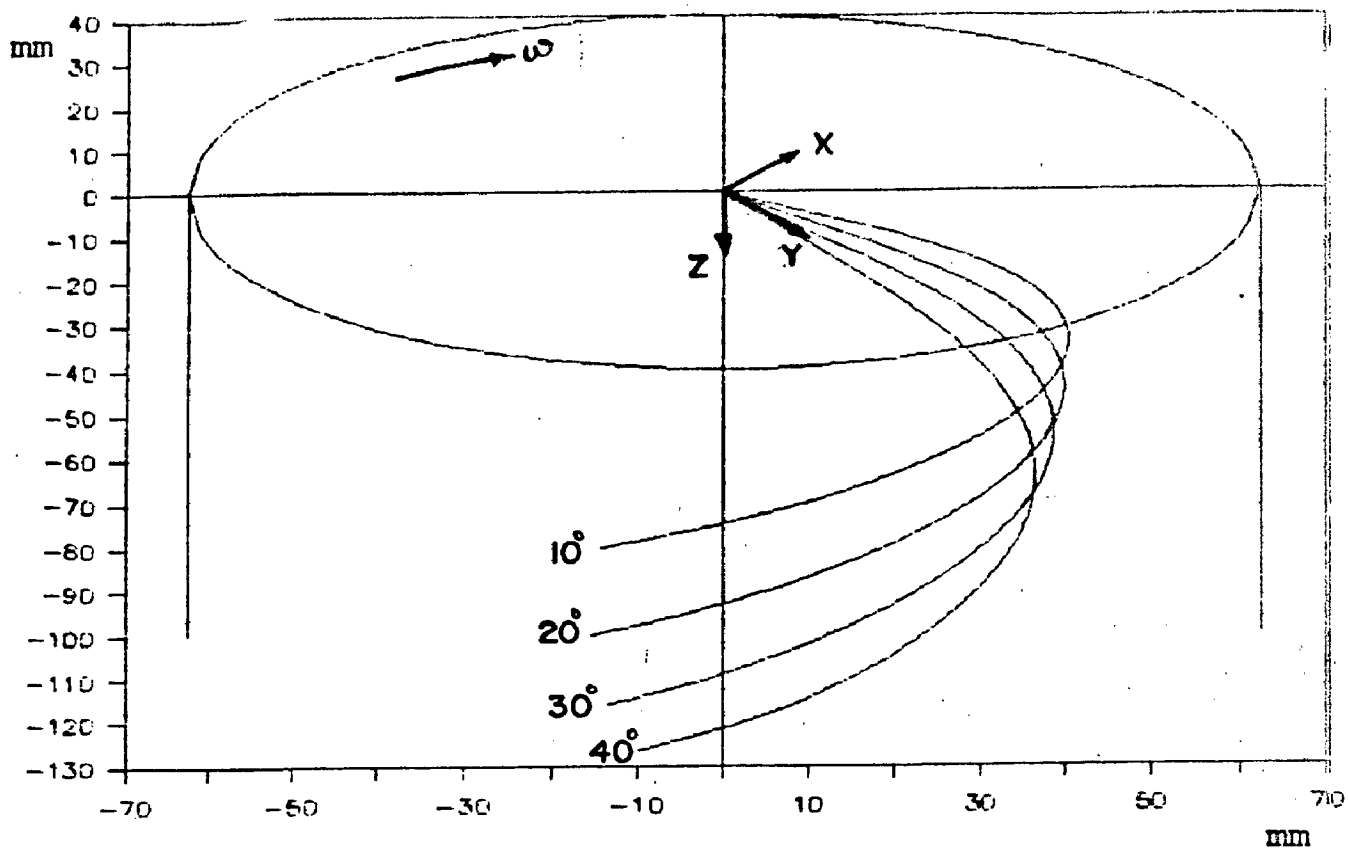


Fig 6.31 Effect of spray angle on trajectory

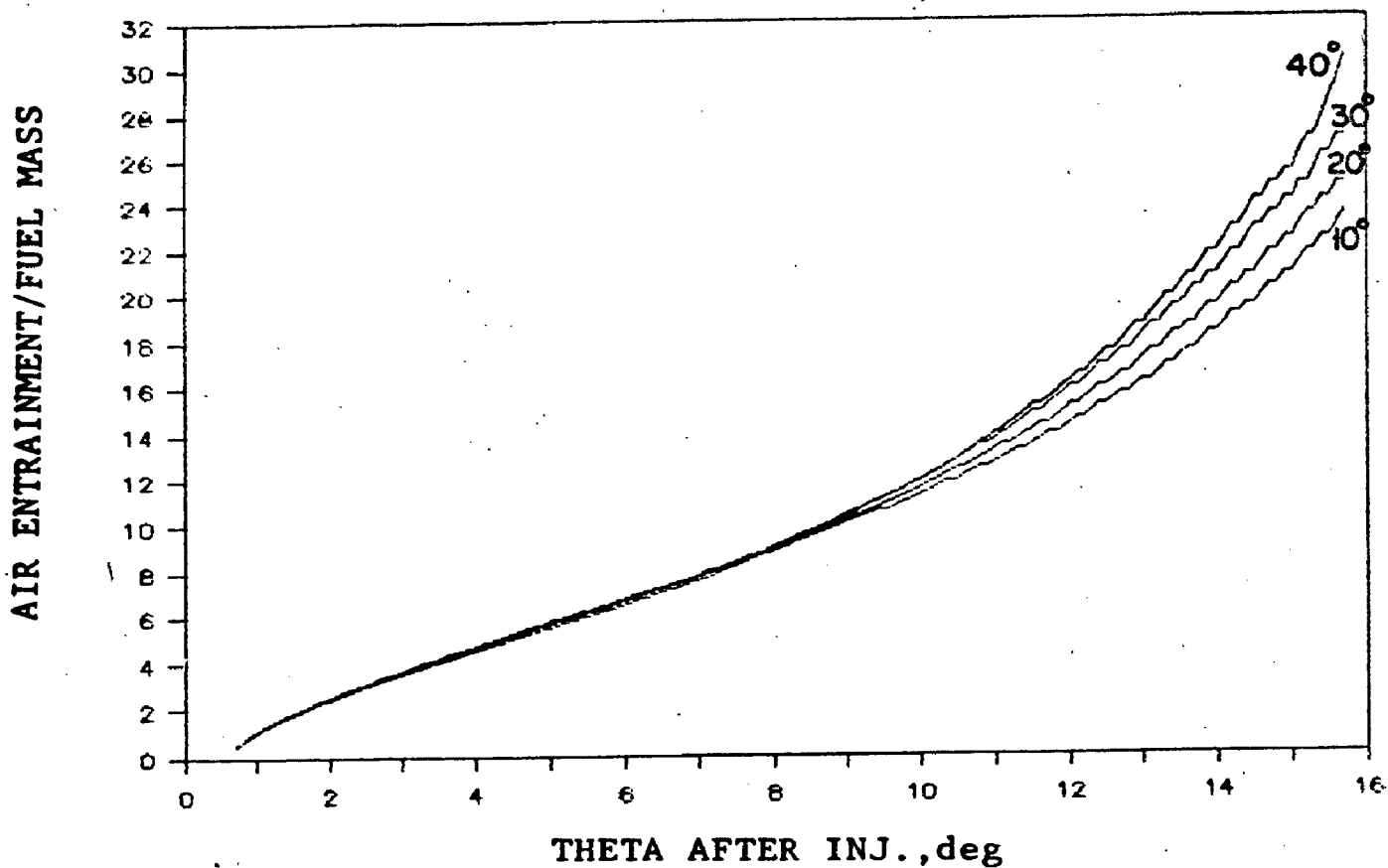


Fig 6.32 Effect of spray angle on air entrainment

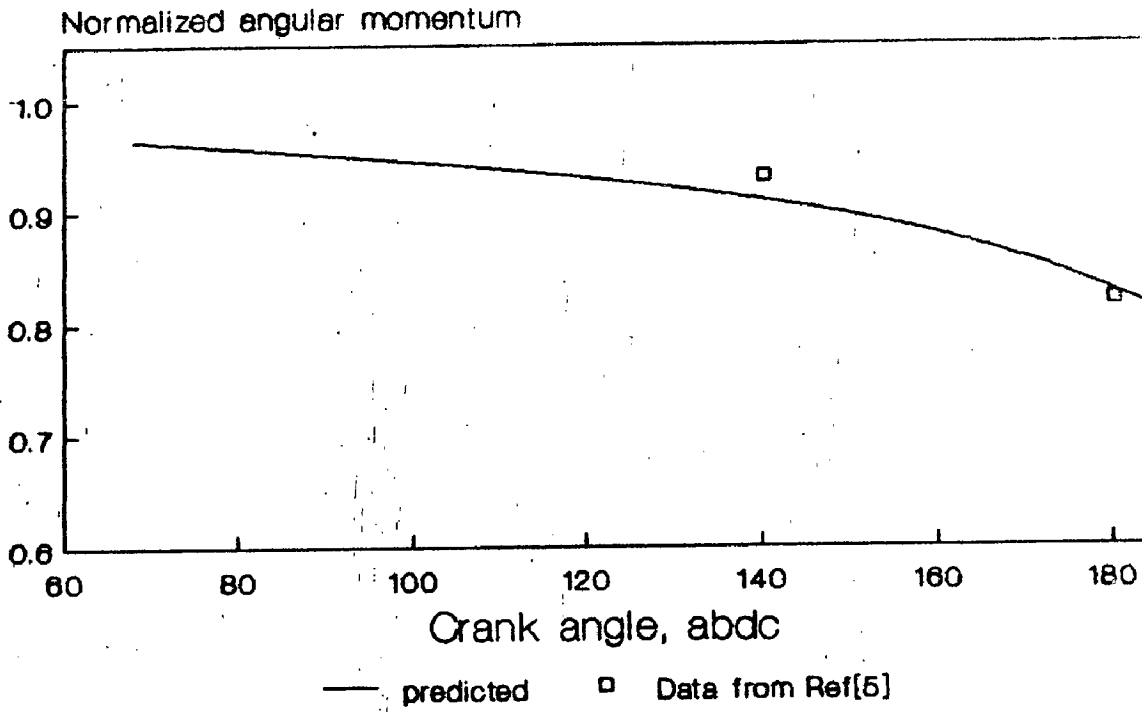


Fig 6.33 Angular swirl momentum comparison

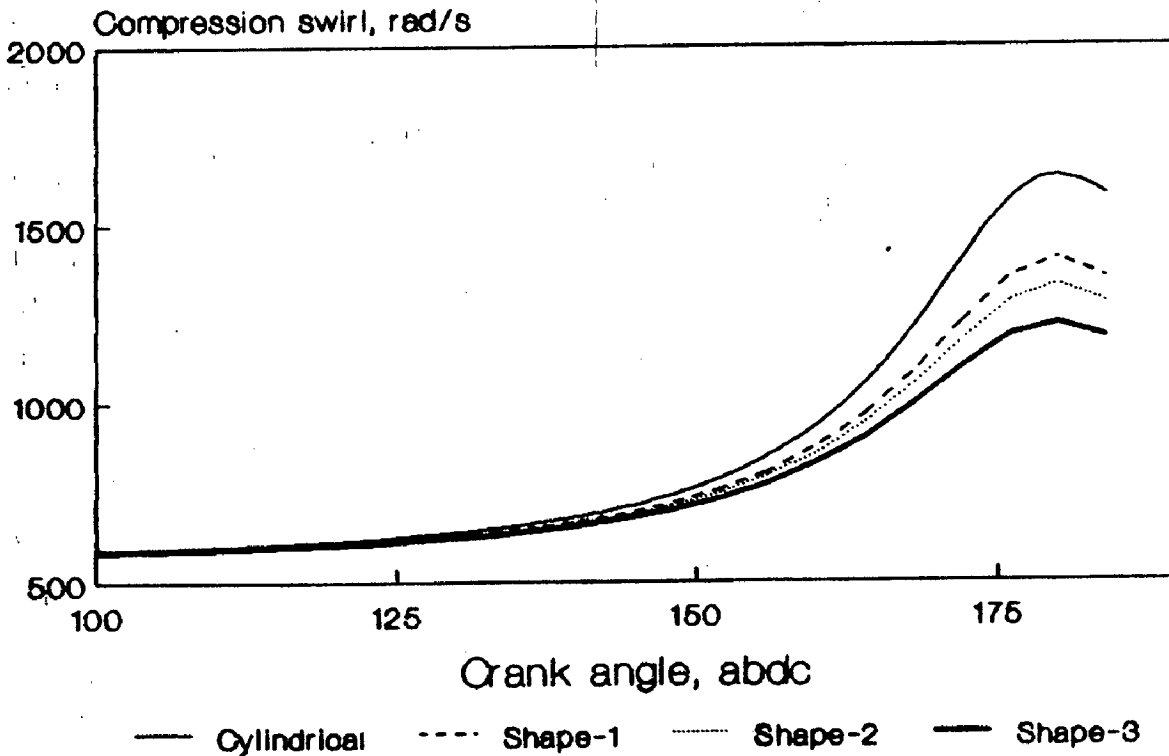


Fig 6.34 Effect of bowl shape on swirl

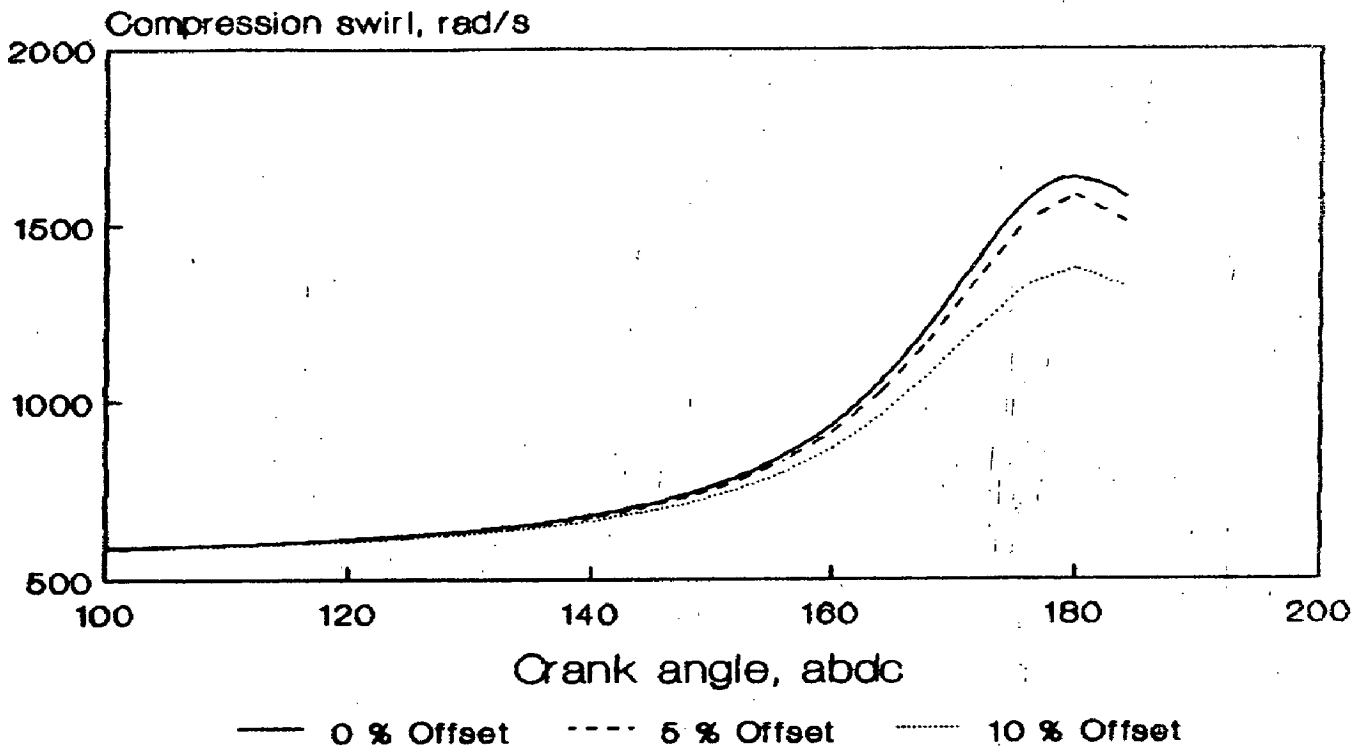


Fig 6.35 Effect of bowl offset on swirl

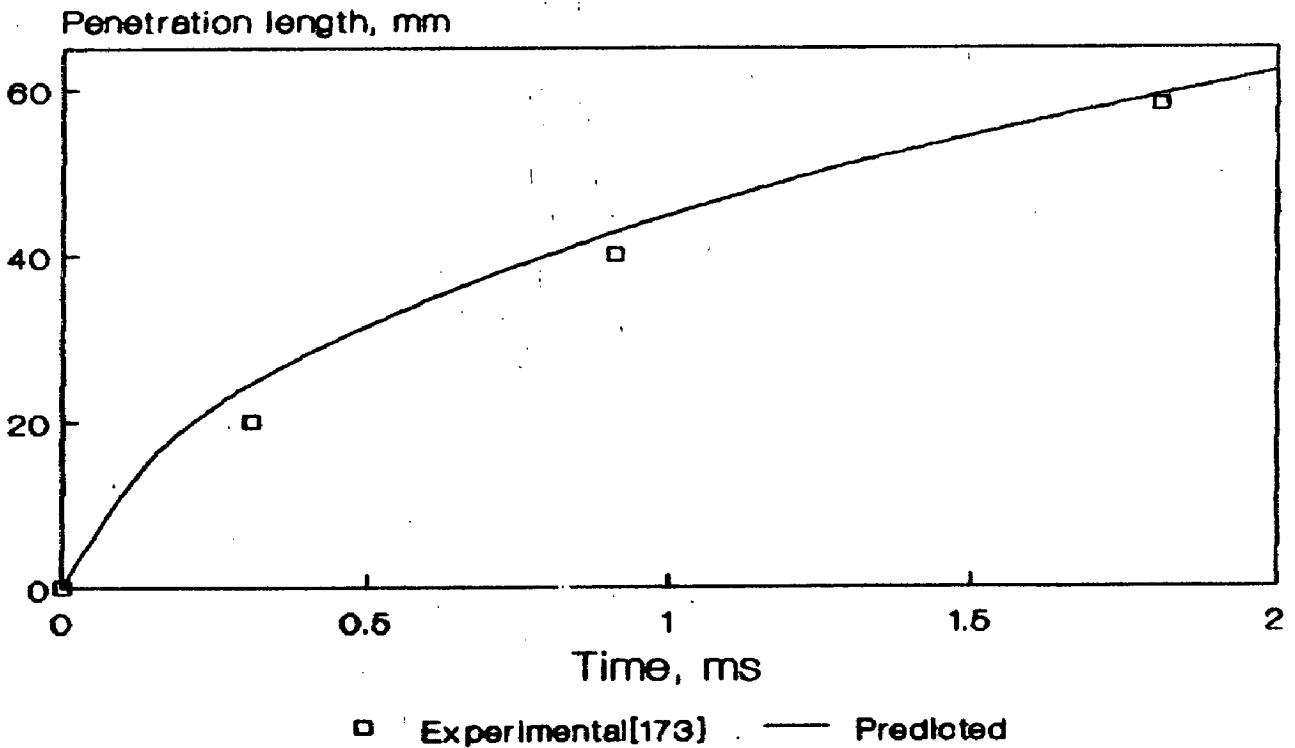


Fig 6.36 Penetration length comparison

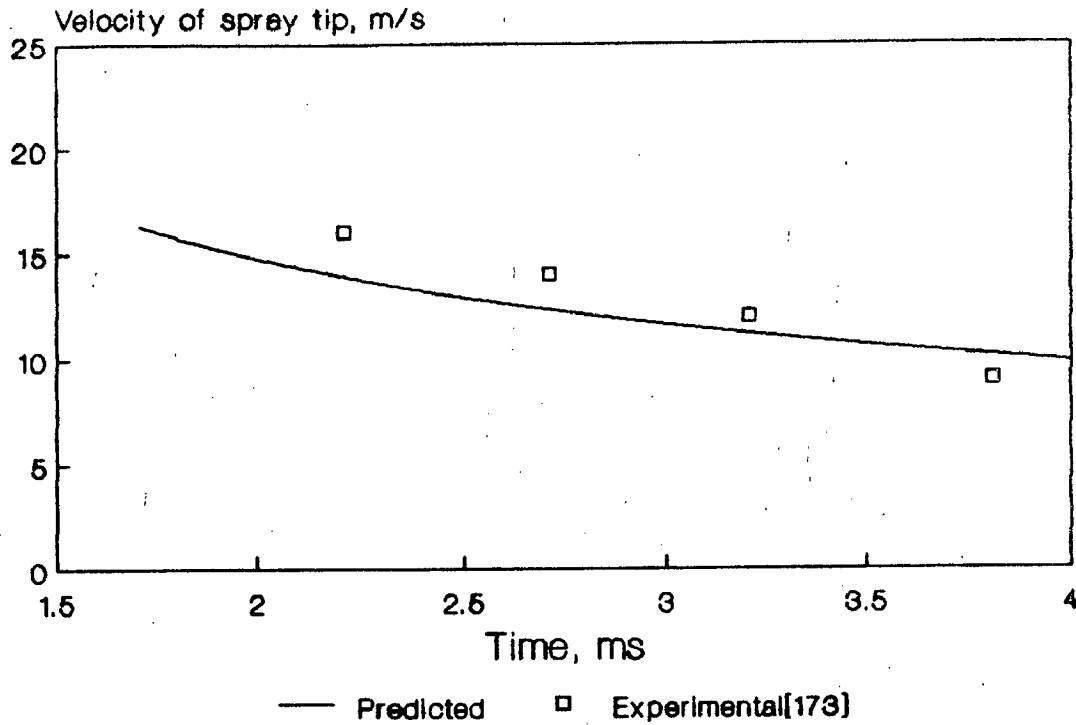


Fig 6.37 Spray velocity comparison

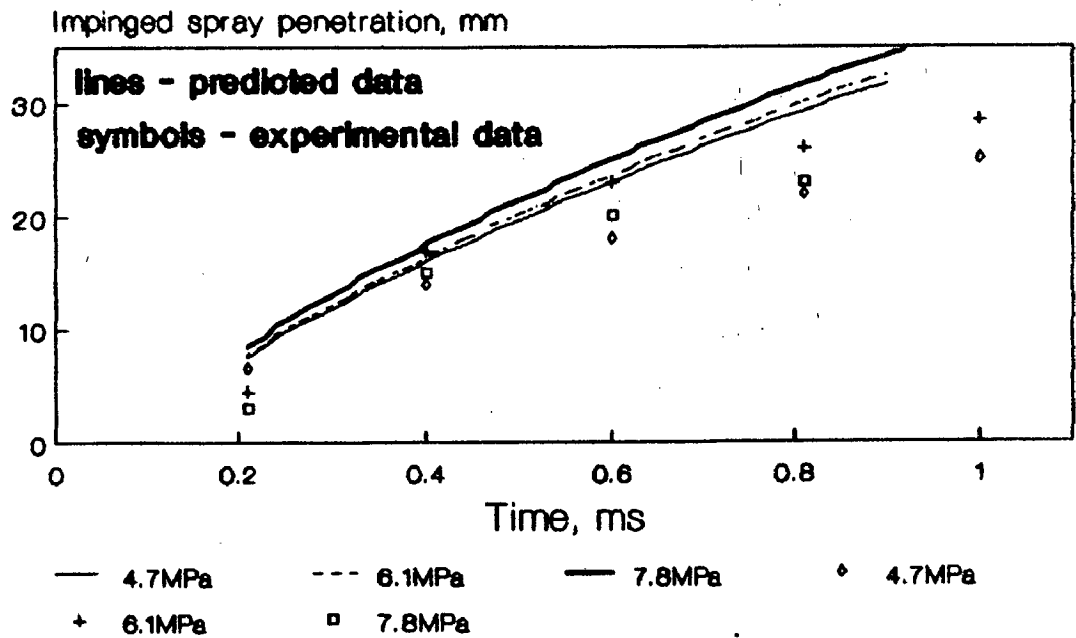


Fig 6.38 Impinged spray penetration comparison at different injection pressures

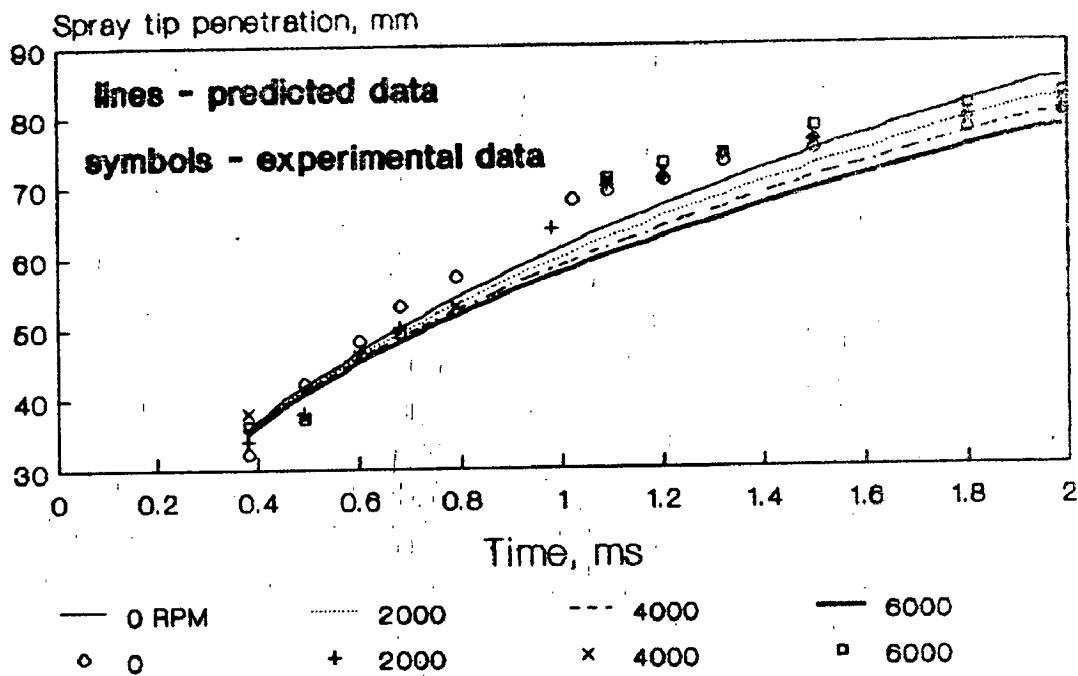


Fig 6.39 Comparison of penetration of impinging spray at different swirler speeds

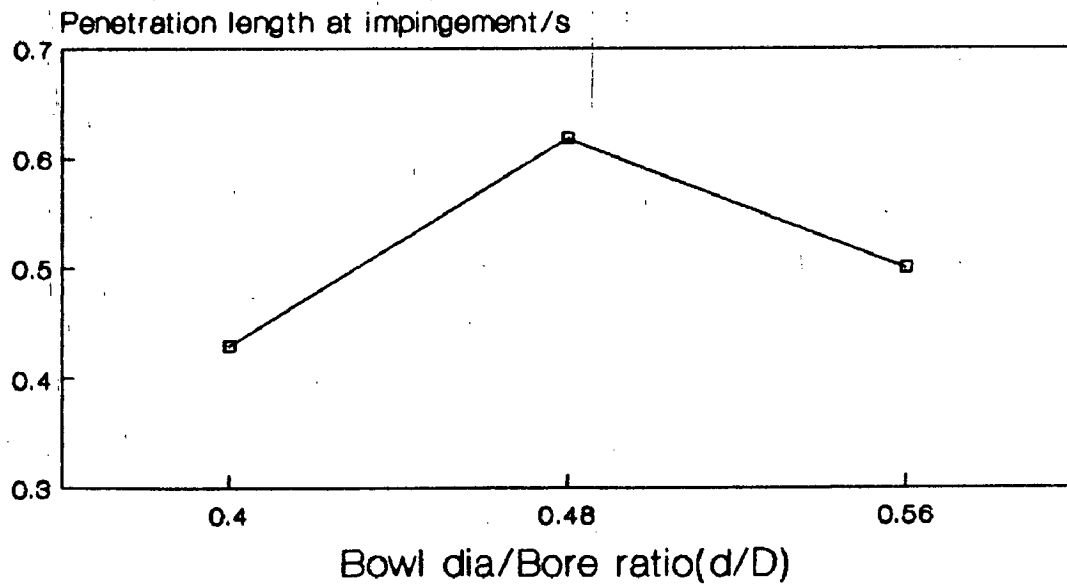


Fig 6.40 Effect of bowl dia/bore ratio on penetration at impingement



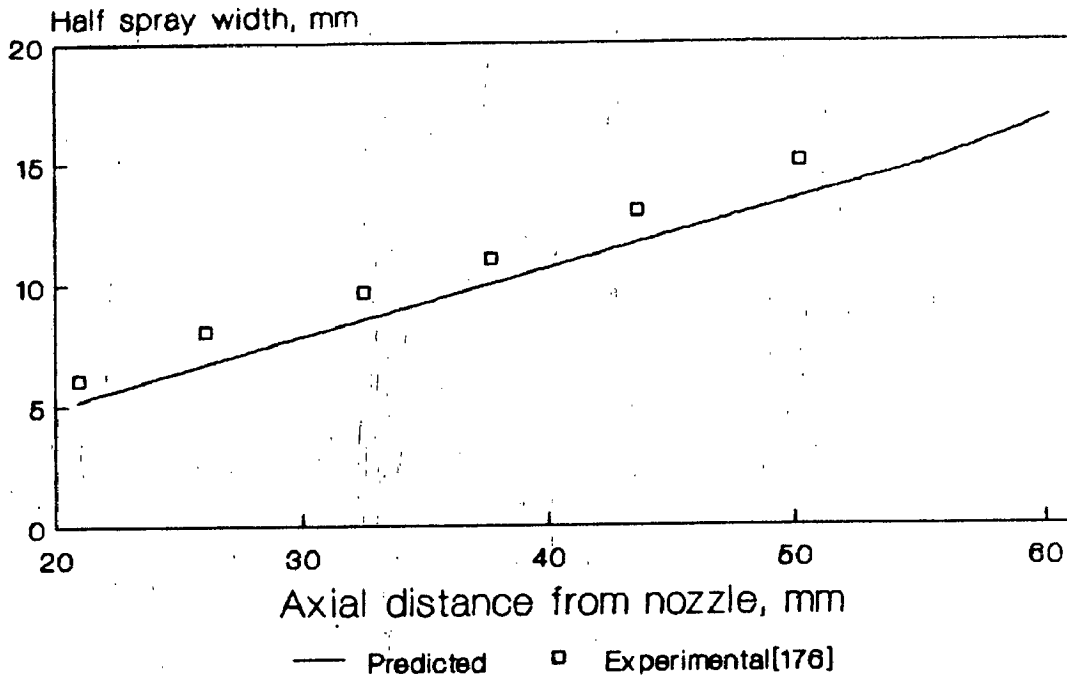


Fig 6.41 Comparison of half spray width

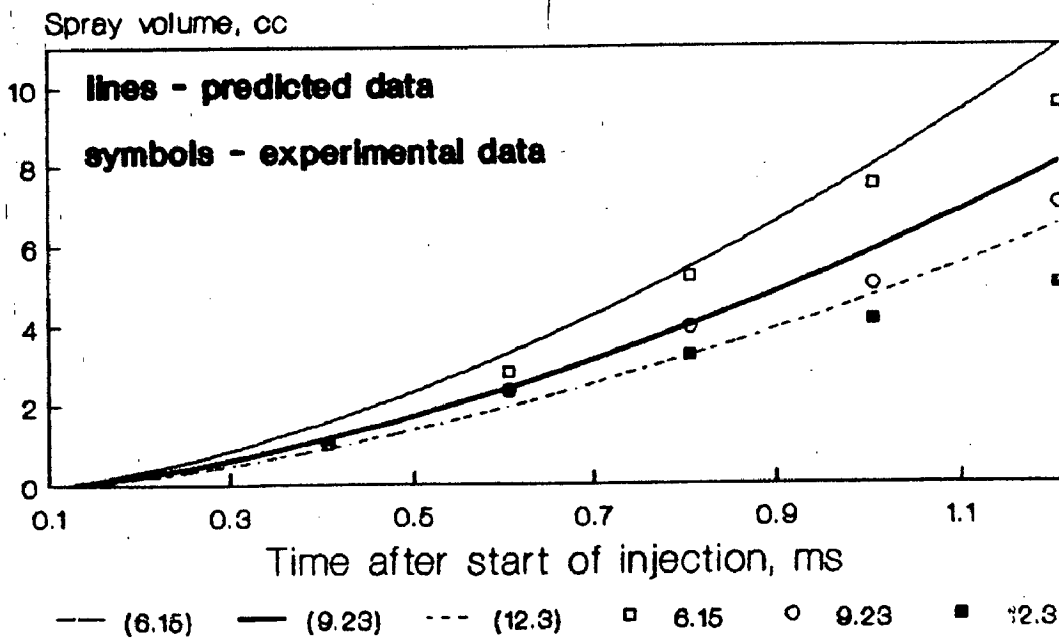


Fig 6.42 Spray volume comparison at different air densities

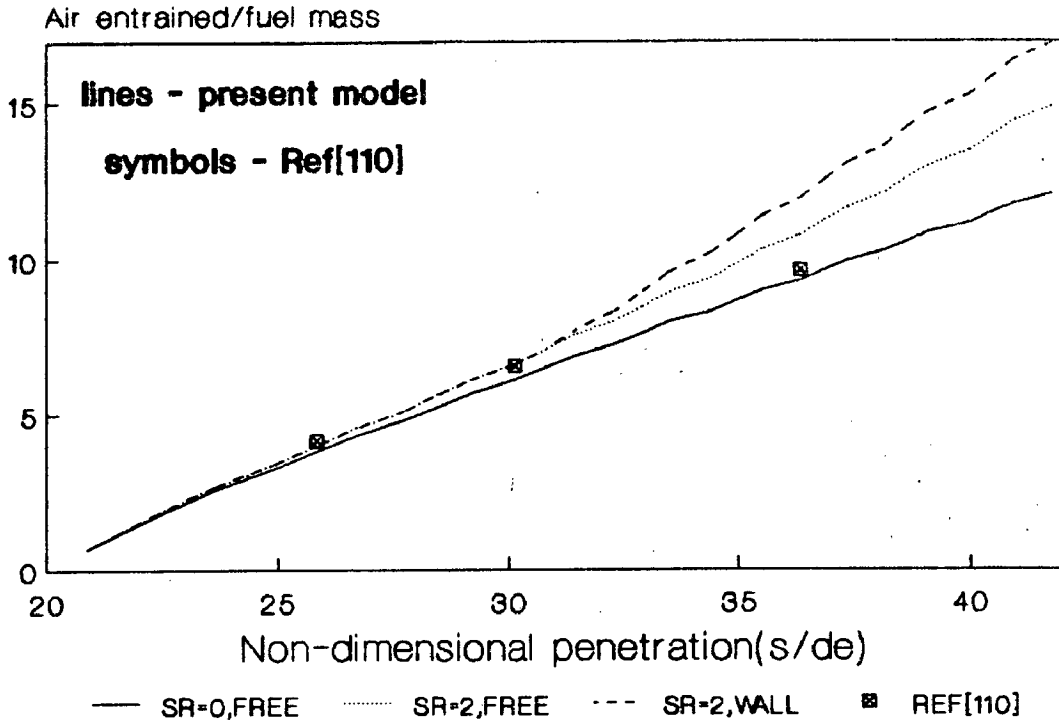


Fig 6.43 Air entrainment comparison

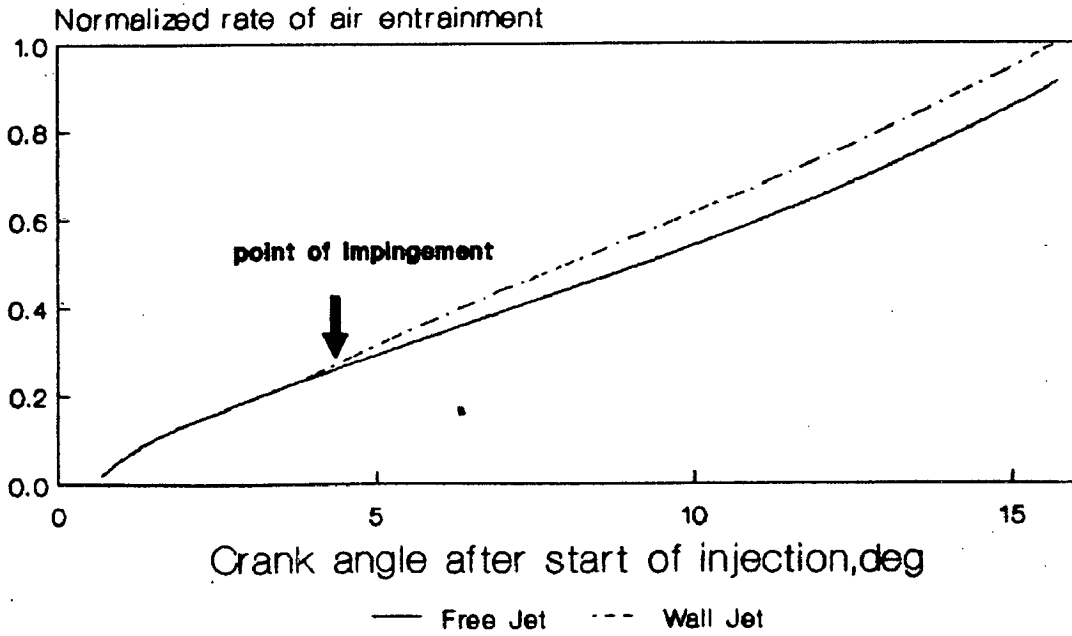


Fig 6.44 Rate of air entrainment for free and wall jet

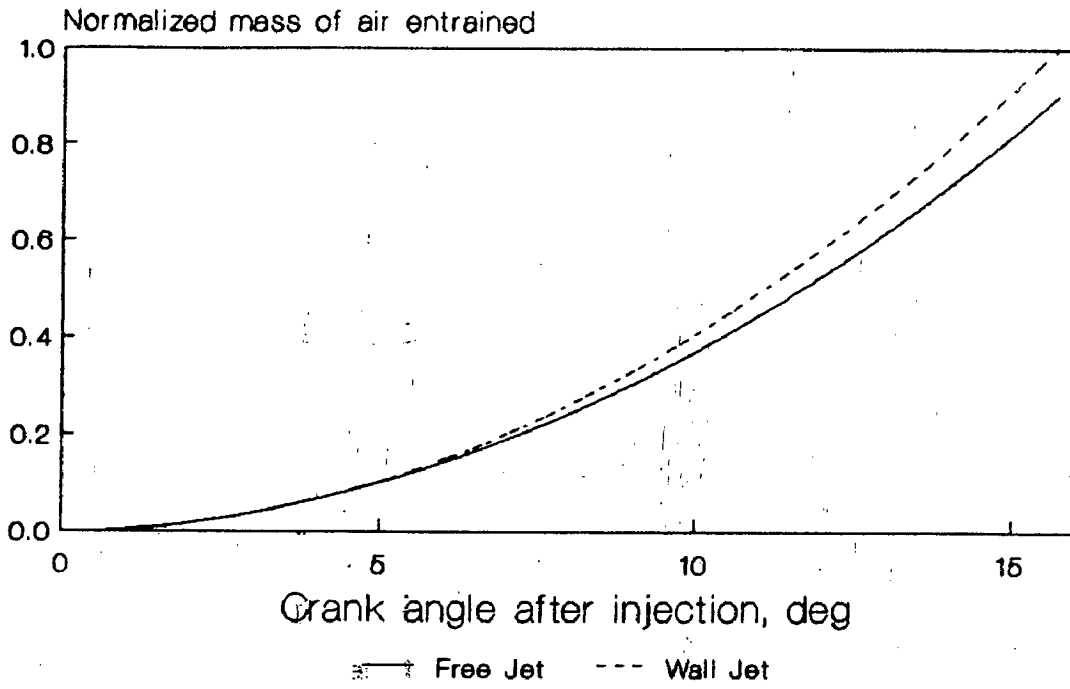


Fig 6.45 Total mass of air entrainment for free and wall jet

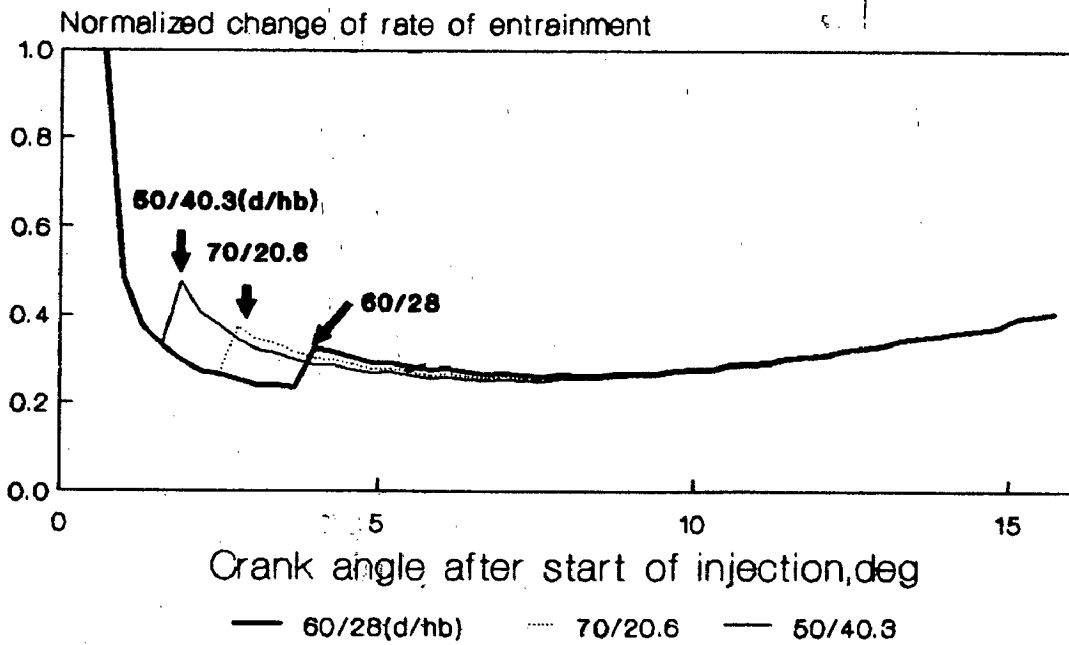


Fig 6.46 Effect of bowl diameter/bore ratio(d/hb) on air entrainment rate

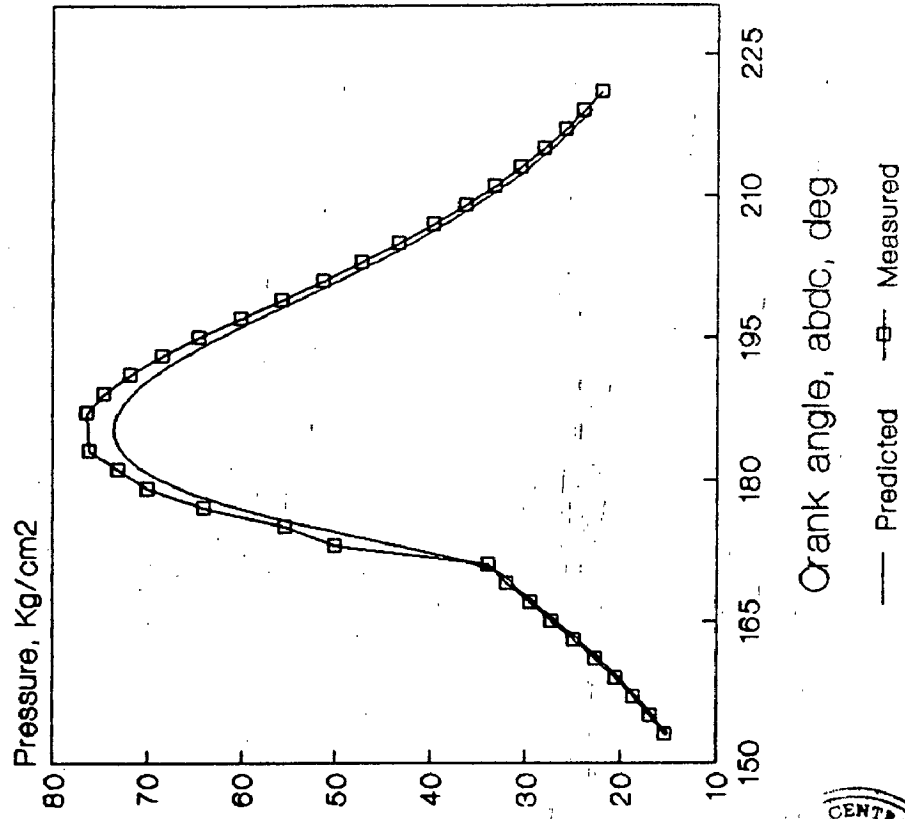


Fig 6.48 Comparison of pressure data for engine-A at 1600 RPM

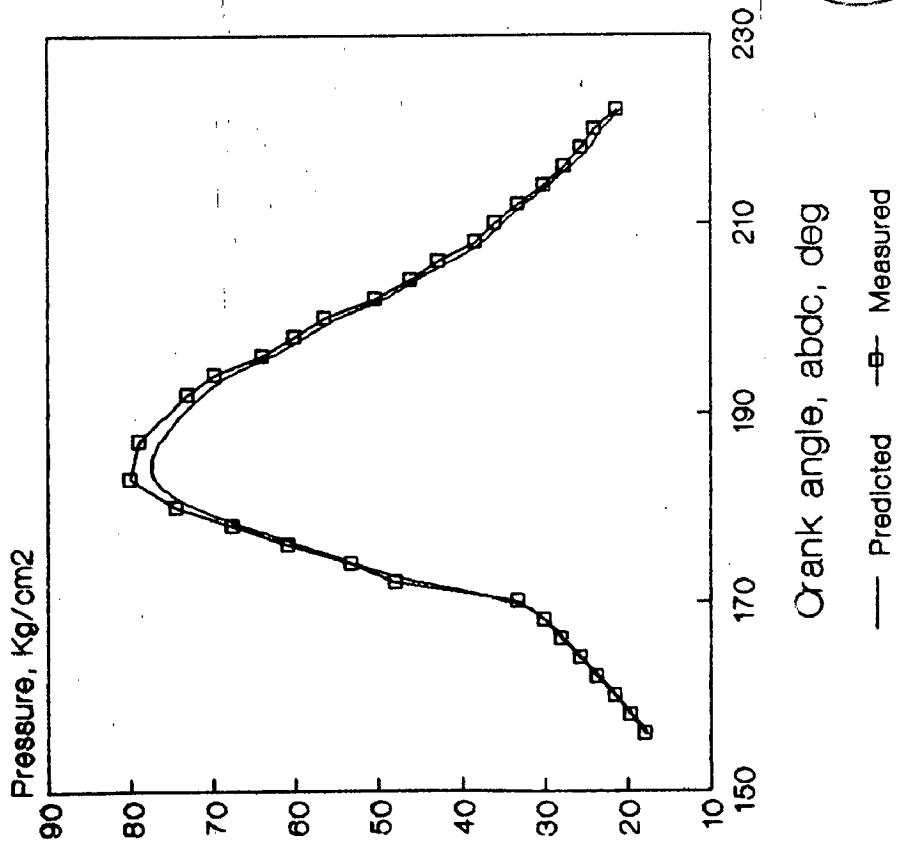


Fig 6.47 Comparison of pressure data for engine-A at 1200 RPM



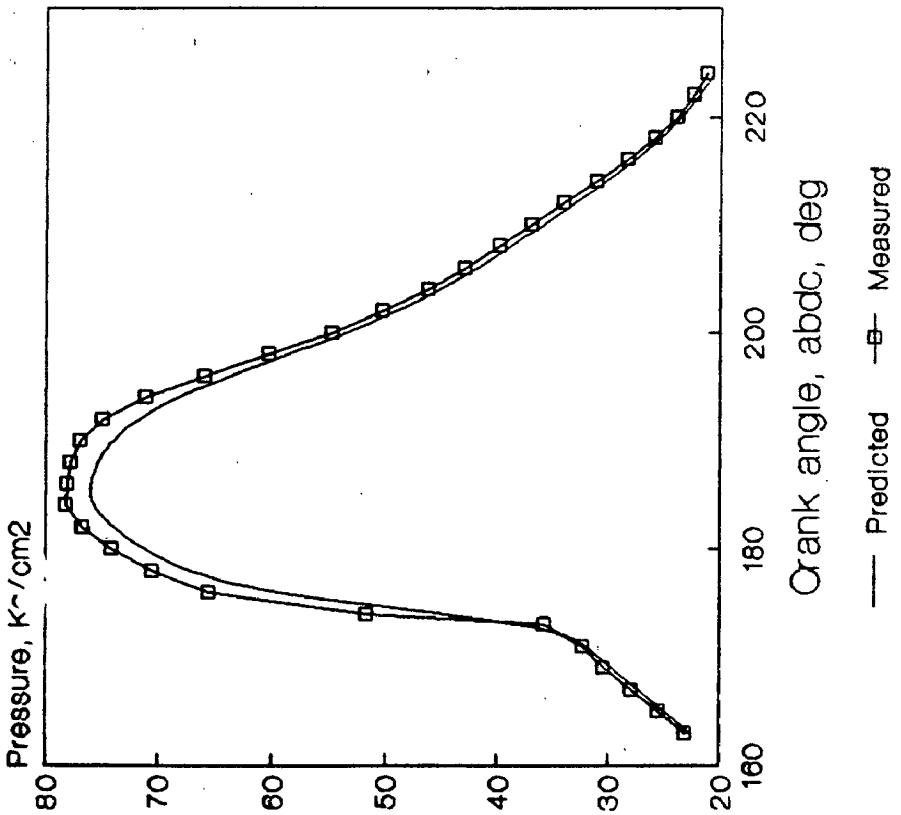


Fig 6.49 Comparison of pressure data for engine-A at 1800 RPM

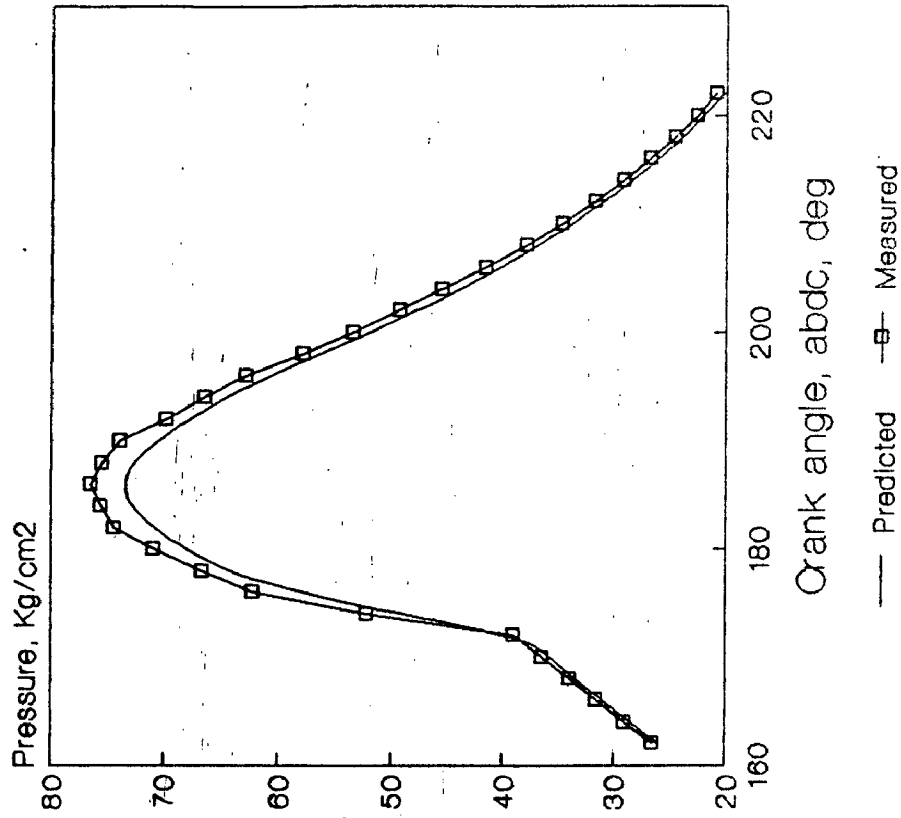


Fig 6.50 Comparison of pressure data for engine-A at 2000 RPM

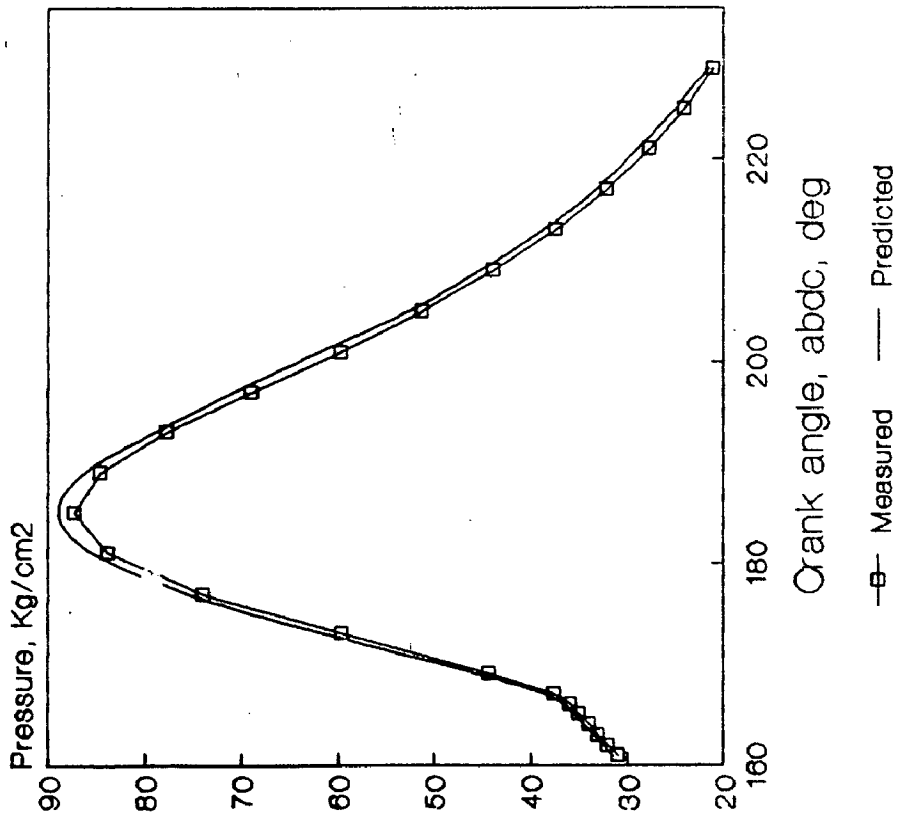


Fig 6.51 Comparison of pressure data for engine-B at 1100 RPM

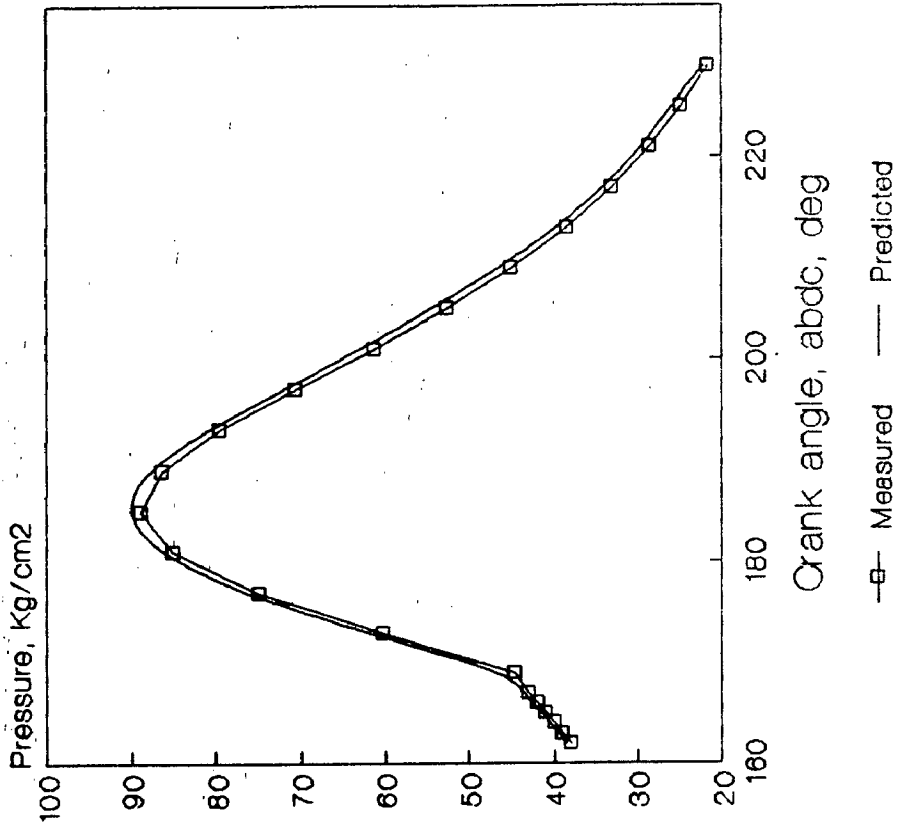


Fig 6.52 Comparison of pressure data for engine-B at 1300 RPM

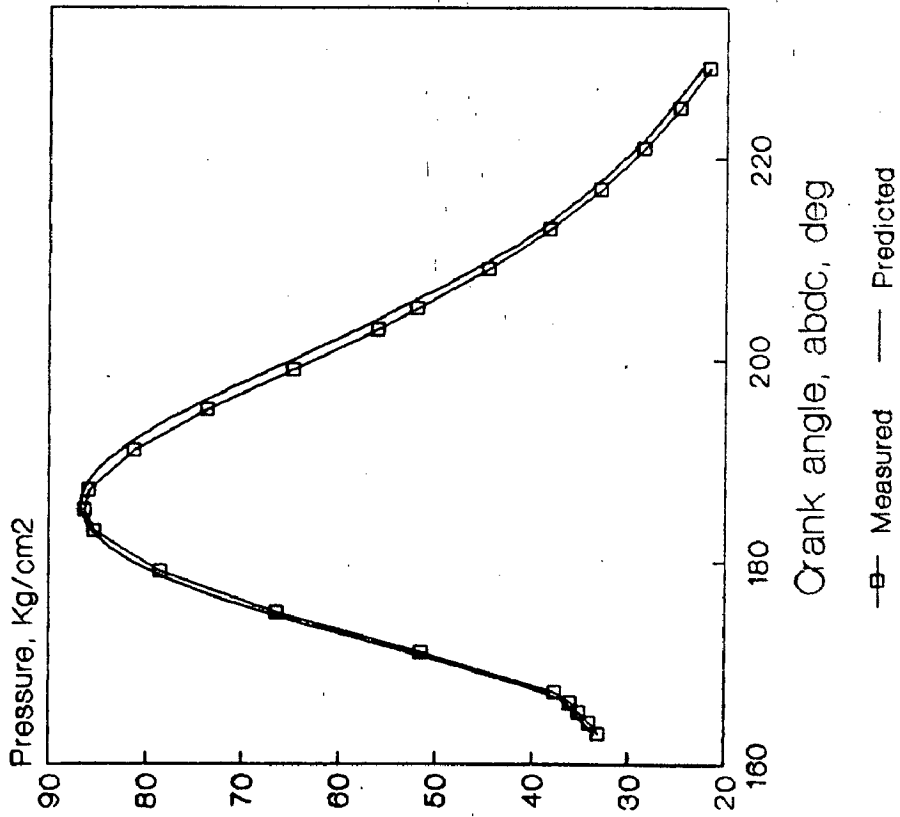


Fig 6.53 Comparison of pressure data for engine-B at 1500 RPM

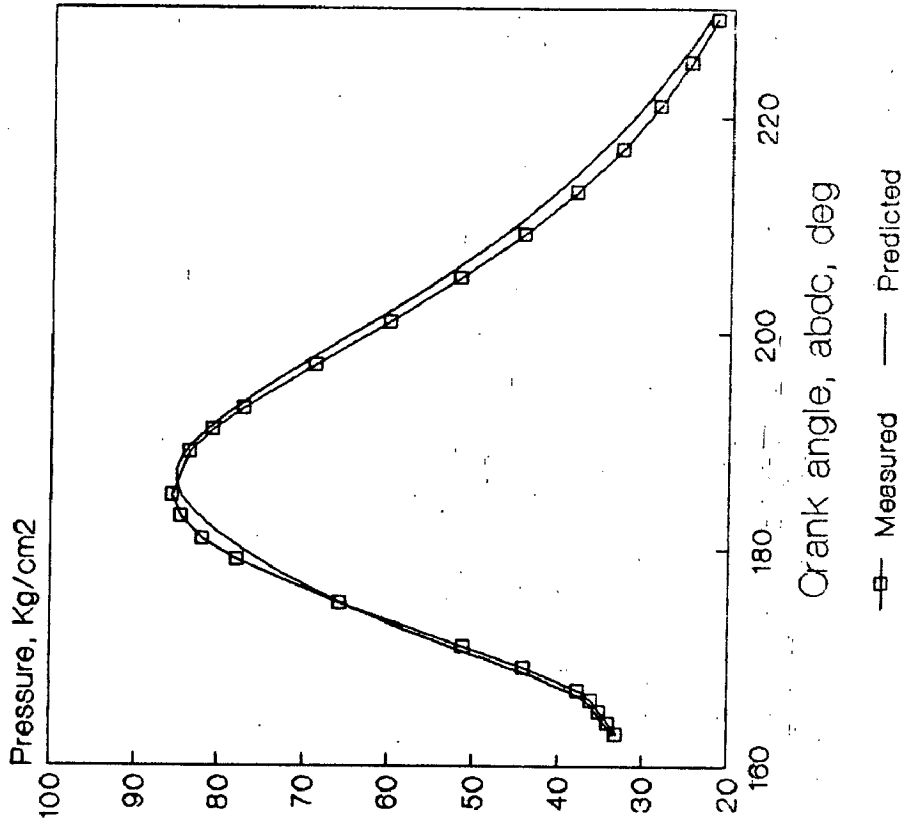


Fig 6.54 Comparison of pressure data for engine-B at 1650 RPM

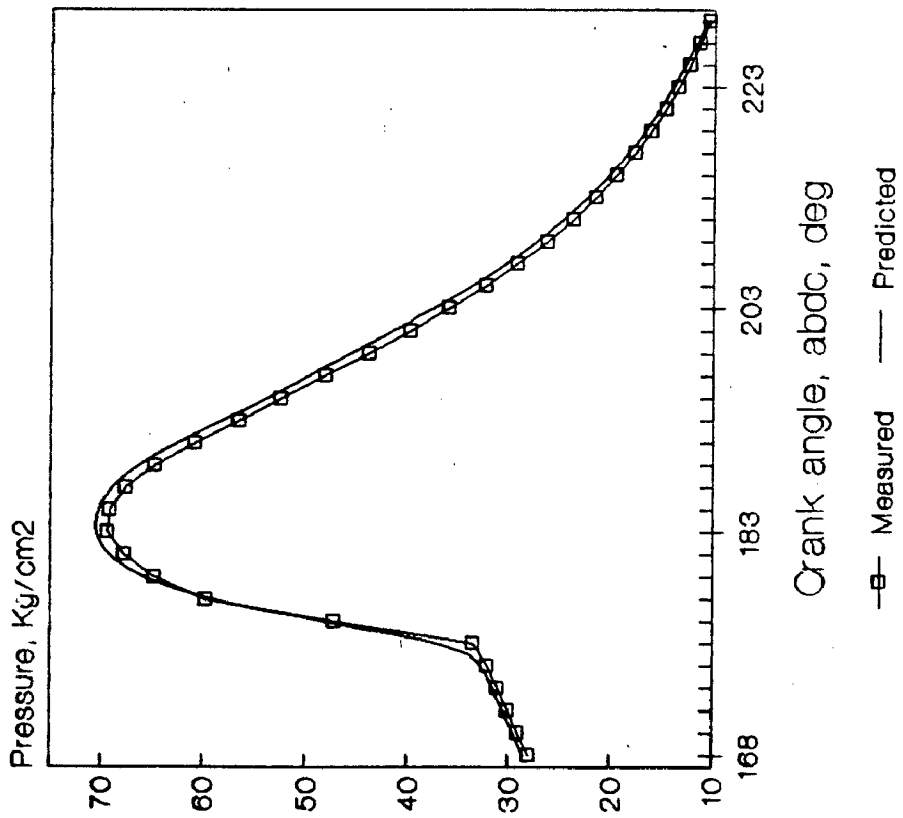


Fig 6.55 Comparison of pressure data for engine-C at 1800 RPM and 23.5 cubic mm fuel delivery

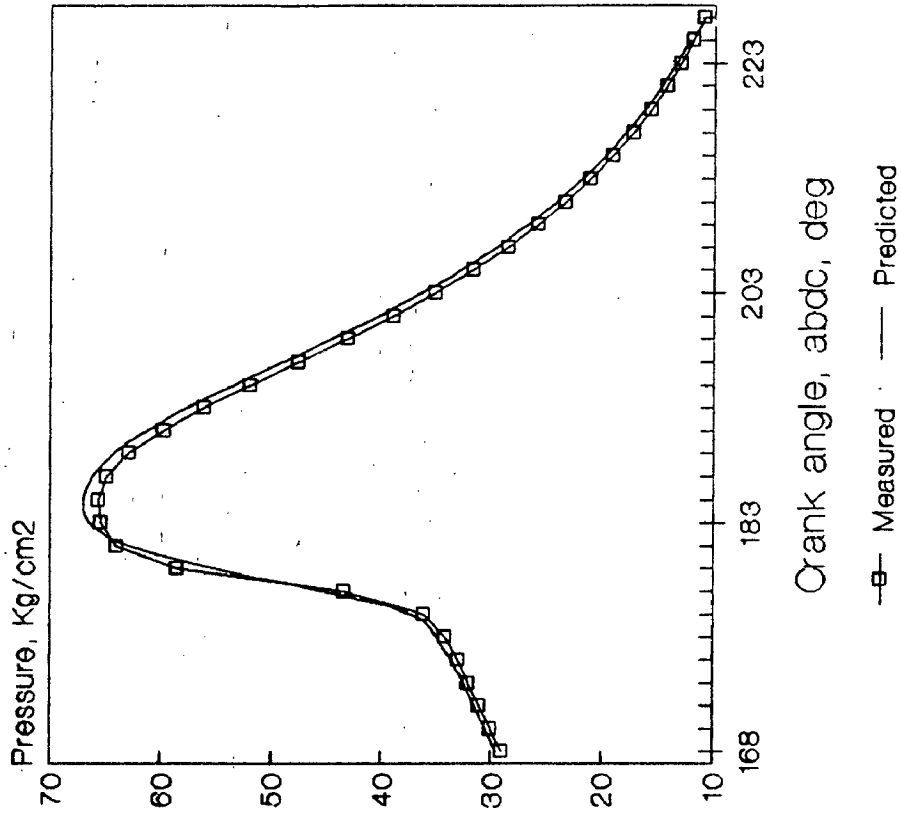


Fig 6.56 Comparison of pressure data for engine-C at 2400 RPM and 19.0 cubic mm fuel delivery



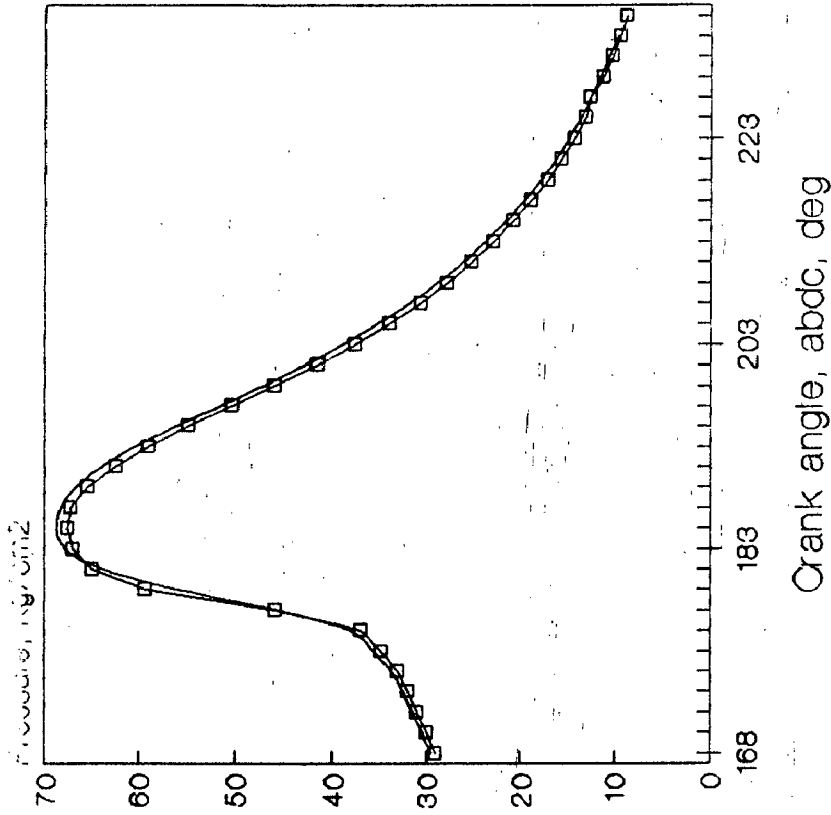


Fig 6.58 Comparison of pressure data for engine-C at 2400 RPM and 23.8 cubic mm fuel delivery

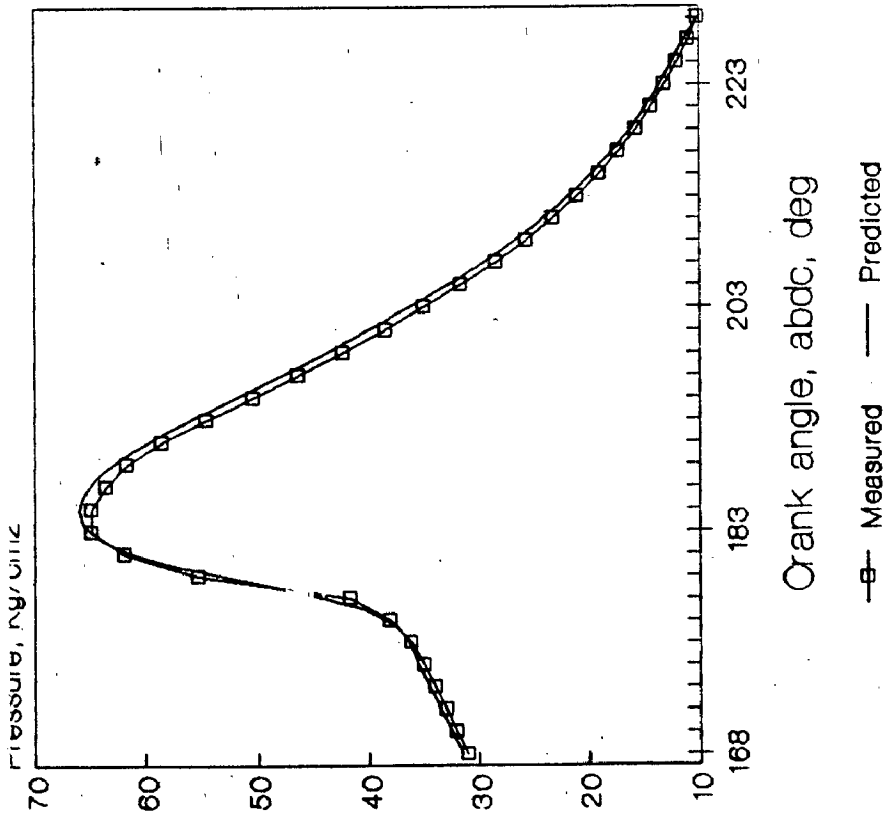


Fig 6.57 Comparison of pressure data for engine-C at 3000 RPM and 18.0 cubic mm fuel delivery

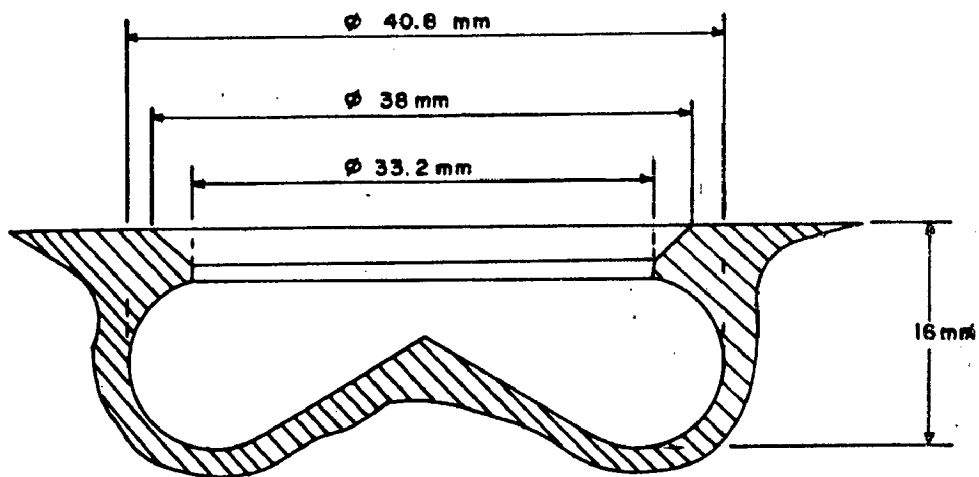


Fig 6.59 Bowl shape of Ricardo engine

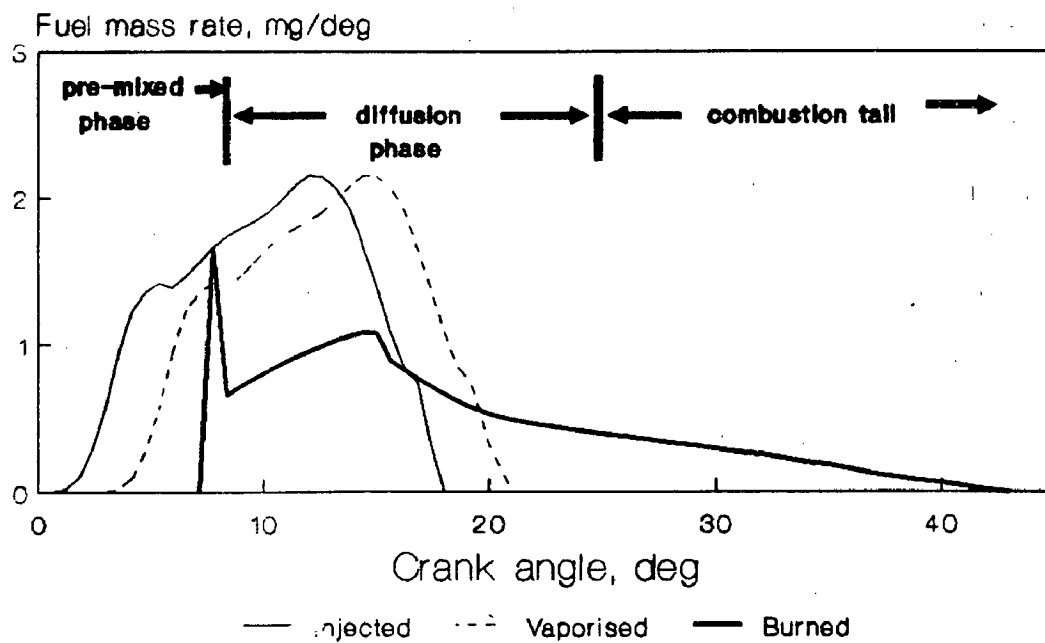


Fig 6.60 Rate of fuel injected, vaporised and burned, mg/deg

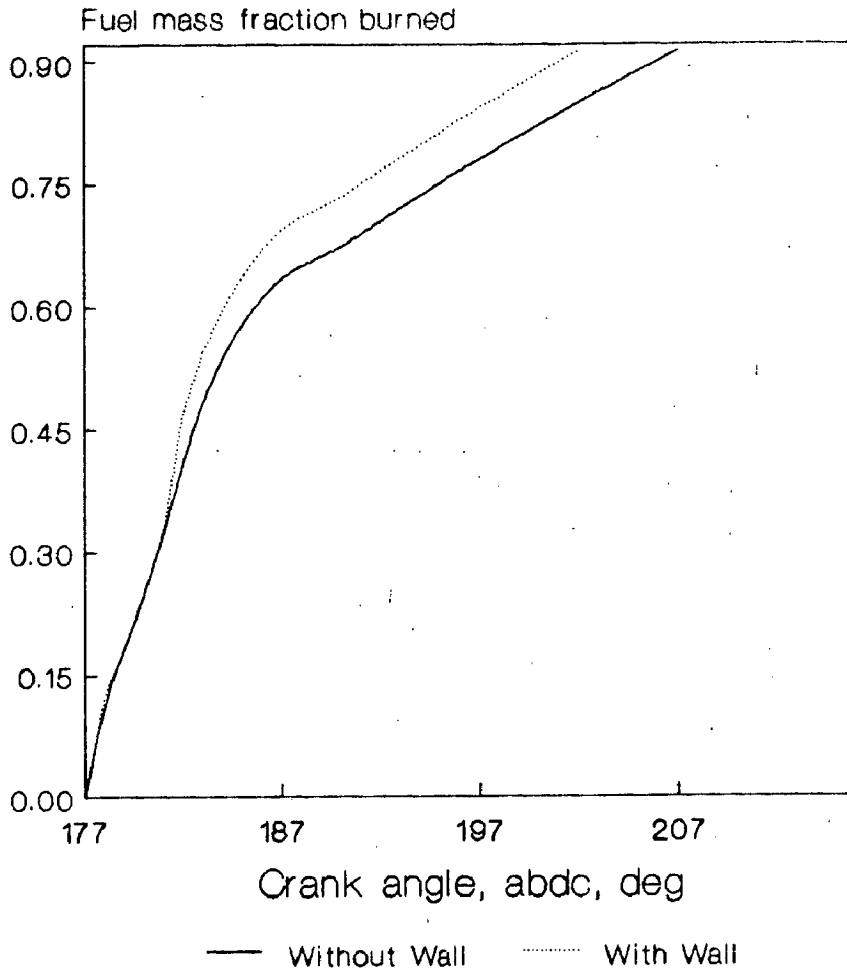


Fig 6.61 Effect of wall on fuel burning

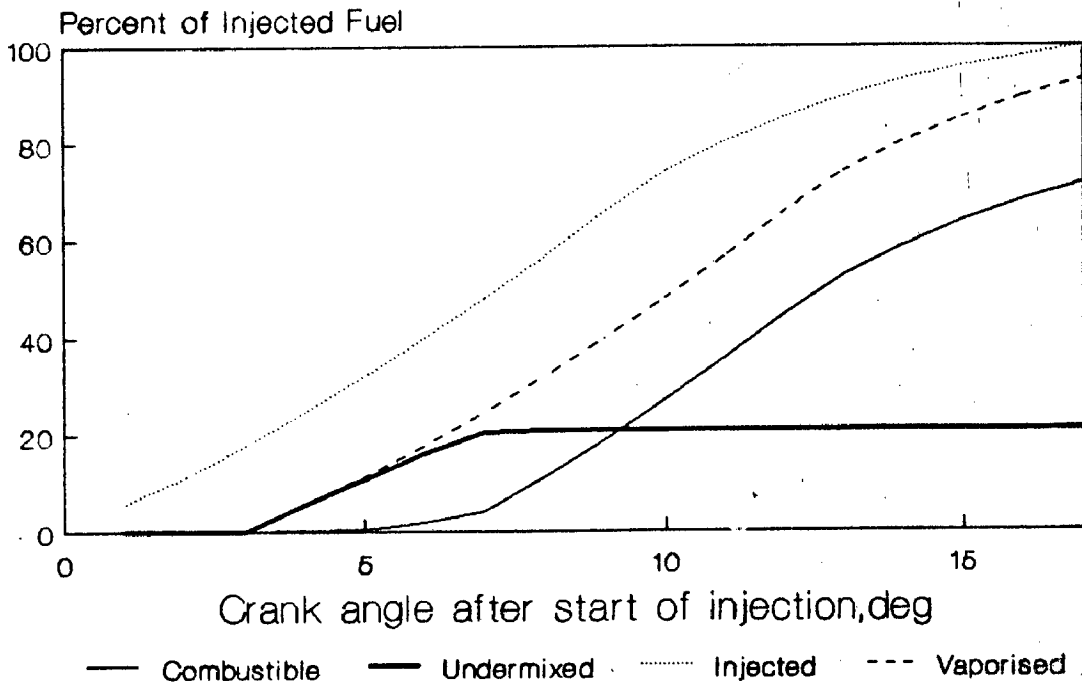


Fig 6.62 Fuel mixing history during injection

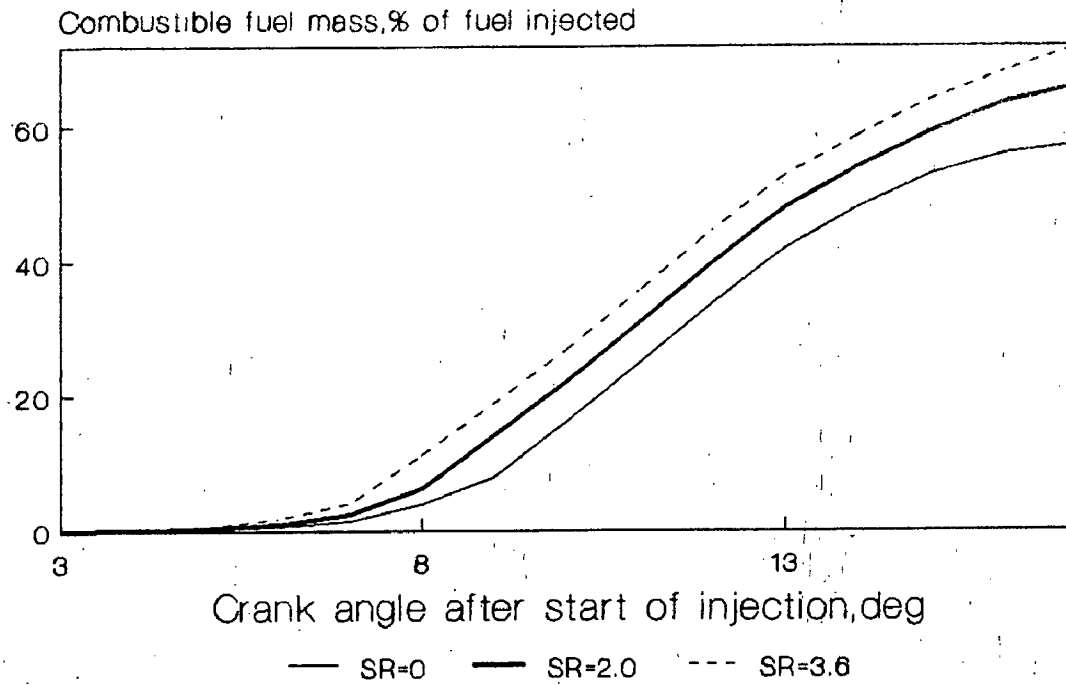


Fig 6.63 Effect of swirl on combustible fuel during injection

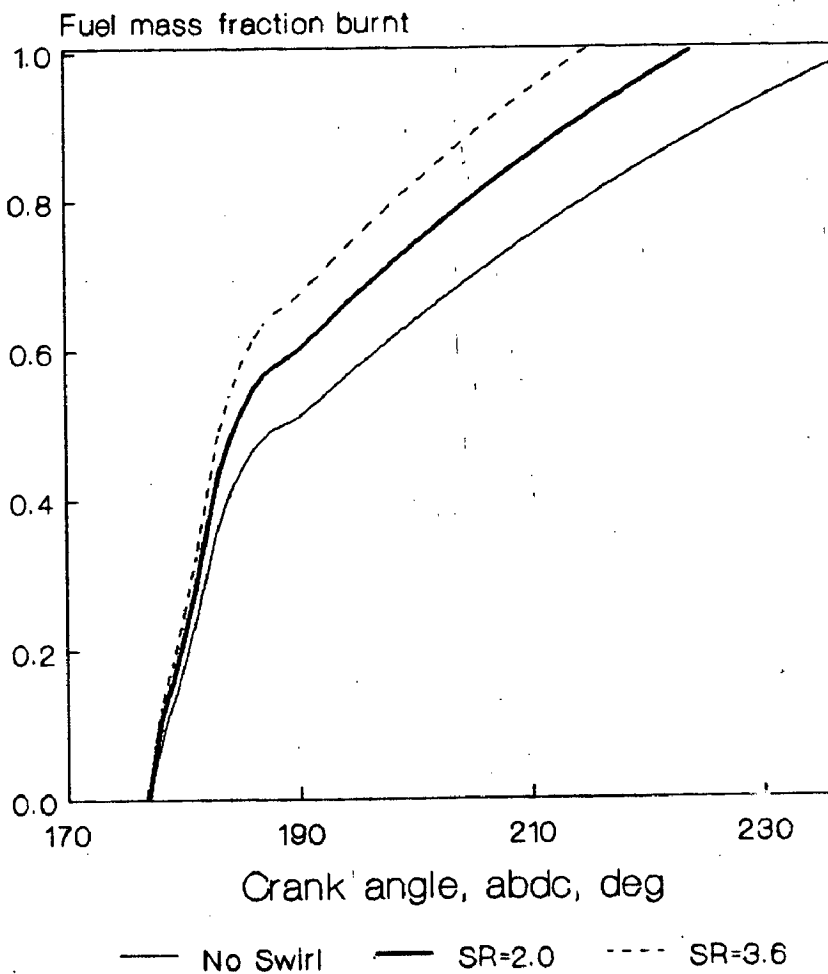


Fig 6.64 Effect of swirl on fuel burning

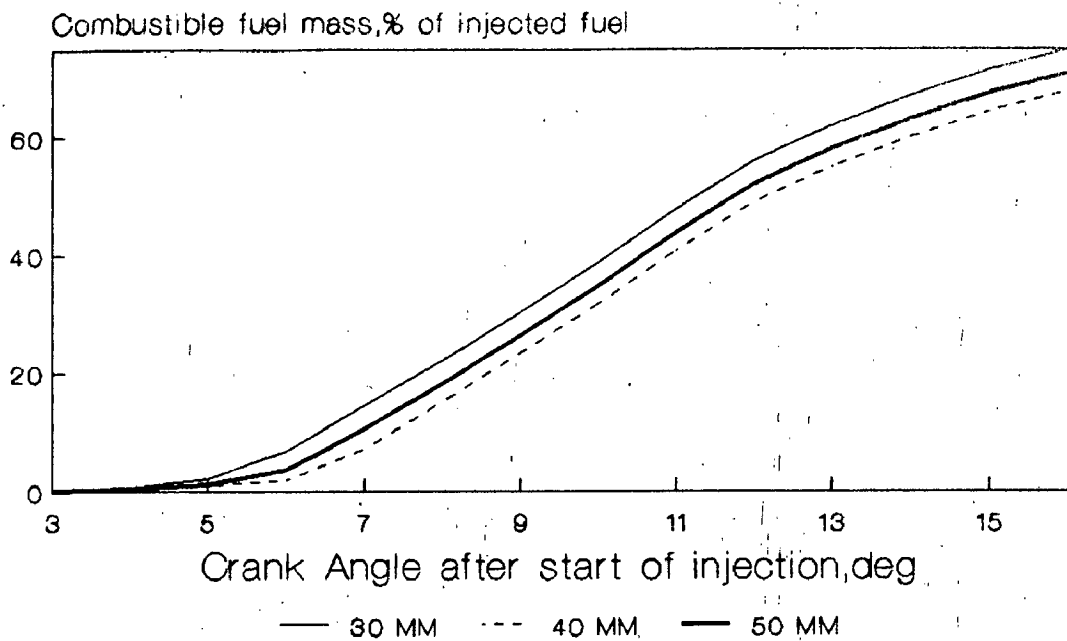


Fig 6.65 Effect of bowl diameter on combustible vapour mass

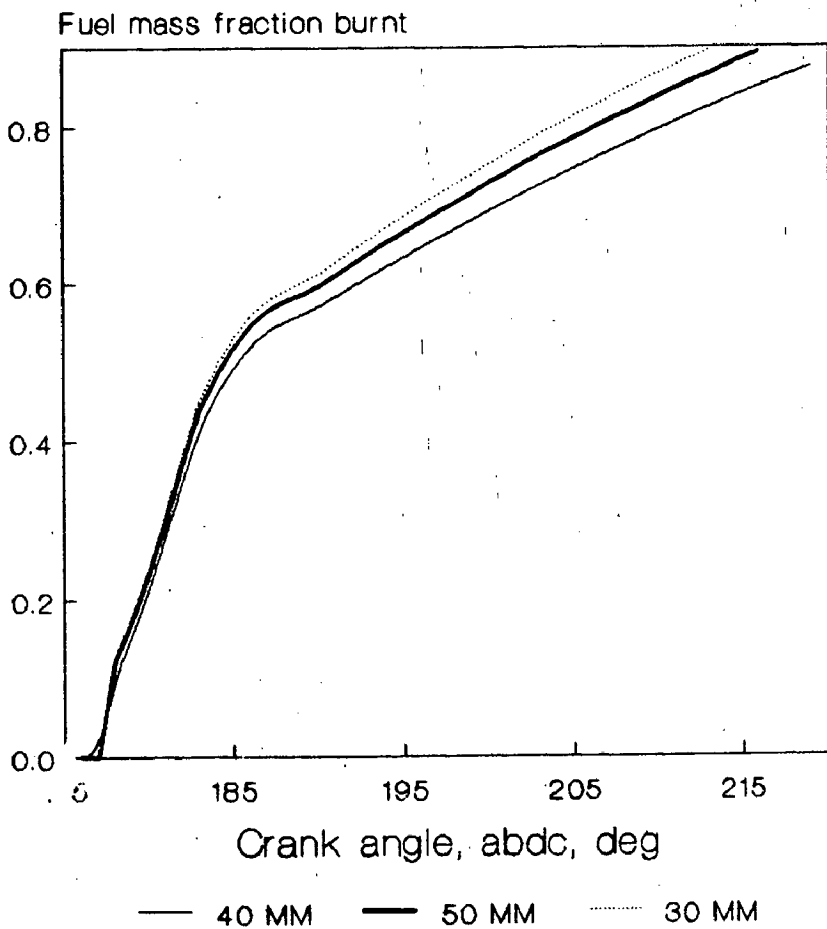


Fig 6.66 Effect of bowl diameter on fuel burning

## CHAPTER - 7

### CONCLUSIONS AND FUTURE WORK

#### 7.1 CONCLUSIONS

From the literature, it is observed that the detailed analysis of the wall jet development in engine situation in the presence of swirl is not adequately done. In the present work, therefore, the spray-swirl-wall interaction model based on the continuum integral approach is formulated by writing mass and momentum conservation equations along the tangential and normal directions to the spray for both free and wall regions. The effect of bowl geometry in terms of moment of inertia and the wall friction on the instantaneous swirl level during compression is also considered.

The spray-swirl-wall interaction model is validated for fuel-air mixing characteristics i.e the spray penetration, growth, air entrainment etc. with the published data from literature. The model predictions show good correlation with the experimental data and respond well to the variations in input parameters.

In the multizone spray structure of the model, the simulation of atomization, droplet-size distribution, evaporation, turbulent mixing and combustion processes is included. The comparison of experimental engine pressure-time history at various test conditions are made.

From the results it is concluded that;

- (i) The rate of air entrainment is enhanced during the wall jet flow due to the combined effect of increased axial

entrainment, increased surface area available for entrainment and the wall shear stress.

- (ii) Although, early impingement in small engines results in wall wetting, once fuel is vaporized, the wall jet formation helps in enhanced mixing due to the higher rates of air entrainment.
- (iii) The initial rate of injection and mass averaged injection pressure play significant role in the air-fuel mixing.
- (iv) The rate of entrainment is higher in the central injection case in comparison to the other injector locations in the cylinder.
- (v) Changes in nozzle orifice size affect fuel-air mixing. The effect is, however, predominantly injection pressure controlled.
- (vi) The predictions in terms of the burning rates and under-mixedness suggest that, if the spray is fully vaporized prior to the impingement, the rate of burning is found to be faster in the presence of the wall.
- (vii) The level of predictions from the model is satisfactory.

A proper matching of injection characteristics, bowl shape and air motion is necessary and can be accomplished with the help of the present model.

## 7.2 FUTURE WORK

A detailed analysis of the spray break-up and evaporation can be done in order to predict the wall wetting effects for a small DI diesel engine.

The prediction of soot and  $(NO)_x$  can be made and a trade-off

study between them can be done.

In the model, the mutual interaction of sprays in multi-spray nozzles can be incorporated.



## REFERENCES

1. Obert E.F. Internal Combustion engines and air pollution ,Intext educational Publishers, New York, 1973.
2. Beck N.J., Weselch W.E., Barkhimer R.L. and Johnson W.P. CRIDEC- A practical solution to high performance, all electronics fuel injection for diesel engines, FISITA Proc., 1984.
3. Heywood J.B. Fluid motion within the cylinder of internal Combustion engines- The 1986 Freeman Scholar lecture, Journal of Fluid Engineering, Vol 109, March 1987.
4. Gosman A.D. Multi-dimensional modelling of cold flows and turbulence in reciprocating engines, SAE paper 850344, 1985.
5. Mckinley T.L., Primus R.J., O'Rourke P.J. and Buttler T.D. Comparison of computed and measured air motion in circular and square piston cups, SAE paper 881612.
6. Liou T.M., Hall M., Santavicca D.A. and Bracco F.V. Laser Doppler Velocitometry measurements in valved and ported engines, SAE paper 840375, 1984.
7. Arcoumanis C. and Whitelaw J.H. Fluid mechanics and internal combustion engines- a review, Proc. Instn mech Engrs, Vol 201, No.1, 1987.
8. Hirt C.W., Amsden A.A. and Cook J.L. An arbitrary Lagrangian Eulerian Computing method for all flow speeds , J of compu. Phy., Vol 14, No.3, March 1974, pp 227-253.
9. Rivard W.C., Farmer C.A. and Butler T.D. RICE- A computer program for multi-dimensional chemically reactive flows at all speeds, Los Alamos Scientific research Laboratory report LA-5812, Nov. 1974.
10. Gosman A.D., Johns R.J.R. and Watkins A.P. Development of prediction methods for in-cylinder process in reciprocating engines, Combustion Modelling in Reciprocating Engines, ed. Mattavi J.N. and Amman C.A., Plenum Press, 1980.
11. Wakisaka T., Shamamoto Y. and Isshiki Y. Three-dimensional numerical analysis of in-cylinder flows in reciprocating engines, SAE paper 860464, 1986.
12. Johns R.J.R. A unified method for calculating engine flows, A ME paper No.84-DGP-18, 1984.
13. O'Rourke P.J., Amsden A.A., Butler T.D. and Mckinley T.L. Improvement of the KIVA-II computer program for numerical combustion, Third Int Conf on Numerical Combustion, Antibis, France.
14. Vafidis C. and Whitelaw J.H. Intake valve and in-cylinder flow

development in a reciprocating model engine, Proc. Inst of mech Engrs, 200, C2, 1986.

15. Monaghan M.L. and Pettifer H.F. Air Motion and its effect on diesel performance and emissions, SAE paper 810255, 1981.
16. Wigley G. and Hawkins M.G. Three-dimensional velocity measurements by Laser Anemometry in a diesel engine cylinder under steady state inlet flow conditions, SAE paper 780060, 1978.
17. Wigley G., Patterson A.C. and Rehshaw. Swirl velocity measurements in a firing production systems, Fluid mechanics of combustion system, Boulder, ASME, 29-30, 1981.
18. Brandstatter W., Johns R.J.R. and Wigley G. The effect of inlet port geometry on in-cylinder flow structure, SAE paper 850499, 1985.
19. Cough A., Brunello G. and Tassi E. Effects of intake ports on the in-cylinder air motion under steady flow conditions, SAE paper 880384, 1988.
20. Tanabe S., Hamamoto Y. and Ohigashi S. Swirl in four stroke cycle engine cylinder, Bulletin JSME, 21, 152, 1978.
21. Tanabe S., Iwata H. and Kashiwada Y. Effects of intake port design on swirl characteristics in a four stroke engine, Trans JSME, 50, 457, 1984.
22. Arcoumanis C., Bicen A.F. and whitelaw J.H. Measurements in a motored four stroke reciprocating model engine, ASME, Journal of Fluid Engineering, Vol 104, June 1982.
23. Arcoumanis C., Bicen A.F., Vafidis C. and Whitelaw J.H. Three-dimensional flow field in four stroke model engines, SAE paper 841360, 1984.
24. Arcoumanis C., Bicen A.F. and Whitelaw J.H. Effects of inlet parameters on the flow characteristics in a four stroke model engines, SAE paper 820750, 1982.
25. Dent J.C. and Derham J.A. Air motion in a four stroke direct injection diesel engine, Proc. Instn mech Engrs, Vol 188, 21/74, 1974.
26. Vafidis C. Influence of induction swirl and piston configuration on air flow in a four stroke model engine, Proc Instn Mech Engrs, Vol 198 C, No.8, 1984.
27. Arcoumanis C., Bicen A.F. and Whitelaw J.H. Squish and swirl-squish interaction in motored model engines, ASME, J of Fluid Engg, 105, 1983.
28. Glover A.R., Hundleby G.E. and Hadded O. The development of scanning LDA for the measurement of turbulence in engines, SAE paper 880379, 1988.

29. Iijima T. and Bracco F.V. LDV measurements in an engine with square and circular piston cups, SAE paper 872073, 1987.
30. Shimoda M., Shigemori M. and Tsuruoka S. Effect of Combustion Chamber Configuration on in-cylinder air motion and combustion characteristics of DI diesel engine, SAE paper 850070, 1985.
31. Matsuoka S., Kamimoto T., Urushihara T., Mochimaru Y. and Morita H. LDA measurements and a theoretical analysis of in-cylinder air motion in a DI diesel engine, SAE paper 850106, 1985.
32. Fansler T.D. Laser Velocimetry measurements of swirl and squish flows in an engine with a cylindrical piston bowl, SAE paper 850124, 1985.
33. Fansler T.D. and French D.T. Cycle-resolved laser velocimetry measurements in a re-entrant bowl-in-piston engine, SAE paper 880377, 1988.
34. Frase R.A. and Bracco F.V. Cycle-resolved LDV integral length scale measurements in an IC engine, SAE paper 880381, 1988.
35. Brandl F., Reverencic J., Cartellieri W. and Dent J.C. Turbulent air flow in the combustion bowl of a DI diesel engine and its effect on engine performance, SAE paper 790040, 1979.
36. Williams T.J. and Tindal M.J. Gas flow velocities in DI diesel engines with re-entrant combustion chamber, SAE paper 800027, 1980.
37. Tindal M.J., Williams T.J. and El-khafaji A.H.A. Gas flow measurements in engine cylinders, SAE paper 740719, 1974.
38. El-khafaji A.H.A., Tindal M.J. and Williams T.J. Measurements of induction gas velocities in reciprocating engine cylinder, SAE paper 720115, 1972.
39. Arnolds M.J., Williams T.J. and Tindal M.J. Measurement of induction gas velocities in a reciprocating engine cylinder, SAE paper 720115, 1972.
40. Tindal M.J., Cheung R.S. and Yianneskis M. Velocity characteristics of steady flow through engine inlet ports and cylinders, SAE paper 880383, 1988.
41. Mckinley T.L. and Primus R.J. The influence of bowl off-set on air motion in a direct injection diesel engine, SAE paper 881611, 1988.
42. Cernez Anton. Fuel injection phenomenon, Technical Report, UNDP project no. DP/IND/82/001, 1987.
43. Burman G.P. and Frank Deluka. Fuel injection and control for internal combustion engine, 1962.
44. Bech N.J., Uyehara O.A. and Johnson W.P. Effects of fuel

- injection on diesel combustion, SAE paper 880299, 1988.
45. Becci G.A. The analytic investigation of phenomena concerning the fuel injection in fast diesel engines carried out at the design stage by means of electronics computer, Fiat Stabilimento Grandi Motori, Technical Bulletin, XV-N2, 33-62, April-June 1962.
  46. Becci G.A. Analytical simulation of fuel injection in diesel engines, SAE paper 710568, 1971.
  47. Knight B. E. Fuel injection system calculation, Proc Instn Mech Engrs (Auto Div.), No.61, 25-33, 1960-62.
  48. Wylie E.B., Bolt J.A. and El-Erian M.E. Diesel fuel injection system simulation and experimental correlation, SAE paper 710, 1971.
  49. Reitz R.D. and Bracco F.V. Mechanism of atomization of a liquid jet, Phys Fluid, Vol 25, No.10, pp 1730-1742, 1982.
  50. Arai M., Tanabe M., Hiroyasu H. and Simuzu M. Disintegrating process and spray characterization of fuel jet injected by a diesel nozzle, SAE paper 840275, 1984.
  51. Yule A.J. and Aval S.M. Cyclic variations of diesel sprays, FUEL, Vol 68, Dec. 1989.
  52. Bracco F.V. Modeling of engine sprays, SAE paper 850394, 1985.
  53. Reitz R.D. and Diwakar R. Effect of drop break-up on fuel sprays, SAE paper 860469, 1986.
  54. Bower G., Cheng S.K., Corradini M.L., El-Beshbeeshy M., Martin J.K. and Krueger J. Physical mechanisms for atomization of a jet spray: A comparison of models and experiments, SAE paper 881318, 1988.
  55. Reitz R.D. and Diwakar R. Structure of high pressure fuel sprays, SAE paper 870598, 1987.
  56. Koo J.Y. and Martin J.K. Droplet sizes and Velocities in a transient diesel fuel spray, SAE paper 900397, 1990
  - 57.. Chin J.S. and Lefebvre A.H. Some comments on the characterization of drop-size distribution in sprays, Proc. ICLASS, 1985.
  58. Arroumanis C., Cossali E., Magini R and Whitelaw J.H. Measurements in diesel sprays, I Mech Engrs, paper C372/42, 1989.
  59. Hiroyasu H. and Kadota T. Fuel droplet size distribution in diesel Combustion Chamber, SAE paper 740715, 1974.
  60. Varde K.S., Popa D.M. and Varde L.K. Spray angle and atomization in diesel sprays, SAE paper 841055, 1984.

61. Elkotb M.M. and Abdalla M.A. Atomization of multi-fuel sprays, Proc. Second ICLASS, 237-244, 1982.
62. Rosin P. and Rammler E. The laws governing the fitness of powdered coal, J. Inst Fuel, Vol. 7, 1933, pp 29-36.
63. Nukiyama S. and Tanasawa Y. An experiment on the atomization of liquid, Trans Soc Mech Engrs (Japanese), Vol 4-6, 1938-40.
64. Mugele R.A. and Evans H.D. Droplet size distribution in sprays, Ind Eng Chem, Vol 43, No.6, 1961, pp 1317-1324.
65. Kamimoto T., Ahn S.K., Cheng Y.J., Kobayashi H. and Matsuoka S. Measurement of droplet diameter and fuel concentration in a non-evaporating diesel sprays by mean of an image analysis of shadow photograph, SAE paper 840276, 1984.
66. Sangeorzan B.P., Uyehara O.A. and Myers P.S. Time resolved drop size measurements in an intermittent high pressure fuel spray, SAE paper 841316, 1984.
67. Hay N. and Jones P.L. Comparison of the various correlations for spray penetration, SAE paper 720776, 1972.
68. Wakuri Y. et al. Journal of JSME, 3, 1960.
69. Dent J.C. A basis for the comparison of various experimental methods for studying spray penetration, SAE paper 710571.
70. Harrington D.L. Analysis of spray penetration and velocity dissipation for non-steady fuel injection, ASME, 84-DGP-13, 1984.
71. Ricou F.P. and spalding D.B. Measurements by axi-symmetrical turbulent jets, J. Fluid Mechanics, 1960, Vol 11, pp 21-22.
72. Townsend A.A. The Mechanism of entrainment in free turbulent flow, J. Fluid Mechanics, 1966, Vol 26, part 4, pp 689-715.
73. Keffer J.F. and Baines W.D. The round turbulent jet in a cross-wind, J. Fluid Mechanics, April 1963, pp 483-496.
74. Patrick M.A. Experimental investigation of the mixing and penetration of a round turbulent jet injected perpendicularly into a transverse stream, Trans Instn Chem Engrs, 1967, Vol 45, pp T 16-31.
75. Hoult D.P. and Weil J.C. Turbulent plume in a laminar cross flow, Atmospheric environment, Vol 6, 1972, pp513-531.
76. Stoy R.L. and Ben-haim Y. Turbulent jets in a confined cross flow, J. Fluid Engineering, Dec.1973, pp551-556.
77. Adler D. and Baron A. Prediction of a three-dimensional circular turbulent jet in cross-flow, AIAA, 1979, vol 17, No.2, pp 168-174.
78. Rife J. and Heywood J.B. Photographic and performance studies

of diesel combustion with a rapid compression machine, SAE paper 740948, 1974.

79. Sinnamon J.F., Lancaster D.R. and Steiner J.C. An experimental and analytical study of engine spray trajectories, SAE paper 800135, 1980.
80. Kamotani Y. and Greber I. Experiments on a turbulent jet in a cross-flow, AIAA, 1972, Vol 10, No.11, pp 1425-1429.
81. Glauert M.B. The wall jet, Journal of Fluid Mechanics, Vol 1, 4, 1956, pp 625-643.
82. Searle N. Entrainment by axi-symmetric jets impinging on a flat plate, thesis 17/7, 1964, Cranfield college of Aeronautics, Cranfield, England.
83. Skifstad J.G. Aerodynamics of jets pertinent to VTOL aircraft, J of Aircraft, Vol 7, 1970.
84. Campbell J.F. Turbulent wall jet in a co-flowing stream, NASA TN D8025, 1975.
85. Escudier M.P. and Nicoll W.B. The entrainment function in turbulent boundary layer and wall jet calculation, J. Fluid Mechanics, Vol 25, 1966.
86. Kyriakides S.C., Dent J.C. and Mehta P.S. Phenomenological diesel combustion model including smoke and No emission, SAE paper 860330, 1986.
87. Thring M.W. and Newby M.P. Combustion length of enclosed turbulent jet flames, 4th Int Sym on Combustion, 1953, pp 789-796.
88. Henein N.A. Combustion and emission formation in fuel sprays injected in swirling air, SAE paper 710220, 1971
89. Adler D. and Lyn W.T. The steady evaporation and mixing of a spray in a gaseous swirl, Int J. Heat and Mass Transfer, 1971, 14, 793-812.
90. Elkotb M.M. and Rafat N.M. Fuel spray trajectory in diesel engines, ASME, 100, 326-332, 1978.
91. Dent J.C., Mehta P.S. and Swan J. A predictive model for automotive DI diesel engine performance and smoke emissions, I. Mech E conference on Diesel engines for passenger cars and light duty vehicles, 1982, paper C 126/82, 237-245.
92. Chiu S., Shahed S.M. and Lyn W.T. A transient spray mixing model for diesel combustion, SAE paper 760128, 1976.
93. Hiroyasu H., and Kadota T. Models for Combustion and formation of nitric oxide and soot in direct-injection diesel engines, SAE Trans. 1976, 85, 513-526.
94. Khan I.M., Greeves G. and Probert D.M. Prediction of soot and

nitric oxide concentration in diesel engine exhaust, symposium on Pollution control in transport engines, I Mech E (Lond), 1971.

95. Meguerdichian M., and Watson N. Prediction of mixture formation and heat release in diesel engines, SAE paper 780225, 1978.
96. Demuren A.O. Modeling turbulent jets in cross-flow, Encyclopedia of Fluid Mechanics.
97. Chen C.L.H. Aufrollung eines Zylindrischen Strahles durch querwind, doctoral dissertation, University of Gottingen, Gottingen, W. Germany, 1942.
98. Strauber M. Berechnung Von Strahlkonturen mit Hilfe eines Wirbelringmodells, Zeitschrift fur Flugwissenschaften, Vol 23, 1975, pp 394-400.
99. Schwartz J and Tulin M.P. Chimney plumes in natural and stable surrounding, Atmospheric Environment, Vol 6, 1972, pp 19-35.
100. Mehta P.S. and Gupta A.K. Modelling of spray-swirl interaction in direct injection diesel engine combustion chambers, Proc Instn Mech Engrs, Vol 199, No.D3, 1985.
101. Packer J.P., Adler D., Wilson M. and Wallace F.J. An integral model of jet mixing in an arbitrary cross flow including the effects of concentration, temperature and pressure gradient, 18th Israel Conference on Mech Engg, Hafia, 1984.
102. Wilson M. and Wallace F.J. A comprehensive phenomenological model of the jet mixing process in DI diesel engines, SAE paper 861273, 1986.
103. Reynolds W.C. Modelling of fluid motions in engines- An introductory overview, Combustion Modelling in Reciprocating Engines, Ed Mattavi J.N. and Amman C.A., Plenum press, 1980, pp 69-124.
104. Gosman A.D. and Johns R.J.R. Computer analysis of fuel-air mixing in direct injection engines, SAE paper 800091, 1980.
105. Watkins A.P., Gosman A.D. and Tabrizi B.S. Calculation of three-dimensional spray motion in engines, SAE paper 860468, 1986.
106. Arsdan A.A., Butler T.D., O'Rourke P.J. and Ramshaw J.D. KIVA- $\tau$  comprehensive model for 2-D and 3-D engine simulation, SAE paper 850554, 1985.
107. Katsura N., Saito M., Senda J. and Fujimoto H. Characteristics of a diesel spray impinging on a flat wall, SAE paper 890264, 1989.
108. Lakshminarayan P.A. and Dent J.C. Interferometric studies of vaporizing and combusting sprays, SAE paper 830244, 1983.

109. Dent J.C. and Mehta P.S. Phenomenological combustion model for a quiescent chamber diesel engine, SAE paper 811235, 1981.
110. Payri F., Benajes J. and Tinaut F.V. A Phenomenological combustion model for direct injection, compression ignition engines, Appl Math Modelling, Butterworth Publishers, 1988, Vol 12.
111. Rajaratnam N. Turbulent jets, Elsevier, New York, 1976.
112. Harris A.E. et al. VTOL transport exhaust gas ingestion model tests, NAPTC-IES Environmental Conference paper 67-ENV-17, 1976, Lockheed-Georgia Co. Marietta, Ga.
113. Arbuckle J.A. Investigation of density effects on entrainment by impinging jets, thesis 18/14, 1965, Cranfield College of Aeronautics, Cranfield, England.
114. Spalding D.B. A unified theory of friction, heat transfer and mass transfer in the turbulent boundary layer and wall jet, ARC current papers 829, 1965.
115. Khan I.M. and Greeves G. A Method of calculating emissions of soot and nitric oxide from diesel engines, SAE paper 730169, 1973.
116. Hertel H. Stromungsvorgange beim Freien Hubstrahler, Luft Farttechnik, Vol 8, 1962.
117. Naber J.D. and Reitz R.D. Modeling engine spray/wall impingement, SAE paper 880107, 1988.
118. Taylor G.I. Oblique impact of a jet on a plane surface, Phil Trans Soc, 1167-1187.
- ✓ 119. Lyn W.T. Study of burning rate and nature of combustion in diesel engines, Ninth Symposium (Int) on Combustion, 1963.
120. Borman G.L. Mathematical simulation of internal Combustion engine processes and performance including comparison with experiments, Ph.D thesis, University of Wisconsin, U.S.A., 1964.
- ✓ 121. Whitehouse N.D. and Way R. Rate of heat release in diesel engines and its correlation with fuel injection data, Proc. I. Mech E, Vol 184, 1969-70.
122. Shipinski J., Myers P.S. and Uyehara O.A. A spray droplet Model for diesel combustion, Proc. I. Mech. E, Vol 184, Part 3 J, 1969-70.
123. Adler D. and Lyn W.T. The evaporation and mixing of liquid fuel spray in a diesel air swirl, Proc. I. Mech.E, Vol 184, 1969-70.
124. Grigg H.C. and Syed M.H. The problem of predicting rate of heat release in diesel engines, Proc. I. Mech. E., Vol 184, 1969-70.



125. Bastress E.K., Chung K.M. and Dix D.M. Models of Combustion and nitrogen oxide formation in direct and indirect injection compression ignition engines, SAE paper 719053, 1971.
126. Shahed S.M., Chiu W.S. and Yumlu V.S. A preliminary model for the formation of nitric oxide in direct injection diesel engines and its application on parametric studies, SAE paper 730083, 1973.
127. Whitehouse N.D. and Sareen B.K. Prediction of heat release in a quiescent chamber diesel engine allowing for fuel-air mixing, SAE paper 740084, 1974.
128. Shahed S.M., Chiu W.S. and Lyn W.T. A mathematical model of diesel Combustion, I. Mech E Conference on Combustion in Engines, Cranfield, 1975.
129. Hodgetts D. and Shroff H.D. More on the formation of nitric oxide and soot in direct injection diesel engines, I. Mech E. Conference on Combustion in Engines, Cranfield, 1975.
130. Kau C.J., Tyson T.J. and Heap M.P. Study of oxides of nitrogen and Carbon formation in diesel engines, Final report, EPA report No.EPA-460/3-76-008-a, 1976.
131. Hiroyasu H., Kadota T. and Arai M. Development and use of a spray Combustion modelling to predict diesel engine efficiency and pollutant emissions, Bulletin JSME, 1983, 26, 569-575.
132. Kono S., Nagao A. and Motooka M. Prediction of in-cylinder flow and spray formation effects on Combustion of direct injection diesel engine, SAE paper 850108, 1985.
133. Gupta A.K., Mehta P.S. and Gupta C.P. Model for predicting air-fuel mixing and combustion for direct injection diesel engine, SAE paper 860331, 1986.
134. Lipkea W.H. and Deejoode A.D. A model of a direct injection diesel Combustion system for use in cycle simulation and optimization studies, SAE paper 870573, 1987.
135. Khan I.M., Wang C.H.T. and Langride B.E. Coagulation and combustion of soot particles in diesel engines, Combustion and Flame, Vol 17, 409-419, 1971.
136. Khan I.M., Greeves G. and Wang C.H.T. Factors affecting smoke and gaseous emissions from DI engines and a method of calculation, SAE paper 730169, 1973.
137. Khan I.M., Greeves G. Heat transfer in flames, Ed. by N.H. Afgan and J.M. Beer, John Wiley and Sons, NY, 391-404, 1975.
138. Schweitzer P.H. Penetration of oil sprays, Pennsylvania st-coll Bull, No.46, 1937.
139. Wilson R.P., Waldman C.H. and Muzio L.J. Foundation for modelling (No)x and smoke formation in diesel flames, EPA

Final report Phase-I, EPA-460/3-74/002a, 1974.

140. Abramovich G.N. The theory of turbulent jets, MIT press, Mass, 1963.
141. Anand W.J.D. Heat transfer in the cylinders of reciprocating internal combustion engines, Proc. I.Mech.E, Vol 177, 36, pp 973, 1963.
142. Woschni G. A universally applicable equation for instantaneous heat transfer co-efficient in the internal combustion engine, SAE paper 670931, 1967.
143. Watson N. and Janota M.S. Development and application of a comprehensive turbocharged diesel engine model, Symp of Universities, I.C. Engines group and sponsored by the Science Research Council, King's college, London, April, 1980.
144. Giralt F., Chia C.J. and Trass O. Characterization of the impingement region in an axi-symmetric turbulent jet, Ind. Engg Chem (Fundamentals), Vol 16, 1977.
145. Era Y. and Saima A. An investigation of impinging jets (Experiments by air, hot air and carbon dioxide), Bulletin JSME, Vol 19.
146. Simmons H.C. The correlation of drop-size distribution in fuel nozzle sprays - Part II: The drop-size/number distribution, J. Engg Power, ASME, 315-319, 1977.
147. Mehta P.S., Dent J.C. and Gupta A.K. Computational schemes for atomization and evaporation of diesel fuel spray, Proc. Third ICLASS, IB/3/1-10, 1985.
148. Corrsin S. Simple theory of an idealized turbulent mixer, A.I.Ch.E. Journal, Vol 3, No.3, 1957.
149. Brodkey R.S. Turbulence in mixing operations, Academic Press, London, 1975.
150. Dent J.C. Turbulent mixing rate - Its effect on smoke and hydrocarbon emissions from diesel engines, SAE paper 800092, 1980.
151. Hardenberg H.O. and Hase F.W. An empirical formula for computing the pressure rise delay of a fuel from its cetane number and from the relevant parameters of direct injection diesel engines, SAE paper 790493, 1979.
152. Glassman I. Combustion, Academic press, New York, 1977.
153. Levich V.G. Physico-chemical hydrodynamic, Prentice-Hall, Englewood Cliffs, N.J., 1962.
154. Hiroyasu H., Kadota T and Arai M. Supplementary comments : Fuel spray characterization in diesel engines, J.N. Mattavi and C.A. Amman (Editors), Combustion Modelling in Reciprocating Engines, pp 369-408, Plenum press, 1980.

155. Faeth G.M. Evaporation and Combustion of sprays, Prog. Energy Combust Sci, 9, pp 1-76, 1983.
156. Ranz W.E. and Marshall W.R. Evaporation from drops, Chemical Engg. Progress, 48, pp 141-146, 1952.
157. Patrick M.A. Experimental investigation of mixing and flow in a round turbulent jet issuing perpendicularly into a main stream, Sheffield University, Fuel Society Journal, Vol 16, pp 46-61, 1965.
158. Patrick M.A. Experimental investigation of mixing and flow in round turbulent jet issuing perpendicularly into a main stream, Journal of the Inst of Fuel, pp 425-432, 1965.
159. Borgnakke C., Davis G.C. and Tabaczynski. Prediction of in-cylinder swirl velocity and turbulence intensity for an open chamber cup in piston engine, SAE paper 810224, 1981.
160. Uyehara O.A. Factors that affect BSFC emissions for diesel engines: Part 1- Presentation of concepts, SAE paper 870343, 1987.
161. Fitzgeorge D and Allison J.L. Air swirl in a road vehicle diesel engine, Proc I.Mech.E(A.D), 1963-63.
162. Streeter V.L. Handbook of fluid dynamics, McGraw Hill book co. Inc, 1961.
163. Kuo T.W. and Bracco F.V. Computation of drop sizes in pulsating sprays and of liquid core length in vaporizing sprays, SAE paper 820133.
164. Lee D.W. The effect of nozzle design and operating conditions on the atomization and distribution of fuel sprays, NASA Report 425, 1932.
165. Henein N.A and Bolt J.A. Ignition delay in diesel engines, SAE paper 670007, 1967.
166. Plee S.L. and Ahmad T. Relative roles of pre-mixed and diffusion burning in diesel combustion, SAE paper 831733, 1983.
167. Belardeni D. and Bertoli C., Corcine F.E and Police G. Ignition delay measurement in a direct injection diesel engine, I.Mech.E, Int Conf. on Combustion in Engineering, paper No. C86/83, 1983.
168. Kamimoto T and Matsuoka S. Prediction of spray evaporation in reciprocating engines, SAE paper 770413, 1977.
169. Chappel M.S and Cockshut E.P. Gas turbine cycle calculator: Thermodynamic data tables for air and combustion products for three system of units, NRC, Canada, Aeronautical Report LR-679, 1974.

170. Spiers H.M. Technical data on fuel, The British National Committee, World Power Conference, London, 1961.
171. Kuo T.W and Bracco F.V. On the scaling of transient laminar, turbulent and spray jets, SAE 820038, 1982.
172. Kamimoto T., Aoyagi Y., Matsui Y. and Matsuoka S. The effects of some engine variables on measured rates of air entrainment and heat release in a DI diesel engine, SAE paper 800253, 1980.
173. Tsunemoto H. and Ishitani H. The behavior of impinged fuel sprays on simulated combustion chamber walls in direct injection diesel engines, JSAE Review, 3, pp9-14, 1982.
174. Naber J. Enright B. and Farrel P. Fuel impingement in a direct injection diesel engine, SAE paper 881316, 1988.
175. Hiroyasu H. and Nishida K. Fuel spray trajectory and dispersion in a DI diesel combustion chamber, SAE paper 890462, 1989.
176. Nishida K., Murakami N. and Hiroyasu H. Holographic measurement of evaporating diesel sprays at high pressure and temperature, JSME International Journal, Vol 30, 259, 1987.

## APPENDIX A

### THE TORQUE FORCE DUE TO WALL FRICTION

The torque force due to the wall friction( $T_f$ ) is estimated as;

#### (a) Friction on Cylinder liner

Wall shear stress( $\tau$ ) and friction factor( $C_f$ ) as given by flat plate formulae are estimated as ;

$$\tau = \frac{1}{2} \rho \left( \omega \frac{D}{2} \right)^2 C_f \quad (\text{A.1})$$

$$C_f = 0.037 \lambda R_s^{-0.2} \quad (\text{A.2})$$

The value of constant  $\lambda = 1.5$  is taken from(3) and is equivalent of flat plate Reynold number( $R_s$ ), which is estimated as ;

$$R_s = \rho \left( D \frac{\omega}{2} \right) \frac{(\pi D)}{\mu} \quad (\text{A.3})$$

Restraining torque( $T_1$ ) exerted by cylinder liner at any crank angle is given by :

$$T_1 = \tau \pi D S(\theta) \frac{D}{2} \quad (\text{A.4})$$

Substitution of equation(A.1) into equation(A.4) yields:

$$T_1 = C_f \rho \frac{\omega^2}{16} \pi D^4 S(\theta) \quad (\text{A.5})$$

#### (b) Friction on cylindrical wall of bowl

Friction torque exerted by side walls of bowl( $T_b$ ) is estimated

by replacing bore(D) with bowl diameter(d) and instantaneous stroke length(S( $\theta$ )) with bowl depth( $h_b$ ) respectively, in equation(A.5):

$$T_b = C_f \rho \frac{\omega^2}{16} \pi d^4 h_b \quad (\text{A.6})$$

Similarly, Reynold number( $R_{\mu}$ ) is estimated as;

$$R_{\mu} = \rho \left( d \frac{\omega}{2} \right) \frac{(\pi d)}{\mu} \quad (\text{A.7})$$

**(c) Friction on Cylinder head and piston crown**

Assuming that the torque exerted by these surfaces acts at mean cylinder radius(D/4), the wall shear stress( $\tau$ ), Reynold number( $R_{\mu}$ ) and the torque exerted on cylinder head ( $T_h$ ) and piston crown( $T_p$ ) are estimated by :

$$\tau = \frac{1}{2} \rho \left( \omega \frac{D}{4} \right)^2 C_f \quad (\text{A.8})$$

$$R_{\mu} = \frac{\rho \left( \omega \frac{D}{4} \right) \left( \frac{D}{4} \right)}{\mu} \quad (\text{A.9})$$

$$T_h = T_p = \tau \frac{\pi}{4} D^2 \frac{D}{4} \quad (\text{A.10})$$

Substitution of equation(A.8) into equation(A.10) gives;

$$T_h = T_p = C_f \rho \frac{\omega^2 \pi D^5}{512} \quad (\text{A.11})$$

The torque due to the friction for all the surfaces( $T_f$ ) is:

$$T_f = T_1 + T_2 + T_h + T_p \quad (\text{A.12})$$

## APPENDIX B

### FUEL INJECTION SIMULATION MODEL

Referring Fig B.1(42),

(1) The continuity equation for pump plunger

Volume displacement of plunger = Flow through control of port + Flow through delivery valve + Compressibility effect of fuel.

$$A_k S_k - \mu_c A_c \sqrt{\frac{2}{\rho_f} (p_k - p_c)} + \mu_v A_v \sqrt{\frac{2}{\rho_f} (p_k - p_1)} + A_v S_v + \frac{V_k dp_k}{E dt} \quad (B.1)$$

Where  $S_k$  and  $S_v$  are velocities of pump plunger and relief valve piston respectively.  $\mu_c$  and  $\mu_v$  are the discharge coefficients for control port and delivery valve respectively.  $V_k$  is the pump volume (over the plunger) and  $p_k$ ,  $p_c$ ,  $p_1$  are the pressures at sections as shown in Fig B.1.  $E$  is the bulk modulus of elasticity. Eq(B.1) can be written as ;

$$\frac{dp_k}{dt} = \frac{E}{V_k} [A_k S_k - \mu_c A_c \sqrt{\frac{2}{\rho_f} (p_k - p_c)} - \mu_v A_v \sqrt{\frac{2}{\rho_f} (p_k - p_1)} - A_v S_v] \quad (B.2)$$

(2) Continuity equation for relief valve holder

Volume displacement by delivery valve + Flow from chamber to delivery valve chamber  
 = Compressibility effect of fuel + Out-flow into high pressure pipe

$$A_v S_v + \mu_v A_v \sqrt{\frac{2}{\rho_f} (p_k - p_l)} = \frac{V_k L}{E} \frac{dp_l}{dt} + A_c W_l \quad (\text{B.3})$$

Where  $W_l$  is the in-flow fuel velocity at section(I-I).  $L$  is length of the high pressure pipe. Eq(B.3) can be written as;

$$\frac{dp_l}{dt} = \left[ \mu_v A_v \sqrt{\frac{2}{\rho_f} (p_k - p_l)} + A_v S_v - A_c W_l \right] \frac{E}{V_k L} \quad (\text{B.4})$$

### (3) The Equilibrium of forces at the relief valve

Inertia force = Fluid pressure force - Reaction of seat on valve - Spring force

$$m_v \frac{d^2 h_v}{dt^2} = A_v (p_k - p_l) - C_v h_v - F_{v0} \quad (\text{B.5})$$

Where  $h_v$  is the relief valve piston lift,  $C_v$  is the relief valve spring rate and  $F_{v0}$  is opening force of the relief valve spring.  $m_v$  is the mass of the relief valve moving parts. Taking  $S_v = \frac{dh_v}{dt}$  and rewriting Eq(B.5),

$$\frac{dS_v}{dt} = \left[ A_v (p_k - p_l) - F_{v0} - C_v h_v \right] \frac{1}{m_v} \quad (\text{B.6})$$

### (4) The Continuity equation for injector

Fuel flow into injector from high pressure pipe = Discharge through nozzle + Volume exerted by needle lift + Compressibility effect.

$$A_c W_{II} = \mu_v A_v \sqrt{\frac{2}{\rho_f} (p_{II} - p_s)} + A_i S_i + \frac{dp_{II} V_d}{dt E} \quad (\text{B.7})$$

Where  $S_i$  is the needle lift and  $V_d$  is the injector dead volume.



Rewriting Eq(B.7);

$$\frac{dp_{II}}{dt} = [A_c W_{II} - \mu_b A_b \sqrt{\frac{2}{\rho_f} (p_{II} - p_x)} - A_1 S_1] \frac{E}{V_i} \quad (B.8)$$

(5) Force Equilibrium equation at the injector

Inertia force due + Force caused + Injector spring  
to accelerated by pressing force  
mass of injector the injector  
moving parts spring

= Force caused by fuel pressure  $P_{IX}$  + Force caused by fuel pressure  $p_b$  on needle seat area

$$m_i \frac{d^2 h_i}{dt^2} + C_{ob} h_i + F_{ob} = (A_1 - A_x) p_{II} + A_x p_b \quad (B.9)$$

Where  $C_{ob}$ ,  $F_{ob}$  and  $m_i$  are the spring rate, opening force of the spring and mass of the injector respectively. Eq(B.9) can be written as;

$$\frac{dS_i}{dt} = [(A_1 - A_x) p_{II} + A_x p_b - F_{ob} - h_i C_{ob}] \frac{1}{m_i} \quad (B.10)$$

Equations(B.2), (B.4), (B.6), (B.8) and (B.10) are ordinary differential equations and are solved with 4th order Runge-Kutta method. These equations calculate in-pump pressure, pressure at the beginning of high pressure pipe, relief valve piston velocity, pressure at the end of high pressure pipe and needle velocity as a function of time. The rate of injection with crank angle is then computed. The flow areas used in the above equations are computed by correlations.



## APPENDIX C

### IMPINGEMENT OF SPRAY ON PISTON WALLS

Referring Fig C.1 ;

The spray angle ( $\psi$ ) is given as ;

$$\frac{\psi}{2} = \sin^{-1} \left[ \frac{1}{\left(\frac{l_y}{r} - 1\right)} \right] \quad (C.1)$$

Length of spray tip tangent is :

$$\overline{AB} = \overline{AC} = Z_t = (l_y - r) \cos\left(\frac{\psi}{2}\right) \quad (C.2)$$

Co-ordinates of characteristic points are ;

$$X_B = X_A + Z_t \sin\left(\alpha - \frac{\psi}{2}\right) \quad (C.3)$$

$$Y_B = Y_A - Z_t \cos\left(\alpha - \frac{\psi}{2}\right) \quad (C.4)$$

$$X_C = X_A + Z_t \sin\left(\alpha + \frac{\psi}{2}\right) \quad (C.5)$$

$$Y_C = Y_A - Z_t \cos\left(\alpha + \frac{\psi}{2}\right) \quad (C.6)$$

$$X_O = X_A + (l_y - r) \sin \alpha \quad (C.7)$$

$$Y_O = Y_A - (l_y - r) \cos \alpha \quad (C.8)$$

$$X_I = X_O + r \quad (C.9)$$

$$Y_I = Y_O \quad (C.10)$$

$$X_F = X_O + r \sin \alpha \quad (C.11)$$

$$Y_F = Y_O + r \cos \alpha \quad (C.12)$$

$X_K$  and  $Y_K$  are co-ordinates of corresponding points K of the piston bowl

Case 1 If  $X_K \leq X_B$

$$Y_D = Y_A + (Y_B - Y_A) \frac{X_K - X_A}{X_B - X_A} \quad (C.13)$$

$$Y_C = Y_A - (Y_C - Y_A) \frac{X_K - X_A}{X_C - X_A} \quad (C.14)$$

Case 2 If  $X_B < X_K \leq X_C$

$$Y_D = Y_0 - \sqrt{\Gamma^2 - (X_K - X_0)^2} \quad (C.15)$$

$$Y_C = Y_A + (Y_C - Y_A) \frac{X_K - X_A}{X_C - X_A} = Y_C(\text{Case 1}) \quad (C.16)$$

Case 3 If  $X_C < X_K < X_E$

$$Y_D = Y_0 - \sqrt{\Gamma^2 - (X_K - X_0)^2} = Y_D(\text{Case 2}) \quad (C.17)$$

$$Y_C = Y_0 + \sqrt{\Gamma^2 - (X_K - X_0)^2} \quad (C.18)$$

If condition  $Y_D \leq Y_K \leq Y_C$  is fulfilled, contact between the spray and engine piston is evaluated on the piston at point K.

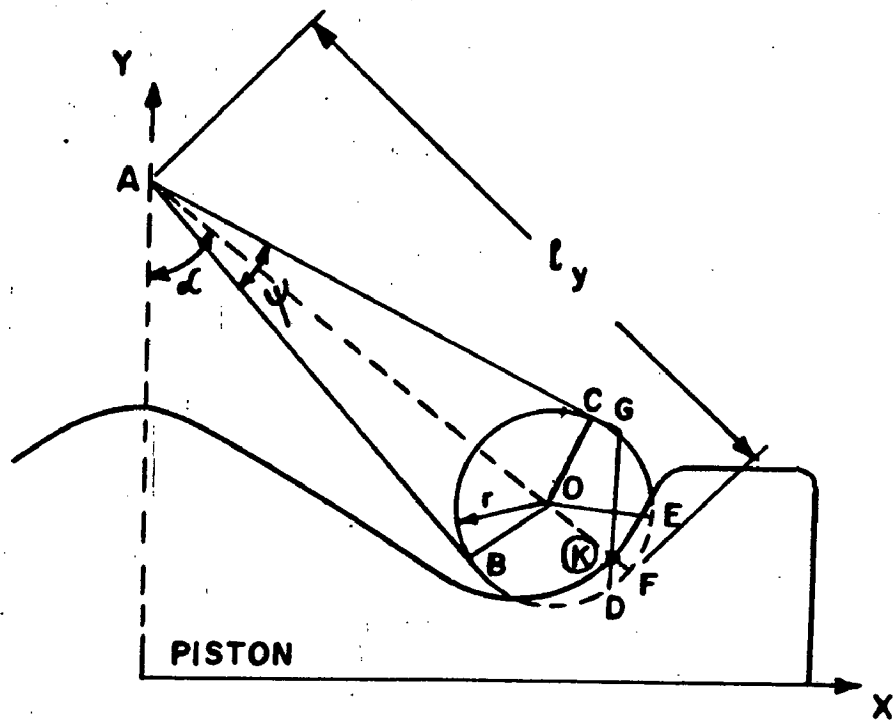


Fig C.1 Co-ordinate system for spray impingement analysis

## APPENDIX D

### AIR ENTRAINMENT IN THE WALL JET

The relation for the rate of mass flow in a wall jet formed by an impinging jet, as shown by Skifstad (83), has been used ;

$$\frac{\dot{m}}{\dot{m}_0} = 0.68 \frac{s}{d_0} \quad (D.1)$$

Differentiating equation (D.1) with respect to s:

$$\frac{d\dot{m}}{ds} = 0.68 \frac{\dot{m}_0}{d_0} \quad (D.2)$$

Using the concept of equivalent diameter for injected fluids of different densities, equation(D.2) modifies to :

$$\frac{d\dot{m}}{ds} = 0.68 \frac{\dot{m}_0}{d_0} \quad (D.3)$$

Mass flow rate through the nozzle orifice is :

$$\dot{m}_0 = \frac{\pi}{4} d_0^2 u_0 \rho_0 C_d \quad (D.4)$$

Orifice diameter( $d_0$ ) in relation to equivalent diameter ( $d_e$ ) is :

$$d_0 = d_e \left( \frac{\rho_e}{\rho_0} \right)^{1/2} \quad (D.5)$$

Substitution of equations(D.4-D.5) into equation(D.3), taking  $C_d = 0.7$  gives :

$$\frac{dm}{ds} = 0.3738 \rho_a d u_a \quad (D.6)$$

Considering equation (3.10) for air entrainment rate for non-burning free jet in the absence of air swirl ( $U_t$  and  $U_n$  equal to zero) and proper substitution of relationship between jet centre-line velocity and the initial jet velocity ( $u_0$ ), taking jet cone angle of  $22^\circ$  and  $C_d = 0.7$ , equation (3.10) reduces to :

$$\frac{dm}{ds} = 5.025 a_1 u_a d (\rho_a \rho_m)^{1/2} \quad (D.7)$$

Equation (D.6) and equation (D.7) are similar provided  $\rho_m$  taken equal to  $\rho_a$  in equation (D.7). Hence, the value of  $a_1 = 0.074$  is estimated by comparing equation (D.6) and equation (D.7). Thus, the estimated value of  $a_1 = 0.074$  is used and adopted in equation (3.10) for the wall jet. The value of normal entrainment parameter  $a_2 = 0.05$  following Sinnamon's work (79) is adopted for the wall jet as well. Hence, the following values of axial and normal entrainment parameters are used in equation (3.10);

$a_1 = 0.035$  for free jet

$= 0.074$  for wall jet

$a_2 = 0.05$  both for free and wall jet.

## APPENDIX E

### THE DETAILS OF DERIVATION OF MODEL EQUATIONS

Equations(3.11-3.22) can be combined to yield the following four conservation equations :

Fuel mass

$$\frac{d}{ds} \left[ P_2 \pi b_j^2 \rho_s u_m \int_0^1 \frac{c_m f^3 y dy}{1 - c_m f \beta} \right] = 0 \quad (E.1)$$

Total mass

$$\begin{aligned} \frac{d}{ds} \left[ P_2 \pi \rho_s u_m b_j^2 \int_0^1 \frac{f^2 y dy}{1 - c_m f \beta} \right] \\ = P \pi b_j (\rho_m \rho_s)^{1/2} [a_1 (u_m - U_t) + a_2 (U_s)] \end{aligned} \quad (E.2)$$

Tangential momentum

$$\begin{aligned} \frac{d}{ds} \left[ P_2 \pi \rho_s u_m^2 b_j^2 \int_0^1 \frac{f^4 y dy}{1 - c_m f \beta} \right] \\ = P \pi b_j (\rho_m \rho_s)^{1/2} [a_1 (u_m - U_t) + a_2 (U_s)] U_t + C_t b_j \frac{\rho_s}{2} (u_m - U_t)^2 \hat{t} \end{aligned} \quad (E.3)$$

Normal momentum

$$\begin{aligned} -P_2 \pi \rho_s u_m^2 b_j^2 \left[ \int_0^1 \frac{f^4 y dy}{1 - c_m f \beta} \right] \frac{d\alpha}{ds} \\ = P \pi b_j (\rho_m \rho_s)^{1/2} [a_1 (u_m - U_t) + a_2 (U_s)] U_s \end{aligned} \quad (E.4)$$

Where f refers to f(y)



$$E = \frac{[a_1(u_m - U_t) + a_2(U_m)]}{(1 - c_m \beta)^{1/2}}$$

$$I_1 = \int_0^1 \frac{f^3 y dy}{(1 - c_m f \beta)^2}$$

$$I_2 = \int_0^1 \frac{c_m f^3 y dy}{(1 - c_m f \beta)}$$

$$I_3 = \int_0^1 \frac{\beta f^3 y dy}{(1 - c_m f \beta)^2}$$

$$I_4 = \int_0^1 \frac{f^2 y dy}{1 - c_m f \beta}$$

$$I_5 = \int_0^1 \frac{\beta f^5 y dy}{(1 - c_m f \beta)^2}$$

$$I_6 = \int_0^1 \frac{f^4 y dy}{(1 - c_m f \beta)}$$

### Constants

$$P_2 = 2 \text{ for free jet}$$

$$= 0.5 \text{ for wall jet}$$

$$P = 2 \text{ for free jet}$$

$$= 0.79 \text{ for wall jet}$$

## APPENDIX F

### THERMODYNAMIC GAS AND FUEL PROPERTIES

For calculation of thermodynamic properties of the gases at any temperature and composition, the polynomial relations proposed by Chappel and Cockshut (169) have been used. These are based on specific heat data of Fielding and Topps and the values agree closely with Keenan and Kay's gas tables. The assumptions made are;

- (a) Dry air and products of combustion are assumed to be semi-perfect gases.
- (b) Dissociation effects are neglected

The specific heat data for dry air represented as fifth order polynomials of temperature ;

$$C_{p,s} = C_0 + C_1 T + C_2 T^2 + C_3 T^3 + C_4 T^4 + C_5 T^5 \quad (\text{F.1})$$

$$h_s = \int_0^T C_{p,s} dT = C_0 T + \frac{C_1}{2} T^2 + \frac{C_2}{3} T^3 + \frac{C_3}{4} T^4 + \frac{C_4}{5} T^5 + \frac{C_5}{6} T^6 + CH \quad (\text{F.2})$$

Where CH is the constant of integration chosen to yield minimum discrepancy from tabulated data and  $C_0 - C_5$  are constant.

The corrections applied to the air data for computing the properties of products of combustion of varying composition are by means of the theta functions defined as;

$$H_{cp} = \left( \frac{1 + F_s}{F_s} \right) (C_{p,s} - C_{p,a}) \quad (\text{F.3})$$

$$H_h = \left( \frac{1 + F_s}{F_s} \right) (h_s - h_a) \quad (\text{F.4})$$

Where  $F_s$  is the fuel-air ratio of stoichiometric mixture and  $C_{p,s}$  and  $h_s$  are the specific heat and enthalpy of stoichiometric mixture.

The above correction factors are then used to define the properties of products of combustion as follows ;

$$C_{p,prod} = C_{p,s} + \frac{F}{1+F} H_{cp} \quad (F.5)$$

$$h_{prod} = h_s + \frac{F}{1+F} H_h \quad (F.6)$$

Where  $F$  is the fuel-air ratio.

The theta functions are represented as fifth order polynomials in temperature ;

$$H_{cp} = CP_0 + CP_1 T + CP_2 T^2 + CP_3 T^3 + CP_4 T^4 + CP_5 T^5 \quad (F.7)$$

$$H_h = CH_0 + CH_1 T + CH_2 T^2 + CH_3 T^3 + CH_4 T^4 + CH_5 T^5 \quad (F.8)$$

Where  $CP_0-CP_5$  and  $CH_0-CH_5$  are constants.

The liquid phase specific heat for hydrocarbon fuel is computed from the relation (170) given as;

$$C_{p,l} = \frac{(38692.0 + 53.585 T)}{\rho_l^{0.8}} \quad (F.9)$$

The constant pressure specific heat for hydrocarbon fuel vapour is evaluated using the correlation given in reference (170) as ;

$$C_{p,v} = (0.296285 + 0.000586 T)(4000 - \rho_v) \quad (F.10)$$

## LIST OF PAPERS FROM THE THESIS

1. Modelling spray/wall interaction in swirling flows for DI diesel engines.

Proc Instn Mech Engrs (London), Journal of Automobile Engg., Vol 204, No. D4, 1990.

2. Modelling of Spray-Swirl interaction in DI Diesel Engine - Influence of Injection Characteristics.

Paper presented in SAE International Off-Highway and Powerplant Congress and Expositions, Wisconsin, Sep 11-14, 1989, SAE paper 891914.

3. Prediction of influence of Injection parameters on Diesel Sprays in Swirling Flows.

Paper presented in 11th National Conference on I.C Engines and Combustion at Madras(India), Dec 11-15, 1989.